Nuclear Science

OECD

Physics of Plutonium Recycling

Volume VII: BWR MOX Benchmark – Specification and Results

NUCLEAR • ENERGY • AGENCY

Nuclear Science

Physics of Plutonium Recycling

Volume VII

BWR MOX Benchmark Specification and Results

NUCLEAR ENERGY AGENCY
ORGANISATION FOR ECONOMIC CO-OPERATION AND DEVELOPMENT

ORGANISATION FOR ECONOMIC CO-OPERATION AND DEVELOPMENT

Pursuant to Article 1 of the Convention signed in Paris on 14th December 1960, and which came into force on 30th September 1961, the Organisation for Economic Co-operation and Development (OECD) shall promote policies designed:

- to achieve the highest sustainable economic growth and employment and a rising standard of living in Member countries, while maintaining financial stability, and thus to contribute to the development of the world economy;
- to contribute to sound economic expansion in Member as well as non-member countries in the process of economic development; and
- to contribute to the expansion of world trade on a multilateral, non-discriminatory basis in accordance with international obligations.

The original Member countries of the OECD are Austria, Belgium, Canada, Denmark, France, Germany, Greece, Iceland, Ireland, Italy, Luxembourg, the Netherlands, Norway, Portugal, Spain, Sweden, Switzerland, Turkey, the United Kingdom and the United States. The following countries became Members subsequently through accession at the dates indicated hereafter: Japan (28th April 1964), Finland (28th January 1969), Australia (7th June 1971), New Zealand (29th May 1973), Mexico (18th May 1994), the Czech Republic (21st December 1995), Hungary (7th May 1996), Poland (22nd November 1996), Korea (12th December 1996) and the Slovak Republic (14 December 2000). The Commission of the European Communities takes part in the work of the OECD (Article 13 of the OECD Convention).

NUCLEAR ENERGY AGENCY

The OECD Nuclear Energy Agency (NEA) was established on 1st February 1958 under the name of the OEEC European Nuclear Energy Agency. It received its present designation on 20th April 1972, when Japan became its first non-European full Member. NEA membership today consists of 28 OECD Member countries: Australia, Austria, Belgium, Canada, Czech Republic, Denmark, Finland, France, Germany, Greece, Hungary, Iceland, Ireland, Italy, Japan, Luxembourg, Mexico, the Netherlands, Norway, Portugal, Republic of Korea, Slovak Republic, Spain, Sweden, Switzerland, Turkey, the United Kingdom and the United States. The Commission of the European Communities also takes part in the work of the Agency.

The mission of the NEA is:

- to assist its Member countries in maintaining and further developing, through international co-operation, the scientific, technological and legal bases required for a safe, environmentally friendly and economical use of nuclear energy for peaceful purposes, as well as
- to provide authoritative assessments and to forge common understandings on key issues, as input to government decisions on nuclear energy policy and to broader OECD policy analyses in areas such as energy and sustainable development.

Specific areas of competence of the NEA include safety and regulation of nuclear activities, radioactive waste management, radiological protection, nuclear science, economic and technical analyses of the nuclear fuel cycle, nuclear law and liability, and public information. The NEA Data Bank provides nuclear data and computer program services for participating countries.

In these and related tasks, the NEA works in close collaboration with the International Atomic Energy Agency in Vienna, with which it has a Co-operation Agreement, as well as with other international organisations in the nuclear field.

FOREWORD

The OECD/NEA Working Party on the Physics of Plutonium Fuels and Innovative Fuel Cycles (WPPR, formerly the Working Party on Physics of Plutonium Recycling) was established in 1993 and reports to the OECD/NEA Nuclear Science Committee. Its main activity has been to analyse physics code benchmarks for problems related to the physics of plutonium fuels. Past volumes of published work have examined the physics of plutonium-fuelled pressurised water reactors (PWRs), the physics of metal- and oxide-fuelled fast reactors and multiple recycling in conventional and high-moderation PWRs. Altogether, six volumes of work have been published comprising:

- Volume I: Issues and Perspectives (OECD/NEA, 1995);
- Volume II: Plutonium Recycling in Pressurised Water Reactors (OECD/NEA, 1995);
- Volume III: Void Reactivity Effect in Pressurised Water Reactors (OECD/NEA, 1995);
- Volume IV: Fast Plutonium Burner Reactors: Beginning of Life (OECD/NEA, 1995);
- Volume V: Plutonium Recycling in Fast Reactors (OECD/NEA, 1996);
- Volume VI: Multiple Plutonium Recycling in Advanced PWRs (OECD/NEA, 2002).

The present Volume VII describes the results of a theoretical benchmark of a boiling water reactor (BWR) assembly containing MOX fuel rods. Addressing this issue was timely as there are now advanced plans for commercial-scale deployment of MOX in BWRs. Volume VIII of this series will be devoted to plutonium fuel in high-temperature reactors (HTRs).

While all of the earlier work consisted of theoretical benchmarks comparing different nuclear codes and nuclear data libraries, comparisons against experimental measurements were made possible by SCK-CEN using data from the VENUS-2 reactor. The VENUS-2 data concerned an experimental mock-up of a PWR core containing UO_2 and mixed-oxide (MOX) assemblies. The results of this benchmark were published in *Benchmark on the VENUS-2 MOX Core Measurements* (OECD/NEA, 2000). The benchmark was carried out under the joint auspices of the WPPR and the Task Force on Reactor-based Plutonium Disposition (TFRPD). Another benchmark was undertaken for three critical core configurations of the KRITZ reactor: two with UO_2 fuel and one with MOX fuel. Measurements were performed for room temperature as well as elevated temperatures (~245°C). The results are due to be published soon.

Acknowledgements

The Secretariat expresses its sincere gratitude to the participants who devoted their time and effort to this benchmark exercise.

TABLE OF CONTENTS

CONTRIBUTORS

TEXT	*HESKETH, Kevin*	BNFL	UK
	TCHISTIAKOV, Andrei	Consultant	France
	DELPECH, Marc	CEA	France
	TIMM, Wolf	Framatome-ANP	Germany
TEXT REVIEW	*SARTORI, Enrico*	OECD/NEA	
	GEHIN Jess	ORNL	USA
TEXT PROCESSING/LAYOUT	*DÉRY, Hélène*	OECD/NEA	
SPECIFICATION	*SCHLOSSER, Gerhard*	Siemens/KWU	Germany
	TIMM, Wolf	Framatome-ANP	Germany
PARTICIPANTS	*LANCE, Benoit*	Belgonucléaire	Belgium
	DELPECH, Marc	CEA Cadarache	France
	GASTALDI, Bernard	CEA Cadarache	France
	LEE, Yi-Kang	CEA Saclay	France
	MAGAT, Philippe	CEA Saclay	France
	PENELIAU, Yannick	CEA Saclay	France
	ROHART, Michelle	CEA Saclay	France
	TCHISTIAKOV, Andrei	Consultant	France
	HESSE, Ulrich	GRS	Germany
	LUTZ, Dietrich	IKE	Germany
	MATTES, Margarete	IKE	Germany
	MISU, Stefan	Framatome-ANP	Germany
	SCHLOSSER, Gerhard	Siemens/KWU	Germany
	TIMM, Wolf	Framatome-ANP	Germany
	ZWERMANN, Winfried	GRS	Germany
	INOUE, Yuichiro	Toden Software Inc.	Japan
	ISHII, Kazuya	Hitachi Ltd.	Japan
	OKUMURA, Keisuke	JAERI	Japan
	KIM, Taek Kyum	KAERI	Republic of Korea
	KIM, Young-Jin	KAERI	Republic of Korea
	JOO, Hyung Kook	KAERI	Republic of Korea
	FRANCOIS, Juan Luis	UNAM	Mexico
	MARTIN-DEL CAMPO, Cecilia	UNAM	Mexico
	DAMEN, Patricia	NRG	The Netherlands
	KALUGIN Mikhai,l A.	RRC-KI	Russian Federation
	KROUTHEN, Jan	EGL/KKL	Switzerland
	PARATTE, Jean-Marie	PSI	Switzerland
	BAKER, Steven	TransWare Enterprise	USA
	CUEVAS-VIVAS, Gabriel	Texas A&M	USA
	GEHIN, Jess C.	ORNL	USA
	PARISH, Theodore A.	Texas A&M	USA

EXECUTIVE SUMMARY

This report presents the detailed results of a theoretical benchmark of a boiling water reactor (BWR) assembly containing MOX fuel rods. This study was carried out by the OECD/NEA Working Party on Physics of Plutonium Fuels and Innovative Fuel Cycles (WPPR). A modern 10×10 BWR design with large internal water structure was chosen for the exercise, corresponding to an ATRIUM-10 (10-9Q) type with symmetrical water gaps. About 30 solutions were submitted by approximately 20 participants using a dozen different code systems with data from well-known state-of-the-art evaluated nuclear data files, a response which underlines the widespread interest in BWR MOX physics. The discrepancies between the participants for the infinite multiplication factor from beginning of life through burn-ups up to 50 MWd/kgHM are relatively small (less than 1%). The effect due to diverse evaluated data libraries, e.g. JEF and ENDF represents about 1%. The power peaking factor is determined by local phenomena, more dependent on the methods used in the codes, and with lower compensation effects than for reactivity. The discrepancies are larger in value and there are inconsistencies in the location of the peak. The average values with and without the extreme values differ by 2%, implying that the extreme values could be outside the acceptable range. Other parameters examined include the behaviour of the power peaking factor under cold conditions, the evolution of the power peaking factor with burn-up and the effect of voiding the assembly. Close attention was also paid to the depletion behaviour of gadolinia burnable poison, the burn-up evolution of the heavy metals and the effect of control rod insertion. The report presents the results of the benchmark study and comments on the consistency and interpretation of the different solutions.

Chapter 1

INTRODUCTION

Background

The commercial recycling of plutonium as PuO_2/UO_2 mixed oxide (MOX) fuel is established in pressurised water reactors (PWR) in several countries, the main motivation being the consumption of plutonium arising from reprocessing. Although the same motivating factors apply to boiling water reactors (BWRs), they have lagged behind PWRs for various reasons, and MOX utilisation in BWRs is implemented only in a few reactors at present. One reason for this is that the nuclear design of BWR MOX assemblies (or bundles) is more complex than that of PWR assemblies, due the presence of the water gaps between BWR assemblies, the presence of U/Gd rods for reactivity control, water channels inside assemblies and the complex spatial distribution of steam void. Accordingly, in 1998 the OECD/NEA Working Party on the Physics of Plutonium Fuels and Innovative Systems (WPPR) conducted a physics code benchmark test for a BWR assembly. This volume reports on the benchmark results and conclusions that can be drawn from it.

In contrast to PWR fuel assemblies (FAs), BWR FAs are heterogeneous, both radially and, in modern designs, axially as well. For thermal-hydraulics reasons, the BWR fuel bundles are surrounded by channel boxes. The water gaps between assemblies have to provide sufficient space for the cruciform control blades. This also provides additional moderation from unvoided water (the water outside the assemblies is not in direct contact with the fuel rods and therefore is generally non-boiling). Furthermore, modern BWR assemblies incorporate non-boiling internal water channels that are introduced to improve neutron economy. A heterogeneous radial distribution of enrichment is necessary to compensate for the influence of the thermal flux peaks on local power peaking behaviour. Typical designs may have four or more different enrichments across the assembly for both UO_2 and UO_2/PuO_2 assemblies. The dimensions of the structures given in the benchmark are representative of modern BWR assemblies. Figure 1.1 shows a schematic layout for a typical modern UO_2 BWR assembly.

The heterogeneity of BWR assemblies also generally applies axially along the length of an assembly. Not only is it usual to have axial blankets of natural uranium in the top and/or bottom 15 cm, but there may also be an axial variation of the gadolinia loading, there may be fuel rods with more than one enrichment along their length and there may be (usually around 10) part length fuel rods, extending only over the bottom part of the assembly. (Typical axial dimensions are about 370 cm for the total active fuel length and about 200 cm for the part length fuel rods.) All these design features combine with the axial distribution of steam voidage (zero at the bottom of the active core, rising to up to 80% at the top) to create a very complex 3-dimensional calculational problem.

BWR assemblies have a stringent burnable poison requirement, since reactivity control is mainly provided by the Gd and not by the soluble boron system that PWRs largely rely upon. The

gadolinia loading in a BWR assembly is accordingly higher than in a PWR assembly and this is another source heterogeneity, particularly during the first cycle of irradiation.

The presence of MOX assemblies causes pronounced heterogeneity effects at the boundaries with UO_2 assemblies which are superimposed on the existing heterogeneity effects of water gaps. This occurs because MOX assemblies have a relatively low thermal flux (due to the higher thermal neutron absorption). At a UO_2/MOX boundary, thermal neutrons stream into the MOX region, and cause a thermal flux decrease from outside to inside. To counter the effects of this transition, it is normally necessary to have a non-uniform radial distribution of Pu concentrations, with a high concentration in the centre region, an intermediate concentration at the edge and a low concentration at the outside corners (see for example WPPR, Volume 1, "Issues and Perspectives", Figures 2.2-2.5, OECD/NEA 1995). The introduction of MOX rods within a BWR assembly has a similar effect on the within-assembly flux and power distribution, complicating the nuclear design. However, the wide water gaps between assemblies in a BWR tends to reduce the severity of UO_2/MOX interface effects, as the water gaps tend to isolate each assembly from its neighbours.

The neutron physics of MOX fuels in BWR is thus a great challenge for calculational models. Also, there is less practical experience of MOX from operating reactors than is the case for PWRs. Nevertheless, there is a lot of interest in various countries in recycling plutonium in BWRs. This was the reason for the proposal for the WPPR to carry out a BWR physics benchmark exercise. The purpose was to compare lattice code solutions for a single assembly to quantify the extent of any differences arising from the lattice codes and nuclear data libraries. This is a valuable first step towards validating a full nuclear design capability. This proposal was accepted by the WPPR and Siemens compiled and distributed a detailed specification against which participants were invited to submit solutions. These solutions were assembled into a database and discussed, in preliminary form, at the November 1998 meeting of the WPPR. Revised solutions were accepted up to 15 September 1999 and are presented in this volume. Over 20 solutions were submitted, and excellent response which underlines the widespread interest in BWR MOX physics.

Chapter 2 summarises the principal elements of the benchmark. Chapter 3 presents a summary of the main results. Chapter 4 attempts to draw out the main conclusions of the benchmark.

The detailed benchmark specification is provided in the Annex.

The Addendum lists the participants in the benchmark and also indicates the codes and methods used and the nuclear data source.

Figure 1.1. Typical layout of a UO_2 assembly for a BWR – ATRIUM-10 design

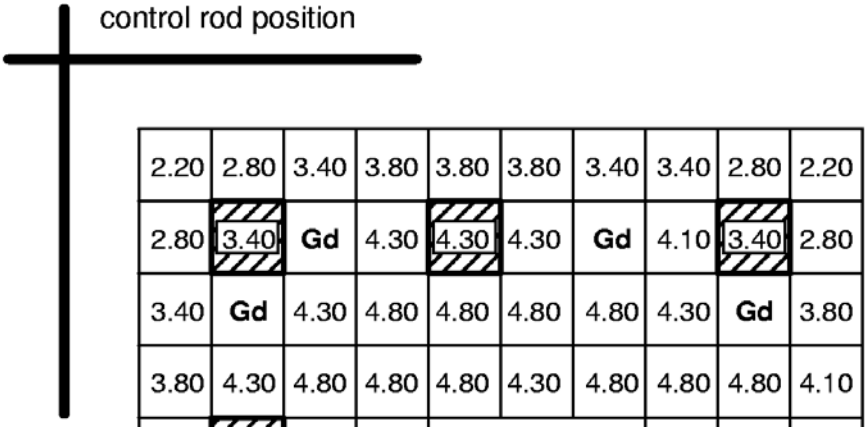

2.20	2.80	3.40	3.80	3.80	3.80	3.40	3.40	2.80	2.20
2.80	3.40	Gd	4.30	4.30	4.30	Gd	4.10	3.40	2.80
3.40	Gd	4.30	4.80	4.80	4.80	4.80	4.30	Gd	3.80
3.80	4.30	4.80	4.80	4.80	4.30	4.80	4.80	4.80	4.10
3.80	4.30	4.80	4.80	W			4.80	Gd	4.10
3.80	4.30	4.80	4.30				4.30	4.30	4.10
3.40	Gd	4.80	4.80				4.30	Gd	3.80
3.40	4.10	4.30	4.80	4.80	4.30	4.30	Gd	4.30	3.40
2.80	3.40	Gd	4.80	Gd	4.30	Gd	4.30	3.40	2.80
2.20	2.80	3.80	4.10	4.10	4.10	3.80	3.40	2.80	2.20

Rod Type (w/o U–235)	Number
2.20	4
2.80	8
3.40	12
3.80	10
4.10	8
4.30	19
4.80	19
Gd (4.30 w/o U–235 + 3.00 w/o Gd_2O_3)	11

Part Length Fuel Rod (PLFR)

W Water Channel

Average Lattice Enrichment: 3.987 w/o U–235

Chapter 2

SUMMARY OF THE BENCHMARK

2.1 Overview

This chapter describes the benchmark only in as much detail as is necessary to understand the results and the discussion presented in Chapters 3 and 4 respectively. The full specification, exactly as used by the various contributors, can be found in Addendum 1.

The benchmark is for a single BWR MOX fuel assembly lattice, which tests the lattice codes and the associated nuclear data libraries, in comparison to Monte Carlo codes. The basic burn-up depletion calculation tests:

1) The multi-group spectrum calculation for the different types of fuel cell within the assembly and within the associated non-fuel volumes (water gaps, water box, assembly shroud and water box shroud).

2) The spectral condensation to the few-group structure used in the whole-assembly diffusion or transport calculation, including the treatment of resonance self-shielding in ^{238}U and ^{240}Pu in particular.

3) The few-group diffusion or transport solution applied to the assembly as a whole to determine the flux distribution radially across the assembly.

4) The fuel depletion calculation, the evolution of fission products with irradiation and depletion of ^{155}Gd and ^{157}Gd within the burnable poison rods.

In addition to these fundamental calculations, the benchmark tests derived parameters, such as:

1) The variation of the infinite multiplication factor k_{inf} with burn-up.

2) The within-assembly radial power distribution.

3) The variation of k_{inf} and radial flux/power distribution with steam void fraction (range from 0 to 100% with intermediate points at 40 and 80%, thus providing void reactivity as a function of void).

The benchmark does not test the whole-core diffusion or transport theory codes and the parameters that derive from them, such as whole-core power distributions, reactivity coefficients etc. Also, since the assembly is formally surrounded by other identical assemblies the question of spectral interactions between MOX and UO_2 or between fresh and irradiated assemblies is not addressed. In the main benchmark, no attempt is made to model the control rods, which are assumed to be

withdrawn completely. However, a separate analysis of control rod effects was carried out and is described at the end of Chapter 3 and is specified Appendix A3 of Addendum 1.

2.2 Geometry and materials specification

Figure A.1 of Annex shows the geometrical layout of the problem. The material number densities are all given, to minimise the possibility of inconsistencies due to material input definitions. The geometry which is representative of modern 10x10 BWR fuel consists of four ATRIUM-10 (10-9Q) assemblies centred around a cruciform control blade position in a 2x2 control cell, which constitutes the basic repeating unit of the core. For reasons of symmetry, the actual calculations are done only for the *bottom right* assembly. The assembly modelled has zero neutron current boundary conditions, corresponding to the reflective symmetry of the physical layout. The water gaps for the ATRIUM-10 are symmetrical (6.75 mm half-width), so that there is no distinction between "wide" and "narrow" water gaps as there are in some BWR cores.

Figure A.2 of Annex shows further details of the assembly, specifically the distribution of plutonium and gadolinium pins radially and the geometry of the water box. The overall design is close to those already in use in modern BWRs, with an assumed rating of 25 W/gHM. The fissile content is set at a level such that the assembly is capable of reaching equilibrium discharge burn-ups of up to 50 MWd/kgHM, which is close to the expected average discharge burn-ups of the present BWR uranium reload assemblies. The isotopic quality of the plutonium feed corresponds to that obtained from UO_2 fuel with a high discharge burn-up in excess of 50 MWd/kgHM; earlier studies by the WPPR for PWRs have shown the nuclear design calculations to be more difficult for such plutonium (which has a fissile fraction <60%), so that this benchmark will present more onerous challenges for the lattice codes and nuclear data libraries.

The radial distribution of plutonium within the assembly reflects the need to counter power peaking wherever there is a concentration of water, which is the principal moderating material. Thus, there are lower concentrations of plutonium in the peripheral fuel rods and still lower concentrations in the corner rods (where there is thermal neutron transport from the water through two sides of the lattice cell). Similarly, there is a grading of plutonium concentrations around the water box, though less pronounced than that at the periphery of the assembly. The gadolinia rods (which are actually UO_2/Gd_2O_3 rods) are clustered around the water box, to take advantage of the fact that the extra moderation in the water box increases the effectiveness of Gd and hence the rate at which ^{155}Gd and ^{157}Gd are depleted by neutron captures. The concentration of gadolinia (Gd_2O_3), at 1.5 w/o, is considerably lower than would normally be used in a UO_2 assembly. This is a necessary adjustment that compensates for the relatively low thermal neutron flux in a MOX assembly compared with a UO_2 assembly: the depletion of ^{155}Gd and ^{157}Gd is dominated by the thermal flux and therefore is slowed down considerably, necessitating a lower initial concentration if these isotopes are to be depleted within the first irradiation cycle of one year.

The UO_2/Gd_2O_3 rods have a smeared oxide density of 9.867 g/cm^3, with a ^{235}U enrichment of 3.95 w/o in the UO_2 matrix. The MOX fuel rods have a density of 9.921 g/cm^3. The UO_2 matrix in the MOX rods is assumed to be composed of depleted uranium, with a ^{235}U enrichment of 0.20 w/o. The plutonium isotopic vector, in weight percentage is:

^{238}Pu	^{239}Pu	^{240}Pu	^{241}Pu	^{242}Pu	Pu_{fiss}
2.2	46.2	29.4	13.4	8.8	59.6

There are six distinct plutonium concentrations used in the assembly, details of the fissile and total plutonium content of which can be seen in Figure A.1 of Annex. The mean Pu_{fiss} concentration is 3.93 w/o, averaged over both MOX and U/Gd-rods. The fuel temperature is set at 627°C.

The densities of non-fuel materials are 6.55 g/cm^3 for the Zircaloy cladding and shroud, and water densities of 0.740 g/cm^3 (at 0% void, hot), 0.458 g/cm^3 (at 40% void, hot), 0.177 g/cm^3 (at 80% void, hot), 0.03676 g/cm^3 (at 100% void, hot) and 0.998 g/cm^3 (at 0% void, cold). At hot conditions, the water temperature is 286°C, while at cold conditions it is 20°C. The shroud (channel box) temperature is set at 327°C in hot conditions and 20°C in cold conditions. Some of the solutions presented will not be at precisely these temperatures if there is no facility to interpolate between library temperature tabulations, in which cases contributors were asked to use the nearest temperature tabulation available.

2.3 Benchmark calculations

There is a beginning of life (zero burn-up) calculation of k_{inf}, the radial fission rate distribution (normalised to 1.0) and the within-assembly radial fission rate peaking factor at the following conditions:

1) Hot, 0% void. This corresponds to an axial position near the bottom of the active core.

2) Hot, 40% void. This corresponds to an axial position near the centre of the active core and is approximately representative of the average behaviour of the whole core.

3) Hot, 80% and 100% void. This corresponds to axial positions near the top of the active core.

4) Cold, 0% void. This is representative of the whole core at cold (shutdown) conditions.

In addition, there is a burn-up calculation at hot, 40% void conditions, with equilibrium xenon. k_{inf} is calculated along with the total flux, the normalised fission rate distribution, within-assembly radial power peaking factors and selected heavy nuclide number densities at irradiations of 0, 5, 10, 30 and 50 MWd/kgHM. Optionally, participants were asked to report microscopic cross-section data, where these were readily available, which might assist with tracing any deviations between codes.

In order to take a closer look at aspects of Gd-burnout, more data such as k_{inf}, concentrations of ^{155}Gd and ^{157}Gd, absorption rates etc. were asked to be reported on a finer burn-up scale from 0 to 10 MWd/kgHM. This was optional in the specification. As a further option, detailed data for three different types of selected fuel pins (such as reaction rates, spectral information etc.) were requested.

Chapter 3

SOLUTIONS AND ANALYSIS

3.1 Participants

Seventeen participants submitted 25 solutions based on deterministic or Monte Carlo methods. The participants are BELGONUCLEAIRE (Belgium), CEA (France), ECN-NRG (The Netherlands), EGL (Switzerland), GRS (Germany), HITACHI (Japan), IKE University (Germany), JAERI (Japan), KAERI (Republic of Korea), Kurchatov Institute (Russian Federation), JLF&CMC (Mexico), ORNL (USA), PSI (Switzerland), FRAMATOME ANP GmbH[1] (Germany), TSI-TEPCO (Japan), TWE (USA), Texas A&M University (USA).

Of the 25 solutions submitted, there were contributions based on WIMS (3 solutions), HELIOS (4 solutions), CASMO-4 (4 solutions), MCNP-4B (3 solutions), CPM-3 (2 solutions), APOLLO-2, BOXER, KENOREST-98, MCU, MVP, RESMOD & RSYST, SCALE 4.4, TRIPOLI-4 and VMONT. The nuclear data libraries used were ENDF B-VI, V or other version (12 solutions), JEF 2 (10 solutions), JENDL 3.2 (3 solutions), MCU DAT, WIMS 97 and WIMS 98.

Codes	**Data**	**Participants**
APOLLO 2	JEF 2	CEA
BOXER	ENDF B	PSI
CASMO 4	ENDF B-VI	PSI
	JEF 2	PSI
	ENDF B/JEF	SIEMENS
	JEF 2	TSI-TEPCO
CPM 3	ENDF B-VI	TWE
	ENDF B-VI	JLF&CMC
SCALE 4.4	JEF 2.2	SIEMENS
HELIOS	ENDF B-VI	EGL
	ENDF B-VI	KAERI
	ENDF B-VI	JLF&CMC
	ENDF B-VI	ORNL

1. Referred to by its former name “SIEMENS Nuclear Power GmbH” in this paper.

Codes	Data	Participants
KENOREST	JEF 2.2	GRS
MCNP 4B	JEF/ENDF B	GRS
	JEF/ENDF B/JENDL	IKE
	ENDF B-V	JLF&CMC
MCU	MCU DAT	KI
MVP	JENDL 3.2	JAERI
RESMOD	JEF 2	IKE
TRIPOLI-4b	JEF 2	CEA
VMONT	JENDL 3.2&2	HITACHI
WIMS 7a	JEF 2	Texas A&M
WIMS 97b	WIMS 97	NRG
WIMS 98a	WIMS 98	BN

PSI submitted two solutions using the same code but two libraries: one based on ENDF/B-VI and one based on JEF 2.

The following comparisons were made between the results described above:

1) Detailed comparison of the fission rate distribution in the assembly (based on JAERI results) at the beginning of cycle (BOL) and during burn-up (24 and 18 solutions correspondingly, including JAERI);

2) Comparison of k_{inf} at BOL and during burn-up (24 and 19 solutions respectively);

3) Comparison of peaking factors at the BOL and during burn-up (24 and 19 solutions respectively);

4) Comparison of average neutron fluxes during burn-up (16 solutions);

5) Comparison of isotopic concentrations (based on average values) during burn-up (for ^{235}U, ^{238}U, ^{238}Pu, ^{239}Pu, ^{240}Pu, ^{241}Pu, ^{242}Pu, ^{241}Am, ^{243}Am, ^{244}Cm; 19 solutions);

6) Comparison of isotopic concentrations for ^{155}Gd and ^{157}Gd, averaged over all gadolinium pins, and of relative absorption reaction rates for all gadolinium isotopes (10 solutions for concentrations and 8 solutions for absorption rates);

7) Comparison of k_{inf} behaviour during burn-up in the "hot, 40% void" situation (8 solutions);

Other comparisons – for example, the comparison between k_{inf} obtained with the same code by different participants – will be presented below.

3.2 Code descriptions

3.2.1 BOXER

BOXER is the fuel assembly computer code of the code system ELCOS. It calculates the neutronic characteristics of two-dimensional LWR configurations. Its main modules concern:

- Cell calculations.
- Homogenisation and group collapsing.
- Group constants of homogeneous materials.
- Two-dimensional calculations.
- Burn-up.

Cell calculations

Sections of a configuration with a heterogeneous structure (fuel pins with their associated moderator, guide tubes, control rods, etc.) are called “cells”. Homogenised group constants over the volume of a cell define a “heterogeneous material”. The materials constituting a cell (for instance fuel, clad and moderator) are called “micro-materials”.

Cells with similar characteristics can be packed together in the same “cell type”. A cell calculation will not be done for each cell of the configuration, but rather for each cell type. The most important cell type of the configuration (with respect to the neutron spectrum) is called the “principal cell type”. It must be defined as the first cell type, and it is computed with white boundary conditions and its outgoing current can be used as the boundary condition (incoming current) for the other cell types and for the homogeneous materials.

A cell calculation can be done either in slab or in cylindrical geometry. It starts with a resonance calculation in 2 zones and about 8 000 lethargy points in the so called “resonance region”, between the energy limits E_i and E_s (in the present cross-section library, E_i = 1.3 eV and E_s = 907 eV), employing the collision probability method. The slowing down source is determined with the assumption that the scattering is isotropic in the centre of mass system. The pointwise flux in the resonance zone is then used as the weighting function for the condensation of the resonance cross-sections into energy groups. By this method all kinds of interactions between the resonance of a particular nuclide as well as of different nuclides are automatically taken into account. Above the resonance range (i.e. for energies greater than E_s) the cross-sections of the resonance nuclides are interpolated over the temperature and the dilution cross-section from the tables produced by ETOBOX, according to the equivalence theorem.

A one-dimensional flux calculation with transport theory in cylindrical or slab geometry and in fine group structure (presently 70 groups) follows. The fission source is assumed to be flat over all zones containing fissile nuclides. The scattering source in each zone can be flat or represented by a polynomial of the radius. In the epithermal range (above 1.3 eV) P_1 corrected isotropic scattering is used. In the thermal energy range the scattering anisotropy can be taken into account by the P_1 matrix (P_2-corrected). The first cell type (the “principal cell type”) is calculated with white boundary

conditions. The outgoing partial current at the boundary of the principal type is used as a fixed incoming current at the boundaries of the secondary types and the homogeneous materials.

During all these calculations the cell type treated is coupled to the neighbouring cells through Dancoff factors, which are calculated for a regular array of the same cells. If the cell array is not regular (as it is the case for BWR fuel assemblies), it is possible to modify the Dancoff factors through input. It is also possible to calculate the correct factors with a Monte Carlo procedure which can determine them in complicated geometries (this option is recommended especially in such configurations as BWR fuel assemblies).

Homogenisation and group collapsing

The macroscopic cross- sections in 70 groups are spatially averaged over the cells using flux-volume weighting. Then a zero-dimensional B_1 transport calculation is performed for the principal cell type using these homogenised cross-sections. In this calculation the buckling can either be given by input or the critical buckling can be searched for. The results of this calculation are the cell average fluxes in 70 groups (fundamental mode spectrum) and the multiplication factors k_{inf} and k_{eff} of the cell. During this step a "re-homogenisation" of the condensed cross-sections is done to preserve the reaction rates of the multi-zone transport calculation. After this, the 70 group cross-sections are collapsed to broad groups (in the present case, 16 groups). The absorption and fission cross-sections as well as the isotropic scattering matrix are flux weighted. The total cross-section and the anisotropic scattering matrix are weighted by the current spectrum. For the principal cell type, the currents are taken from the B_1 calculation; for the secondary types and the homogeneous materials they are approximated as:

$$J_g = D_g \text{ grad } (phi_g),$$

where the diffusion coefficient D_g is determined according to the Bell-Glasstone formula.

As an option, it is possible to obtain the kinetic parameters (fraction of delayed neutrons and prompt generation time) of the cell type through the calculation of the adjoint fluxes in the cell type.

Group constants of homogeneous materials

The homogeneous materials are those which, as opposed to the heterogeneous materials such as fuel rod cells, do not have a fine structure, e.g. water gaps, absorber plates, or reflectors. For the calculation of the weighting spectrum their normally complicated geometry is replaced by a slab whose thickness is chosen so that the mean chord length [4 times (volume/surface)] is preserved.

For homogeneous materials with resonances, e.g. steel, the pointwise spectrum is calculated using the same assumptions as in the cell calculation. The outgoing partial current from the principal type determined in the pointwise flux calculation is used as an incoming current at the boundaries. The resonance cross-sections are then condensed to groups by weighting with the pointwise flux. The 70 group fluxes in the slab are calculated by a one-dimensional transport method using the following assumptions:

- The outgoing partial currents from the principal cell type are used as fixed incoming currents on both faces of the slab.
- The incoming angular fluxes are isotropic.

- The scattering source is isotropic, the total and scattering cross-sections are P_1 transport corrected.
- The transport calculation is performed in a single mesh. The scattering source is represented by a polynomial of the space variable.

Two-dimensional calculations

The few group two-dimensional calculation in detailed X-Y geometry can be performed either by the diffusion module CODIFF or by the transport module QP1. In order to save computing time, CODIFF can also be used to supply a flux guess to QP1.

CODIFF computes the fluxes at the mesh centres by the finite difference method assuming a double linear flux variation in each direction. The QP1 program is based on the transmission probability method. Adjacent meshes are coupled by means of the continuity of the mesh surface current moments. The outgoing current moments are obtained by the solution of the integral transport equation using the following approximations:

- The hemisphere of the flight angles is divided into four quadrants. The surface current in each quadrant is represented by a linear function in space and a first order spherical harmonics expansion in the flight directions:

  J (*x*, theta, phi) = J_0 + J_(1 x) + J_[2 cos(theta) cos(phi)] + J_[3 cos(theta) sin(phi)]

  where *x* is the spatial variable and theta and phi are the polar and azimuthal angles, respectively.

- The scattering and fission source within the mesh is approximated by a linear function of the space variables.
- The scattering anisotropy is taken into account by the P_1 matrix.

In addition to the multiplication factor, two-dimensional flux and power distributions and reaction rates are also computed.

Burn-up

In this module, the evolution of nuclide densities as a function of the time is calculated. Burn-up calculations are possible for cells as well as for two-dimensional configurations.

The coupling between nuclides sensitive to the burn-up is established through 5 matrices. The nuclides are partitioned into 2 classes:

1) The density of most of the nuclides is described by a polynomial function of the time.

2) The density of the nuclides with a large destruction rate is calculated by an asymptotic formula.

During a time step, the microscopic cross-sections are normally assumed constant. For a few nuclides and reactions which are especially sensitive (absorption in ^{239}Pu and capture in ^{240}Pu) the variation of the cross-sections can be taken into account by an empirical formula.

The common assumptions are:

1) The total power in the configuration is kept constant during a time step.

2) Through an input parameter it is possible to mix two different criteria:

   - the shape of the flux distribution between the materials is kept constant;
   - the shape of the absorption distribution is kept constant.

At the end of the time step, new calculations are normally done and new one group cross-sections are produced. These new cross-sections are used for a recalculation of the last time step. The definitive densities are then mean values of the previous and the current calculations (predictor-corrector method). If the materials or the 2-D geometry are modified, the corrector step is not executed.

It is also possible to divide the time step into smaller steps. The code will do it automatically if the accuracy of the polynomials is poorer than a prescribed value.

References

[1] Paratte, J.M., K. Foskolos, P. Grimm, C. Maeder, "EIR Codesystem ELCOS zur stationaeren Berechnung von Leichtwasserreaktoren", Jahrestagung Kerntechnik'88, Luebeck-Travemuende, Bundesrepublik Deutschland, 17-19 May 1988.

[2] Paratte, J.M., K. Foskolos, P. Grimm, J.M. Hollard, "ELCOS: The PSI Code System for LWR Core Analysis. Part I: User's Manual for the Library Preparation Code ETOBOX", PSI Bericht Nr. 96-02, January 1996.

[3] Paratte, J.M., P. Grimm, J.M. Hollard, "ELCOS: The PSI Code System for LWR Core Analysis. Part II: User's Manual for the Fuel Assembly Code BOXER", PSI Report No. 96-08, February 1996.

3.2.2 CASMO-4

Description of method

CASMO-4 is a multi-group two-dimensional transport theory code for burn-up calculations on BWR and PWR assemblies. The standard L-library (based mainly on ENDFB-data) has been used. Alternatively, in some solutions the "JEF" – library based mainly on JEF2 data has been used. These libraries contain microscopic cross-sections in 70 energy groups. The commercially available versions of the code and library of the developer STUDSVIK OF AMERICA INC. have been used. For "industrial" applications STUDSVIK normally recommends usage of the L-library.

Basic data library version

Most of the data is based on ENDF B-IV. For some isotopes (ex. ^{162}Er or ^{170}Tm) data from JEF 1 and JEF 2.1 were used. The shielded resonance data for Pu and Gd-isotopes were taken from JEF libraries.

Data processing code/method used to obtain the cross-section data used NJOY (different versions).

Spectral calculations and data reduction methods used CASMO-4 standard calculation procedures.

Reference

Knott, D., B.H. Forssen, M. Edenius, "CASMO-4, A Fuel Assembly Burnup Program Methodology", Studsvik/SOA-95/2.

3.2.3 CPM3

CPM-3 is an advanced lattice physics burn-up code that performs neutron flux, gamma flux, eigenvalue and isotopic depletion calculations for light water reactor nuclear fuel assemblies. CPM-3 couples deterministic nuclear transport theory methods with an arbitrary geometry modelling capability to provide a highly flexible and accurate tool for analysing fuel assembly lattices of regular and highly irregular geometry design. Two multi-group, two-dimensional transport theory methods are supported: the method of collision probabilities and the method of characteristics. Other important features of CPM-3 include an arbitrary geometry model for determining Dancoff correction factors, a spatial self-shielding method for the explicit treatment of multi-annulus and sectored resonance absorber cells, and an accurate isotopic depletion capability for time-dependent fuel exposure calculations. The CPM-3 code package includes a nuclear data file derived from ENDF/B-VI that contains cross-section data and nuclear parameters in 97 energy groups for over 300 nuclides. CPM-3 is designed for production applications by supporting engineering-style user input and an extensive set of user-selectable edit options. Data may be edited in several forms to accommodate linkage to downstream reactor analysis codes. A restart capability is provided to restart depletion runs or to perform branch reactivity calculations. The CPM-3 code is written in the FORTRAN 90 programming language standard for ease of portability between computing platforms.

97 Group ENDF B-VI cross-section library

Multi-group cross-sections were processed from ENDF B-VI data using the NJOY code system. The following NJOY modules were used to produce the multi-group cross-section data for the CPM-3 nuclear data file:

- RECONR Reconstructs point-wise cross-section data from evaluated physics data in ENDF B files;
- BROADR Performs numerical Doppler broadening for point-wise data generated by RECONR in resonance range;
- UNRESR Processes point-wise data for the unresolved resonance range;

- THERMR Processes thermal scattering laws for free-gas atoms, and for incoherent and coherent scattering from bound molecules; and
- GROUPR Integrates point-wise data with specified weighting function to obtain multi-group cross-sections and scatter matrices.

NJOY weight functions used to average multi-group data

The GROUPR module of NJOY offers several options to represent the weight function used to average multi-group data. If a nuclide is not treated as a resonance material, then only the infinitely dilute cross-sections, and possibly the scatter matrix, is included in the CPM-3 nuclear data file. For these nuclides, the infinitely dilute cross-section is computed in GROUPR using a smooth function obtained from a generic LWR spectrum.

In the case of resonance materials, two different approximations have been used in GROUPR for the weight function. The first approach, which is used for the most significant resonance materials in the CPM-3 nuclear data file, utilises the "computed flux" option of GROUPR for the energy range below 600 eV and the LWR smooth function for weighting cross-sections and shielding factors above this energy. This type of weighting is used to process cross-sections and shielding factors for the uranium and plutonium isotopes.

The second approach used for resonance materials other than those listed above, uses NJOY LWR smooth function over the entire resonance range. These materials consist mainly of fission products and burnable absorber nuclides.

One-dimensional multi-group cross-sections

Over 250 nuclides in the data file contain infinitely dilute cross-sections. The 1-D cross-sections consist of multi-group absorption and, as appropriate, nu-fission cross-sections in the 97 group energy group structure. The absorption cross-section has been adjusted for some nuclides to account for the (n, 2n) reaction. The thermal group structure is represented by 35 thermal energy groups which includes several groups around the 0.3 and 1.0 eV resonances of ^{239}Pu and ^{240}Pu, respectively, to improve the accuracy of the reaction rate computation for these nuclides. The fast group structure is represented by 62 fast groups which provides the capability to represent leakage effects more accurately.

Scattering matrices

In addition to the 1-D cross-sections, the CPM-3 nuclear data file also includes 2-D cross-sections that represent scatter matrices for several nuclides at multiple temperatures. Most of the nuclides in the nuclear data file have transport-corrected, P_0 scatter matrix data. The following nuclides in the data file have P_1 matrices: H (in water), H (in ZrH), Zr (in ZrH), O and C.

In the thermal energy range, the thermal motion of molecules may cause low energy neutrons to gain energy in a scattering reaction. The CPM-3 scatter matrices include up-scattering data for the energy range below 3.928 eV. Thermal scatter cross-sections for most nuclides were processed with the "free-gas" model for molecular motion, which neglects chemical binding effects. However, 2-D thermal cross-sections for the following three nuclides were processed from S(f) data given in

ENDF/B, which describes incoherent, inelastic scatter from bound molecules: H (in water), H (in ZrH), and Zr (in ZrH).

Resonance Data

The resonance methodology implemented in CPM-3 is based on a variation of the widely used "shielding factor method". In this approach the nuclear data file contains pre-calculated, infinitely-dilute cross-sections and shielding factors, tabulated as a function of "background cross-section" that indicates the degree of resonance self-shielding.

Resonance data on the CPM-3 nuclear data file consists of infinitely dilute cross-sections and shielding factors, as function of background cross-section and temperature, for absorption and nu-fission reactions of all resonance materials. Over 70 nuclides are treated for resonance materials. Shielding factors are included in the data file for the energy range between 0.08 eV and 24.79 keV, tabulated over the range of background cross-sections and temperatures expected for each nuclide. In addition to the actinide materials, shielding factor data is provided for several important fission products, burnable absorbers, and control rod materials. Some of the important isotopes include gadolinia, hafnium, erbium, silver and others.

The CPM-3 nuclear data file provides CPM-3 the capability to shield resolved resonances in the thermal and epithermal energy ranges. Shielding factors for thermal energy groups are important to accurately treat Doppler broadening of low energy resonances in nuclides such as ^{230}Pu and ^{240}Pu. CPM-3 also performs self-shielding corrections for the unresolved resonance range of important nuclides such as ^{238}U, ^{235}U, ^{239}Pu, ^{240}Pu and several others.

Potential cross-sections and IR parameters

The CPM-3 resonance methodology utilises the "intermediate resonance (IR) approximation" to determine the value of the background cross-section for self-shielding calculations. This method requires potential cross-sections and IR parameters to treat nuclides that are "intermediate" between the limiting cases of narrow resonance and wide resonance scatterers. The CPM-3 nuclear data file contains values for the product of the IR parameters, and potential cross-sections of essentially all nuclides that contribute to the background cross-section in resonance calculations. These values are a function of temperature and energy.

Ninety-seven energy groups were used for both the flux and burn-up calculation.

The problem was modelled using the collision probability method to solve the transport equation. The lattice was modelled in a heterogeneous geometry, where the fuel rods, clad, water box and channel are modelled explicitly. The UO_2 and MOX fuel rods were modelled as a single rod, and the gadolinia rods were modelled with 8 radial rings. The flux and burn-up calculations were performed in the heterogeneous geometry, in the full 97 energy groups. A weighted spectrum is calculated based on the concentrations of the fission spectrum nuclides. Fission spectra is provided for ^{232}Th, ^{233}Pa, ^{233}U, ^{234}U, ^{235}U, ^{236}U, ^{238}U, ^{237}Np, ^{238}Pu, ^{239}Pu, ^{240}Pu, ^{241}Pu, ^{242}Pu, ^{241}Am, ^{242m}Am, ^{243}Am, ^{242}Cm, and ^{244}Cm.

3.2.4 HELIOS

HELIOS is a two-dimensional neutron and gamma transport code for fuel assembly calculations developed by Studsvik Scandpower, Inc. The particle transport is performed using the current coupling collision probability (CCCP) method in which the space elements are globally coupled using interface currents and local transport with the space element is performed using collision probabilities. The resonance treatment is based on the subgroup method and allows for full interaction of the resonance isotopes.

The HELIOS nuclear data libraries are based on ENDF/B-VI and are available in several group structures ranging from 34-190 neutron energy groups. Two different sets of libraries are available, the production libraries in which the ^{238}U absorption cross-section has been adjusted (reduced) and unadjusted libraries. Depletion is performed using a predictor/corrector method with 29 heavy isotopes and 114 fission products.

Benchmark results computed with HELIOS were submitted by four different organizations: EGL (Switzerland), KAERI (Republic of Korea), JLF&CMC (Mexico), and ORNL (USA). Specific HELIOS code version numbers and calculational details for each of these submissions are briefly discussed below.

EGL (Switzerland)

The calculations have been performed with HELIOS 1.5 using the 35 neutron/18 gamma groups library. The U-Pu pins were radially subdivided in two regions, and the U-Gd pins in five, without any azimuthal subdivision. The resonance option 9 was chosen in order to allow for an individual treatment for each resonance isotope. The burn-up path was segmented in steps of 0.25 GWd/t from 0 up to 10 GWd/t, and then regularly increased to 5 GWd/t up to 50 GWd/t.

KAERI (Republic of Korea)

Calculations were performed with HELIOS version 1.5 using the 35 group adjusted library. In the geometric modelling the MOX fuel pins and the U-Gd pins were subdivided into five radial depletion regions. All calculations were performed with the HELIOS “RES” option set to 9, which each isotope is individually categorised. The interface current coupling order was set to k=4. Depletion calculations were modelled using 0.15 GWd/t steps from 0 to 0.15 GWd/t, 0.35 GWd/t steps from 0.15 to 0.5 GWd/t, 0.5 GWd/t step from 0.5 to 10 GWd/t and 1 GWd/t steps from 10 to 50 GWd/t. The standard HELIOS option of using the critical spectrum for performing depletion was used.

JLF&CMC (Mexico)

Calculations were performed with HELIOS version 1.5 using the 35 group adjusted library. In the geometric modeling the MOX fuel pins were subdivided into two radial depletion regions and the U-Gd pins were subdivided in to five radial and eight azimuthal depletion regions. All calculations were performed with the HELIOS “RES” option set to 4, which results in three resonance categories: ^{238}U, other heavy metals, and non-heavy metals. The interface current coupling order was set to k=4. Depletion calculations were modeled using 0.25 GWd/t steps from 0 to 10 GWd/t, 1 GWd/t steps from 10 to 12 GWd/t, 3 GWd/t step from 12 to 15 GWd/t and 5 GWd/t steps from 15 to 50 GWd/t. The standard HELIOS option of using the critical spectrum for performing depletion was used.

ORNL (USA)

Calculations were performed with HELIOS version 1.4 using the 190 group adjusted library. In the geometric modeling the MOX fuel pins were subdivided into two radial depletion regions and the U-Gd pins were subdivided in to five radial and eight azimuthal depletion regions. All calculations were performed with the HELIOS "RES" option set to 4, which results in three resonance categories: ^{238}U, other heavy metals, and non-heavy metals. Depletion calculations were modeled using 0.5 GWd/t steps from 0 to 10 GWd/t and 2 GWd/t steps from 10 to 50 GWd/t. The standard HELIOS option of using the critical spectrum for performing depletion was disabled.

References

[1] Casal, J.J. *et. al*, "HELIOS: Geometric Capabilities of a New Fuel-Assembly Program", *Proc. Int. Topl. Mtg. Advances in Mathematics, Computations, and Reactor Physics,* Pittsburgh, Pennsylvania, April 28-May 2, 1991, Vol. 2, p. 10.2.1-1.

[2] Villarino, E.A., R.J.J. Stamm'ler, A.A. Ferri, J.J. Casal, "HELIOS: Angularly Dependent Collision Probabilities", *Nuc. Sci. Eng.*, 112, 16-31 (1992).

[3] "FMS: The Scandpower Fuel Management System, HELIOS Documentation", Scandpower A/S (1995).

3.2.5 KENOREST

Computer codes

KENOREST-98, a directly coupled system of KENO-5a /KEN83/ and OREST-98 (/ORS86/, /ORS96/).

Basic data library version

JEF 2.2 /IKE292/ for <KORLIBV2> (KENO) and for <99BWRMOX> (OREST).

Data processing code used for XS

- Data condensing from 292 groups /IKE292/ to 83 groups <KORLIBV2> (for KENO) for the infinite dilution state by the RESMOD code.
- Generation of HAMMER-98 /SUI67/ libraries <99BWRMOX> (for OREST) by the standard LITHE and HELP modules /SUI67/ inside GRS LITHELP code system.

Spectral calculations

- KENO-5a (standard 3-d fuel assembly calculations).
- HAMMER-98 (/SUI67,/ORS96/) (standard 1-d fuel rod calculations).

Number of groups

83-group structure used both in KENO and OREST:

- 29 thermal groups;
- 54 epithermal/fast groups.

Assumptions made for some XS: (n, 2n) XS are directly handled by ORIGEN /BEL67/.

Self-shielding and mutual resonance shielding

- Nordheim resonance self-shielding treatment for ^{235}U, ^{236}U, ^{238}U, ^{237}Np, ^{238}Pu, ^{239}Pu, ^{240}Pu, ^{241}Pu, ^{242}Pu, ^{241}Am, ^{243}Am, ^{155}Gd, ^{156}Gd, ^{157}Gd, ^{158}Gd, ^{160}Gd.
- Mutual resonance shielding inside 29 thermal groups up to 0,625 eV for resolved $^{237}Np/^{239}Pu/^{241}Pu$ /^{241}Am thermal resonances.

Cell lattice calculation methods used

- Boltzmann transport equation is used inside KENO, integral Boltzmann transport equation is used in HAMMER.
- The KENOREST calculation starts with an <infinite dilution> step, followed by resonance shielded OREST single rod calculations. The OREST cross-sections are directly fed back to KENO in 83 groups. This start-up iteration procedure is repeated three times before burn-up.
- The KENOREST burn-up loops, defined by the user, are repeated each 1 GWd/tHM up to 15 GWd/tHM, and each 2.5 GWd/tHM up to 50 GWd/tHM.
- Burn-up calculations are done by ORIGEN.

Supplementary information

- No fuel rod radial subdivision is used, but flat nuclide distribution is assumed inside all pellets during burnout simulation. For Gd-rods the KENOREST acceleration burnout function <gd-set98> is applied.
- Nine water-filled tubes preserving the original area of the water channel are used.
- 1 000 000 neutron histories for each KENO run.
- k_{inf} scatter +/- 0.06% standard deviation.
- Fission rate distribution scatter +/- 0.7%.
- Full ORIGEN isotope inventory calculations (144 actinides and over 800 fission products) are done. Full Gd build-up and depletion chains are used.

3.2.6 MCNP-4B

Origin of cross-section data

ENDF B-V – DLC-105 MCNPDAT Version 4.

Number of energy groups used in the different phases

Continuous energy.

References

J.F. Briesmester, Editor, "MCNP – A General Monte Carlo Code for N-Particle Transport Code, Version 4B", LA-12625-M, Los Alamos National Laboratory, Los Alamos, New Mexico, (March 1997).

3.2.7 MCU ("Kurchatov Institute")

The calculations reported were performed using the MCU-REA Monte Carlo code and the DLC/MCUDAT-2.1 library. MCU-REA code is the advanced version of the MCU-RFFI/A code, certified by Russian safety authorities (Gosatomnadzor GAN, Passport N61 17.10.96).

MCU-REA is a Monte Carlo code for solving the neutron transport and burn-up problems.

MCU-REA is a pointwise continuous energy code permitting one to model systems with any geometry. To describe the unresolved resonance cross-section the subgroup method (analogous to probability table method) is used. It is possible to use a detailed description of cross-sections in the resolved resonance region. For the most important isotopes an "infinite" number of energy points is used to describe the resonance curve. In this case cross-sections are calculated during the Monte Carlo run at every energy point on the basis of the resonance parameter library. It permits one to perform the calculations without preliminary tabulation of cross-sections and allows the user to estimate temperature effects independent of the cross-section library state. Special fast algorithms to calculate resonance cross-sections are used. For the thermal energy region, the Monte Carlo game is played using the $S(\alpha,\beta)$ scattering laws and the coherent elastic cross-sections or free gas model. One may solve the problems taking into account both the prompt neutron and the delayed neutron fission spectra.

The MCU-REA code and MCUDAT library were verified and validated by using the results of more than 400 criticals. However, nuclear data for some important isotopes could not be verified using results of physical benchmarks. This applies principally to data for fission products and other isotopes present at low concentrations in the criticals investigated. It is especially important to understand the reasons for significant discrepancies concerning the plutonium critical calculations published by various authors.

Cross-section representation

- Thermal energy region: Continuous energy S(α, β) representation;
- Resolved resonance region: Infinite number of points;
- Unresolved resonance region: Subgroup method;
- Fast region: 100 keV – 10.5 MeV: Step representation;
- Assumptions: Step function representation for inelastic scattering and (n, 2n) reaction.

3.2.8 MVP-BURN

Code descriptions

MVP-BURN [1, 2] is a coupling code of a continuous energy Monte Carlo code MVP [3, 4] and a burn-up calculation module BURN [2] which solves a depletion equation analytically based on the modified Bateman's method with microscopic capture, fission and (n, 2n) reaction rates obtained by MVP. The MVP-BURN is well validated by several burn-up benchmark calculations and analyses of post irradiation experiments [1]. Features of this code are as follows:

- Very fast computation is realised on vector and / or paralleled computers [5].
- MVP library for arbitrary temperatures can be internally generated [5].
- Burn-up calculation can be applied to the system including a great many coated fuel particles (ex. HTTR: high-temperature engineering test reactor in JAERI) with the statistical geometry model [6].
- Geometry and material composition can be changed during burn-up (ex. motion of control rod, boron concentration, void fraction, fuel temperature distribution, etc.).
- Branch-off calculation is supported to estimate instantaneous reactivity changes at any burn-up time-step point.
- Predictor-corrector method can be applied to any burn-up duration for accurate and efficient calculation for the system including burnable poison.
- Burn-up chain model can be easily changed according to reactor types and computer resources.

Calculation conditions for the BWR MOX benchmark

1) Basic data library version:

   JENDL-3.2 for all nuclides (energy range from 1.0E-5 eV to 20 MeV).

2) Data processing code:

   LICEM; Neutron Cross Section Library Production Code System [7] for Continuous Energy Monte Carlo Code MVP. The LICEM system includes the following sub-codes;

   LINEAR, RECENT, SIGMA1, ACER-J, U3R-J, THERM-J, etc.

3) Depletion calculation:

- number of depletion zones – 142;

  each MOX fuel is not divided, while each UO_2-Gd_2O_3 fuel is divided into 32 depletion zones (8 annuluses * 4 segments).

- number of depletion nuclides (chain model);

  20 heavy nuclides from ^{234}U to ^{245}Cm and 35 fission products including 4 pseudo FPs. Five nuclides (^{234}U, ^{113}Cd, ^{143}Pr, ^{143}Nd, ^{145}Nd) are added in the chain model appeared in [1].

  Point-wise cross-sections are used for all nuclides, however, cross-sections of the pseudo fission products are generated from 107-group constants (JENDL-3.2) of the SRAC95 code [1].

- time step width for MVP-BURN calculation;

  0.5 GWd/t with the predictor-corrector(PC) method from 0 GWd/t to 10 GWd/t,

  1.0 GWd/t with the PC-method from 10 GWd/t to 20 GWd/t,

  1.0 GWd/t without the PC-method from 20 GWd/t to 50 GWd/t.

  Note: In the PC-method, MVP calculations are done twice in each time step (beginning of step and end of step) to get averaged microscopic reaction rates. Each time step is furthermore divided into several sub-steps for solution of depletion equation.

4) Neutron histories in each MVP calculation:

- for BOL calculations:

  1 000 000 = 100 cycles * 10,000 particles/cycle, (not including initially skipped 10 cycles).

- for a burn-up calculation:

  400 000 = 40 cycles * 1,0000 particles/cycle, (not including initially skipped 10 cycles).

References

[1] Okumura, K., T. Mori, M. Nakagawa, K. Kaneko, “Validation of A Continuous Energy Monte Carlo Burn-up Code MVP-BURN and Its Application to Analysis of Post Irradiation Experiment”, J. Nucl. Sci. Technol., Vol. 37, No. 2, pp. 128, (2000).

[2] Okumura, K., M. Nakagawa, K. Kaneko, “Development of Burn-up Calculation Code System MVP-BURN Based on Continuous Energy Monte Carlo Method and Its Validation”, Proc. of Joint Int. Conf. on Mathematical Methods and Supercomputing for Nuclear Applications (M&C and SNA 97), Vol. 1, pp. 495, Saratoga Springs, NY (1997).

[3] Mori, T., M. Nakagawa, M. Sasaki, “Vectorization of Continuous Energy Monte Carlo Method for Neutron Transport Calculation”, J. Nucl. Sci. Technol., Vol. 29, No. 4, pp. 325, (1992).

[4] Nakagawa, M. and T. Mori, "Whole Core Calculation of Power Reactors by Use of Monte Carlo Method", J. Nucl. Sci. Technol., Vol. 30, No. 7, pp. 692, (1993).

[5] Mori, T., K. Okumura, Y. Nagaya, M. Nakagawa, "Application of Continuous Energy Monte Carlo Code MVP to Burn-up Calculation and Whole Core Calculations Using Cross-Sections at Arbitrary Temperatures", Proc. of Int. Conf. Mathematics and Computation, and Environmental Analysis in Nuclear Applications (M&C'99), Vol. 2, pp. 987, Madrid, Spain (1999).

[6] Mori, T., K. Okumura, Y. Nagaya, H. Ando, "Monte Carlo Analysis of HTTR with the MVP Statistical Geometry Model", Trans. Am. Nucl. Soc., Vol. 83, pp. 283 (2000).

[7] Mori, T., M. Nakagawa, K. Kaneko, "Neutron-Cross Section Library Production Code System for Continuous Energy Monte Carlo Code MVP LICEM", JAERI-Data/Code 96-018 (1996) [in Japanese].

3.2.9 VMONT

Origin of cross-section data

- Actinides: JENDL-3.2.
- Other nuclides: JENDL-2.

Spectral calculations and data reduction methods used

1) Monte Carlo neutron transport method.

- Resonance shielding: Self-shielding effects are considered for principal actinides and fission products in whole energy range by self-shielding factors.
- Actinides: ^{228}Th, ^{232}Th, ^{231}Pa, ^{233}Pa, ^{232}U, ^{233}U, ^{234}U, ^{235}U, ^{236}U, ^{238}U, ^{237}Np, ^{239}Np, ^{236}Pu, ^{238}Pu, ^{239}Pu, ^{240}Pu, ^{241}Pu, ^{242}Pu, ^{241}Am, ^{242m}Am, ^{242f}Am, ^{243}Am, ^{242}Cm, ^{243}Cm, ^{244}Cm, ^{245}Cm;
- FPs: ^{83}Kr, ^{93}Zr, ^{95}Mo, ^{97}Mo, ^{98}Mo, ^{99}Tc, ^{100}Ru, ^{101}Ru, ^{103}Rh, ^{105}Rh, ^{105}Pd, ^{107}Pd, ^{108}Pd, ^{109}Ag, ^{113}Cd, ^{129}I, ^{131}Xe, ^{133}Xe, ^{135}Xe, ^{133}Cs, ^{135}Cs, ^{139}La, ^{141}Pr, ^{143}Pr, ^{143}Nd, ^{144}Nd, ^{145}Nd, ^{148}Nd, ^{147}Pm, ^{148m}Pm, ^{148f}Pm, ^{149}Pm, ^{147}Sm, ^{148}Sm, ^{149}Sm, ^{150}Sm, ^{151}Sm, ^{152}Sm, ^{154}Sm, ^{153}Eu, ^{154}Eu, ^{155}Eu, ^{156}Eu, ^{154}Gd, ^{155}Gd, ^{156}Gd, ^{157}Gd, ^{158}Gd.
- Mutual shielding: not considered.
- Fission spectra: mix from all fissile nuclides by production rates weighting.
- (n, 2n) reaction treatment:
  1) (n, 2n) reaction is treated exactly in a Monte Carlo neutron,
  2) transport calculation.
- Number of energy groups: 190.

Cell calculation

- Full assembly calculation without any homogenisations.
- Type of calculation: Heterogeneous.
- Theory used: Transport.
- Method used: Monte Carlo.

Other assumptions and characteristics

- The fuel pellet region of a gadolinia-containing fuel rod is divided into eight regions.
- The fuel pellet region of a fuel rod other than gadolinia-containing fuel rods is treated as one region.

References

[1] Morimoto, Y., *et al.*, "Neutronic Analysis Code for Fuel Assembly Using a Vectorized Monte Carlo Method", Nucl. Sci. Eng., 103, 351 (1989).

[2] Maruyama, H., *et al*., "Development and Performance Evaluation of a Vectorized Monte Carlo Method with Pseudoscattering", Proceedings of the First International Conference on Supercomputing in Nuclear Applications, 156 (1990).

[3] Ishii, K. and H. Maruyama, "Fuel Assembly Analysis Code Based on a Monte Carlo Method with Multi-assembly Analysis Model", Proceedings of the International Conference on the Physics of Reactors PHYSOR96, A-415 (1996).

3.2.10 WIMS

Solution Method

The multi-group neutron transport equation was solved using a characteristics method (WCACTUS) in a x-y geometry integrating along 5 azimuthal angles.

Basic Data Library

JEF 2.2 nuclear data library.

Reference

"The ANSWERS Software Package WIMS. User Guide", ANSWERS/WIMS (95)4. AEA Technology, December 1996.

3.3 Solutions

The parameters for which comparisons of the various solutions are presented are:

- reactivity at BOL (without irradiation, same specification for every one) for hot and cold conditions, with various void fractions and reactivity balance during irradiation,
- isotopic concentrations for heavy nuclides and gadolinium nuclides.

In order to facilitate comparison, the average values of all the solutions are given, together with the range of values. In addition, the average and the range of values are also calculated with the outlying solutions excluded. This avoids the analysis being distorted by single solutions which are particularly discrepant.

Reactivity

Reactivity at BOL

The table shows:

1) The true average n° 1 of all k_{inf}, including the extreme values.
2) The difference between the highest value and the true average 1.
3) The difference between the lowest value and the true average 1.
4) Average of the discrepancies between values and the true average 1.
5) The average n° 2 of all k_{inf}, with the extreme values excluded.
6) Average of the discrepancies between values and the average 2.
7) The average for solutions based on the JEF 2 nuclear data library.
8) The average for solutions based on the ENDF B-VI nuclear data library.

k_{inf} (BOL)	**hot 0% void**	**hot 40% void**	**hot 80% void**	**cold 0% void**
Average =>	1.16459	1.13575	1.10559	1.17681
Discrepancy max. =>	0.00700	0.00637	0.01401	0.00889
Discrepancy min. =>	-0.00804	-0.00671	-0.01779	-0.00751
Average discrepancies (min./max.) =>	0.00365	0.00367	0.00416	0.00325
Average without extreme values =>	1.16464	1.13577	1.10576	1.17675
Average discrepancies (min./max.) =>	0.00329	0.00341	0.00309	0.00280
JEF 2 =>	1.17020	1.13966	1.10651	1.18052
ENDF B-VI =>	1.16083	1.13230	1.10325	1.17291

The following table shows a selection of the data grouped according to solution method. Results calculated by different groups with the same code tend to cluster closely together, as might be expected. There appears to be a difference of around 1% with CASMO, depending on whether the ENDF B-VI or JEF-2.2 nuclear data libraries are used (see PSI solutions with CASMO). There

appears to be no significant difference between the averages of the Monte Carlo solutions and the deterministic solutions.

WIMS	**hot 0% void**	**hot 40% void**	**hot 80% void**	**cold 0% void**
BELGONUCLEAIRE (Belgium)	1.162330	1.13711	1.117240	1.17639
ECN-NRG (The Netherlands)	1.165100	1.13980	1.119600	1.18480
HELIOS	**hot 0% void**	**hot 40% void**	**hot 80% void**	**cold 0% void**
EGL (Switzerland)	1.157670	1.12904	1.102140	1.17392
KAERI (Republic of Korea)	1.156544	1.12918	1.105181	1.17176
JLF&CMC (Mexico)	1.159870	1.13063	1.102370	1.17580
ORNL (USA)	1.160000	1.13120	1.103800	1.17520
CASMO 4	**hot 0% void**	**hot 40% void**	**hot 80% void**	**cold 0% void**
PSI (Switzerland), ENDF B-VI	1.160830	1.13230	1.103250	1.17291
PSI (Switzerland), JEF-2.2	1.170200	1.13966	1.106510	1.18052
TSI (Japan) JEF-2.2	1.170930	1.14021	1.107050	1.18154
SIEMENS (Germany)	1.160840	1.13227	1.103360	1.17347
MCNP	**hot 0% void**	**hot 40% void**	**hot 80% void**	**cold 0% void**
GRS (Germany)	1.167300	1.13840	1.107100	1.17580
IKE University (Germany)	1.170400	1.14130	1.109900	1.17770
JLF&CMC (Mexico)	1.171590	1.14212	1.109700	1.17317
Other MC	**hot 0% void**	**hot 40% void**	**hot 80% void**	**cold 0% void**
CEA (France)	1.165530	1.13595	1.107020	1.17518
GRS (Germany)/KENOREST-98	1.169110	1.13734	1.100780	1.17920
HITACHI (Japan)	1.166200	1.13760	1.106000	1.17770
JAERI (Japan)	1.165900	1.13830	1.104900	1.17400
“Kurchatov Institute” (Russian Fed.)	1.156900	1.12940	1.101600	1.16930
SIEMENS (Germany)/KENO-5	1.168400	1.13270	1.087800	1.18570

Mean values w/o extreme solutions	**1.1646**	**1.1358**	**1.1058**	**1.1768**
Deterministic codes	**1.1627**	**1.1345**	**1.1064**	**1.1758**
Monte Carlo codes	**1.1668**	**1.1370**	**1.1039**	**1.1764**

With the extreme solutions excluded, the various solutions for “hot 0% void” and “hot 40% void” are consistent to within better than ±1% on k_{inf}. The extreme positive data points are only just outside the other data and have no significant impact on the average. Excluding the extreme values, the data are fairly evenly distributed about the mean.

With the extreme solutions excluded, the various solutions for "hot 80% void" are spread over rather more than ±1%. Excluding the extreme solutions, there are three data points approaching or exceeding ±1%, indicating that some of the codes have difficulty coping with the high voidage and hard spectrum (which will increase the relative importance of resonance effects). Interestingly, the remaining data points are clustered closer together, so that the average discrepancy is slightly reduced relative to the 0% and 40% voidage cases.

The situation is similar for the "cold 0% void" case, where the range of values exceeds ±1%. As with the 80% void case, there is evidence of a larger spread in the outlying solutions which is countered by a smaller spread amongst the remaining solutions, giving an average spread which is smaller than the hot 0% and hot 40% void cases. In this case the spectrum is softer and resonance effects are weakened and the behaviour seen suggests that some of the codes may have difficulty with their treatment of the resonances in this condition.

The figures below plot all the data points for the four different conditions relative to the average calculated, excluding the extreme values.

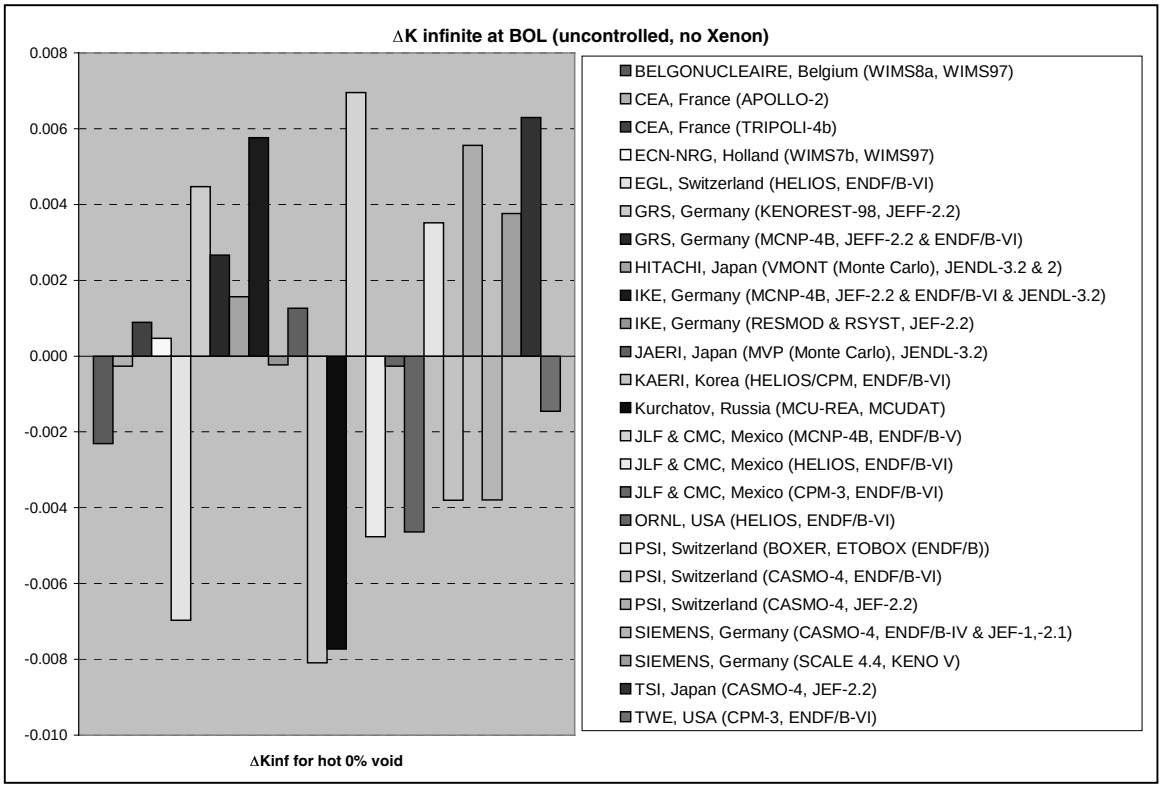

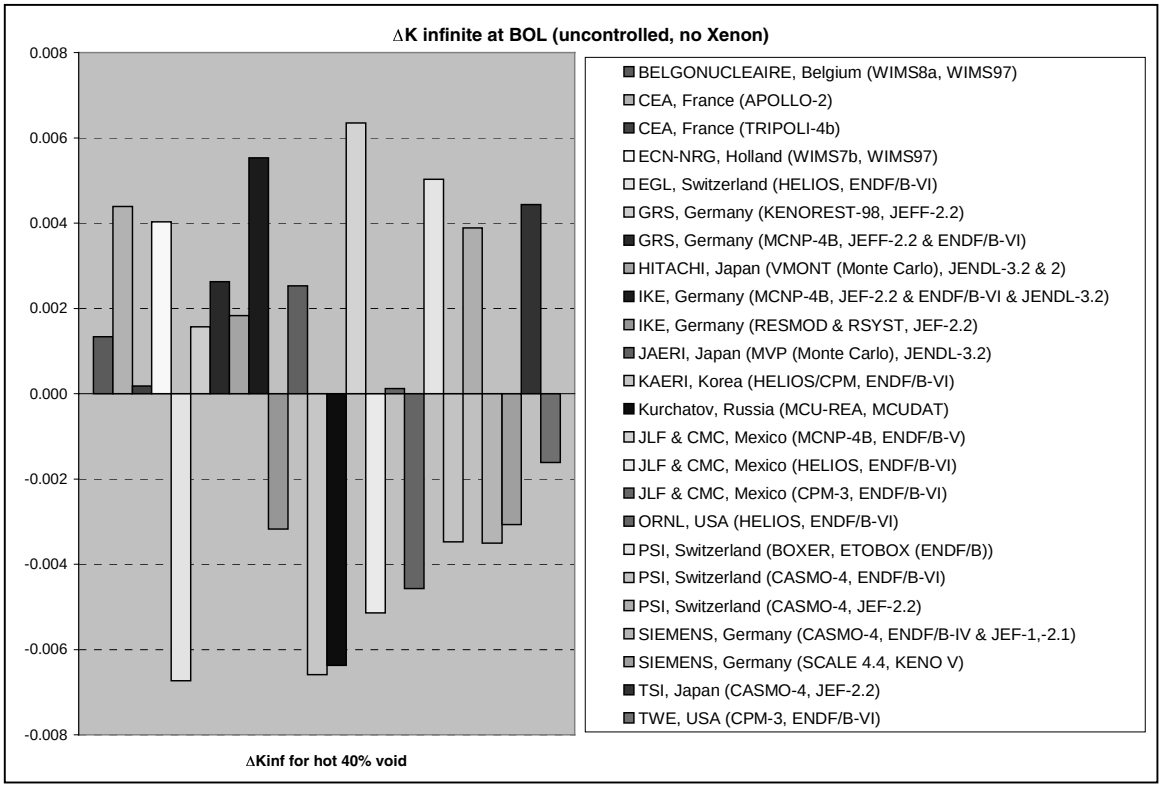
ΔK infinite at BOL (uncontrolled, no Xenon)
0.008
0.006
0.004
0.002
0.000
-0.002
-0.004
-0.006
-0.008
BELGONUCLEAIRE, Belgium (WIMS8a, WIMS97)
CEA, France (APOLLO-2)
CEA, France (TRIPOLI-4b)
ECN-NRG, Holland (WIMS7b, WIMS97)
EGL, Switzerland (HELIOS, ENDF/B-VI)
GRS, Germany (KENOREST-98, JEFF-2.2)
GRS, Germany (MCNP-4B, JEFF-2.2 & ENDF/B-VI)
HITACHI, Japan (VMONT (Monte Carlo), JENDL-3.2 & 2)
IKE, Germany (MCNP-4B, JEF-2.2 & ENDF/B-VI & JENDL-3.2)
IKE, Germany (RESMOD & RSYST, JEF-2.2)
JAERI, Japan (MVP (Monte Carlo), JENDL-3.2)
KAERI, Korea (HELIOS/CPM, ENDF/B-VI)
Kurchatov, Russia (MCU-REA, MCUDAT)
JLF & CMC, Mexico (MCNP-4B, ENDF/B-V)
JLF & CMC, Mexico (HELIOS, ENDF/B-VI)
JLF & CMC, Mexico (CPM-3, ENDF/B-VI)
ORNL, USA (HELIOS, ENDF/B-VI)
PSI, Switzerland (BOXER, ETOBOX (ENDF/B))
PSI, Switzerland (CASMO-4, ENDF/B-VI)
PSI, Switzerland (CASMO-4, JEF-2.2)
SIEMENS, Germany (CASMO-4, ENDF/B-IV & JEF-1,-2.1)
SIEMENS, Germany (SCALE 4.4, KENO V)
TSI, Japan (CASMO-4, JEF-2.2)
TWE, USA (CPM-3, ENDF/B-VI)
ΔKinf for hot 40% void

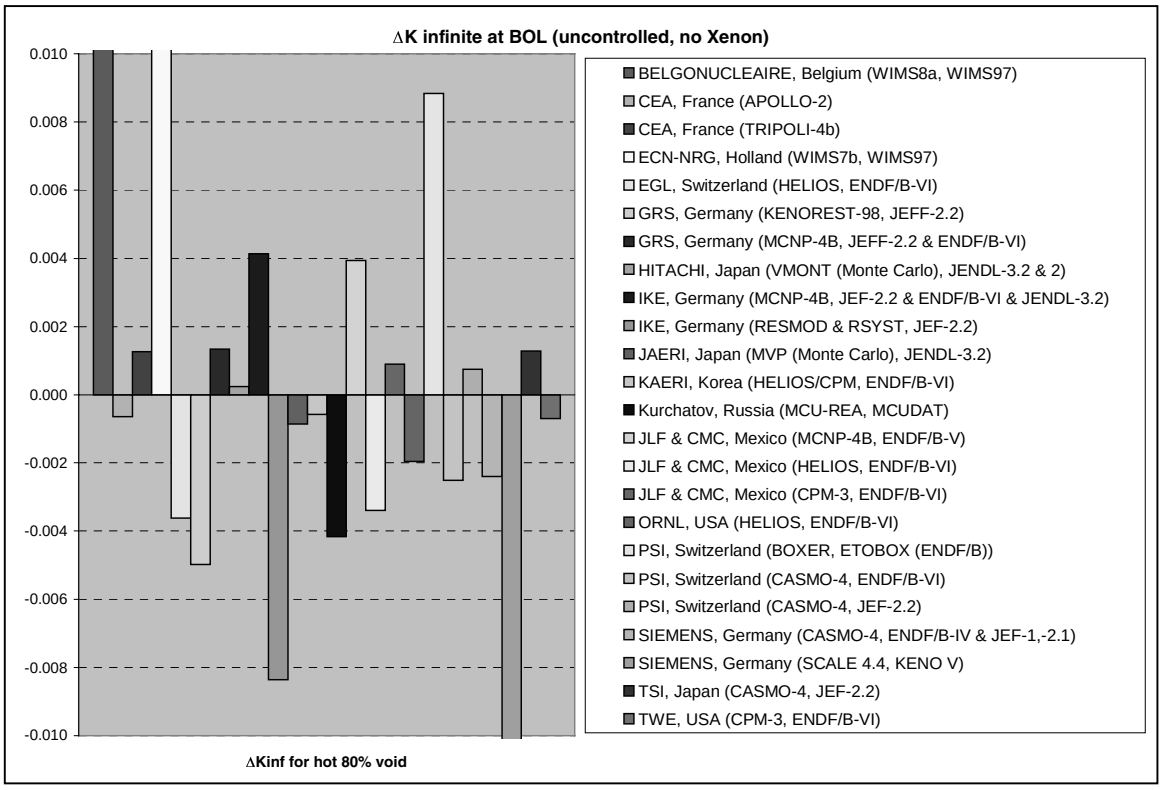
ΔK infinite at BOL (uncontrolled, no Xenon)
0.010
0.008
0.006
0.004
0.002
0.000
-0.002
-0.004
-0.006
-0.008
-0.010
BELGONUCLEAIRE, Belgium (WIMS8a, WIMS97)
CEA, France (APOLLO-2)
CEA, France (TRIPOLI-4b)
ECN-NRG, Holland (WIMS7b, WIMS97)
EGL, Switzerland (HELIOS, ENDF/B-VI)
GRS, Germany (KENOREST-98, JEFF-2.2)
GRS, Germany (MCNP-4B, JEFF-2.2 & ENDF/B-VI)
HITACHI, Japan (VMONT (Monte Carlo), JENDL-3.2 & 2)
IKE, Germany (MCNP-4B, JEF-2.2 & ENDF/B-VI & JENDL-3.2)
IKE, Germany (RESMOD & RSYST, JEF-2.2)
JAERI, Japan (MVP (Monte Carlo), JENDL-3.2)
KAERI, Korea (HELIOS/CPM, ENDF/B-VI)
Kurchatov, Russia (MCU-REA, MCUDAT)
JLF & CMC, Mexico (MCNP-4B, ENDF/B-V)
JLF & CMC, Mexico (HELIOS, ENDF/B-VI)
JLF & CMC, Mexico (CPM-3, ENDF/B-VI)
ORNL, USA (HELIOS, ENDF/B-VI)
PSI, Switzerland (BOXER, ETOBOX (ENDF/B))
PSI, Switzerland (CASMO-4, ENDF/B-VI)
PSI, Switzerland (CASMO-4, JEF-2.2)
SIEMENS, Germany (CASMO-4, ENDF/B-IV & JEF-1,-2.1)
SIEMENS, Germany (SCALE 4.4, KENO V)
TSI, Japan (CASMO-4, JEF-2.2)
TWE, USA (CPM-3, ENDF/B-VI)
ΔKinf for hot 80% void

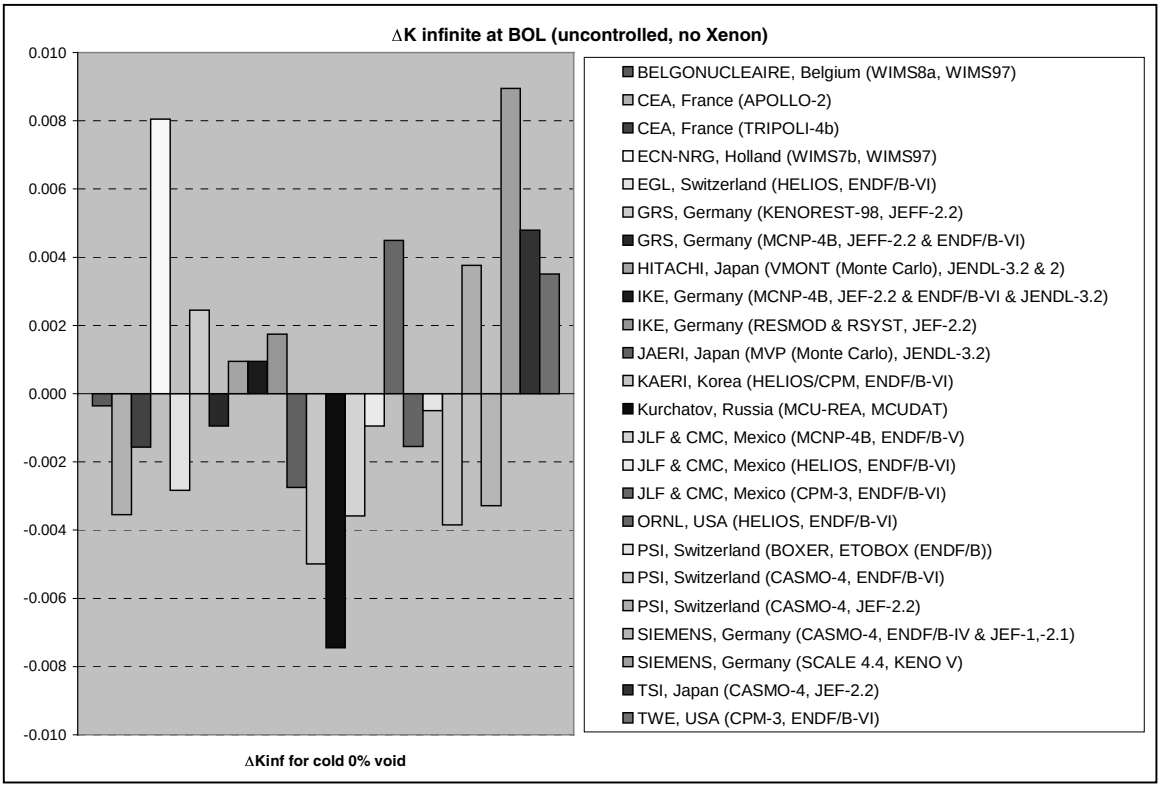

Variation of reactivity with burn-up

The table below shows the k-infinity data and for 5, 10, 30 and 50 GWd/t burn-up steps. All the data correspond to "hot 40% void" conditions.

k_{inf} (BOL)	5 GWd/t	10 GWd/t	30 GWd/t	50 GWd/t
Average =>	1.11210	1.10494	1.004180	0.92107
Discrepancy max. =>	0.00666	0.00501	0.015880	0.02058
Discrepancy min. =>	-0.00687	-0.00634	-0.001068	-0.01429
Average discrepancies (min./max.) =>	0.00330	0.00311	0.004020	0.00528
Average without extreme values =>	1.11212	1.10502	1.003880	0.92070
Average discrepancies (min./max.) =>	0.00289	0.00281	0.002930	0.00384
JEF 2 =>	1.11217	1.10581	1.007990	0.92648
ENDF B-VI =>	1.11620	1.10918	1.008150	0.92466

The number of solutions submitted is reduced: only 19 solutions were available, since some of the Monte Carlo codes are not able to carry out the fuel depletion calculation. The range of discrepancies between solutions is also smaller than at zero burn-up (less than 1%). The extreme negative outlier at zero burn-up is one of the Monte Carlo solutions for which there is no depletion

data and therefore it is not represented in this data. Accordingly, the remaining solutions all lie within a reasonable range and the outliers do not unduly influence the average value. Again, the effect of changing from JEF 2.2 to ENDF B VI in PSI calculations is less than 1%, while the reactivity balance during burn-up is better with ENDF library.

WIMS	**5 GWd/t**	**10 GWd/t**	**30 GWd/t**	**50 GWd/t**
BELGONUCLEAIRE (Belgium)	1.112640	1.10483	1.002160	0.921170
ECN-NRG (The Netherlands)	1.113700	1.10750	1.006400	0.924900
HELIOS	**5 GWd/t**	**10 GWd/t**	**30 GWd/t**	**50 GWd/t**
EGL (Switzerland)	1.107010	1.100090	1.000610	0.918140
KAERI (Republic of Korea)	1.108309	1.102534	1.006233	0.924692
JLF&CMC (Mexico)	1.108900	1.101800	1.002300	0.919800
ORNL (USA)	1.108600	1.101500	1.001800	0.919600
CASMO 4	**5 GWd/t**	**10 GWd/t**	**30 GWd/t**	**50 GWd/t**
PSI (Switzerland), ENDF B-VI	1.112170	1.105810	1.007990	0.926480
PSI (Switzerland), JEF-2.2	1.116200	1.109180	1.008150	0.924660
SIEMENS (Germany)	1.111900	1.105700	1.008100	0.926700
Other MC	**5 GWd/t**	**10 GWd/t**	**30 GWd/t**	**50 GWd/t**
GRS (Germany)/KENOREST-98	1.105230	1.109950	1.020060	0.941650
HITACHI (Japan)	1.115600	1.108100	1.004800	0.922100
JAERI (Japan)	1.114100	1.105600	1.004700	0.920200
“Kurchatov Institute” (Russian Fed.)	1.114400	1.102100	0.993500	0.907900

Mean values w/o extreme solutions	**1.112100**	**1.105000**	**1.003900**	**0.920700**
Deterministic codes	**1.112000**	**1.104500**	**1.003800**	**0.920600**
Monte Carlo codes	**1.112300**	**1.106400**	**1.005700**	**0.923000**

The figures below plot the data for 5, 10, 30 and 50 GWd/t respectively. These show that the outlying solutions have a tendency to spread further apart with increasing burn-up, although the remaining solutions remain tightly clustered about the mean. This causes the average discrepancy to increase with burn-up, but even so remains within ±0.6%.

With the exception of the clear outlier, the calculations are all show very consistent behaviour of k_{inf} as a function of burn-up. As can be seen from the figure below, the shapes of the various curves are very similar and in particular the rapid variation due to gadolinia depletion at around 10 GWd/t appears to be very consistent. Most of the solutions have a very similar gradient of k_{inf} versus burn-up. This means that those solutions which are higher or lower than average at 0 GWd/t tend to remain on the high or low side during irradiation and consequently the BOL spread tends to persist throughout the depletion. However, there appears to be a difference in gradient between ENDF/B and JEF, with the former having a noticeably lower reactivity balance. There is good consistency between the average of the Monte Carlo codes and the average of the deterministic codes.

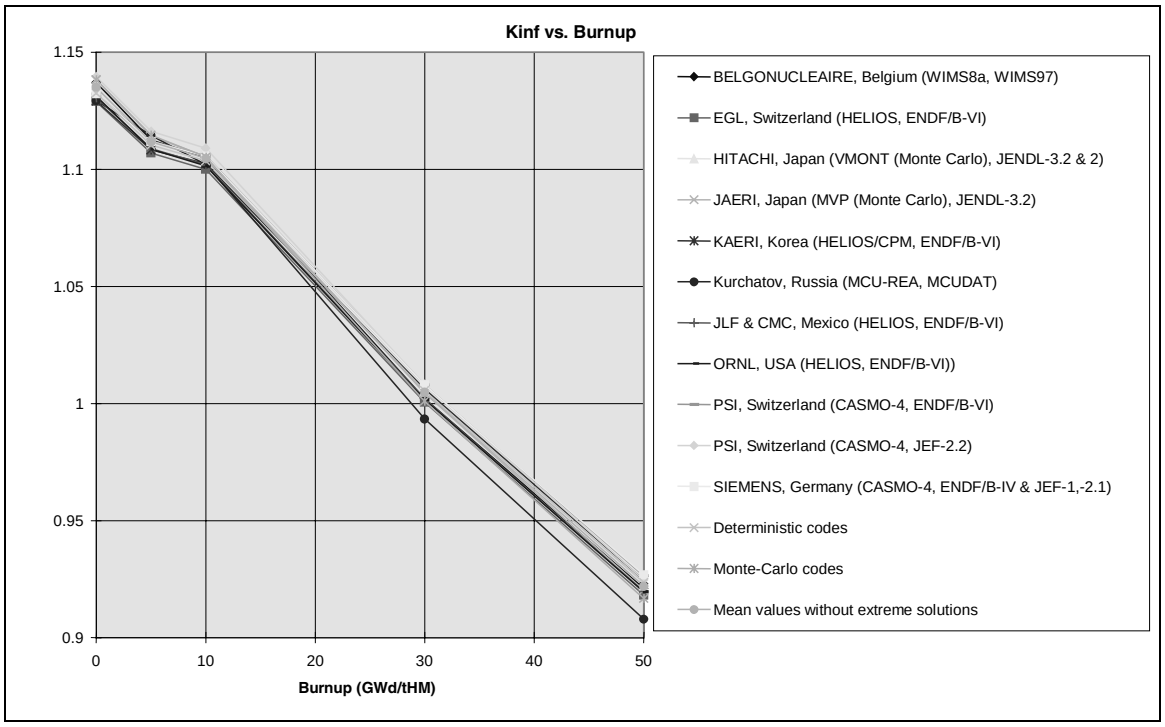
Kinf vs. Burnup
1.15
1.1
1.05
1
0.95
0.9
0
10
20
30
40
50
Burnup (GWd/tHM)
BELGONUCLEAIRE, Belgium (WIMS8a, WIMS97)
EGL, Switzerland (HELIOS, ENDF/B-VI)
HITACHI, Japan (VMONT (Monte Carlo), JENDL-3.2 & 2)
JAERI, Japan (MVP (Monte Carlo), JENDL-3.2)
KAERI, Korea (HELIOS/CPM, ENDF/B-VI)
Kurchatov, Russia (MCU-REA, MCUDAT)
JLF & CMC, Mexico (HELIOS, ENDF/B-VI)
ORNL, USA (HELIOS, ENDF/B-VI))
PSI, Switzerland (CASMO-4, ENDF/B-VI)
PSI, Switzerland (CASMO-4, JEF-2.2)
SIEMENS, Germany (CASMO-4, ENDF/B-IV & JEF-1,-2.1)
Deterministic codes
Monte-Carlo codes
Mean values without extreme solutions

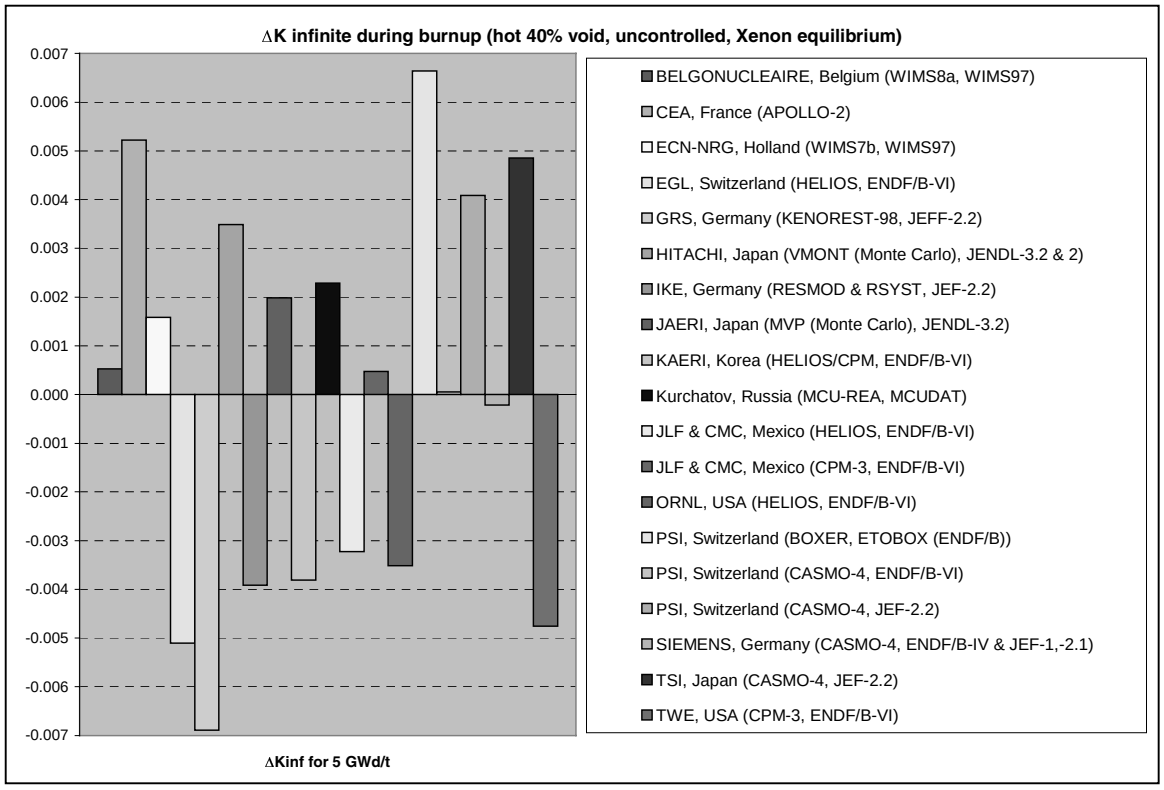
ΔK infinite during burnup (hot 40% void, uncontrolled, Xenon equilibrium)
0.007
0.006
0.005
0.004
0.003
0.002
0.001
0.000
-0.001
-0.002
-0.003
-0.004
-0.005
-0.006
-0.007
ΔKinf for 5 GWd/t
BELGONUCLEAIRE, Belgium (WIMS8a, WIMS97)
CEA, France (APOLLO-2)
ECN-NRG, Holland (WIMS7b, WIMS97)
EGL, Switzerland (HELIOS, ENDF/B-VI)
GRS, Germany (KENOREST-98, JEFF-2.2)
HITACHI, Japan (VMONT (Monte Carlo), JENDL-3.2 & 2)
IKE, Germany (RESMOD & RSYST, JEF-2.2)
JAERI, Japan (MVP (Monte Carlo), JENDL-3.2)
KAERI, Korea (HELIOS/CPM, ENDF/B-VI)
Kurchatov, Russia (MCU-REA, MCUDAT)
JLF & CMC, Mexico (HELIOS, ENDF/B-VI)
JLF & CMC, Mexico (CPM-3, ENDF/B-VI)
ORNL, USA (HELIOS, ENDF/B-VI)
PSI, Switzerland (BOXER, ETOBOX (ENDF/B))
PSI, Switzerland (CASMO-4, ENDF/B-VI)
PSI, Switzerland (CASMO-4, JEF-2.2)
SIEMENS, Germany (CASMO-4, ENDF/B-IV & JEF-1,-2.1)
TSI, Japan (CASMO-4, JEF-2.2)
TWE, USA (CPM-3, ENDF/B-VI)

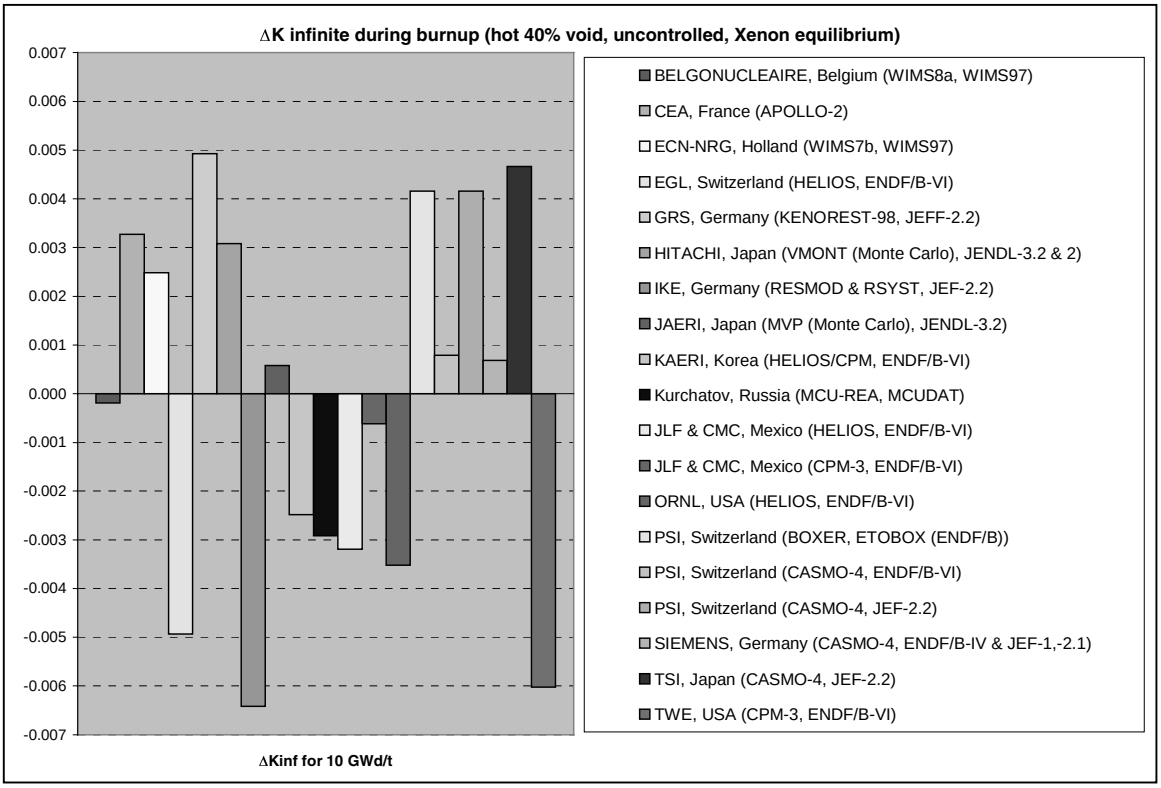
ΔK infinite during burnup (hot 40% void, uncontrolled, Xenon equilibrium)
0.007
0.006
0.005
0.004
0.003
0.002
0.001
0.000
-0.001
-0.002
-0.003
-0.004
-0.005
-0.006
-0.007
ΔKinf for 10 GWd/t
BELGONUCLEAIRE, Belgium (WIMS8a, WIMS97)
CEA, France (APOLLO-2)
ECN-NRG, Holland (WIMS7b, WIMS97)
EGL, Switzerland (HELIOS, ENDF/B-VI)
GRS, Germany (KENOREST-98, JEFF-2.2)
HITACHI, Japan (VMONT (Monte Carlo), JENDL-3.2 & 2)
IKE, Germany (RESMOD & RSYST, JEF-2.2)
JAERI, Japan (MVP (Monte Carlo), JENDL-3.2)
KAERI, Korea (HELIOS/CPM, ENDF/B-VI)
Kurchatov, Russia (MCU-REA, MCUDAT)
JLF & CMC, Mexico (HELIOS, ENDF/B-VI)
JLF & CMC, Mexico (CPM-3, ENDF/B-VI)
ORNL, USA (HELIOS, ENDF/B-VI)
PSI, Switzerland (BOXER, ETOBOX (ENDF/B))
PSI, Switzerland (CASMO-4, ENDF/B-VI)
PSI, Switzerland (CASMO-4, JEF-2.2)
SIEMENS, Germany (CASMO-4, ENDF/B-IV & JEF-1,-2.1)
TSI, Japan (CASMO-4, JEF-2.2)
TWE, USA (CPM-3, ENDF/B-VI)

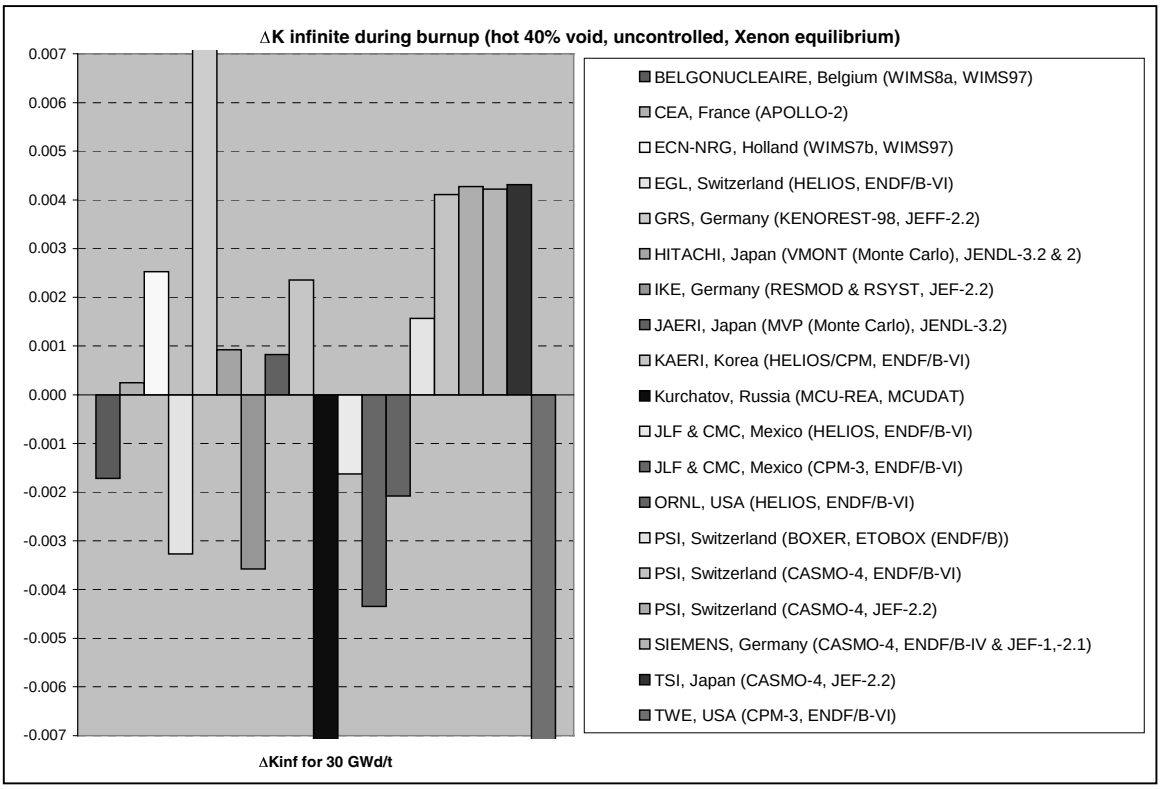
ΔK infinite during burnup (hot 40% void, uncontrolled, Xenon equilibrium)
0.007
0.006
0.005
0.004
0.003
0.002
0.001
0.000
-0.001
-0.002
-0.003
-0.004
-0.005
-0.006
-0.007
ΔKinf for 30 GWd/t
BELGONUCLEAIRE, Belgium (WIMS8a, WIMS97)
CEA, France (APOLLO-2)
ECN-NRG, Holland (WIMS7b, WIMS97)
EGL, Switzerland (HELIOS, ENDF/B-VI)
GRS, Germany (KENOREST-98, JEFF-2.2)
HITACHI, Japan (VMONT (Monte Carlo), JENDL-3.2 & 2)
IKE, Germany (RESMOD & RSYST, JEF-2.2)
JAERI, Japan (MVP (Monte Carlo), JENDL-3.2)
KAERI, Korea (HELIOS/CPM, ENDF/B-VI)
Kurchatov, Russia (MCU-REA, MCUDAT)
JLF & CMC, Mexico (HELIOS, ENDF/B-VI)
JLF & CMC, Mexico (CPM-3, ENDF/B-VI)
ORNL, USA (HELIOS, ENDF/B-VI)
PSI, Switzerland (BOXER, ETOBOX (ENDF/B))
PSI, Switzerland (CASMO-4, ENDF/B-VI)
PSI, Switzerland (CASMO-4, JEF-2.2)
SIEMENS, Germany (CASMO-4, ENDF/B-IV & JEF-1,-2.1)
TSI, Japan (CASMO-4, JEF-2.2)
TWE, USA (CPM-3, ENDF/B-VI)

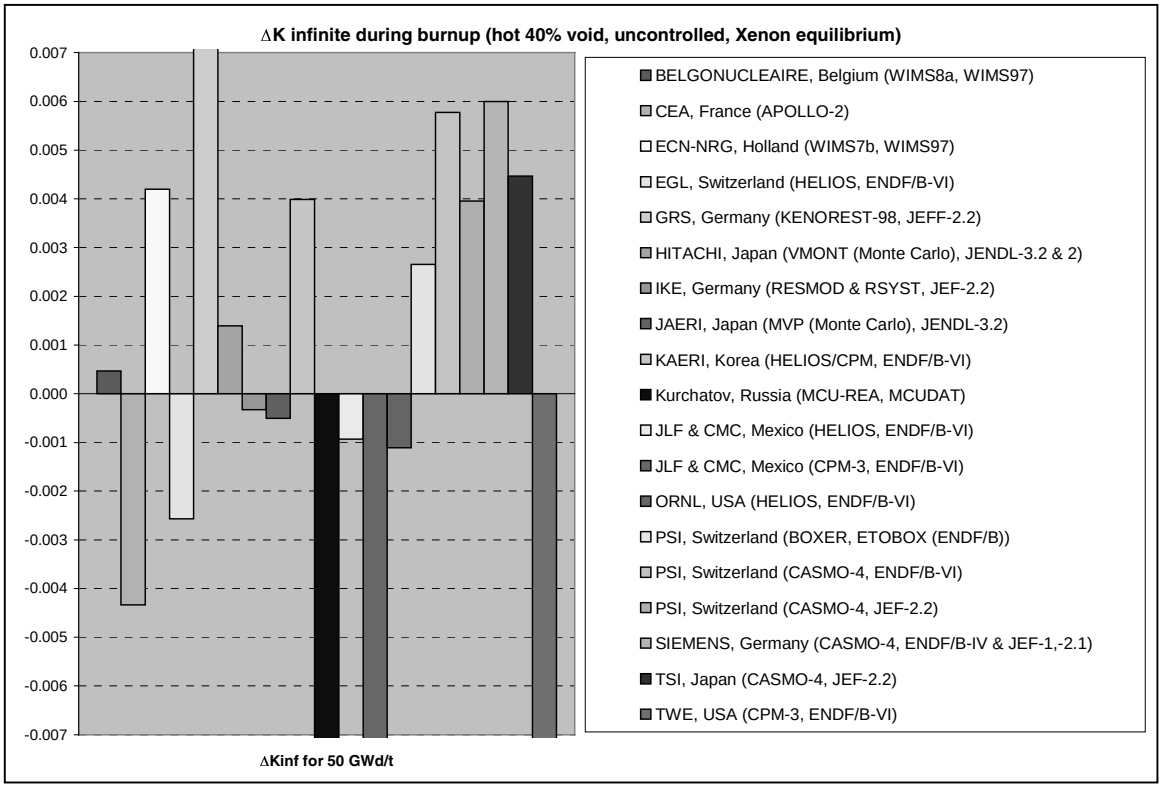

Peaking factors

Peaking factor at BOL

This section presents a comparison of radial power peaking factors within the fuel assembly. The radial peaking factor is an important performance and safety parameter and it tests the ability of the various codes to calculate the spatial variations of neutron flux and fission rate in what is a very heterogeneous problem.

Peaking factor (BOL)	hot 0% void	hot 40% void	hot 80% void	cold 0% void
Average =>	1.24120	1.22959	1.22360	1.33945
Discrepancy max. =>	0.01280	0.01041	0.01640	0.05355
Discrepancy min. =>	-0.01220	-0.01659	-0.04060	-0.07345
Average discrepancies (min./max.) =>	0.00537	0.00695	0.00692	0.02452
Average without extreme values =>	1.24117	1.22987	1.22352	1.34035
Average discrepancies (min./max.) =>	0.00472	0.00636	0.00495	0.02098
JEF 2 =>	1.24500	1.23800	1.22200	1.33600
ENDF B-VI =>	1.24500	1.23800	1.22100	1.33400

The peaking factor is a local parameter which is more dependent on the methods used by the codes, and with lower compensation effects than for reactivity. There are differences between participants both in the magnitude of the peaking factor and its position within the assembly.

WIMS	**hot 0% void**	**hot 40% void**	**hot 80% void**	**cold 0% void**
BELGONUCLEAIRE (Belgium)	1.2440	1.2350	1.2160	1.3250
ECN-NRG (The Netherlands)	1.2370	1.2130	1.1830	1.2660
HELIOS	**hot 0% void**	**hot 40% void**	**hot 80% void**	**cold 0% void**
EGL (Switzerland)	1.2310	1.2140	1.2280	1.3020
KAERI (Republic of Korea)	1.2375	1.2228	1.2337	1.3185
JLF&CMC (Mexico)	1.2360	1.2210	1.2330	1.3190
ORNL (USA)	1.2380	1.2230	1.2360	1.3210
CASMO 4	**hot 0% void**	**hot 40% void**	**hot 80% void**	**cold 0% void**
PSI (Switzerland), ENDF B-VI	1.2440	1.2380	1.2220	1.3360
PSI (Switzerland), JEF-2.2	1.2450	1.2380	1.2210	1.3340
SIEMENS (Germany)	1.2450	1.2370	1.2220	1.3310
MCNP	**hot 0% void**	**hot 40% void**	**hot 80% void**	**cold 0% void**
GRS (Germany)	1.2370	1.2370	1.2230	1.3660
IKE University (Germany)	1.2450	1.2320	1.2260	1.3710
JLF&CMC (Mexico)	1.2540	1.2380	1.2310	1.3710
Other MC	**hot 0% void**	**hot 40% void**	**hot 80% void**	**cold 0% void**
CEA (France)	1.2498	1.2361	1.2218	1.3885
GRS (Germany)/KENOREST-98	1.2360	1.2250	1.2400	1.3590
HITACHI (Japan)	1.2440	1.2360	1.2170	1.3400
JAERI (Japan)	1.2290	1.2320	1.2210	1.3930
“Kurchatov Institute” (Russian Fed.)	1.2480	1.2290	1.2250	1.3600
SIEMENS (Germany)/KENO-5	1.2410	1.2350	1.2240	1.3370

Mean values w/o extreme solutions	**1.2411**	**1.2300**	**1.2235**	**1.3403**
Deterministic codes	**1.2403**	**1.2273**	**1.2225**	**1.3241**
Monte Carlo codes	**1.2426**	**1.2333**	**1.2254**	**1.3651**

The extreme values clearly fall outside a normal distribution and can be regarded as discrepant. Excluding the extreme values, the solutions differ by no more than ±2.0% about the mean at hot conditions. There is evidence of a tendency for a slight increase with void fraction. The cold 0% void case shows a larger range of ±2.5%. For hot conditions, at 0%, 40% and 80% void, there is tight clustering of the solutions, with only 4 solutions showing a difference more than 0.01 in absolute value on the peaking factor. For the cold case, however, 9 solutions differ more than 0.03. This suggests that modelling cold conditions presents a more severe test of the methods. This may be due to the higher moderation causing more pronounced local thermal peaking effects.

The impact of data library between JEF and ENDF is negligible.

The position of the peak is always at A1 for cold conditions, and mainly at E10 for nominal conditions (40% void). There is no difference due to libraries. The positions and the magnitude of the peak calculated HELIOS and CASMO are consistent. The solutions from WIMS show a greater spread.

Participant/Code	hot 0% void	hot 40% void	hot 80% void	cold 0% void
BN/WIMS PSI/CASMO ENDF PSI/CASMO JEF SIEMENS/CASMO TSI-TEPCO/CASMO TWE/CPM-3	E10	E10	E10	A1
CEA/APOLLO GRS/MCNP IKE/MCNP IKE/RESMOD JLF&CMC/CPM-3	E10	E10	D7	A1
CEA/TRIPOLI GRS/KENOREST	A1	E10	D7	A1
HITACHI/VMONT KAERI/HELIOS ORNL/HELIOS EGL/HELIOS JLF&CMC/HELIOS	E10	E10	K9	A1
JAERI/MVP	A1	E10	D7	A1
KI/MCU	A1	A1	D7	A1
NRG/WIMS	A1	A6	A6	A1
JLF&CMC/MCNP PSI/BOXER SIEMENS/SCALE-KENO	E10	H10	D7	A1

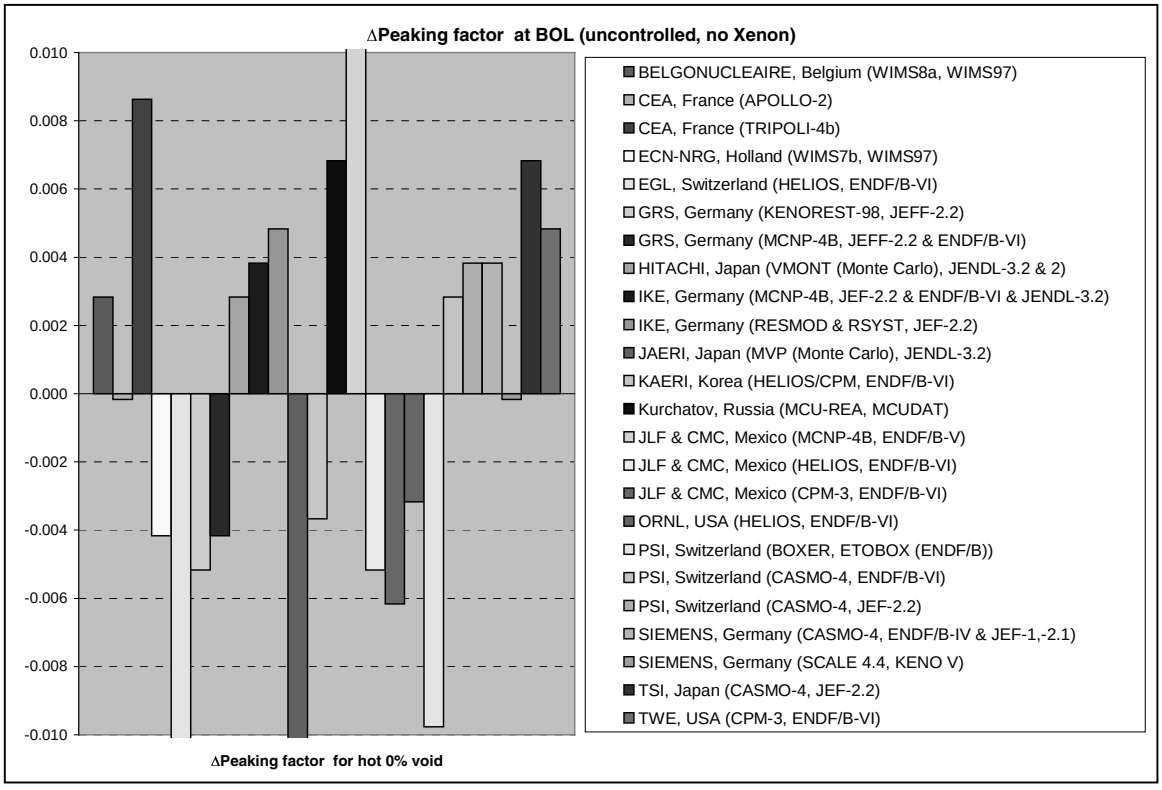
ΔPeaking factor at BOL (uncontrolled, no Xenon)
0.010
0.008
0.006
0.004
0.002
0.000
-0.002
-0.004
-0.006
-0.008
-0.010
BELGONUCLEAIRE, Belgium (WIMS8a, WIMS97)
CEA, France (APOLLO-2)
CEA, France (TRIPOLI-4b)
ECN-NRG, Holland (WIMS7b, WIMS97)
EGL, Switzerland (HELIOS, ENDF/B-VI)
GRS, Germany (KENOREST-98, JEFF-2.2)
GRS, Germany (MCNP-4B, JEFF-2.2 & ENDF/B-VI)
HITACHI, Japan (VMONT (Monte Carlo), JENDL-3.2 & 2)
IKE, Germany (MCNP-4B, JEF-2.2 & ENDF/B-VI & JENDL-3.2)
IKE, Germany (RESMOD & RSYST, JEF-2.2)
JAERI, Japan (MVP (Monte Carlo), JENDL-3.2)
KAERI, Korea (HELIOS/CPM, ENDF/B-VI)
Kurchatov, Russia (MCU-REA, MCUDAT)
JLF & CMC, Mexico (MCNP-4B, ENDF/B-V)
JLF & CMC, Mexico (HELIOS, ENDF/B-VI)
JLF & CMC, Mexico (CPM-3, ENDF/B-VI)
ORNL, USA (HELIOS, ENDF/B-VI)
PSI, Switzerland (BOXER, ETOBOX (ENDF/B))
PSI, Switzerland (CASMO-4, ENDF/B-VI)
PSI, Switzerland (CASMO-4, JEF-2.2)
SIEMENS, Germany (CASMO-4, ENDF/B-IV & JEF-1,-2.1)
SIEMENS, Germany (SCALE 4.4, KENO V)
TSI, Japan (CASMO-4, JEF-2.2)
TWE, USA (CPM-3, ENDF/B-VI)
ΔPeaking factor for hot 0% void

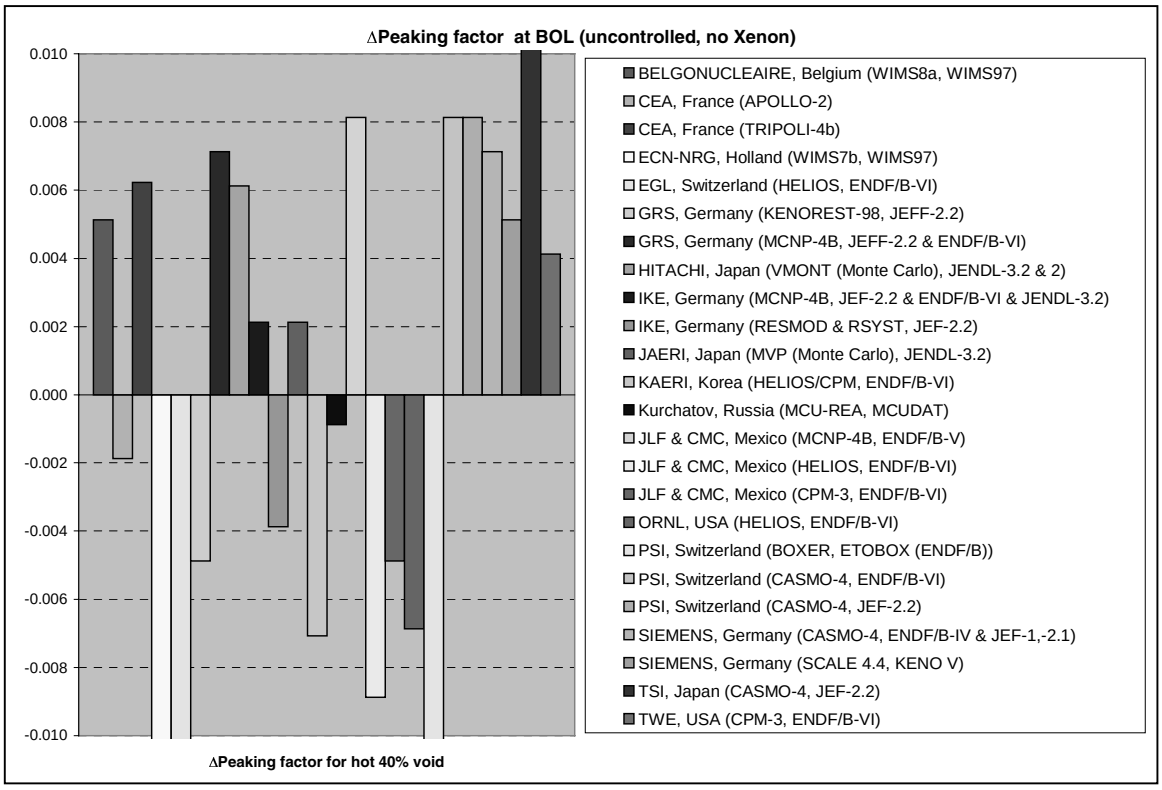
ΔPeaking factor at BOL (uncontrolled, no Xenon)
0.010
0.008
0.006
0.004
0.002
0.000
-0.002
-0.004
-0.006
-0.008
-0.010
BELGONUCLEAIRE, Belgium (WIMS8a, WIMS97)
CEA, France (APOLLO-2)
CEA, France (TRIPOLI-4b)
ECN-NRG, Holland (WIMS7b, WIMS97)
EGL, Switzerland (HELIOS, ENDF/B-VI)
GRS, Germany (KENOREST-98, JEFF-2.2)
GRS, Germany (MCNP-4B, JEFF-2.2 & ENDF/B-VI)
HITACHI, Japan (VMONT (Monte Carlo), JENDL-3.2 & 2)
IKE, Germany (MCNP-4B, JEF-2.2 & ENDF/B-VI & JENDL-3.2)
IKE, Germany (RESMOD & RSYST, JEF-2.2)
JAERI, Japan (MVP (Monte Carlo), JENDL-3.2)
KAERI, Korea (HELIOS/CPM, ENDF/B-VI)
Kurchatov, Russia (MCU-REA, MCUDAT)
JLF & CMC, Mexico (MCNP-4B, ENDF/B-V)
JLF & CMC, Mexico (HELIOS, ENDF/B-VI)
JLF & CMC, Mexico (CPM-3, ENDF/B-VI)
ORNL, USA (HELIOS, ENDF/B-VI)
PSI, Switzerland (BOXER, ETOBOX (ENDF/B))
PSI, Switzerland (CASMO-4, ENDF/B-VI)
PSI, Switzerland (CASMO-4, JEF-2.2)
SIEMENS, Germany (CASMO-4, ENDF/B-IV & JEF-1,-2.1)
SIEMENS, Germany (SCALE 4.4, KENO V)
TSI, Japan (CASMO-4, JEF-2.2)
TWE, USA (CPM-3, ENDF/B-VI)
ΔPeaking factor for hot 40% void

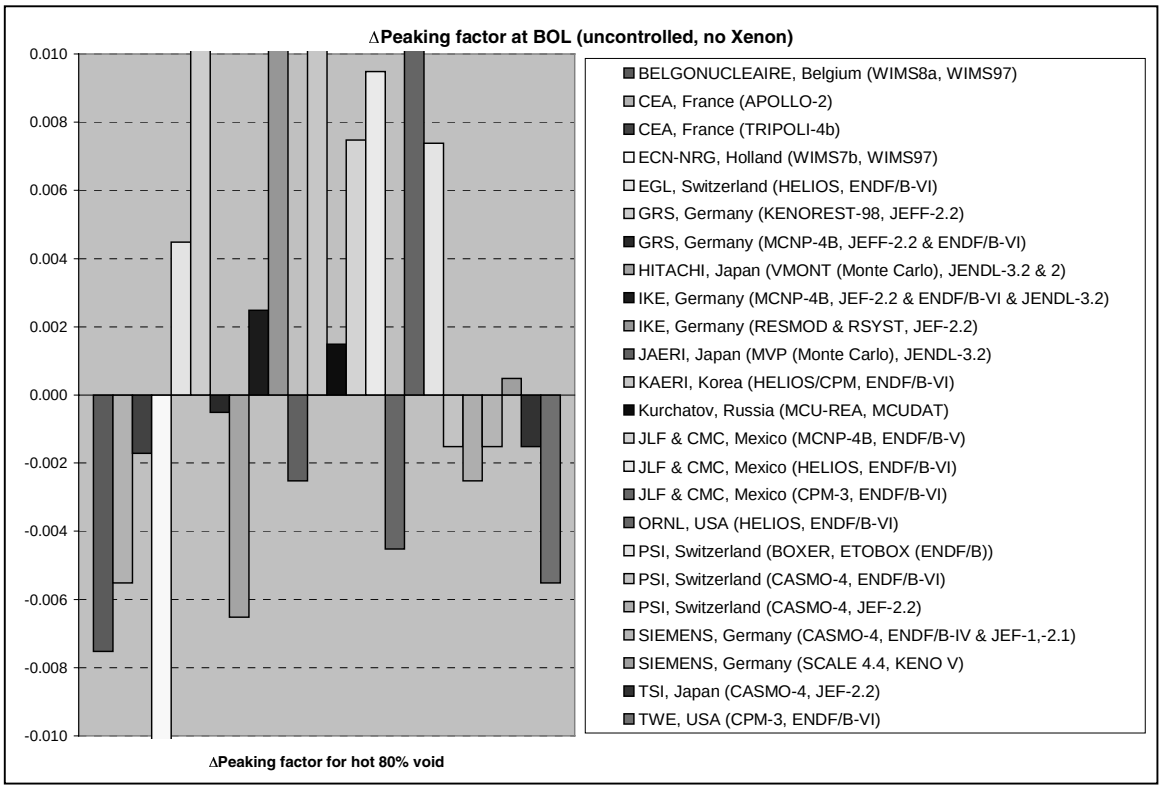
ΔPeaking factor at BOL (uncontrolled, no Xenon)
0.010
0.008
0.006
0.004
0.002
0.000
-0.002
-0.004
-0.006
-0.008
-0.010
ΔPeaking factor for hot 80% void
BELGONUCLEAIRE, Belgium (WIMS8a, WIMS97)
CEA, France (APOLLO-2)
CEA, France (TRIPOLI-4b)
ECN-NRG, Holland (WIMS7b, WIMS97)
EGL, Switzerland (HELIOS, ENDF/B-VI)
GRS, Germany (KENOREST-98, JEFF-2.2)
GRS, Germany (MCNP-4B, JEFF-2.2 & ENDF/B-VI)
HITACHI, Japan (VMONT (Monte Carlo), JENDL-3.2 & 2)
IKE, Germany (MCNP-4B, JEF-2.2 & ENDF/B-VI & JENDL-3.2)
IKE, Germany (RESMOD & RSYST, JEF-2.2)
JAERI, Japan (MVP (Monte Carlo), JENDL-3.2)
KAERI, Korea (HELIOS/CPM, ENDF/B-VI)
Kurchatov, Russia (MCU-REA, MCUDAT)
JLF & CMC, Mexico (MCNP-4B, ENDF/B-V)
JLF & CMC, Mexico (HELIOS, ENDF/B-VI)
JLF & CMC, Mexico (CPM-3, ENDF/B-VI)
ORNL, USA (HELIOS, ENDF/B-VI)
PSI, Switzerland (BOXER, ETOBOX (ENDF/B))
PSI, Switzerland (CASMO-4, ENDF/B-VI)
PSI, Switzerland (CASMO-4, JEF-2.2)
SIEMENS, Germany (CASMO-4, ENDF/B-IV & JEF-1,-2.1)
SIEMENS, Germany (SCALE 4.4, KENO V)
TSI, Japan (CASMO-4, JEF-2.2)
TWE, USA (CPM-3, ENDF/B-VI)

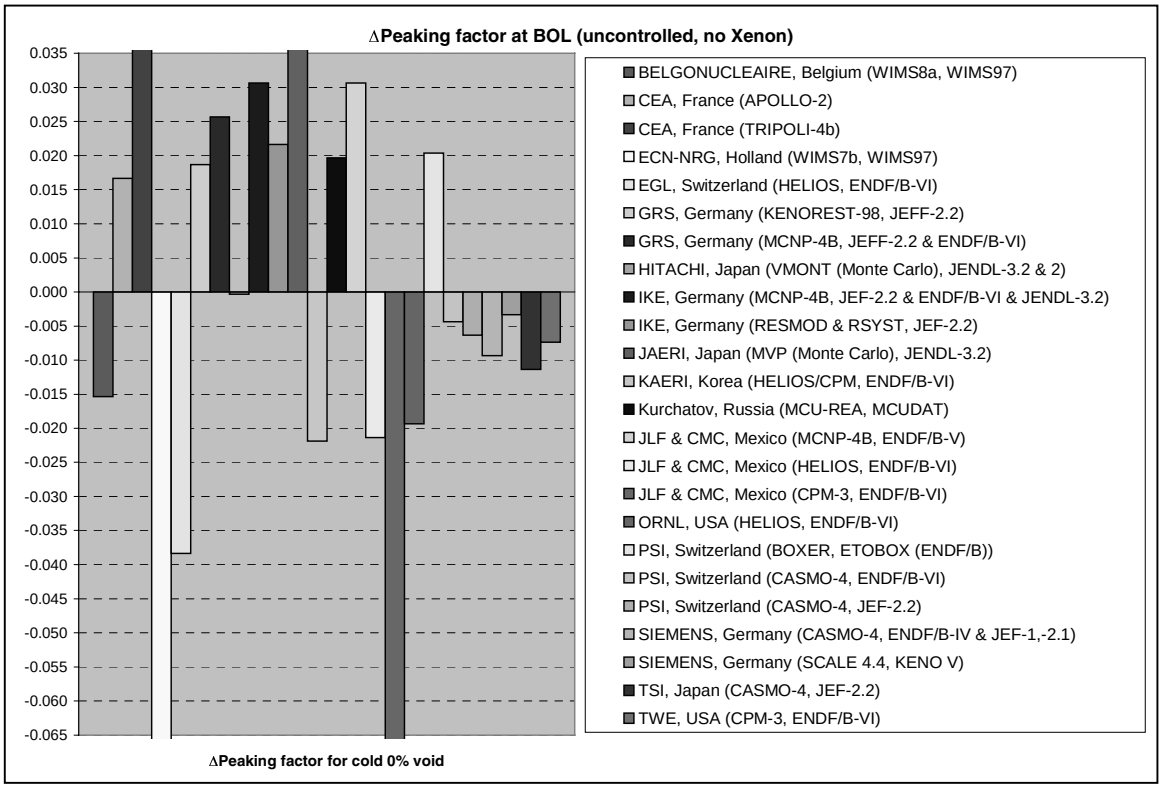
ΔPeaking factor at BOL (uncontrolled, no Xenon)
0.035
0.030
0.025
0.020
0.015
0.010
0.005
0.000
-0.005
-0.010
-0.015
-0.020
-0.025
-0.030
-0.035
-0.040
-0.045
-0.050
-0.055
-0.060
-0.065
ΔPeaking factor for cold 0% void
BELGONUCLEAIRE, Belgium (WIMS8a, WIMS97)
CEA, France (APOLLO-2)
CEA, France (TRIPOLI-4b)
ECN-NRG, Holland (WIMS7b, WIMS97)
EGL, Switzerland (HELIOS, ENDF/B-VI)
GRS, Germany (KENOREST-98, JEFF-2.2)
GRS, Germany (MCNP-4B, JEFF-2.2 & ENDF/B-VI)
HITACHI, Japan (VMONT (Monte Carlo), JENDL-3.2 & 2)
IKE, Germany (MCNP-4B, JEF-2.2 & ENDF/B-VI & JENDL-3.2)
IKE, Germany (RESMOD & RSYST, JEF-2.2)
JAERI, Japan (MVP (Monte Carlo), JENDL-3.2)
KAERI, Korea (HELIOS/CPM, ENDF/B-VI)
Kurchatov, Russia (MCU-REA, MCUDAT)
JLF & CMC, Mexico (MCNP-4B, ENDF/B-V)
JLF & CMC, Mexico (HELIOS, ENDF/B-VI)
JLF & CMC, Mexico (CPM-3, ENDF/B-VI)
ORNL, USA (HELIOS, ENDF/B-VI)
PSI, Switzerland (BOXER, ETOBOX (ENDF/B))
PSI, Switzerland (CASMO-4, ENDF/B-VI)
PSI, Switzerland (CASMO-4, JEF-2.2)
SIEMENS, Germany (CASMO-4, ENDF/B-IV & JEF-1,-2.1)
SIEMENS, Germany (SCALE 4.4, KENO V)
TSI, Japan (CASMO-4, JEF-2.2)
TWE, USA (CPM-3, ENDF/B-VI)

Variation of peaking factor with burn-up

The following table shows the average radial peaking factor and the range of values about the average as a function of burn-up.

Peaking factor (BOL)	**5 GWd/t**	**10 GWd/t**	**30 GWd/t**	**50 GWd/t**
Average =>	1.22244	1.22047	1.20943	1.20366
Discrepancy max. =>	0.02416	0.02793	0.03007	0.06934
Discrepancy min. =>	-0.05244	-0.08747	-0.06143	-0.04866
Average discrepancies (min./max.) =>	0.01053	0.01261	0.01065	0.01293
Average without extreme values =>	1.22410	1.23279	1.21052	1.20245
Average discrepancies (min./max.) =>	0.00730	0.00730	0.00650	0.00750
JEF 2 =>	1.22800	1.23700	1.21600	1.20900
ENDF B-VI =>	1.22700	1.23600	1.21500	1.20700

The fuel composition changes rapidly with burn-up and in turn affects the location and magnitude of the power peaking factor. For a BWR, the radial power peaking factor is a key parameter and it is important to calculate it accurately. Since some of the Monte Carlo solutions are unable to calculate the fuel depletion behaviour, there are fewer solutions available (19) and the homogeneity of the results is improved. The average values with and without the extreme values are not very different (2%) in relative value. The calculation of the power peaking factor with burn-up is strongly dependent on the methods used for the thermal flux calculation and the depletion calculation. The impact of the nuclear data library is again negligible, as indicated by comparing the solutions using ENDF/B and JEF.

WIMS	5 GWd/t	10 GWd/t	30 GWd/t	50 GWd/t
BELGONUCLEAIRE (Belgium)	1.2200	1.2280	1.2090	1.1940
ECN-NRG (The Netherlands)	1.1700	1.1420	1.1480	1.1550
HELIOS	**5 GWd/t**	**10 GWd/t**	**30 GWd/t**	**50 GWd/t**
EGL (Switzerland)	1.2100	1.2180	1.1970	1.1940
KAERI (Republic of Korea)	1.2235	1.2322	1.2134	1.2148
JLF&CMC (Mexico)	1.2200	1.2270	1.2060	1.2020
ORNL (USA)	1.2220	1.2280	1.2090	1.2020
CASMO 4	**5 GWd/t**	**10 GWd/t**	**30 GWd/t**	**50 GWd/t**
PSI (Switzerland), ENDF B-VI	1.2270	1.2360	1.2150	1.2070
PSI (Switzerland), JEF-2.2	1.2280	1.2370	1.2160	1.2090
SIEMENS (Germany)	1.2260	1.2350	1.2140	1.2070
Other MC	**5 GWd/t**	**10 GWd/t**	**30 GWd/t**	**50 GWd/t**
GRS (Germany)/KENOREST-98	1.2350	1.2400	1.2260	1.2080
HITACHI (Japan)	1.2300	1.2380	1.2140	1.2010
JAERI (Japan)	1.2110	1.2330	1.2070	1.1910
"Kurchatov Institute" (Russian Fed.)	1.2380	1.2380	1.2100	1.1980

Mean values w/o extreme solutions	**1.2241**	**1.2328**	**1.2105**	**1.2024**
Deterministic codes	**1.2208**	**1.2274**	**1.2081**	**1.2048**
Monte Carlo codes	**1.2285**	**1.2373**	**1.2143**	**1.1995**

The position of the peak factor is almost the same for the 19 solutions given for burn-up.

Participant/Code	5 GWd/t	10 GWd/t	30 GWd/t	50 GWd/t
GRS/KENOREST	E10	D7	D7	D9
NRG/WIMS	E10	E10	D7	D7
IKE/RESMOD	D7	D7	D7	D7
All other solutions	D7	D7	D7	D9

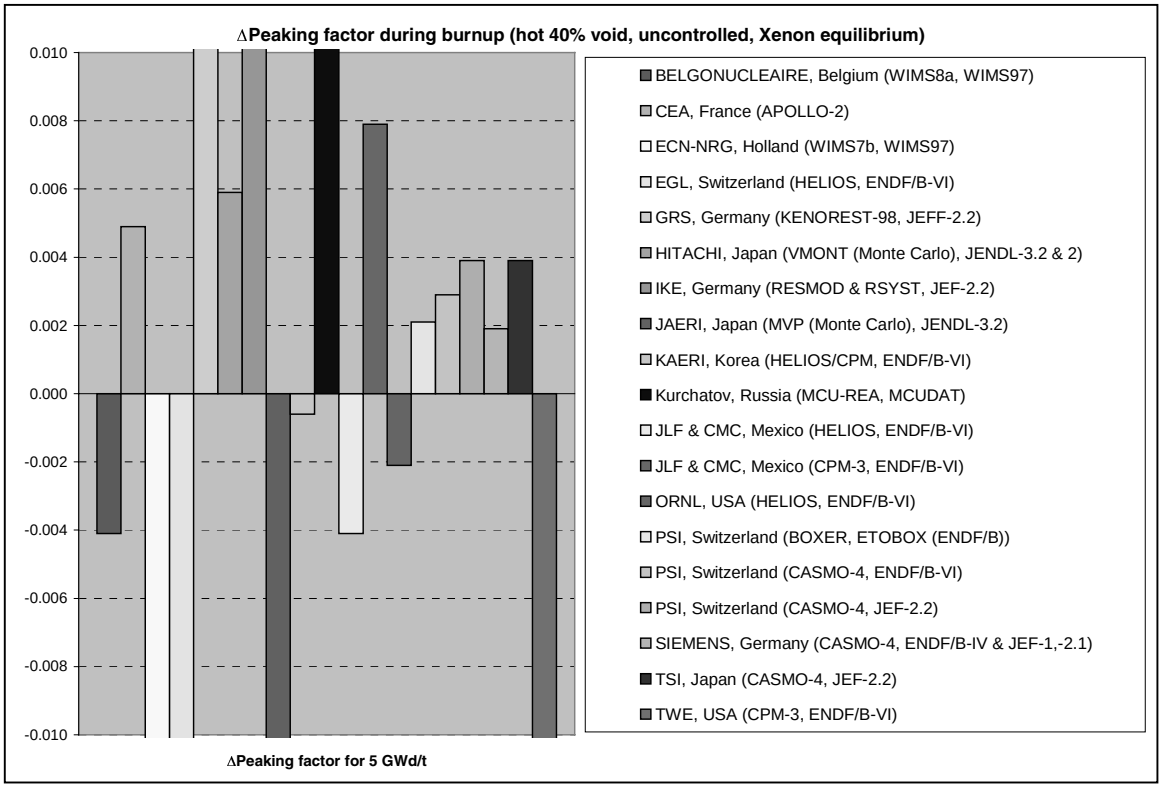
ΔPeaking factor during burnup (hot 40% void, uncontrolled, Xenon equilibrium)
0.010
0.008
0.006
0.004
0.002
0.000
-0.002
-0.004
-0.006
-0.008
-0.010
ΔPeaking factor for 5 GWd/t
BELGONUCLEAIRE, Belgium (WIMS8a, WIMS97)
CEA, France (APOLLO-2)
ECN-NRG, Holland (WIMS7b, WIMS97)
EGL, Switzerland (HELIOS, ENDF/B-VI)
GRS, Germany (KENOREST-98, JEFF-2.2)
HITACHI, Japan (VMONT (Monte Carlo), JENDL-3.2 & 2)
IKE, Germany (RESMOD & RSYST, JEF-2.2)
JAERI, Japan (MVP (Monte Carlo), JENDL-3.2)
KAERI, Korea (HELIOS/CPM, ENDF/B-VI)
Kurchatov, Russia (MCU-REA, MCUDAT)
JLF & CMC, Mexico (HELIOS, ENDF/B-VI)
JLF & CMC, Mexico (CPM-3, ENDF/B-VI)
ORNL, USA (HELIOS, ENDF/B-VI)
PSI, Switzerland (BOXER, ETOBOX (ENDF/B))
PSI, Switzerland (CASMO-4, ENDF/B-VI)
PSI, Switzerland (CASMO-4, JEF-2.2)
SIEMENS, Germany (CASMO-4, ENDF/B-IV & JEF-1,-2.1)
TSI, Japan (CASMO-4, JEF-2.2)
TWE, USA (CPM-3, ENDF/B-VI)

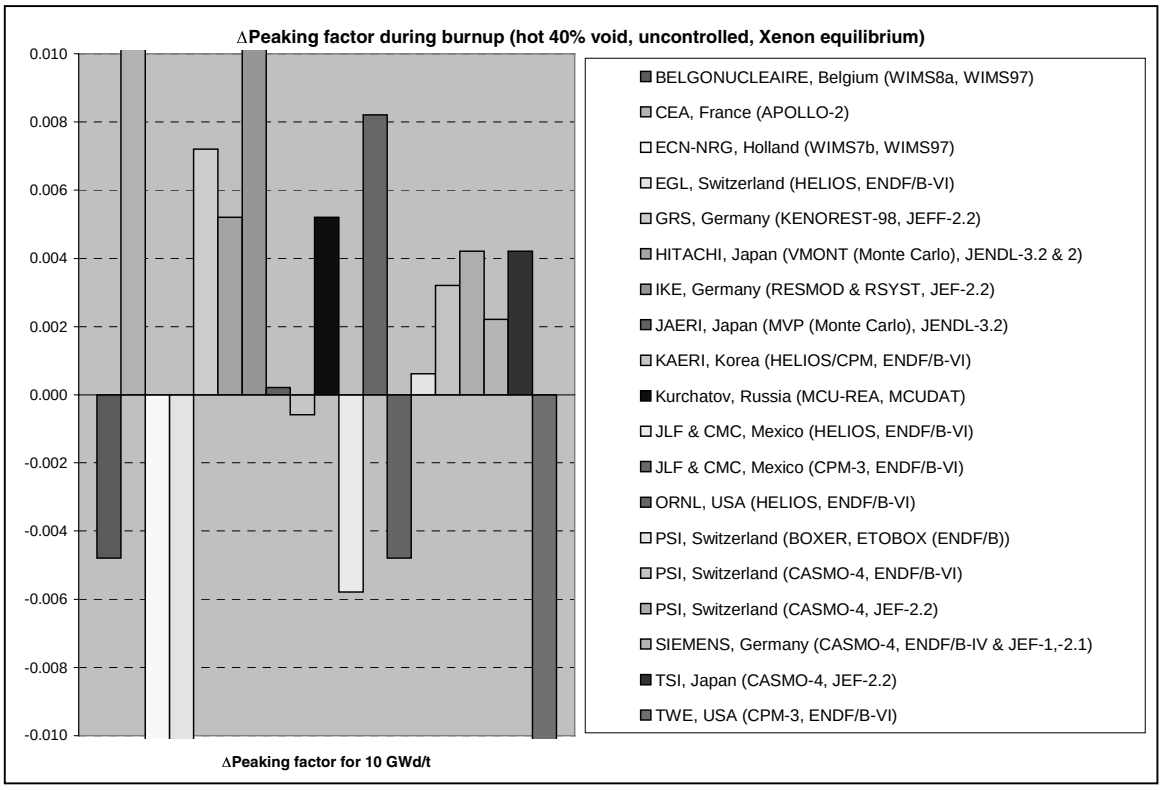
ΔPeaking factor during burnup (hot 40% void, uncontrolled, Xenon equilibrium)
0.010
0.008
0.006
0.004
0.002
0.000
-0.002
-0.004
-0.006
-0.008
-0.010
ΔPeaking factor for 10 GWd/t
BELGONUCLEAIRE, Belgium (WIMS8a, WIMS97)
CEA, France (APOLLO-2)
ECN-NRG, Holland (WIMS7b, WIMS97)
EGL, Switzerland (HELIOS, ENDF/B-VI)
GRS, Germany (KENOREST-98, JEFF-2.2)
HITACHI, Japan (VMONT (Monte Carlo), JENDL-3.2 & 2)
IKE, Germany (RESMOD & RSYST, JEF-2.2)
JAERI, Japan (MVP (Monte Carlo), JENDL-3.2)
KAERI, Korea (HELIOS/CPM, ENDF/B-VI)
Kurchatov, Russia (MCU-REA, MCUDAT)
JLF & CMC, Mexico (HELIOS, ENDF/B-VI)
JLF & CMC, Mexico (CPM-3, ENDF/B-VI)
ORNL, USA (HELIOS, ENDF/B-VI)
PSI, Switzerland (BOXER, ETOBOX (ENDF/B))
PSI, Switzerland (CASMO-4, ENDF/B-VI)
PSI, Switzerland (CASMO-4, JEF-2.2)
SIEMENS, Germany (CASMO-4, ENDF/B-IV & JEF-1,-2.1)
TSI, Japan (CASMO-4, JEF-2.2)
TWE, USA (CPM-3, ENDF/B-VI)

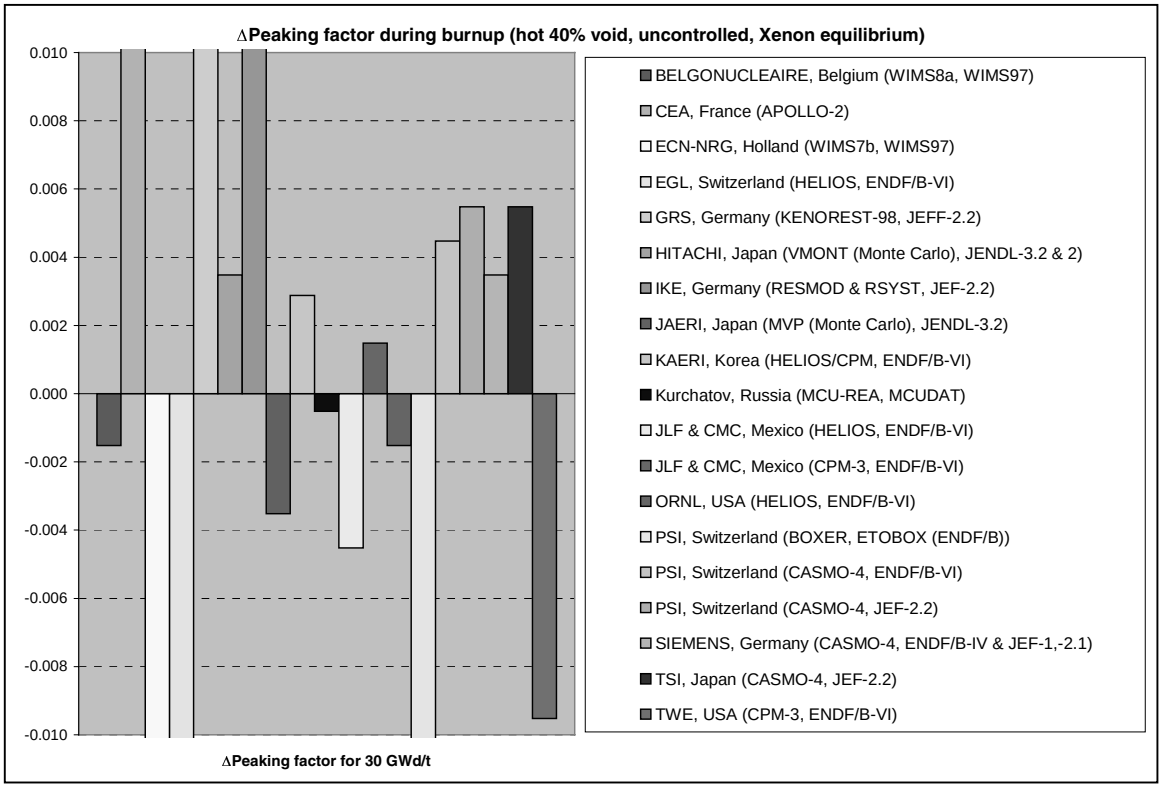
ΔPeaking factor during burnup (hot 40% void, uncontrolled, Xenon equilibrium)
0.010
0.008
0.006
0.004
0.002
0.000
-0.002
-0.004
-0.006
-0.008
-0.010
ΔPeaking factor for 30 GWd/t
BELGONUCLEAIRE, Belgium (WIMS8a, WIMS97)
CEA, France (APOLLO-2)
ECN-NRG, Holland (WIMS7b, WIMS97)
EGL, Switzerland (HELIOS, ENDF/B-VI)
GRS, Germany (KENOREST-98, JEFF-2.2)
HITACHI, Japan (VMONT (Monte Carlo), JENDL-3.2 & 2)
IKE, Germany (RESMOD & RSYST, JEF-2.2)
JAERI, Japan (MVP (Monte Carlo), JENDL-3.2)
KAERI, Korea (HELIOS/CPM, ENDF/B-VI)
Kurchatov, Russia (MCU-REA, MCUDAT)
JLF & CMC, Mexico (HELIOS, ENDF/B-VI)
JLF & CMC, Mexico (CPM-3, ENDF/B-VI)
ORNL, USA (HELIOS, ENDF/B-VI)
PSI, Switzerland (BOXER, ETOBOX (ENDF/B))
PSI, Switzerland (CASMO-4, ENDF/B-VI)
PSI, Switzerland (CASMO-4, JEF-2.2)
SIEMENS, Germany (CASMO-4, ENDF/B-IV & JEF-1,-2.1)
TSI, Japan (CASMO-4, JEF-2.2)
TWE, USA (CPM-3, ENDF/B-VI)

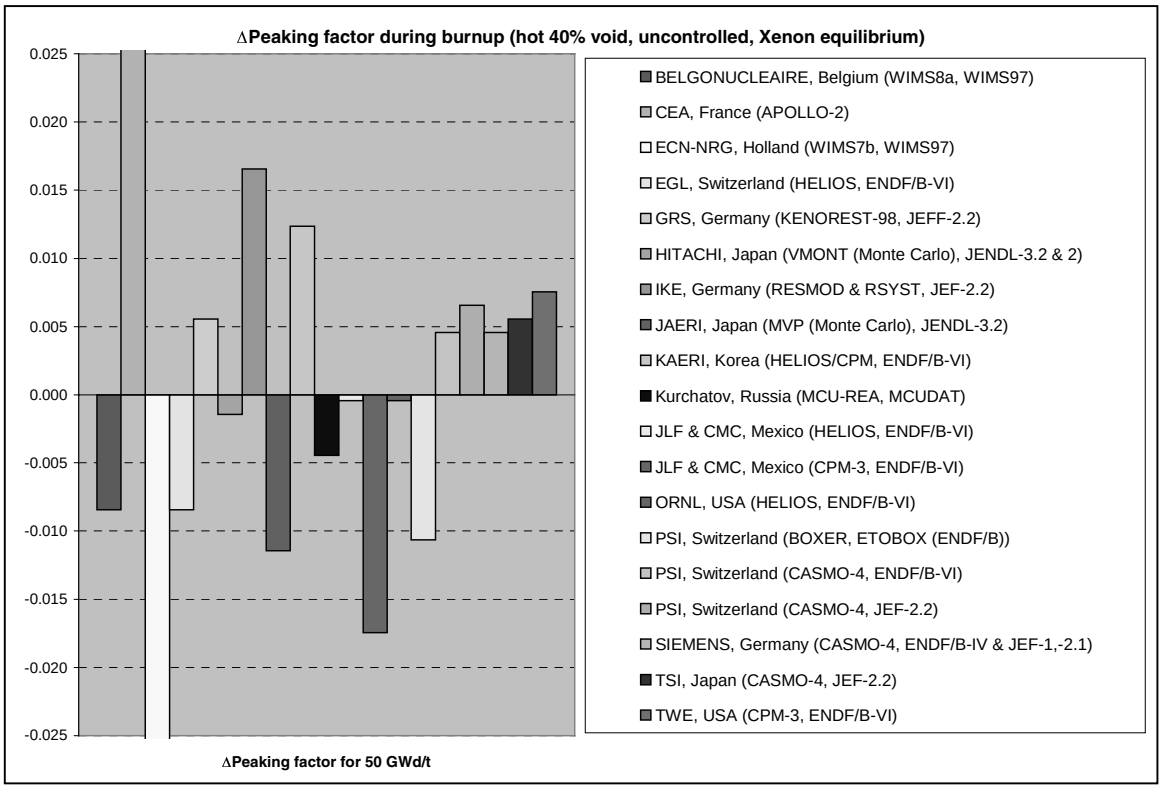
ΔPeaking factor during burnup (hot 40% void, uncontrolled, Xenon equilibrium)
0.025
0.020
0.015
0.010
0.005
0.000
-0.005
-0.010
-0.015
-0.020
-0.025
ΔPeaking factor for 50 GWd/t
BELGONUCLEAIRE, Belgium (WIMS8a, WIMS97)
CEA, France (APOLLO-2)
ECN-NRG, Holland (WIMS7b, WIMS97)
EGL, Switzerland (HELIOS, ENDF/B-VI)
GRS, Germany (KENOREST-98, JEFF-2.2)
HITACHI, Japan (VMONT (Monte Carlo), JENDL-3.2 & 2)
IKE, Germany (RESMOD & RSYST, JEF-2.2)
JAERI, Japan (MVP (Monte Carlo), JENDL-3.2)
KAERI, Korea (HELIOS/CPM, ENDF/B-VI)
Kurchatov, Russia (MCU-REA, MCUDAT)
JLF & CMC, Mexico (HELIOS, ENDF/B-VI)
JLF & CMC, Mexico (CPM-3, ENDF/B-VI)
ORNL, USA (HELIOS, ENDF/B-VI)
PSI, Switzerland (BOXER, ETOBOX (ENDF/B))
PSI, Switzerland (CASMO-4, ENDF/B-VI)
PSI, Switzerland (CASMO-4, JEF-2.2)
SIEMENS, Germany (CASMO-4, ENDF/B-IV & JEF-1,-2.1)
TSI, Japan (CASMO-4, JEF-2.2)
TWE, USA (CPM-3, ENDF/B-VI)

Gadolinium concentration during burn-up

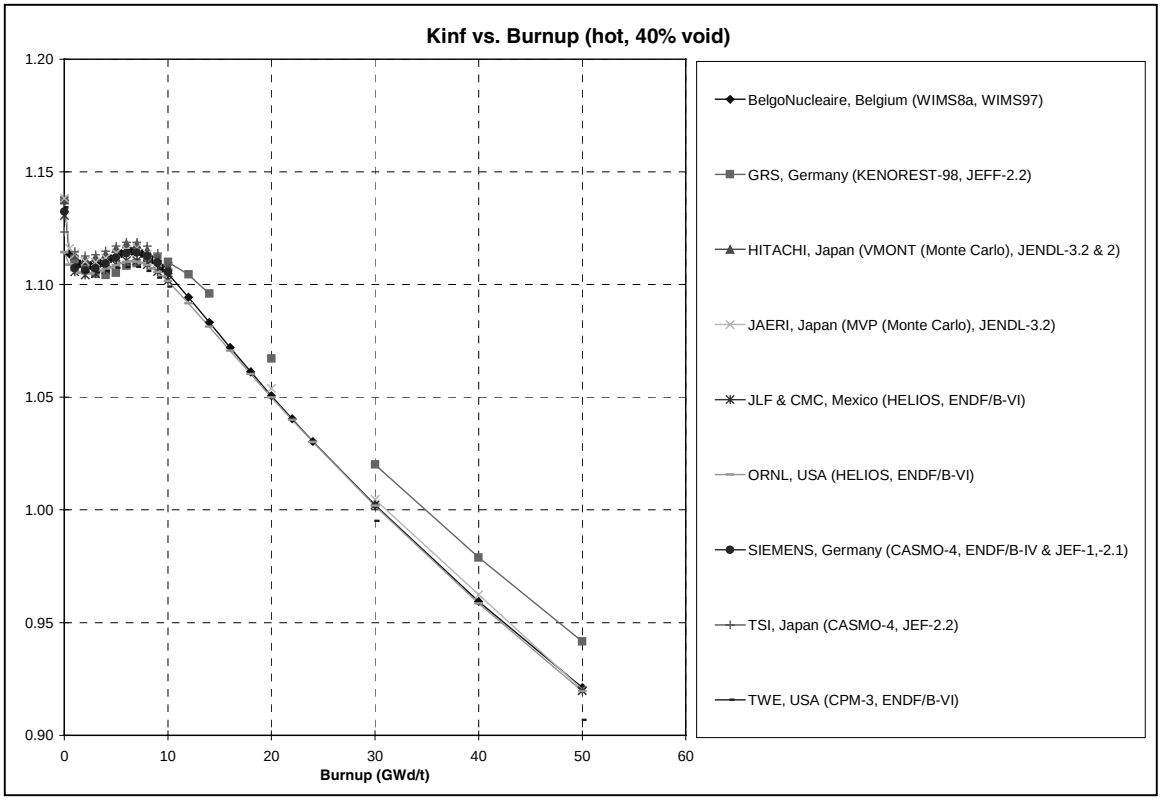

The figure shows k_{inf} as a function of burn-up, with small burn-up steps up to 10 GWd/t to resolve the rapid variation due to gadolinia depletion between 0 and 10 GWd/t. The use of gadolinia to hold down excess reactivity early in life is an essential feature of BWRs. The depletion behaviour of the gadolinia affects both reactivity as a function of burn-up and the radial flux/fission rate distribution. The gadolinia depletion is a strongly local effect and is difficult to calculate due to a combination of strong self-shielding and rapid burn-out effects.

Thus, the calculation of the depletion reactivity and peak factor might be expected to show significant differences due to nuclear data and the methods (self-shielding, predictor-corrector methods for depletion behaviour, spatial resolution of gadolinia rods, etc.).We therefore present more detailed information on reactivity and the gadolinia concentration during burn-up.

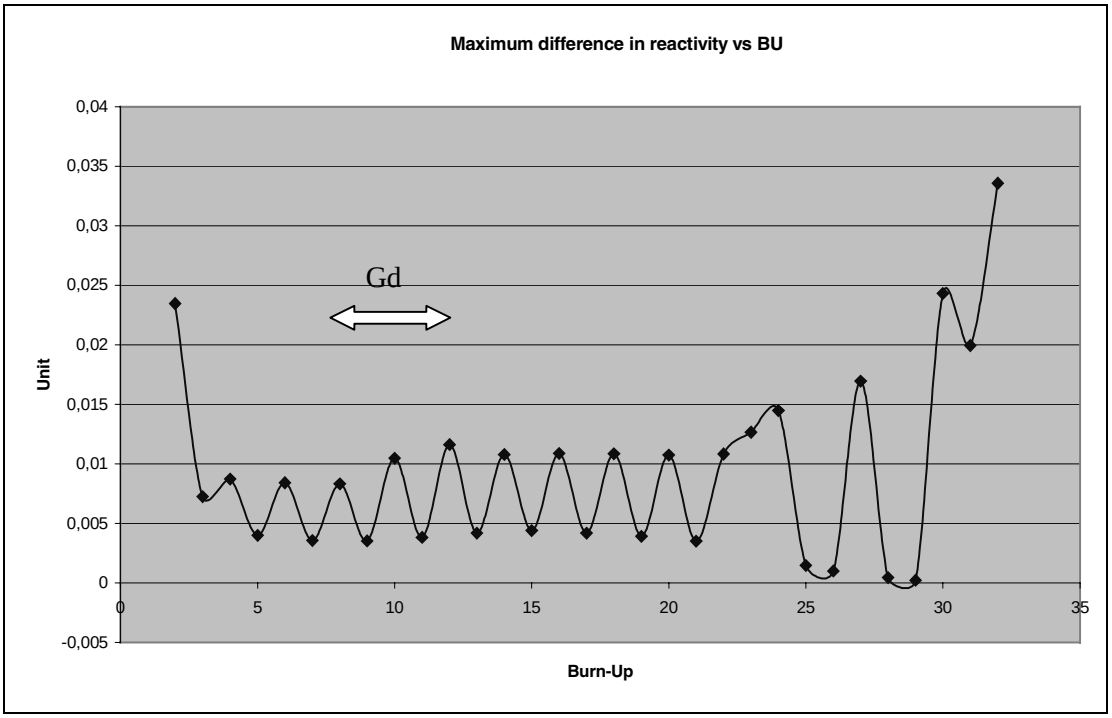

The figure above shows the maximum range of values seen on k_{inf} and its variation with burn-up. The oscillatory effect is due to different participants reporting the gadolinia depletion at different burn-up steps. The differences are quite small for most of the depletion (<1%) but increase at high burn-ups. It is the behaviour between 0 and 10 GWd/t that is important, when the gadolinia has a strong influence on k_{inf}. At higher burn-ups the deviation increases. This must be due to other effects associated with the fuel depletion, since by then the gadolinia has been depleted down to levels where it can have no impact.

Following table and figures shows that the differences in ^{155}Gd, one of the heavily absorbing gadolinia isotopes, increasing during burn-up. However, at 10 GWd/t, the concentration of ^{155}Gd is reduced by a factor 30, so that the impact on reactivity is strongly reduced. The range of deviations starts off at zero since all participants started with the same initial concentration. As might be expected, errors accumulate during burn-up leading to quite a large range of deviations at 10 GWd/t, with some clearly anomalous solutions. Large relative errors could reasonably be expected on a parameter which is decreasing rapidly with burn-up.

^{155}Gd concentration [10^{24} a/cm^3]	2 GWd/t	5 GWd/t	8 GWd/t	10 GWd/t
Average =>	8.7689E-07	4.2269E-07	9.4965E-08	3.6605E-05
Discrepancy max. =>	0.92%	-61.68%	19.50%	263%
Discrepancy min. =>	-1.48%	-9.58%	-26.25%	-36.78%
Average discrepancies (min./max.) =>	0.55%	10.50%	11.52%	45.47%
Average without extreme values =>	8.7739E-07	4.0357E-07	9.5610E-08	3.0351E-08
Average discrepancies (min./max.) =>	0.39%	4.92%	8.68%	22.22%

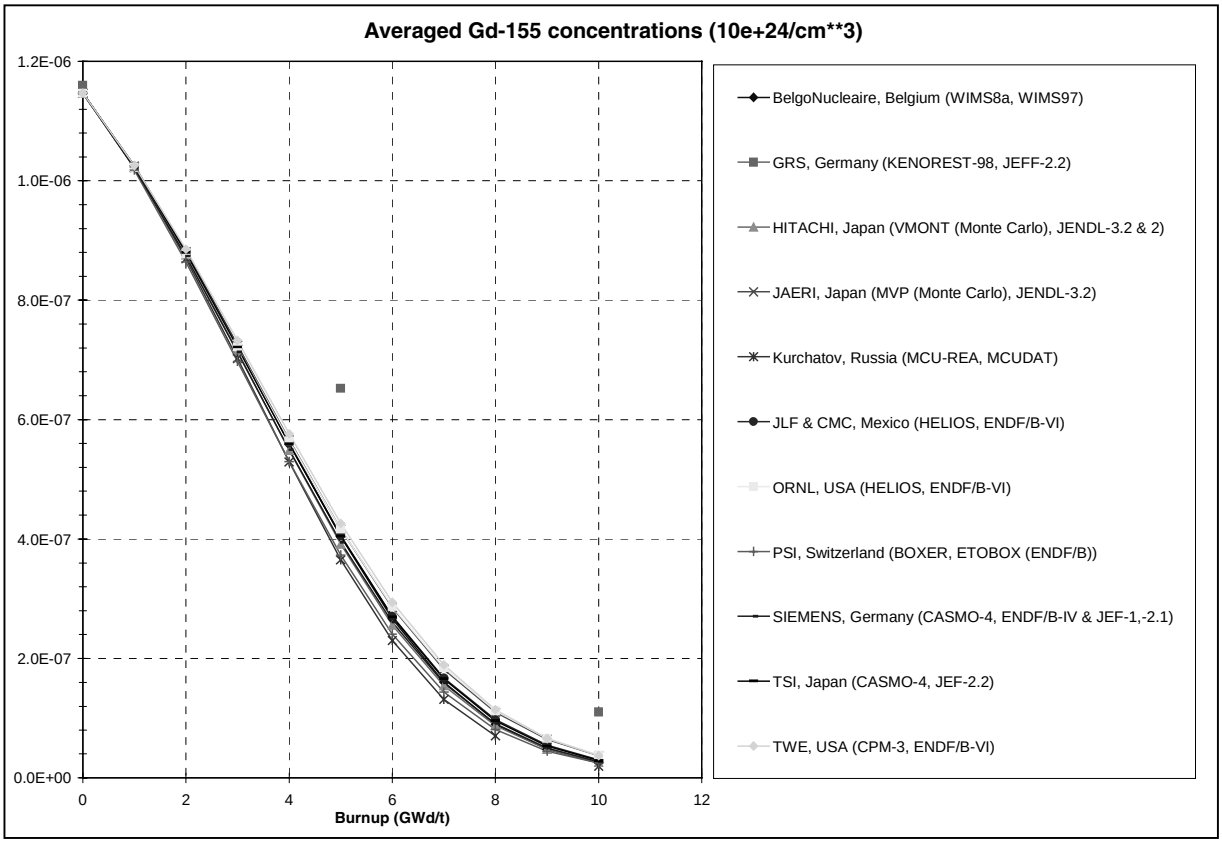

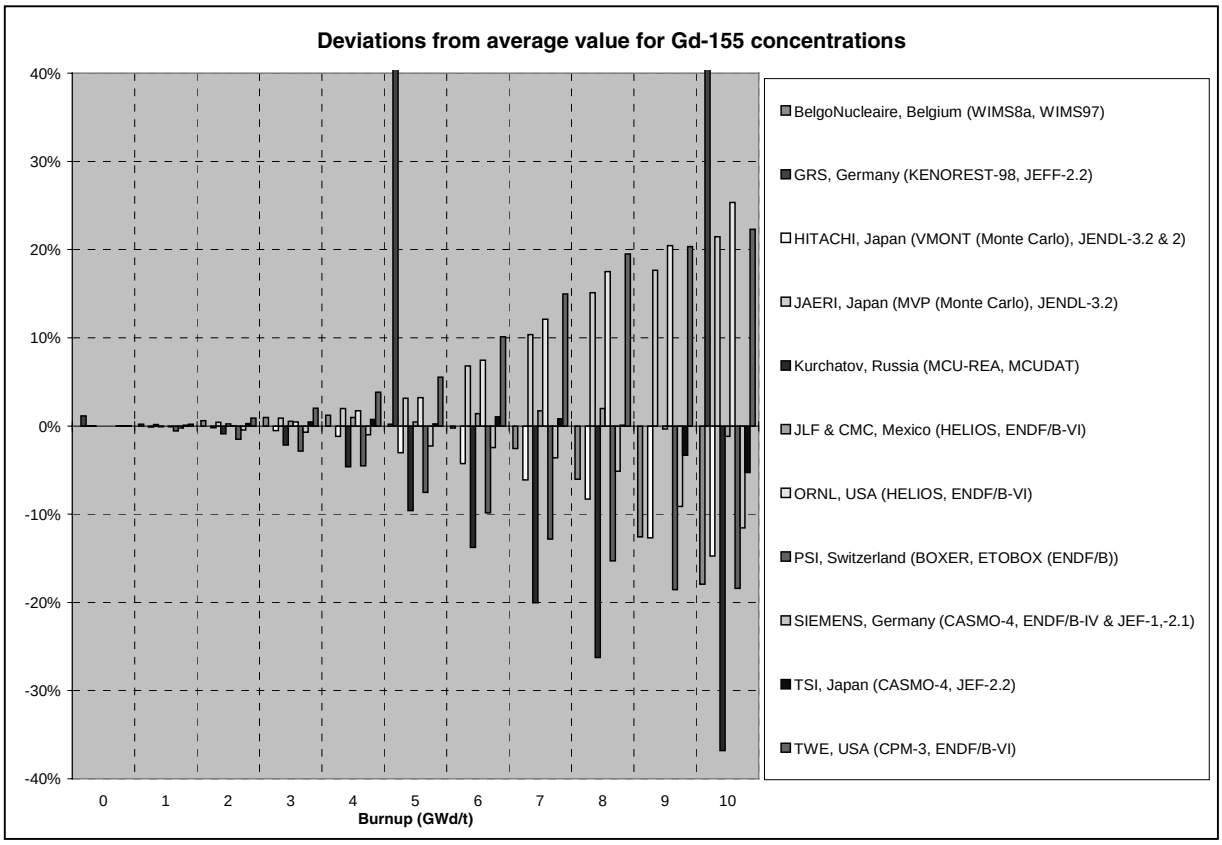

A comparison of the concentrations of ^{157}Gd versus burn-up is given in the following table and figures. For ^{157}Gd the kinetics of its burn-out is faster, due to its cross-section being even higher than for ^{155}Gd and the discrepancies are correspondingly larger and grow more quickly.

^{157}Gd concentration [10^{24} a/cm^3]	**2 GWd/t**	**5 GWd/t**	**8 GWd/t**	**10 GWd/t**
Average =>	5.3403E-07	6.8647E-08	3.2055E-09	2.7910E-09
Discrepancy max. =>	3.54%	180%	83.83%	111%
Discrepancy min. =>	-4.25%	-27.32%	-34.77%	-37.59%
Average discrepancies (min./max.) =>	1.84%	16.83%	23.98%	47.07%
Average without extreme values =>	5.3441E-07	6.0289E-08	3.0556E-09	2.6172E-09
Average discrepancies (min./max.) =>	1.33%	16.83%	23.98%	41.06%

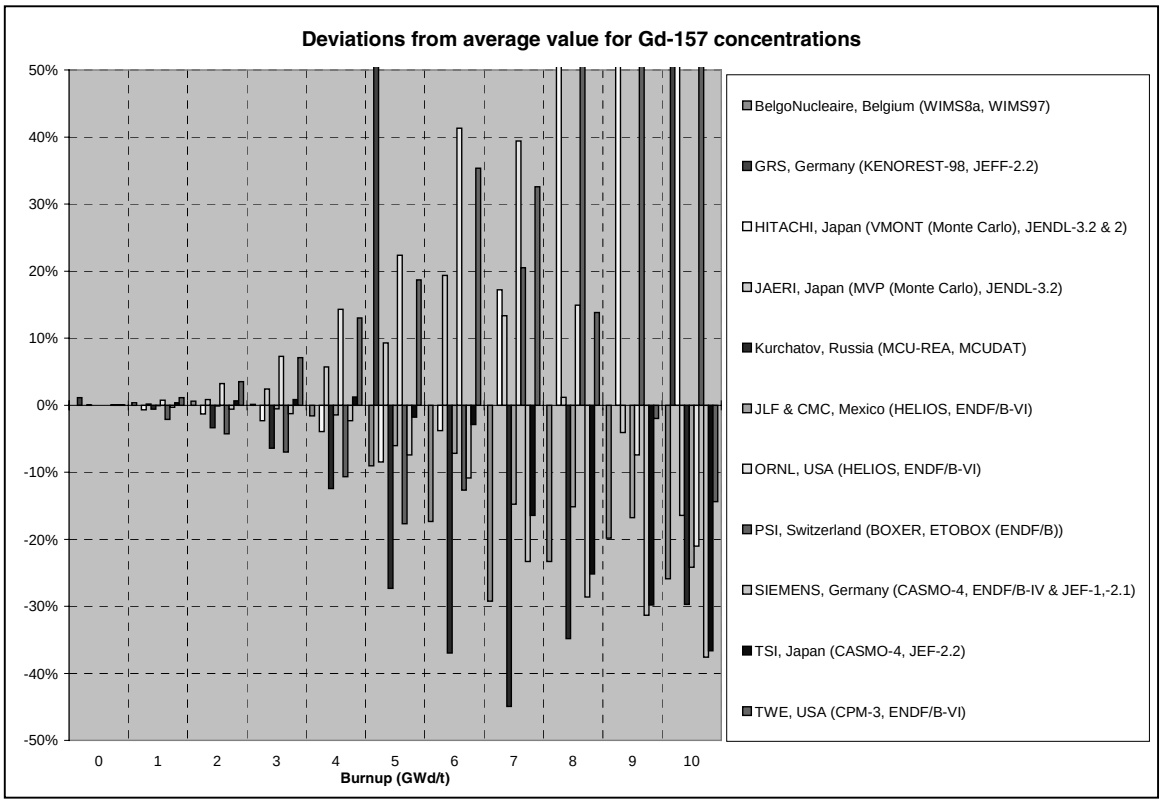

As the following figure shows, the relative absorption rate for Gd isotopes is reduced by more than a factor 10 at 10 GWd/t after which it maintains a nearly constant level.

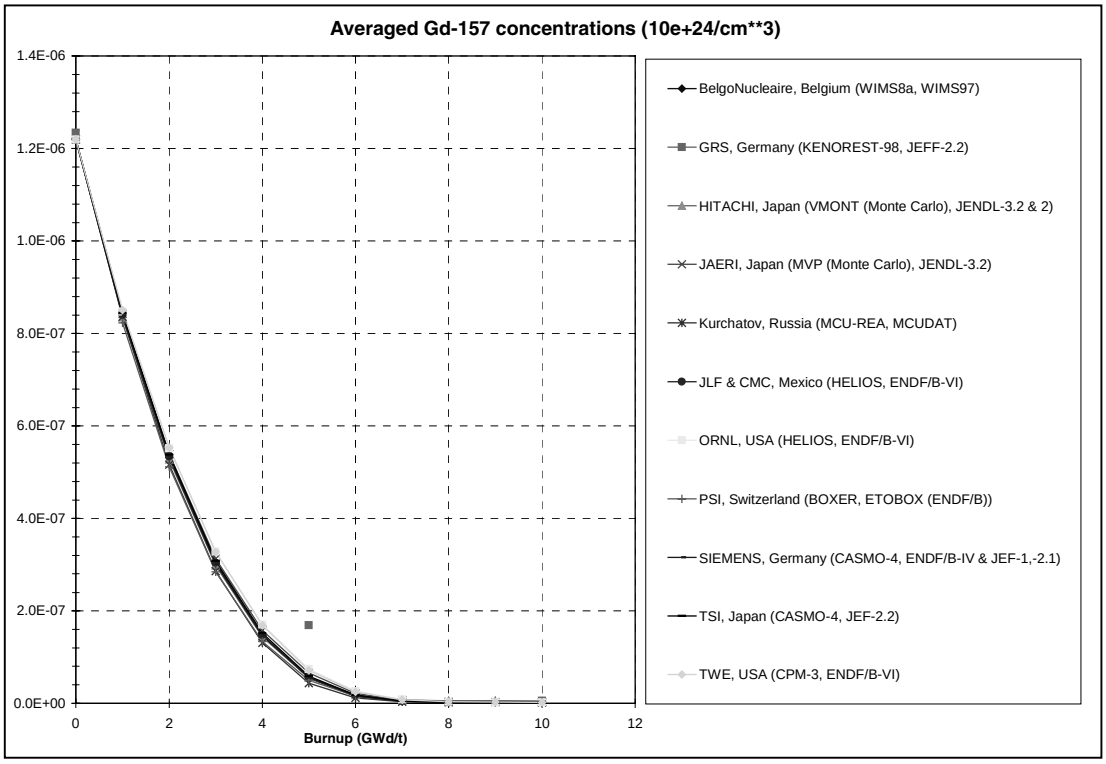

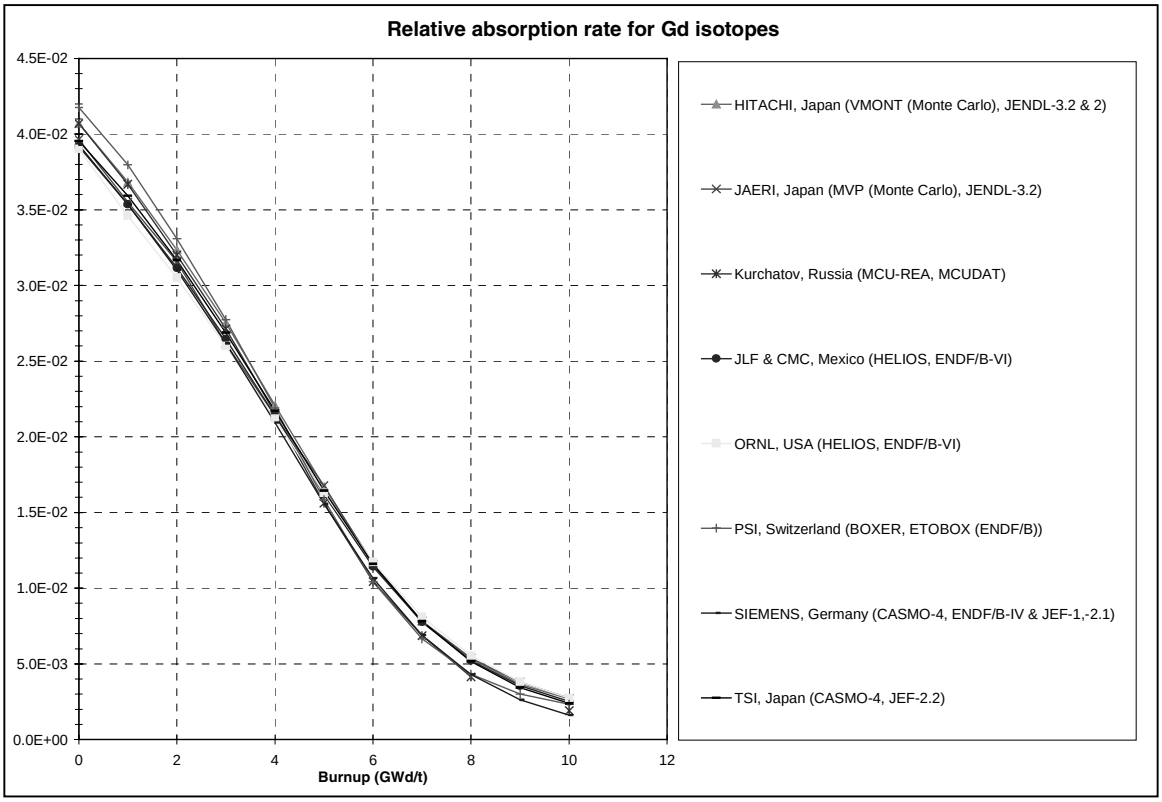
Relative absorption rate for Gd isotopes
4.5E-02
4.0E-02
3.5E-02
3.0E-02
2.5E-02
2.0E-02
1.5E-02
1.0E-02
5.0E-03
0.0E+00
0
2
4
6
8
10
12
Burnup (GWd/t)
HITACHI, Japan (VMONT (Monte Carlo), JENDL-3.2 & 2)
JAERI, Japan (MVP (Monte Carlo), JENDL-3.2)
Kurchatov, Russia (MCU-REA, MCUDAT)
JLF & CMC, Mexico (HELIOS, ENDF/B-VI)
ORNL, USA (HELIOS, ENDF/B-VI)
PSI, Switzerland (BOXER, ETOBOX (ENDF/B))
SIEMENS, Germany (CASMO-4, ENDF/B-IV & JEF-1,-2.1)
TSI, Japan (CASMO-4, JEF-2.2)

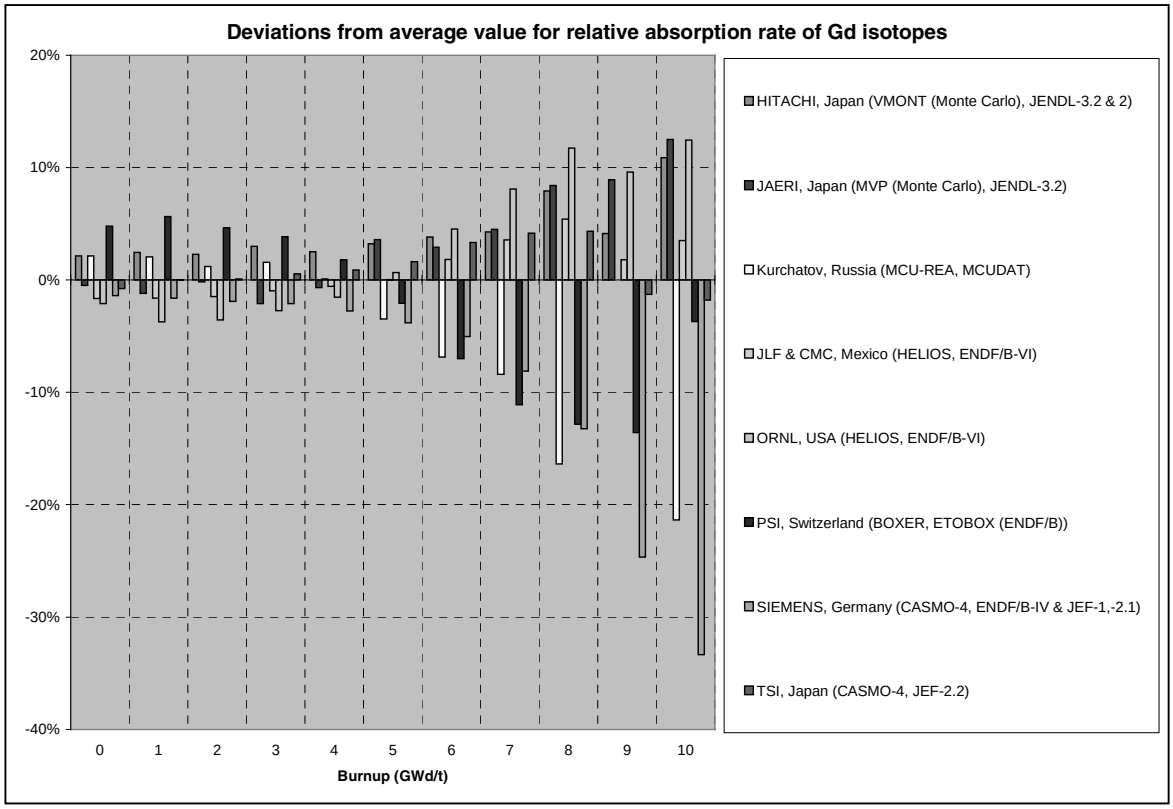
Deviations from average value for relative absorption rate of Gd isotopes
20%
10%
0%
-10%
-20%
-30%
-40%
0
1
2
3
4
5
6
7
8
9
10
Burnup (GWd/t)
HITACHI, Japan (VMONT (Monte Carlo), JENDL-3.2 & 2)
JAERI, Japan (MVP (Monte Carlo), JENDL-3.2)
Kurchatov, Russia (MCU-REA, MCUDAT)
JLF & CMC, Mexico (HELIOS, ENDF/B-VI)
ORNL, USA (HELIOS, ENDF/B-VI)
PSI, Switzerland (BOXER, ETOBOX (ENDF/B))
SIEMENS, Germany (CASMO-4, ENDF/B-IV & JEF-1,-2.1)
TSI, Japan (CASMO-4, JEF-2.2)

Heavy nuclide concentrations during burn-up

The following series of tables and figures show the average values, range of individual heavy nuclide concentrations and discrepancies of concentrations from average for different burn-up (see figures). These are generally in reasonable agreement, though there are outlying solutions that are clearly discrepant. Naturally, errors are largest for nuclides such as ^{244}Cm which are a long way up the chain of neutron captures and whose absolute concentration is small. The figures in this section plot the differences between the individual solutions and the true average.

^{235}U concentration (10^{24} a/cm^3)	5 GWd/t	10 GWd/t	30 GWd/t	50 GWd/t
Average =>	2.1407E-05	1.9493E-05	1.2612E-05	7.5520E-06
Discrepancy max. =>	1.05%	1.85%	5.14%	12.96%
Discrepancy min. =>	-0.46%	-1.15%	-3.92%	-8.77%
Average discrepancies (min./max.) =>	0.16%	0.39%	1.08%	2.45%
Average without extreme values =>	2.1400E-05	1.9485E-05	1.2603E-05	7.5334E-06
Average discrepancies (min./max.) =>	0.09%	0.26%	0.68%	1.46%

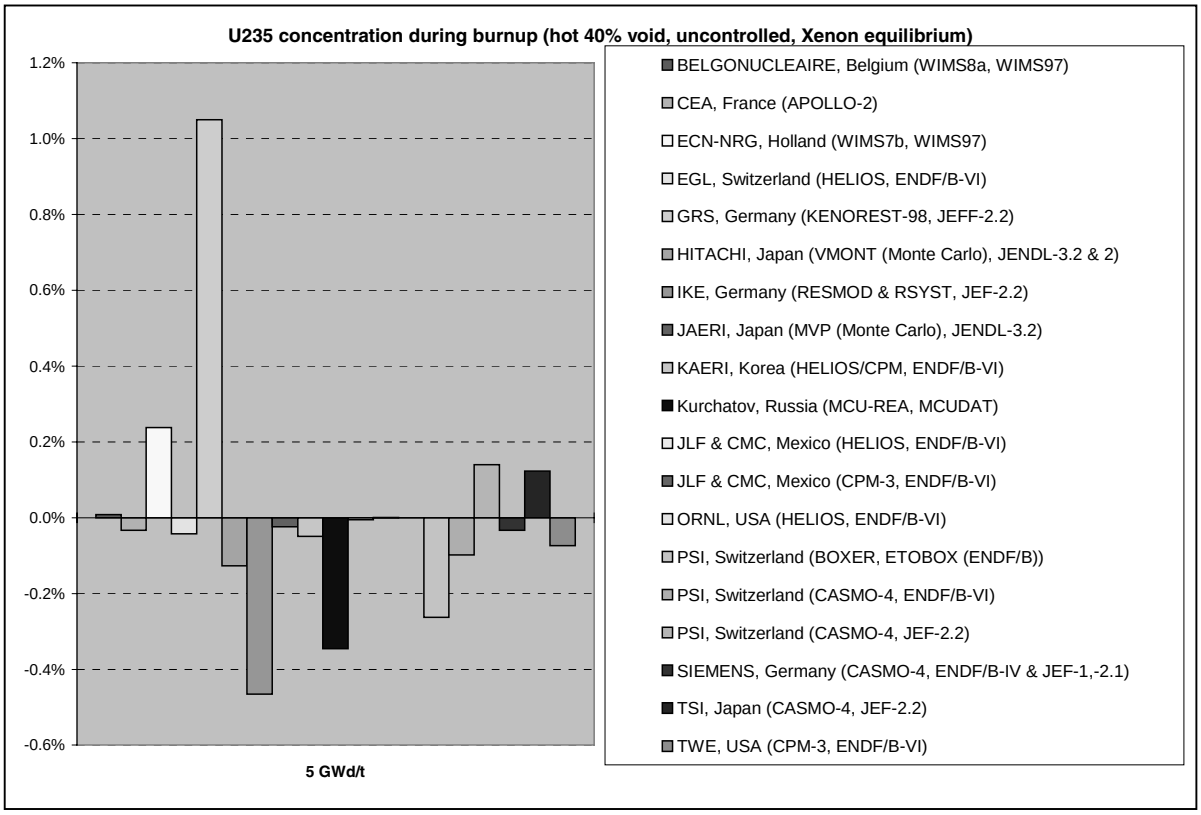

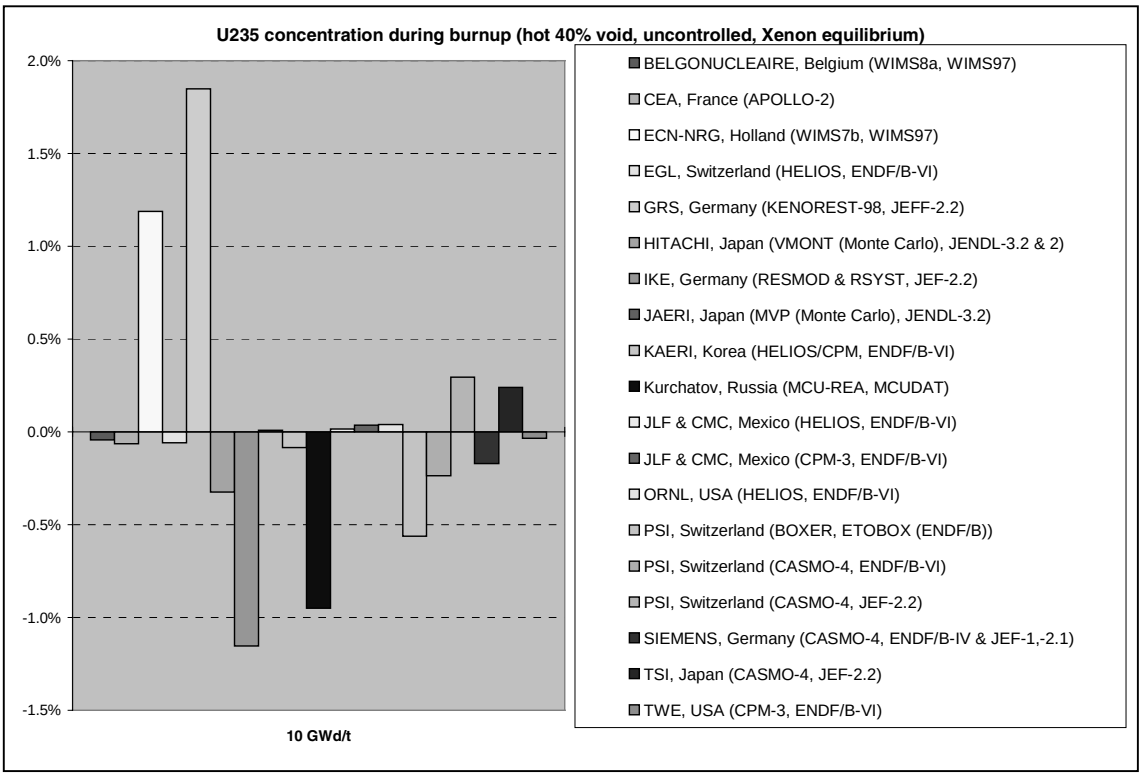
U235 concentration during burnup (hot 40% void, uncontrolled, Xenon equilibrium)
2.0%
1.5%
1.0%
0.5%
0.0%
-0.5%
-1.0%
-1.5%
10 GWd/t
BELGONUCLEAIRE, Belgium (WIMS8a, WIMS97)
CEA, France (APOLLO-2)
ECN-NRG, Holland (WIMS7b, WIMS97)
EGL, Switzerland (HELIOS, ENDF/B-VI)
GRS, Germany (KENOREST-98, JEFF-2.2)
HITACHI, Japan (VMONT (Monte Carlo), JENDL-3.2 & 2)
IKE, Germany (RESMOD & RSYST, JEF-2.2)
JAERI, Japan (MVP (Monte Carlo), JENDL-3.2)
KAERI, Korea (HELIOS/CPM, ENDF/B-VI)
Kurchatov, Russia (MCU-REA, MCUDAT)
JLF & CMC, Mexico (HELIOS, ENDF/B-VI)
JLF & CMC, Mexico (CPM-3, ENDF/B-VI)
ORNL, USA (HELIOS, ENDF/B-VI)
PSI, Switzerland (BOXER, ETOBOX (ENDF/B))
PSI, Switzerland (CASMO-4, ENDF/B-VI)
PSI, Switzerland (CASMO-4, JEF-2.2)
SIEMENS, Germany (CASMO-4, ENDF/B-IV & JEF-1,-2.1)
TSI, Japan (CASMO-4, JEF-2.2)
TWE, USA (CPM-3, ENDF/B-VI)

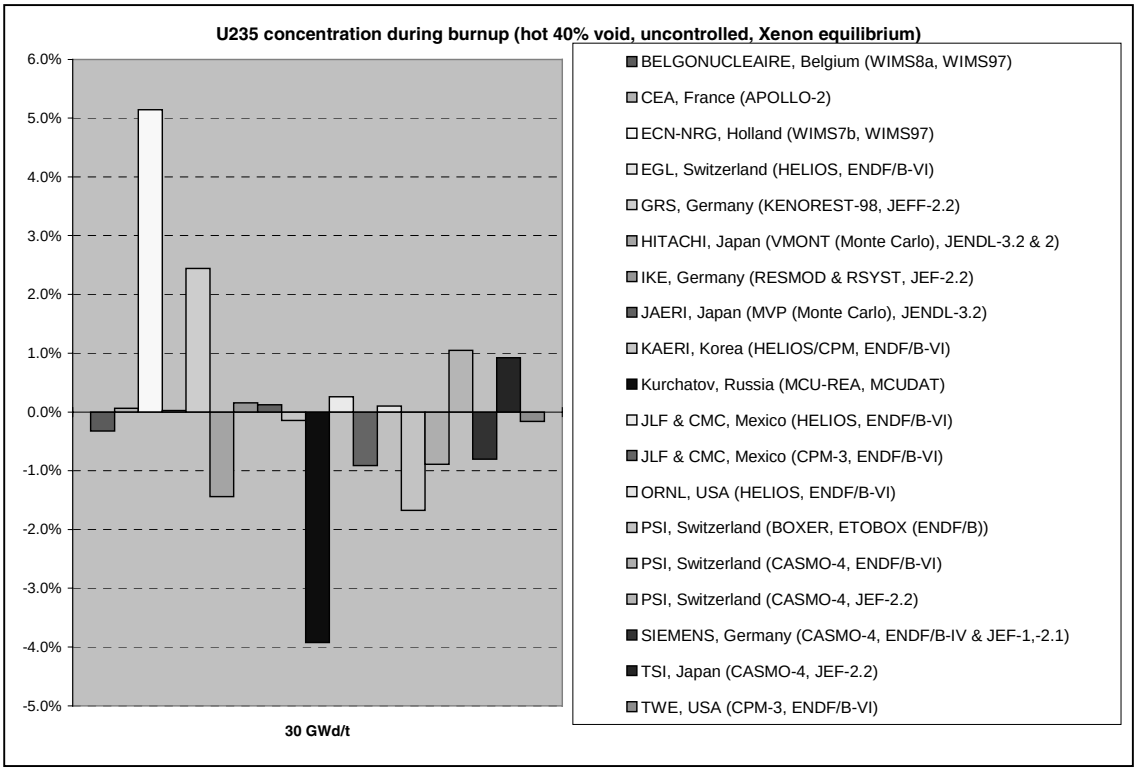
U235 concentration during burnup (hot 40% void, uncontrolled, Xenon equilibrium)
6.0%
5.0%
4.0%
3.0%
2.0%
1.0%
0.0%
-1.0%
-2.0%
-3.0%
-4.0%
-5.0%
30 GWd/t
BELGONUCLEAIRE, Belgium (WIMS8a, WIMS97)
CEA, France (APOLLO-2)
ECN-NRG, Holland (WIMS7b, WIMS97)
EGL, Switzerland (HELIOS, ENDF/B-VI)
GRS, Germany (KENOREST-98, JEFF-2.2)
HITACHI, Japan (VMONT (Monte Carlo), JENDL-3.2 & 2)
IKE, Germany (RESMOD & RSYST, JEF-2.2)
JAERI, Japan (MVP (Monte Carlo), JENDL-3.2)
KAERI, Korea (HELIOS/CPM, ENDF/B-VI)
Kurchatov, Russia (MCU-REA, MCUDAT)
JLF & CMC, Mexico (HELIOS, ENDF/B-VI)
JLF & CMC, Mexico (CPM-3, ENDF/B-VI)
ORNL, USA (HELIOS, ENDF/B-VI)
PSI, Switzerland (BOXER, ETOBOX (ENDF/B))
PSI, Switzerland (CASMO-4, ENDF/B-VI)
PSI, Switzerland (CASMO-4, JEF-2.2)
SIEMENS, Germany (CASMO-4, ENDF/B-IV & JEF-1,-2.1)
TSI, Japan (CASMO-4, JEF-2.2)
TWE, USA (CPM-3, ENDF/B-VI)

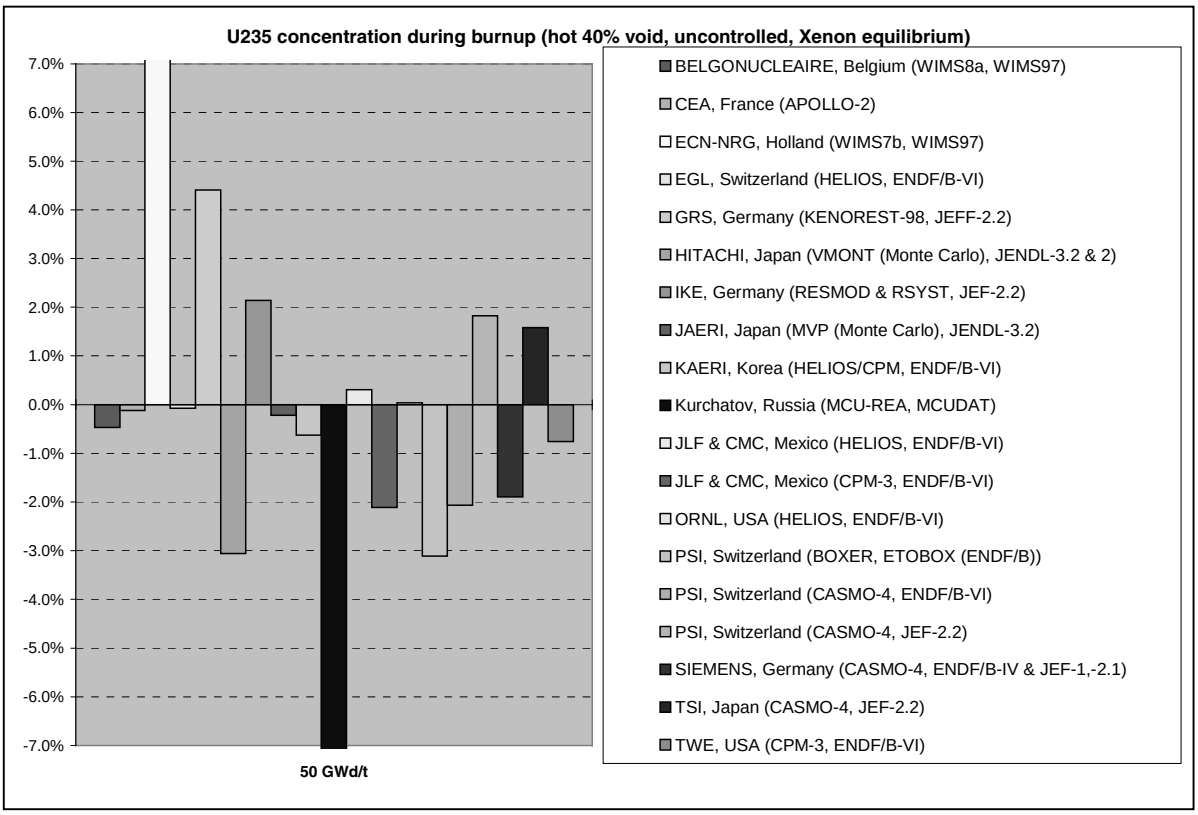

^{238}U concentration (10^{24} a/cm^3)	5 GWd/t	10 GWd/t	30 GWd/t	50 GWd/t
Average =>	4.9187E-03	4.9042E-03	4.8404E-03	4.7701E-03
Discrepancy max. =>	0.01%	0.13%	0.09%	0.08%
Discrepancy min. =>	-0.04%	-0.09%	-0.24%	-0.36%
Average discrepancies (min./max.) =>	0.01%	0.02%	0.04%	0.06%
Average without extreme values =>	4.9188E-03	4.9041E-03	4.8408E-03	4.7709E-03
Average discrepancies (min./max.) =>	0.01%	0.01%	0.02%	0.04%

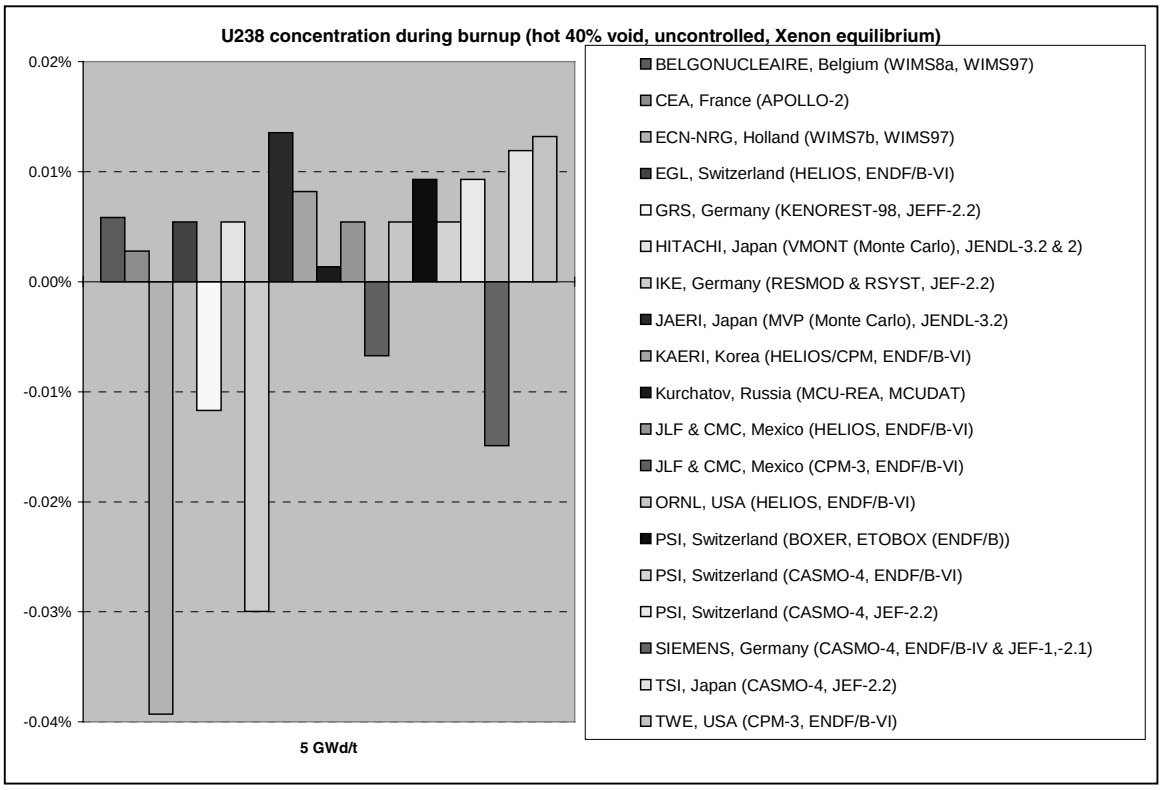
U238 concentration during burnup (hot 40% void, uncontrolled, Xenon equilibrium)
0.02%
0.01%
0.00%
-0.01%
-0.02%
-0.03%
-0.04%
5 GWd/t
BELGONUCLEAIRE, Belgium (WIMS8a, WIMS97)
CEA, France (APOLLO-2)
ECN-NRG, Holland (WIMS7b, WIMS97)
EGL, Switzerland (HELIOS, ENDF/B-VI)
GRS, Germany (KENOREST-98, JEFF-2.2)
HITACHI, Japan (VMONT (Monte Carlo), JENDL-3.2 & 2)
IKE, Germany (RESMOD & RSYST, JEF-2.2)
JAERI, Japan (MVP (Monte Carlo), JENDL-3.2)
KAERI, Korea (HELIOS/CPM, ENDF/B-VI)
Kurchatov, Russia (MCU-REA, MCUDAT)
JLF & CMC, Mexico (HELIOS, ENDF/B-VI)
JLF & CMC, Mexico (CPM-3, ENDF/B-VI)
ORNL, USA (HELIOS, ENDF/B-VI)
PSI, Switzerland (BOXER, ETOBOX (ENDF/B))
PSI, Switzerland (CASMO-4, ENDF/B-VI)
PSI, Switzerland (CASMO-4, JEF-2.2)
SIEMENS, Germany (CASMO-4, ENDF/B-IV & JEF-1,-2.1)
TSI, Japan (CASMO-4, JEF-2.2)
TWE, USA (CPM-3, ENDF/B-VI)

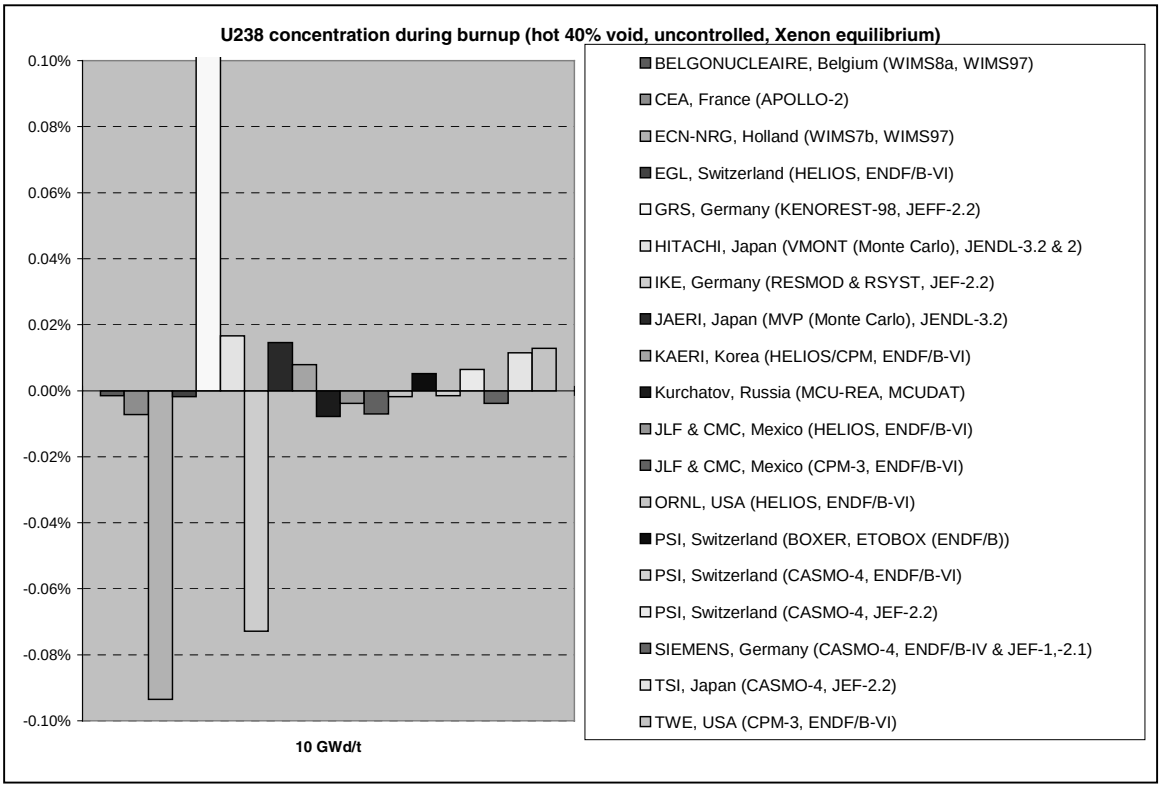
U238 concentration during burnup (hot 40% void, uncontrolled, Xenon equilibrium)
0.10%
0.08%
0.06%
0.04%
0.02%
0.00%
-0.02%
-0.04%
-0.06%
-0.08%
-0.10%
10 GWd/t
BELGONUCLEAIRE, Belgium (WIMS8a, WIMS97)
CEA, France (APOLLO-2)
ECN-NRG, Holland (WIMS7b, WIMS97)
EGL, Switzerland (HELIOS, ENDF/B-VI)
GRS, Germany (KENOREST-98, JEFF-2.2)
HITACHI, Japan (VMONT (Monte Carlo), JENDL-3.2 & 2)
IKE, Germany (RESMOD & RSYST, JEF-2.2)
JAERI, Japan (MVP (Monte Carlo), JENDL-3.2)
KAERI, Korea (HELIOS/CPM, ENDF/B-VI)
Kurchatov, Russia (MCU-REA, MCUDAT)
JLF & CMC, Mexico (HELIOS, ENDF/B-VI)
JLF & CMC, Mexico (CPM-3, ENDF/B-VI)
ORNL, USA (HELIOS, ENDF/B-VI)
PSI, Switzerland (BOXER, ETOBOX (ENDF/B))
PSI, Switzerland (CASMO-4, ENDF/B-VI)
PSI, Switzerland (CASMO-4, JEF-2.2)
SIEMENS, Germany (CASMO-4, ENDF/B-IV & JEF-1,-2.1)
TSI, Japan (CASMO-4, JEF-2.2)
TWE, USA (CPM-3, ENDF/B-VI)

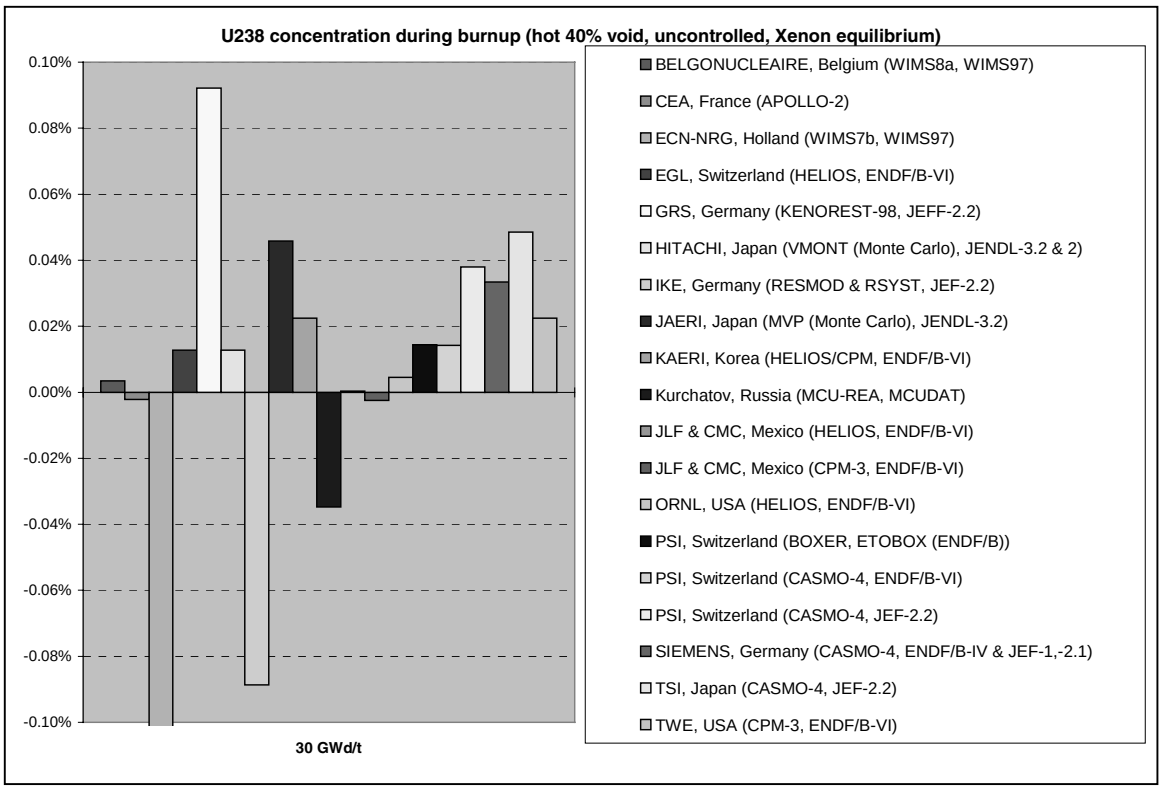
U238 concentration during burnup (hot 40% void, uncontrolled, Xenon equilibrium)
0.10%
0.08%
0.06%
0.04%
0.02%
0.00%
-0.02%
-0.04%
-0.06%
-0.08%
-0.10%
30 GWd/t
BELGONUCLEAIRE, Belgium (WIMS8a, WIMS97)
CEA, France (APOLLO-2)
ECN-NRG, Holland (WIMS7b, WIMS97)
EGL, Switzerland (HELIOS, ENDF/B-VI)
GRS, Germany (KENOREST-98, JEFF-2.2)
HITACHI, Japan (VMONT (Monte Carlo), JENDL-3.2 & 2)
IKE, Germany (RESMOD & RSYST, JEF-2.2)
JAERI, Japan (MVP (Monte Carlo), JENDL-3.2)
KAERI, Korea (HELIOS/CPM, ENDF/B-VI)
Kurchatov, Russia (MCU-REA, MCUDAT)
JLF & CMC, Mexico (HELIOS, ENDF/B-VI)
JLF & CMC, Mexico (CPM-3, ENDF/B-VI)
ORNL, USA (HELIOS, ENDF/B-VI)
PSI, Switzerland (BOXER, ETOBOX (ENDF/B))
PSI, Switzerland (CASMO-4, ENDF/B-VI)
PSI, Switzerland (CASMO-4, JEF-2.2)
SIEMENS, Germany (CASMO-4, ENDF/B-IV & JEF-1,-2.1)
TSI, Japan (CASMO-4, JEF-2.2)
TWE, USA (CPM-3, ENDF/B-VI)

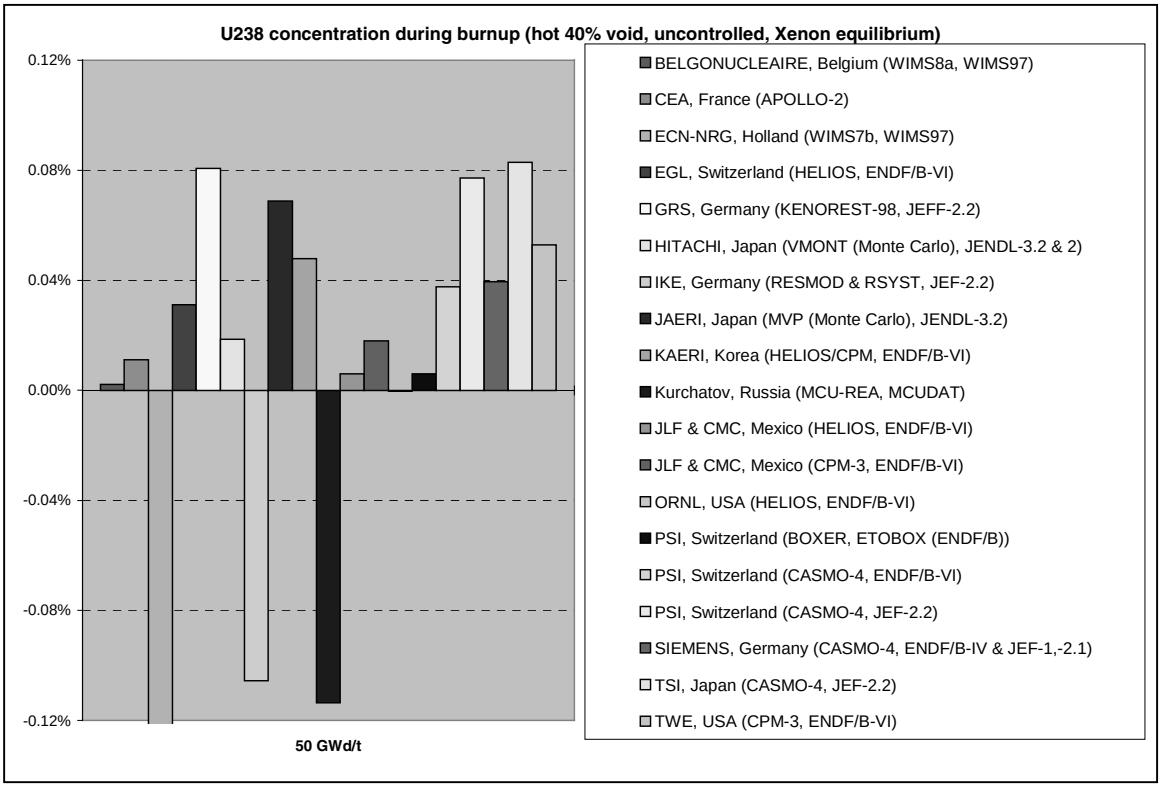
U238 concentration during burnup (hot 40% void, uncontrolled, Xenon equilibrium)
0.12%
0.08%
0.04%
0.00%
-0.04%
-0.08%
-0.12%
50 GWd/t
BELGONUCLEAIRE, Belgium (WIMS8a, WIMS97)
CEA, France (APOLLO-2)
ECN-NRG, Holland (WIMS7b, WIMS97)
EGL, Switzerland (HELIOS, ENDF/B-VI)
GRS, Germany (KENOREST-98, JEFF-2.2)
HITACHI, Japan (VMONT (Monte Carlo), JENDL-3.2 & 2)
IKE, Germany (RESMOD & RSYST, JEF-2.2)
JAERI, Japan (MVP (Monte Carlo), JENDL-3.2)
KAERI, Korea (HELIOS/CPM, ENDF/B-VI)
Kurchatov, Russia (MCU-REA, MCUDAT)
JLF & CMC, Mexico (HELIOS, ENDF/B-VI)
JLF & CMC, Mexico (CPM-3, ENDF/B-VI)
ORNL, USA (HELIOS, ENDF/B-VI)
PSI, Switzerland (BOXER, ETOBOX (ENDF/B))
PSI, Switzerland (CASMO-4, ENDF/B-VI)
PSI, Switzerland (CASMO-4, JEF-2.2)
SIEMENS, Germany (CASMO-4, ENDF/B-IV & JEF-1,-2.1)
TSI, Japan (CASMO-4, JEF-2.2)
TWE, USA (CPM-3, ENDF/B-VI)

^{238}Pu concentration (10^{24} a/cm^3)	5 GWd/t	10 GWd/t	30 GWd/t	50 GWd/t
Average =>	7.3251E-06	7.0326E-05	6.7628E-06	7.3316E-06
Discrepancy max. =>	0.34%	0.67%	3.36%	6.81%
Discrepancy min. =>	-0.44%	-0.84%	-1.62%	-5.05%
Average discrepancies (min./max.) =>	0.16%	0.29%	1.01%	2.04%
Average without extreme values =>	7.3255E-06	7.0333E-06	6.7559E-06	7.3240E-06
Average discrepancies (min./max.) =>	0.13%	0.24%	0.84%	1.59%

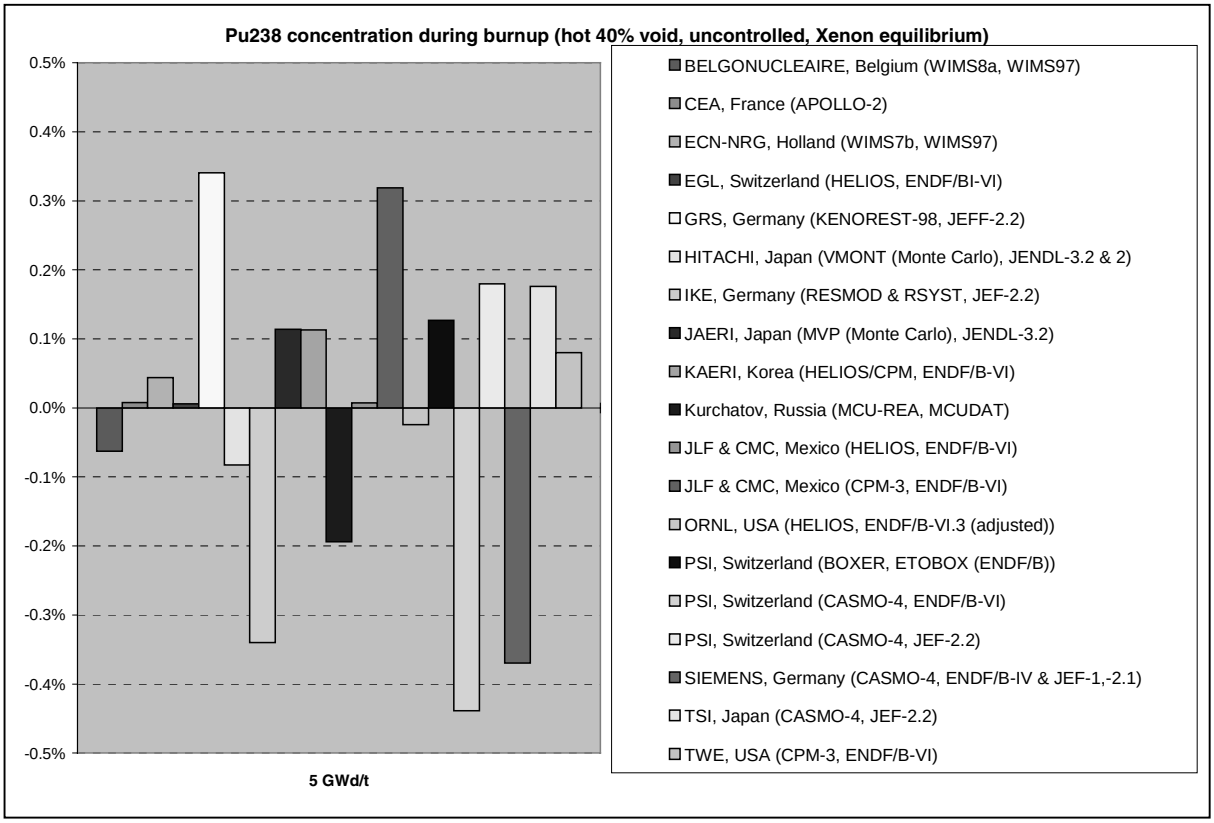

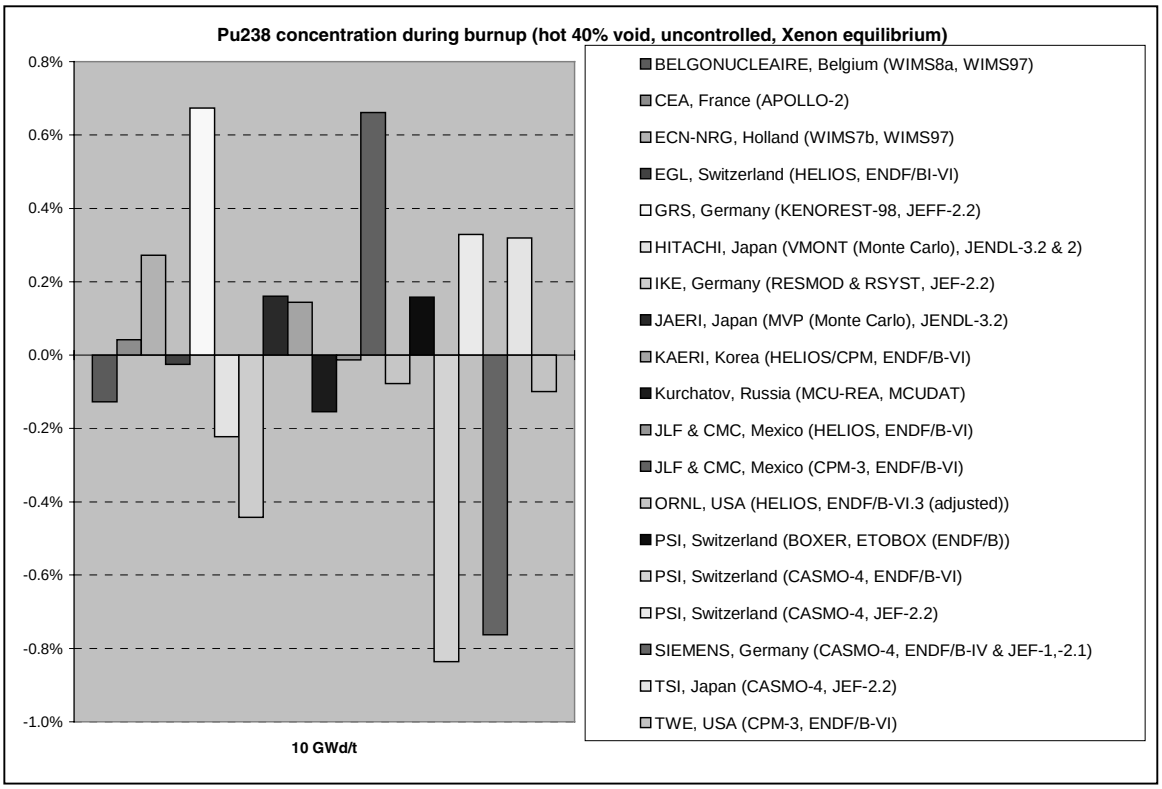
Pu238 concentration during burnup (hot 40% void, uncontrolled, Xenon equilibrium)
0.8%
0.6%
0.4%
0.2%
0.0%
-0.2%
-0.4%
-0.6%
-0.8%
-1.0%
10 GWd/t
BELGONUCLEAIRE, Belgium (WIMS8a, WIMS97)
CEA, France (APOLLO-2)
ECN-NRG, Holland (WIMS7b, WIMS97)
EGL, Switzerland (HELIOS, ENDF/BI-VI)
GRS, Germany (KENOREST-98, JEFF-2.2)
HITACHI, Japan (VMONT (Monte Carlo), JENDL-3.2 & 2)
IKE, Germany (RESMOD & RSYST, JEF-2.2)
JAERI, Japan (MVP (Monte Carlo), JENDL-3.2)
KAERI, Korea (HELIOS/CPM, ENDF/B-VI)
Kurchatov, Russia (MCU-REA, MCUDAT)
JLF & CMC, Mexico (HELIOS, ENDF/B-VI)
JLF & CMC, Mexico (CPM-3, ENDF/B-VI)
ORNL, USA (HELIOS, ENDF/B-VI.3 (adjusted))
PSI, Switzerland (BOXER, ETOBOX (ENDF/B))
PSI, Switzerland (CASMO-4, ENDF/B-VI)
PSI, Switzerland (CASMO-4, JEF-2.2)
SIEMENS, Germany (CASMO-4, ENDF/B-IV & JEF-1,-2.1)
TSI, Japan (CASMO-4, JEF-2.2)
TWE, USA (CPM-3, ENDF/B-VI)

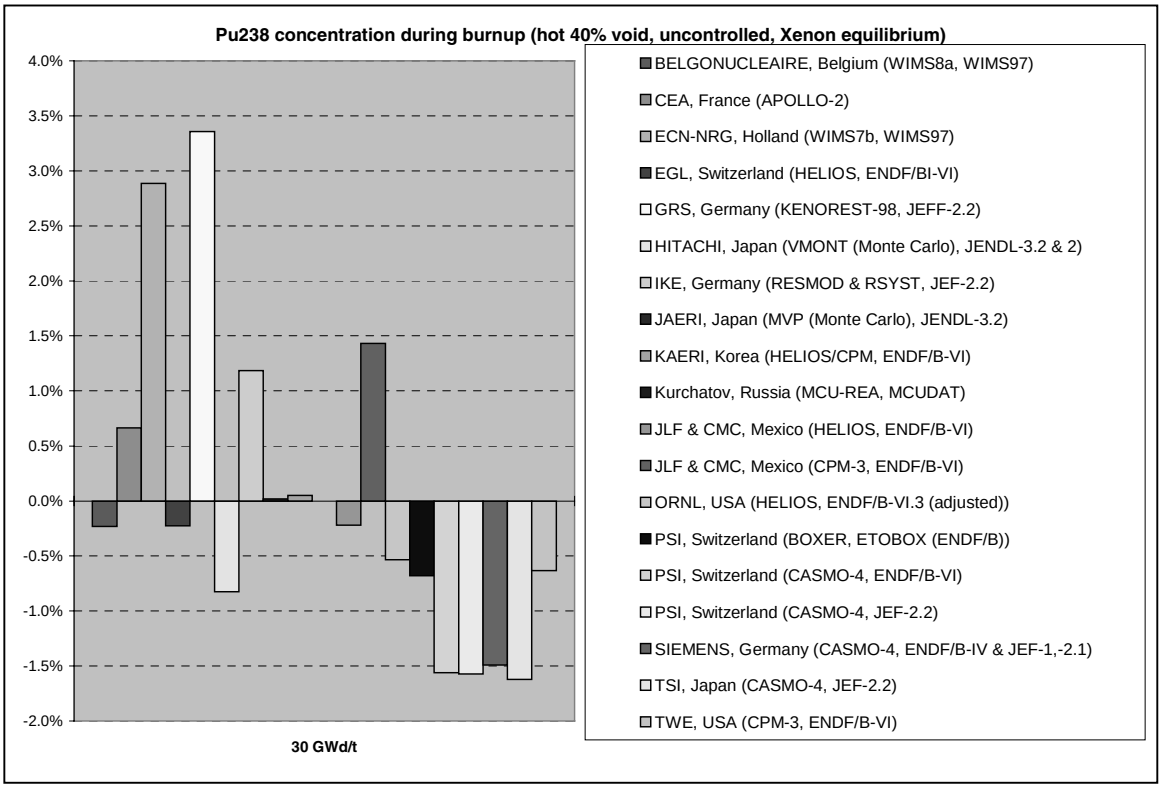
Pu238 concentration during burnup (hot 40% void, uncontrolled, Xenon equilibrium)
4.0%
3.5%
3.0%
2.5%
2.0%
1.5%
1.0%
0.5%
0.0%
-0.5%
-1.0%
-1.5%
-2.0%
30 GWd/t
BELGONUCLEAIRE, Belgium (WIMS8a, WIMS97)
CEA, France (APOLLO-2)
ECN-NRG, Holland (WIMS7b, WIMS97)
EGL, Switzerland (HELIOS, ENDF/BI-VI)
GRS, Germany (KENOREST-98, JEFF-2.2)
HITACHI, Japan (VMONT (Monte Carlo), JENDL-3.2 & 2)
IKE, Germany (RESMOD & RSYST, JEF-2.2)
JAERI, Japan (MVP (Monte Carlo), JENDL-3.2)
KAERI, Korea (HELIOS/CPM, ENDF/B-VI)
Kurchatov, Russia (MCU-REA, MCUDAT)
JLF & CMC, Mexico (HELIOS, ENDF/B-VI)
JLF & CMC, Mexico (CPM-3, ENDF/B-VI)
ORNL, USA (HELIOS, ENDF/B-VI.3 (adjusted))
PSI, Switzerland (BOXER, ETOBOX (ENDF/B))
PSI, Switzerland (CASMO-4, ENDF/B-VI)
PSI, Switzerland (CASMO-4, JEF-2.2)
SIEMENS, Germany (CASMO-4, ENDF/B-IV & JEF-1,-2.1)
TSI, Japan (CASMO-4, JEF-2.2)
TWE, USA (CPM-3, ENDF/B-VI)

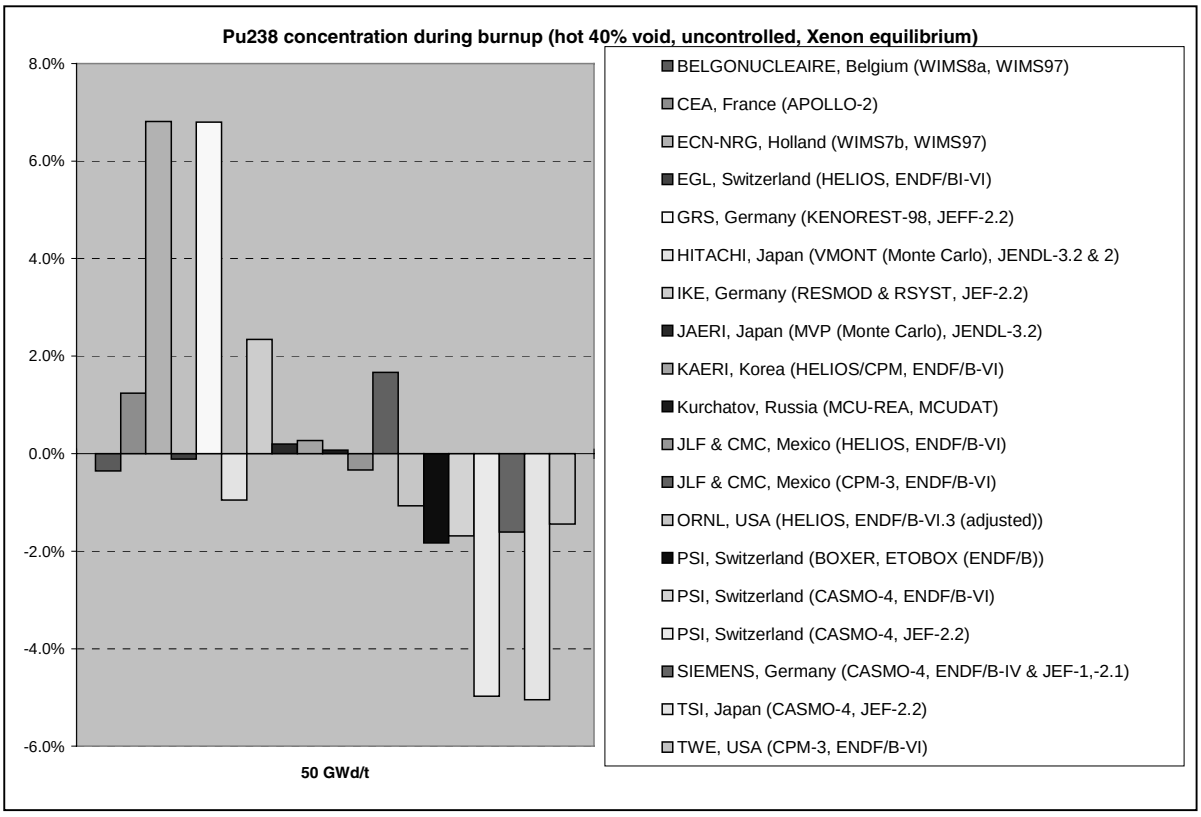

^{239}Pu concentration (10^{24} a/cm^3)	5 GWd/t	10 GWd/t	30 GWd/t	50 GWd/t
Average =>	1.4763E-04	1.3552E-04	9.6452E-05	6.9939E-05
Discrepancy max. =>	1.65%	3.57%	12.93%	24.10%
Discrepancy min. =>	-0.54%	-1.07%	-2.97%	-6.22%
Average discrepancies (min./max.) =>	0.24%	0.53%	1.77%	3.32%
Average without extreme values =>	1.4753E-04	1.3532E-04	9.5887E-05	6.9203E-05
Average discrepancies (min./max.) =>	0.14%	0.32%	1.04%	1.93%

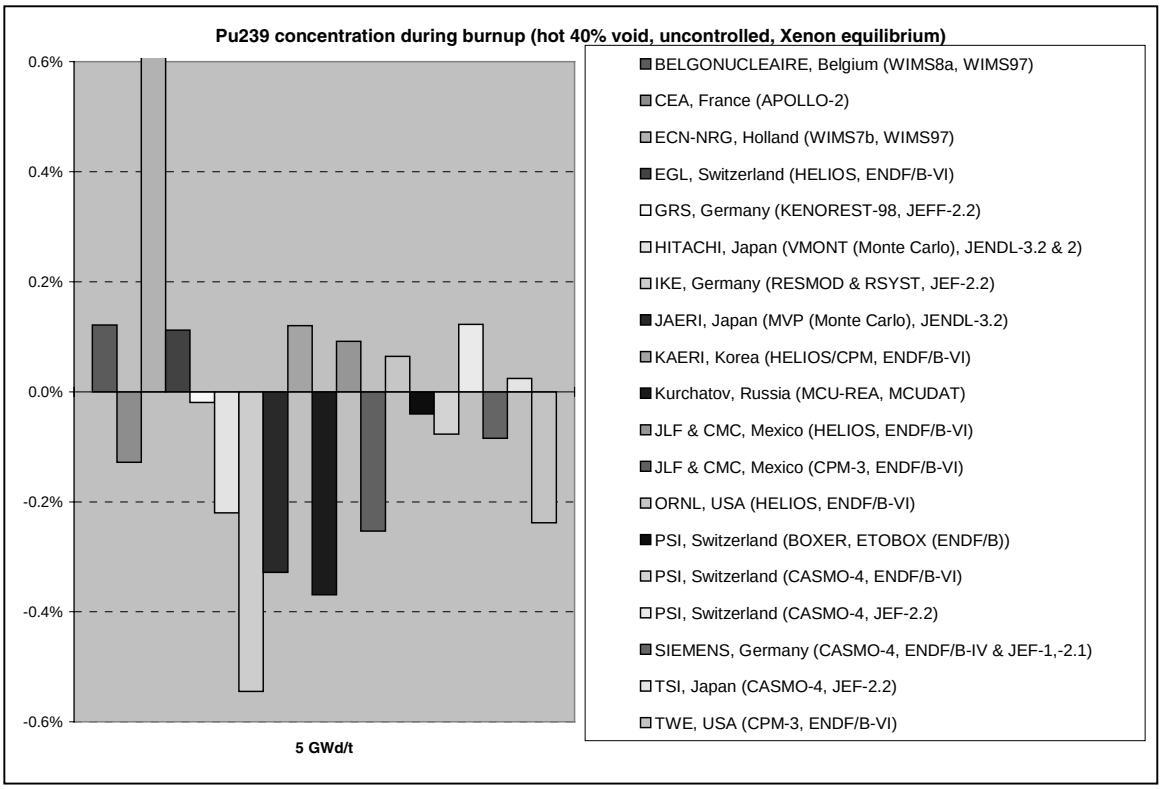
Pu239 concentration during burnup (hot 40% void, uncontrolled, Xenon equilibrium)
0.6%
0.4%
0.2%
0.0%
-0.2%
-0.4%
-0.6%
5 GWd/t
BELGONUCLEAIRE, Belgium (WIMS8a, WIMS97)
CEA, France (APOLLO-2)
ECN-NRG, Holland (WIMS7b, WIMS97)
EGL, Switzerland (HELIOS, ENDF/B-VI)
GRS, Germany (KENOREST-98, JEFF-2.2)
HITACHI, Japan (VMONT (Monte Carlo), JENDL-3.2 & 2)
IKE, Germany (RESMOD & RSYST, JEF-2.2)
JAERI, Japan (MVP (Monte Carlo), JENDL-3.2)
KAERI, Korea (HELIOS/CPM, ENDF/B-VI)
Kurchatov, Russia (MCU-REA, MCUDAT)
JLF & CMC, Mexico (HELIOS, ENDF/B-VI)
JLF & CMC, Mexico (CPM-3, ENDF/B-VI)
ORNL, USA (HELIOS, ENDF/B-VI)
PSI, Switzerland (BOXER, ETOBOX (ENDF/B))
PSI, Switzerland (CASMO-4, ENDF/B-VI)
PSI, Switzerland (CASMO-4, JEF-2.2)
SIEMENS, Germany (CASMO-4, ENDF/B-IV & JEF-1,-2.1)
TSI, Japan (CASMO-4, JEF-2.2)
TWE, USA (CPM-3, ENDF/B-VI)

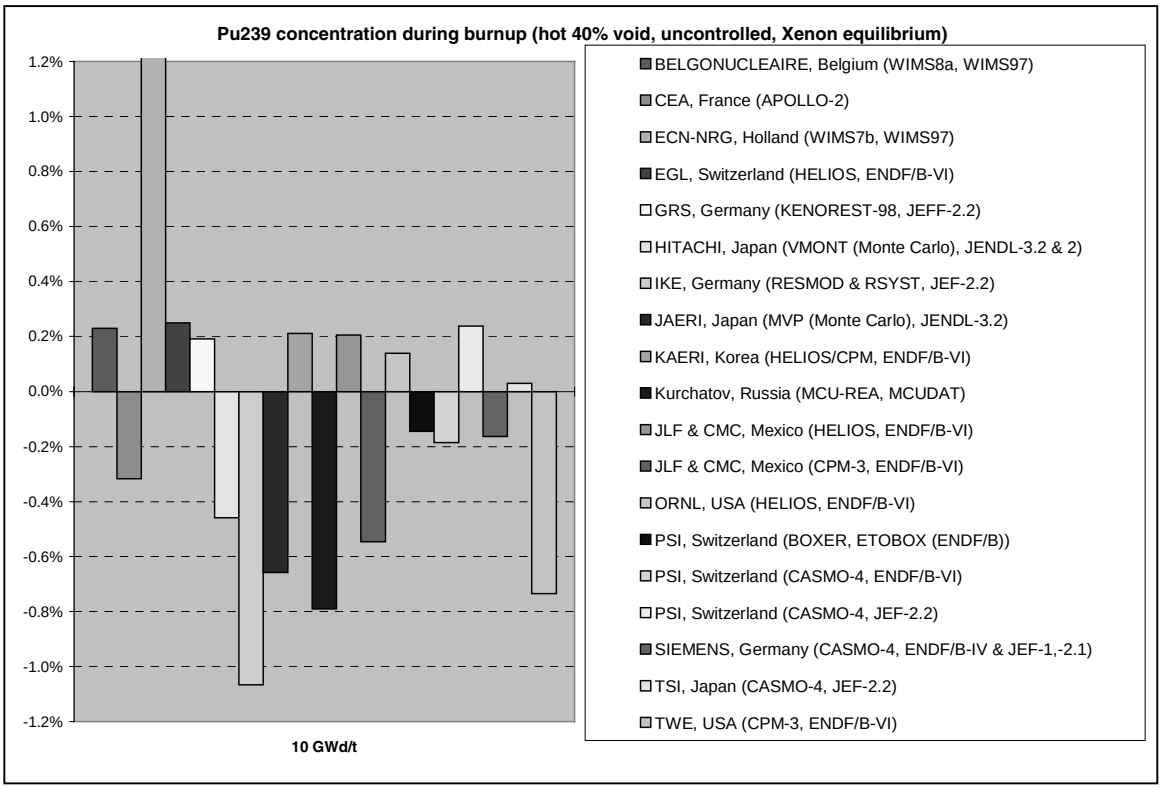
Pu239 concentration during burnup (hot 40% void, uncontrolled, Xenon equilibrium)
1.2%
1.0%
0.8%
0.6%
0.4%
0.2%
0.0%
-0.2%
-0.4%
-0.6%
-0.8%
-1.0%
-1.2%
10 GWd/t
BELGONUCLEAIRE, Belgium (WIMS8a, WIMS97)
CEA, France (APOLLO-2)
ECN-NRG, Holland (WIMS7b, WIMS97)
EGL, Switzerland (HELIOS, ENDF/B-VI)
GRS, Germany (KENOREST-98, JEFF-2.2)
HITACHI, Japan (VMONT (Monte Carlo), JENDL-3.2 & 2)
IKE, Germany (RESMOD & RSYST, JEF-2.2)
JAERI, Japan (MVP (Monte Carlo), JENDL-3.2)
KAERI, Korea (HELIOS/CPM, ENDF/B-VI)
Kurchatov, Russia (MCU-REA, MCUDAT)
JLF & CMC, Mexico (HELIOS, ENDF/B-VI)
JLF & CMC, Mexico (CPM-3, ENDF/B-VI)
ORNL, USA (HELIOS, ENDF/B-VI)
PSI, Switzerland (BOXER, ETOBOX (ENDF/B))
PSI, Switzerland (CASMO-4, ENDF/B-VI)
PSI, Switzerland (CASMO-4, JEF-2.2)
SIEMENS, Germany (CASMO-4, ENDF/B-IV & JEF-1,-2.1)
TSI, Japan (CASMO-4, JEF-2.2)
TWE, USA (CPM-3, ENDF/B-VI)

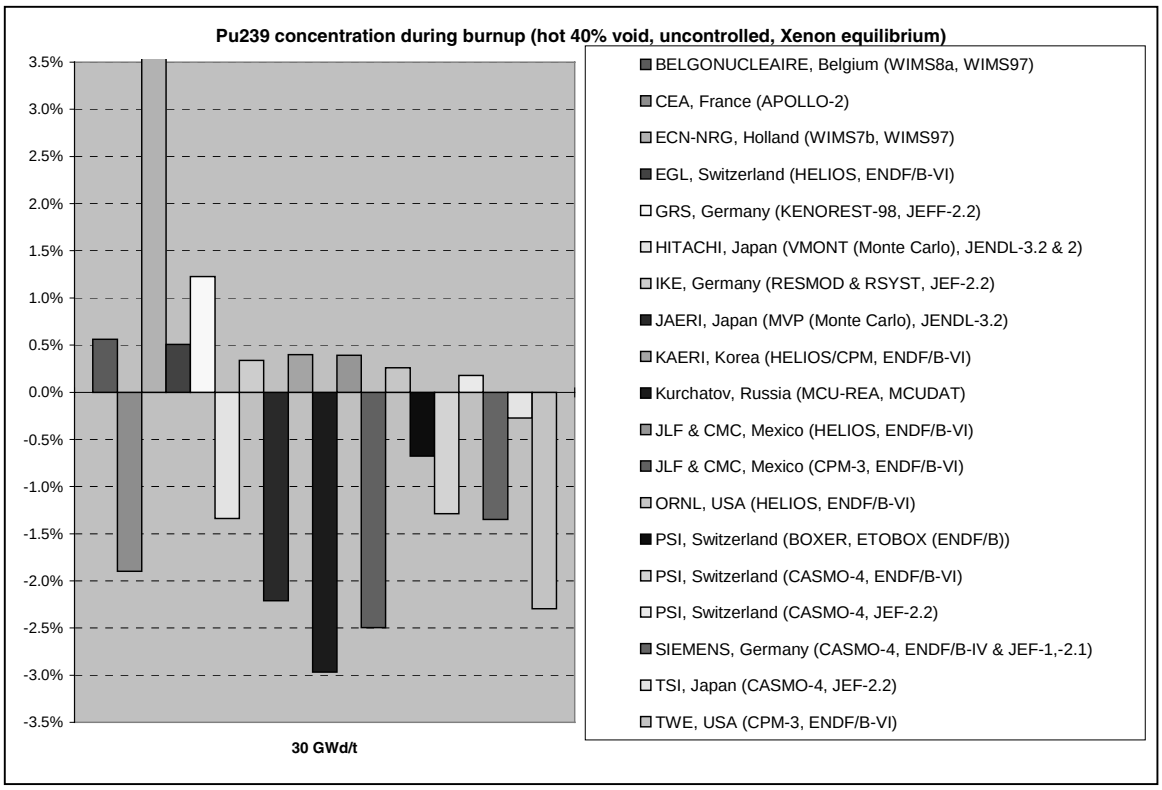
Pu239 concentration during burnup (hot 40% void, uncontrolled, Xenon equilibrium)
3.5%
3.0%
2.5%
2.0%
1.5%
1.0%
0.5%
0.0%
-0.5%
-1.0%
-1.5%
-2.0%
-2.5%
-3.0%
-3.5%
30 GWd/t
BELGONUCLEAIRE, Belgium (WIMS8a, WIMS97)
CEA, France (APOLLO-2)
ECN-NRG, Holland (WIMS7b, WIMS97)
EGL, Switzerland (HELIOS, ENDF/B-VI)
GRS, Germany (KENOREST-98, JEFF-2.2)
HITACHI, Japan (VMONT (Monte Carlo), JENDL-3.2 & 2)
IKE, Germany (RESMOD & RSYST, JEF-2.2)
JAERI, Japan (MVP (Monte Carlo), JENDL-3.2)
KAERI, Korea (HELIOS/CPM, ENDF/B-VI)
Kurchatov, Russia (MCU-REA, MCUDAT)
JLF & CMC, Mexico (HELIOS, ENDF/B-VI)
JLF & CMC, Mexico (CPM-3, ENDF/B-VI)
ORNL, USA (HELIOS, ENDF/B-VI)
PSI, Switzerland (BOXER, ETOBOX (ENDF/B))
PSI, Switzerland (CASMO-4, ENDF/B-VI)
PSI, Switzerland (CASMO-4, JEF-2.2)
SIEMENS, Germany (CASMO-4, ENDF/B-IV & JEF-1,-2.1)
TSI, Japan (CASMO-4, JEF-2.2)
TWE, USA (CPM-3, ENDF/B-VI)

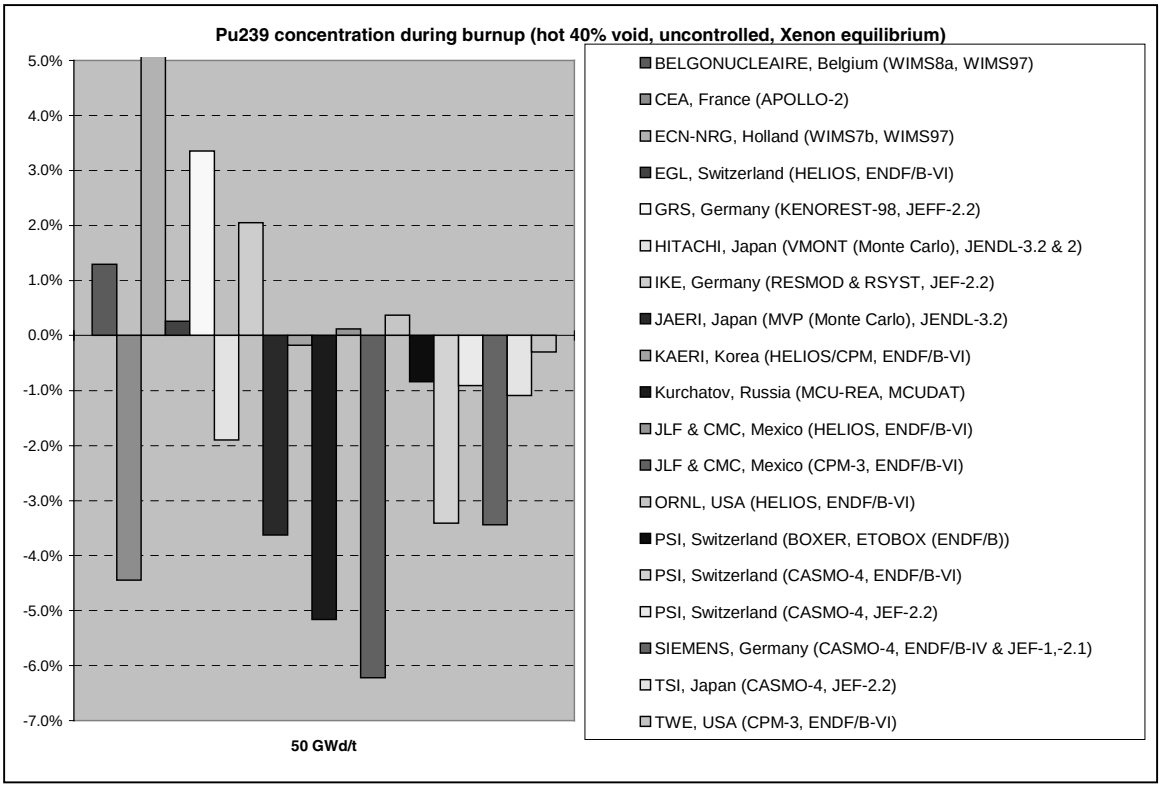
Pu239 concentration during burnup (hot 40% void, uncontrolled, Xenon equilibrium)
5.0%
4.0%
3.0%
2.0%
1.0%
0.0%
-1.0%
-2.0%
-3.0%
-4.0%
-5.0%
-6.0%
-7.0%
50 GWd/t
BELGONUCLEAIRE, Belgium (WIMS8a, WIMS97)
CEA, France (APOLLO-2)
ECN-NRG, Holland (WIMS7b, WIMS97)
EGL, Switzerland (HELIOS, ENDF/B-VI)
GRS, Germany (KENOREST-98, JEFF-2.2)
HITACHI, Japan (VMONT (Monte Carlo), JENDL-3.2 & 2)
IKE, Germany (RESMOD & RSYST, JEF-2.2)
JAERI, Japan (MVP (Monte Carlo), JENDL-3.2)
KAERI, Korea (HELIOS/CPM, ENDF/B-VI)
Kurchatov, Russia (MCU-REA, MCUDAT)
JLF & CMC, Mexico (HELIOS, ENDF/B-VI)
JLF & CMC, Mexico (CPM-3, ENDF/B-VI)
ORNL, USA (HELIOS, ENDF/B-VI)
PSI, Switzerland (BOXER, ETOBOX (ENDF/B))
PSI, Switzerland (CASMO-4, ENDF/B-VI)
PSI, Switzerland (CASMO-4, JEF-2.2)
SIEMENS, Germany (CASMO-4, ENDF/B-IV & JEF-1,-2.1)
TSI, Japan (CASMO-4, JEF-2.2)
TWE, USA (CPM-3, ENDF/B-VI)

^{240}Pu concentration (10^{24} a/cm^3)	5 GWd/t	10 GWd/t	30 GWd/t	50 GWd/t
Average =>	1.0117E-04	9.9954E-05	9.1197E-05	7.8117E-05
Discrepancy max. =>	0.44%	0.89%	2.49%	3.96%
Discrepancy min. =>	-0.69%	-1.22%	-3.18%	-5.65%
Average discrepancies (min./max.) =>	0.18%	0.38%	0.88%	1.31%
Average without extreme values =>	1.0118E-04	9.9973E-05	9.1234E-05	7.8295E-05
Average discrepancies (min./max.) =>	0.14%	0.30%	0.88%	0.90%

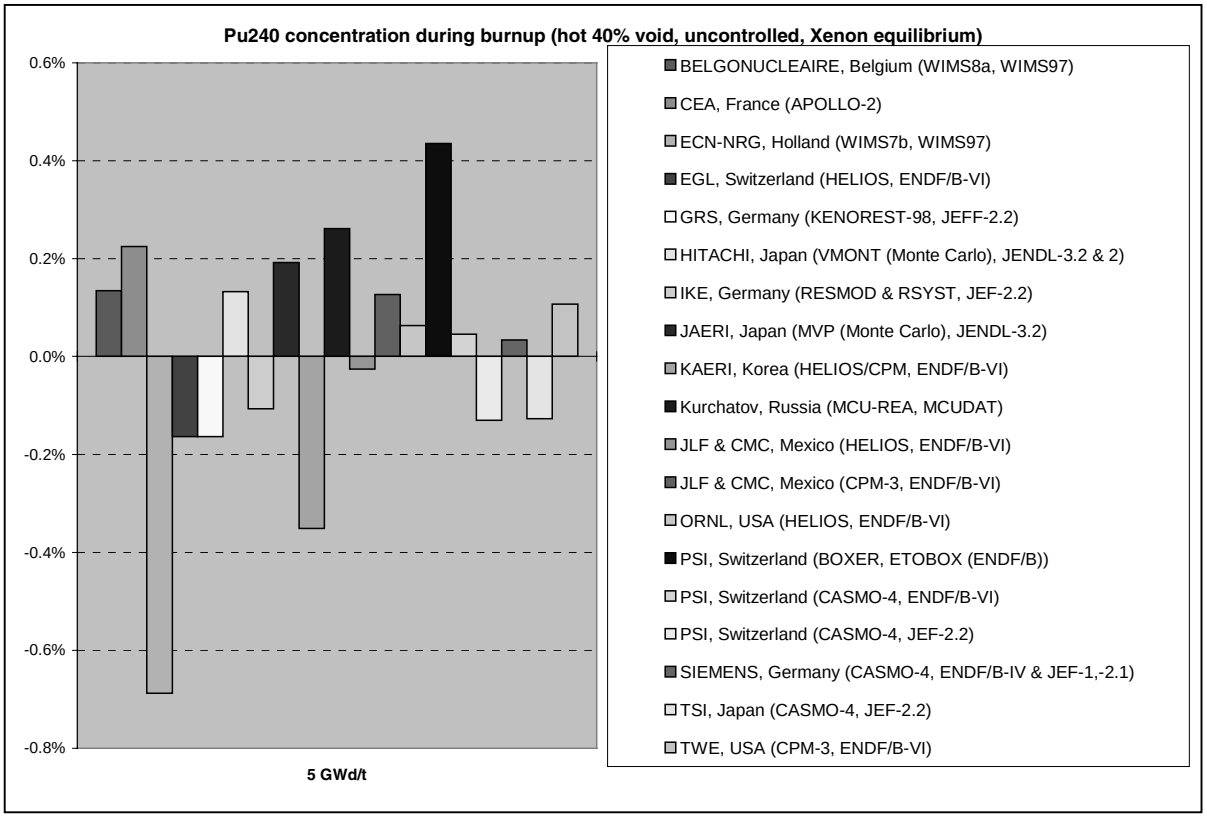

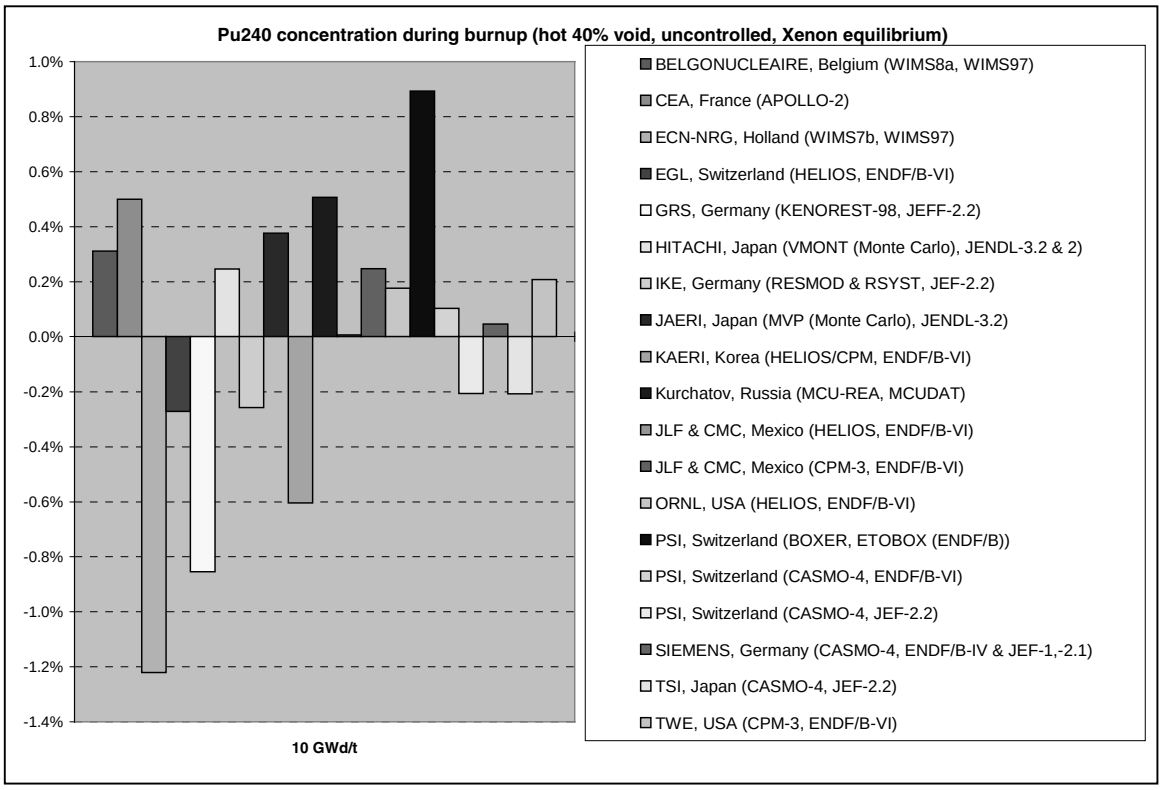
Pu240 concentration during burnup (hot 40% void, uncontrolled, Xenon equilibrium)
1.0%
0.8%
0.6%
0.4%
0.2%
0.0%
-0.2%
-0.4%
-0.6%
-0.8%
-1.0%
-1.2%
-1.4%
10 GWd/t
BELGONUCLEAIRE, Belgium (WIMS8a, WIMS97)
CEA, France (APOLLO-2)
ECN-NRG, Holland (WIMS7b, WIMS97)
EGL, Switzerland (HELIOS, ENDF/B-VI)
GRS, Germany (KENOREST-98, JEFF-2.2)
HITACHI, Japan (VMONT (Monte Carlo), JENDL-3.2 & 2)
IKE, Germany (RESMOD & RSYST, JEF-2.2)
JAERI, Japan (MVP (Monte Carlo), JENDL-3.2)
KAERI, Korea (HELIOS/CPM, ENDF/B-VI)
Kurchatov, Russia (MCU-REA, MCUDAT)
JLF & CMC, Mexico (HELIOS, ENDF/B-VI)
JLF & CMC, Mexico (CPM-3, ENDF/B-VI)
ORNL, USA (HELIOS, ENDF/B-VI)
PSI, Switzerland (BOXER, ETOBOX (ENDF/B))
PSI, Switzerland (CASMO-4, ENDF/B-VI)
PSI, Switzerland (CASMO-4, JEF-2.2)
SIEMENS, Germany (CASMO-4, ENDF/B-IV & JEF-1,-2.1)
TSI, Japan (CASMO-4, JEF-2.2)
TWE, USA (CPM-3, ENDF/B-VI)

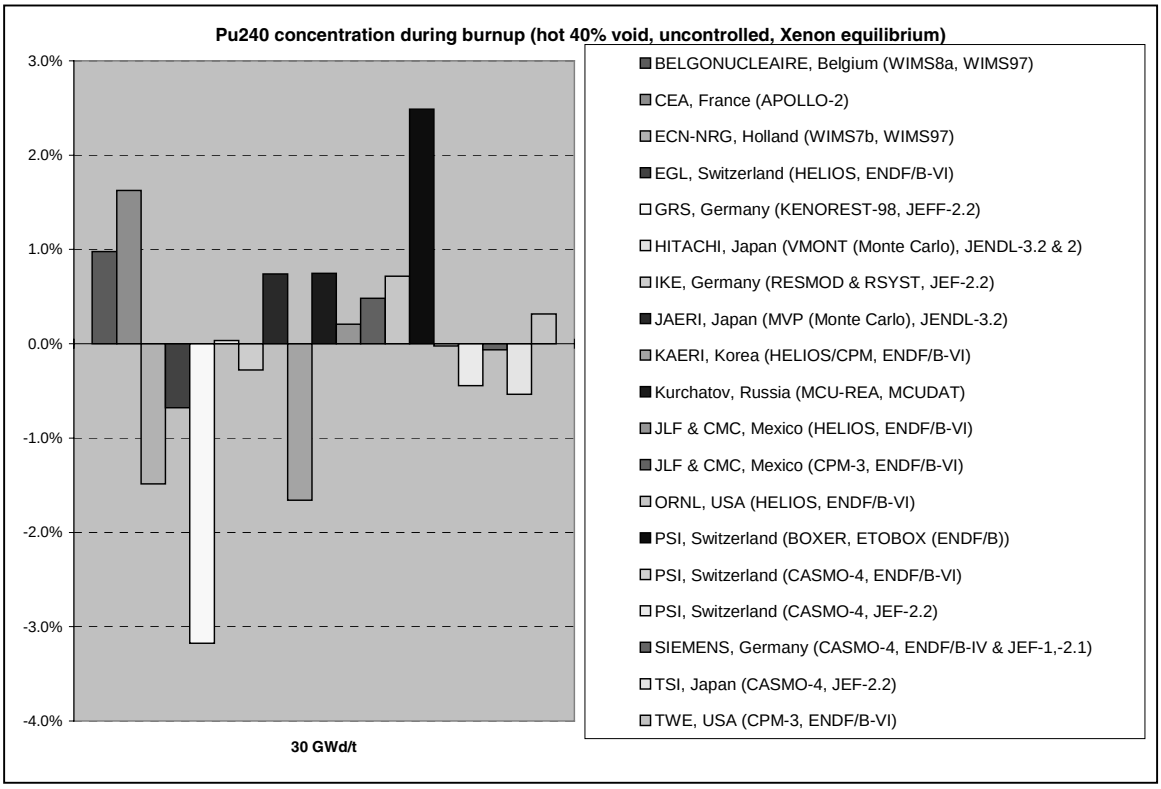
Pu240 concentration during burnup (hot 40% void, uncontrolled, Xenon equilibrium)
3.0%
2.0%
1.0%
0.0%
-1.0%
-2.0%
-3.0%
-4.0%
30 GWd/t
BELGONUCLEAIRE, Belgium (WIMS8a, WIMS97)
CEA, France (APOLLO-2)
ECN-NRG, Holland (WIMS7b, WIMS97)
EGL, Switzerland (HELIOS, ENDF/B-VI)
GRS, Germany (KENOREST-98, JEFF-2.2)
HITACHI, Japan (VMONT (Monte Carlo), JENDL-3.2 & 2)
IKE, Germany (RESMOD & RSYST, JEF-2.2)
JAERI, Japan (MVP (Monte Carlo), JENDL-3.2)
KAERI, Korea (HELIOS/CPM, ENDF/B-VI)
Kurchatov, Russia (MCU-REA, MCUDAT)
JLF & CMC, Mexico (HELIOS, ENDF/B-VI)
JLF & CMC, Mexico (CPM-3, ENDF/B-VI)
ORNL, USA (HELIOS, ENDF/B-VI)
PSI, Switzerland (BOXER, ETOBOX (ENDF/B))
PSI, Switzerland (CASMO-4, ENDF/B-VI)
PSI, Switzerland (CASMO-4, JEF-2.2)
SIEMENS, Germany (CASMO-4, ENDF/B-IV & JEF-1,-2.1)
TSI, Japan (CASMO-4, JEF-2.2)
TWE, USA (CPM-3, ENDF/B-VI)

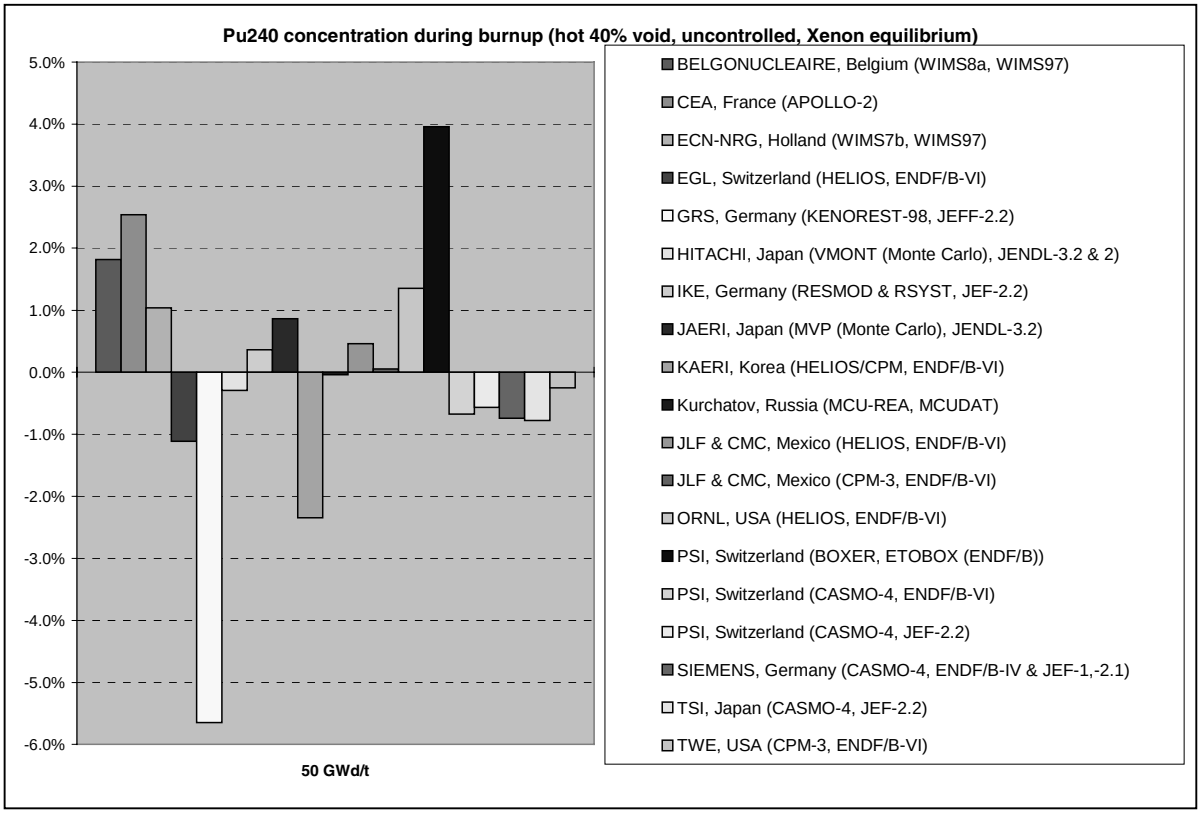

^{241}Pu concentration (10^{24} a/cm^3)	5 GWd/t	10 GWd/t	30 GWd/t	50 GWd/t
Average =>	4.6405E-05	4.6169E-05	4.2700E-05	3.6745E-05
Discrepancy max. =>	1.71%	3.10%	6.79%	11.29%
Discrepancy min. =>	-0.94%	-1.71%	-3.93%	-5.80%
Average discrepancies (min./max.) =>	0.46%	0.76%	1.70%	2.51%
Average without extreme values =>	4.6384E-05	4.6131E-05	4.2628E-05	3.6626E-05
Average discrepancies (min./max.) =>	0.36%	0.56%	1.27%	1.80%

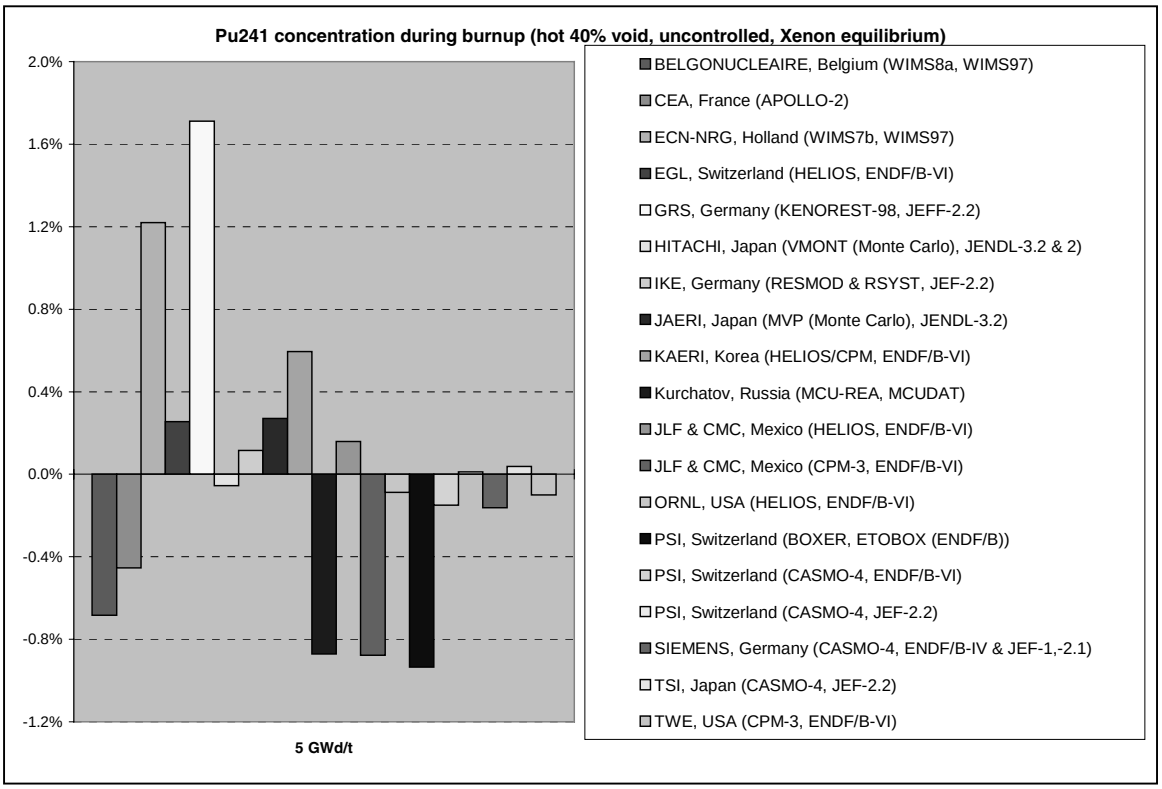
Pu241 concentration during burnup (hot 40% void, uncontrolled, Xenon equilibrium)
2.0%
1.6%
1.2%
0.8%
0.4%
0.0%
-0.4%
-0.8%
-1.2%
5 GWd/t
BELGONUCLEAIRE, Belgium (WIMS8a, WIMS97)
CEA, France (APOLLO-2)
ECN-NRG, Holland (WIMS7b, WIMS97)
EGL, Switzerland (HELIOS, ENDF/B-VI)
GRS, Germany (KENOREST-98, JEFF-2.2)
HITACHI, Japan (VMONT (Monte Carlo), JENDL-3.2 & 2)
IKE, Germany (RESMOD & RSYST, JEF-2.2)
JAERI, Japan (MVP (Monte Carlo), JENDL-3.2)
KAERI, Korea (HELIOS/CPM, ENDF/B-VI)
Kurchatov, Russia (MCU-REA, MCUDAT)
JLF & CMC, Mexico (HELIOS, ENDF/B-VI)
JLF & CMC, Mexico (CPM-3, ENDF/B-VI)
ORNL, USA (HELIOS, ENDF/B-VI)
PSI, Switzerland (BOXER, ETOBOX (ENDF/B))
PSI, Switzerland (CASMO-4, ENDF/B-VI)
PSI, Switzerland (CASMO-4, JEF-2.2)
SIEMENS, Germany (CASMO-4, ENDF/B-IV & JEF-1,-2.1)
TSI, Japan (CASMO-4, JEF-2.2)
TWE, USA (CPM-3, ENDF/B-VI)

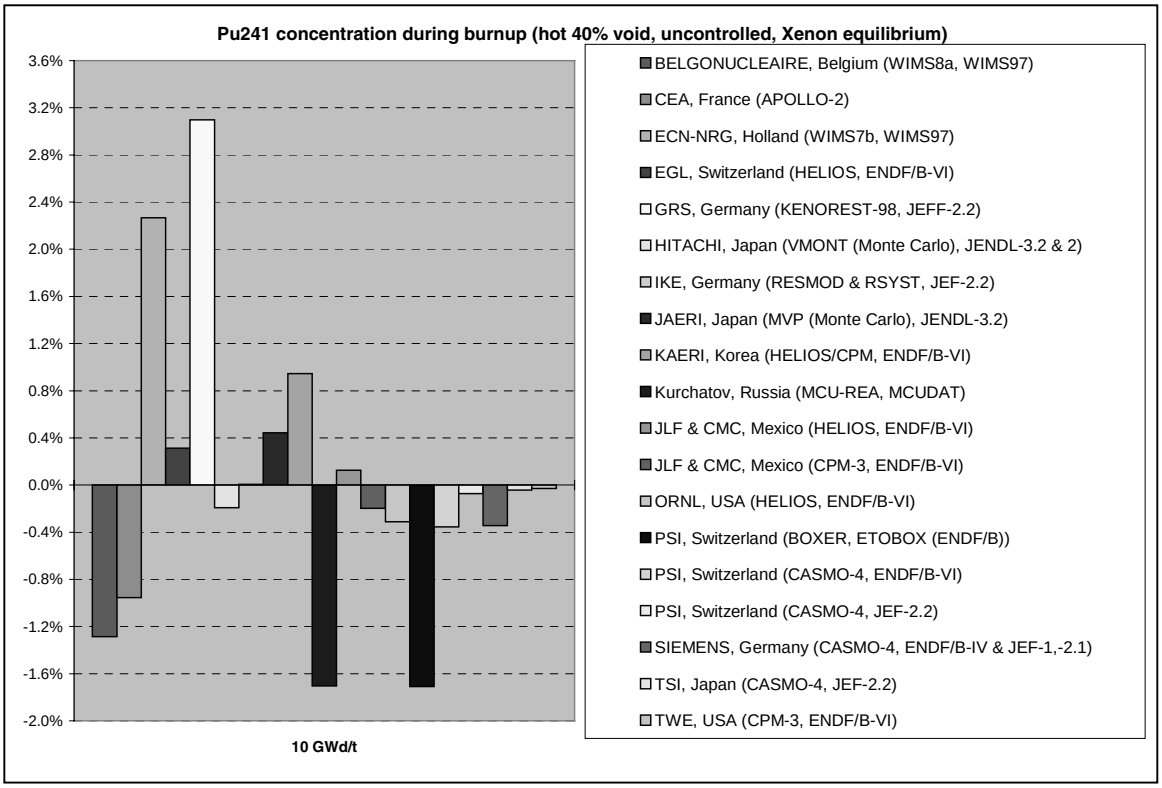
Pu241 concentration during burnup (hot 40% void, uncontrolled, Xenon equilibrium)
3.6%
3.2%
2.8%
2.4%
2.0%
1.6%
1.2%
0.8%
0.4%
0.0%
-0.4%
-0.8%
-1.2%
-1.6%
-2.0%
10 GWd/t
BELGONUCLEAIRE, Belgium (WIMS8a, WIMS97)
CEA, France (APOLLO-2)
ECN-NRG, Holland (WIMS7b, WIMS97)
EGL, Switzerland (HELIOS, ENDF/B-VI)
GRS, Germany (KENOREST-98, JEFF-2.2)
HITACHI, Japan (VMONT (Monte Carlo), JENDL-3.2 & 2)
IKE, Germany (RESMOD & RSYST, JEF-2.2)
JAERI, Japan (MVP (Monte Carlo), JENDL-3.2)
KAERI, Korea (HELIOS/CPM, ENDF/B-VI)
Kurchatov, Russia (MCU-REA, MCUDAT)
JLF & CMC, Mexico (HELIOS, ENDF/B-VI)
JLF & CMC, Mexico (CPM-3, ENDF/B-VI)
ORNL, USA (HELIOS, ENDF/B-VI)
PSI, Switzerland (BOXER, ETOBOX (ENDF/B))
PSI, Switzerland (CASMO-4, ENDF/B-VI)
PSI, Switzerland (CASMO-4, JEF-2.2)
SIEMENS, Germany (CASMO-4, ENDF/B-IV & JEF-1,-2.1)
TSI, Japan (CASMO-4, JEF-2.2)
TWE, USA (CPM-3, ENDF/B-VI)

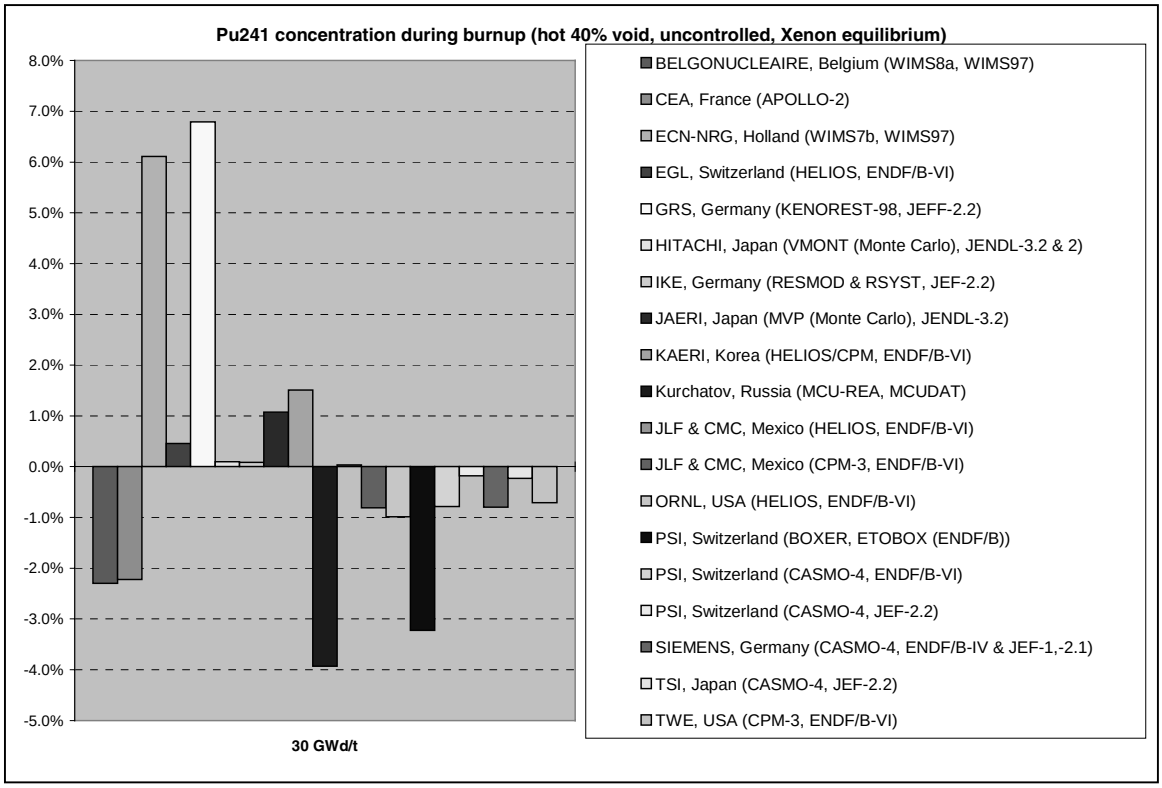
Pu241 concentration during burnup (hot 40% void, uncontrolled, Xenon equilibrium)
8.0%
7.0%
6.0%
5.0%
4.0%
3.0%
2.0%
1.0%
0.0%
-1.0%
-2.0%
-3.0%
-4.0%
-5.0%
30 GWd/t
BELGONUCLEAIRE, Belgium (WIMS8a, WIMS97)
CEA, France (APOLLO-2)
ECN-NRG, Holland (WIMS7b, WIMS97)
EGL, Switzerland (HELIOS, ENDF/B-VI)
GRS, Germany (KENOREST-98, JEFF-2.2)
HITACHI, Japan (VMONT (Monte Carlo), JENDL-3.2 & 2)
IKE, Germany (RESMOD & RSYST, JEF-2.2)
JAERI, Japan (MVP (Monte Carlo), JENDL-3.2)
KAERI, Korea (HELIOS/CPM, ENDF/B-VI)
Kurchatov, Russia (MCU-REA, MCUDAT)
JLF & CMC, Mexico (HELIOS, ENDF/B-VI)
JLF & CMC, Mexico (CPM-3, ENDF/B-VI)
ORNL, USA (HELIOS, ENDF/B-VI)
PSI, Switzerland (BOXER, ETOBOX (ENDF/B))
PSI, Switzerland (CASMO-4, ENDF/B-VI)
PSI, Switzerland (CASMO-4, JEF-2.2)
SIEMENS, Germany (CASMO-4, ENDF/B-IV & JEF-1,-2.1)
TSI, Japan (CASMO-4, JEF-2.2)
TWE, USA (CPM-3, ENDF/B-VI)

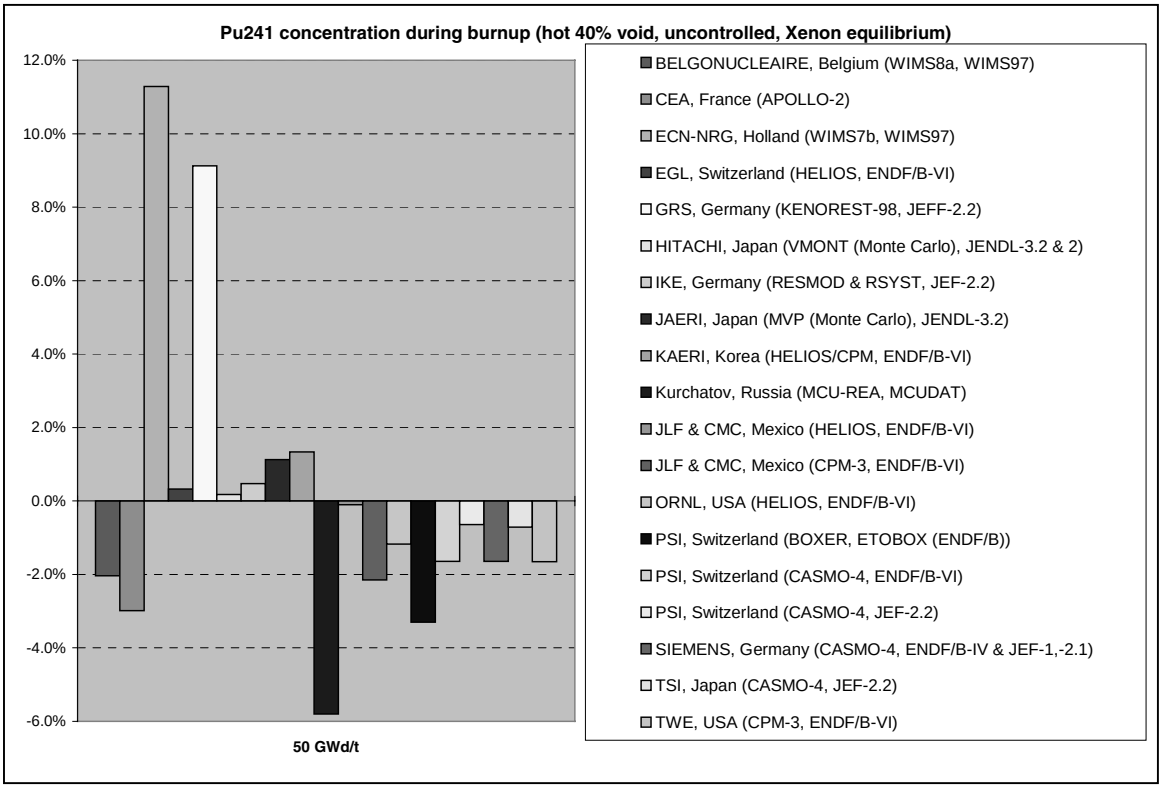
Pu241 concentration during burnup (hot 40% void, uncontrolled, Xenon equilibrium)
12.0%
10.0%
8.0%
6.0%
4.0%
2.0%
0.0%
-2.0%
-4.0%
-6.0%
50 GWd/t
BELGONUCLEAIRE, Belgium (WIMS8a, WIMS97)
CEA, France (APOLLO-2)
ECN-NRG, Holland (WIMS7b, WIMS97)
EGL, Switzerland (HELIOS, ENDF/B-VI)
GRS, Germany (KENOREST-98, JEFF-2.2)
HITACHI, Japan (VMONT (Monte Carlo), JENDL-3.2 & 2)
IKE, Germany (RESMOD & RSYST, JEF-2.2)
JAERI, Japan (MVP (Monte Carlo), JENDL-3.2)
KAERI, Korea (HELIOS/CPM, ENDF/B-VI)
Kurchatov, Russia (MCU-REA, MCUDAT)
JLF & CMC, Mexico (HELIOS, ENDF/B-VI)
JLF & CMC, Mexico (CPM-3, ENDF/B-VI)
ORNL, USA (HELIOS, ENDF/B-VI)
PSI, Switzerland (BOXER, ETOBOX (ENDF/B))
PSI, Switzerland (CASMO-4, ENDF/B-VI)
PSI, Switzerland (CASMO-4, JEF-2.2)
SIEMENS, Germany (CASMO-4, ENDF/B-IV & JEF-1,-2.1)
TSI, Japan (CASMO-4, JEF-2.2)
TWE, USA (CPM-3, ENDF/B-VI)

^{242}Pu concentration (10^{24} a/cm^3)	5 GWd/t	10 GWd/t	30 GWd/t	50 GWd/t
Average =>	3.1031E-05	3.1907E-05	3.6122E-05	4.0653E-05
Discrepancy max. =>	0.78%	1.55%	4.17%	6.52%
Discrepancy min. =>	-0.57%	-1.18%	-3.65%	-5.89%
Average discrepancies (min./max.) =>	0.34%	0.65%	1.63%	2.40%
Average without extreme values =>	3.1027E-05	3.1900E-05	3.6111E-05	4.0638E-05
Average discrepancies (min./max.) =>	0.30%	0.57%	1.36%	1.95%

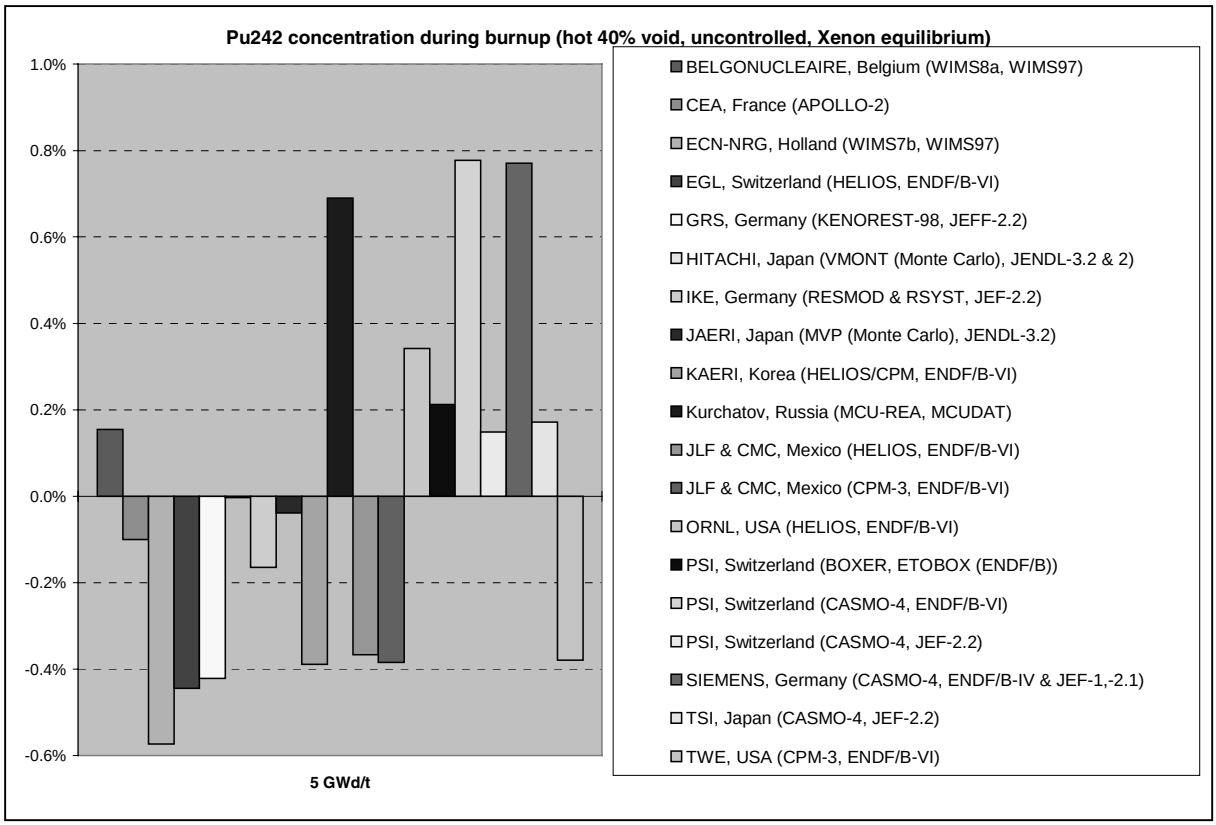

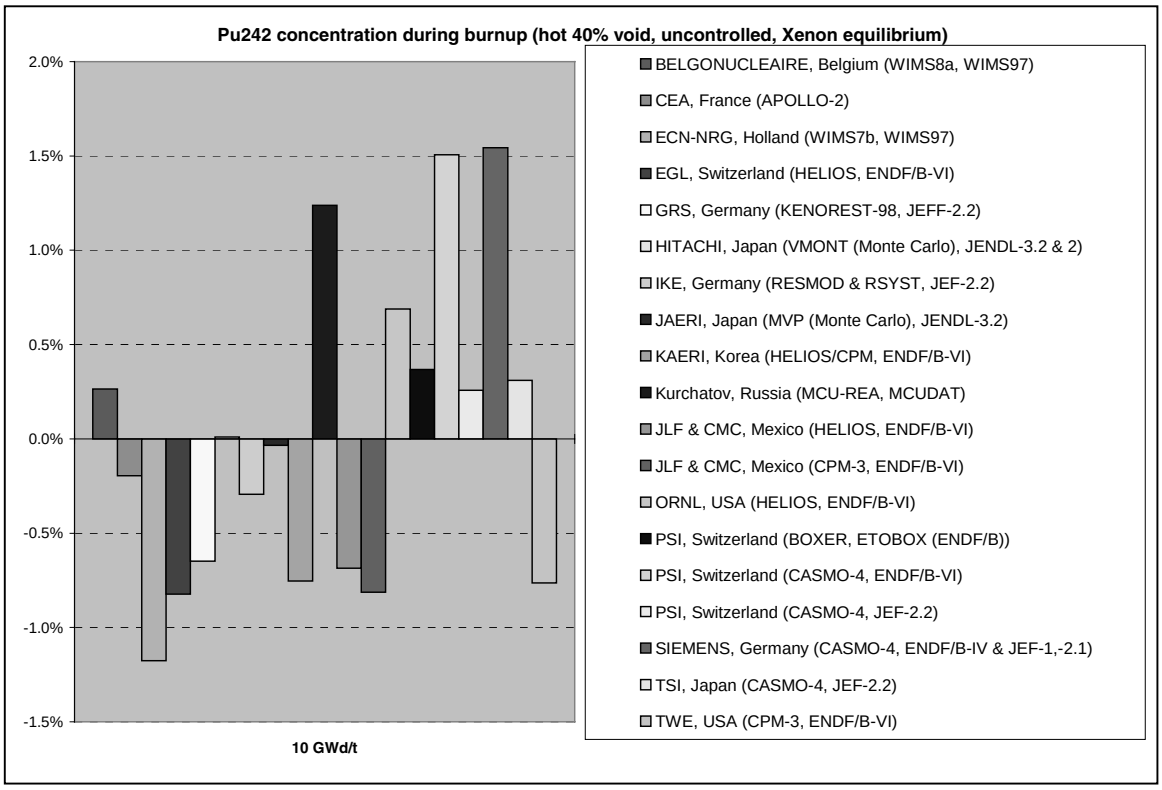
Pu242 concentration during burnup (hot 40% void, uncontrolled, Xenon equilibrium)
2.0%
1.5%
1.0%
0.5%
0.0%
-0.5%
-1.0%
-1.5%
10 GWd/t
BELGONUCLEAIRE, Belgium (WIMS8a, WIMS97)
CEA, France (APOLLO-2)
ECN-NRG, Holland (WIMS7b, WIMS97)
EGL, Switzerland (HELIOS, ENDF/B-VI)
GRS, Germany (KENOREST-98, JEFF-2.2)
HITACHI, Japan (VMONT (Monte Carlo), JENDL-3.2 & 2)
IKE, Germany (RESMOD & RSYST, JEF-2.2)
JAERI, Japan (MVP (Monte Carlo), JENDL-3.2)
KAERI, Korea (HELIOS/CPM, ENDF/B-VI)
Kurchatov, Russia (MCU-REA, MCUDAT)
JLF & CMC, Mexico (HELIOS, ENDF/B-VI)
JLF & CMC, Mexico (CPM-3, ENDF/B-VI)
ORNL, USA (HELIOS, ENDF/B-VI)
PSI, Switzerland (BOXER, ETOBOX (ENDF/B))
PSI, Switzerland (CASMO-4, ENDF/B-VI)
PSI, Switzerland (CASMO-4, JEF-2.2)
SIEMENS, Germany (CASMO-4, ENDF/B-IV & JEF-1,-2.1)
TSI, Japan (CASMO-4, JEF-2.2)
TWE, USA (CPM-3, ENDF/B-VI)

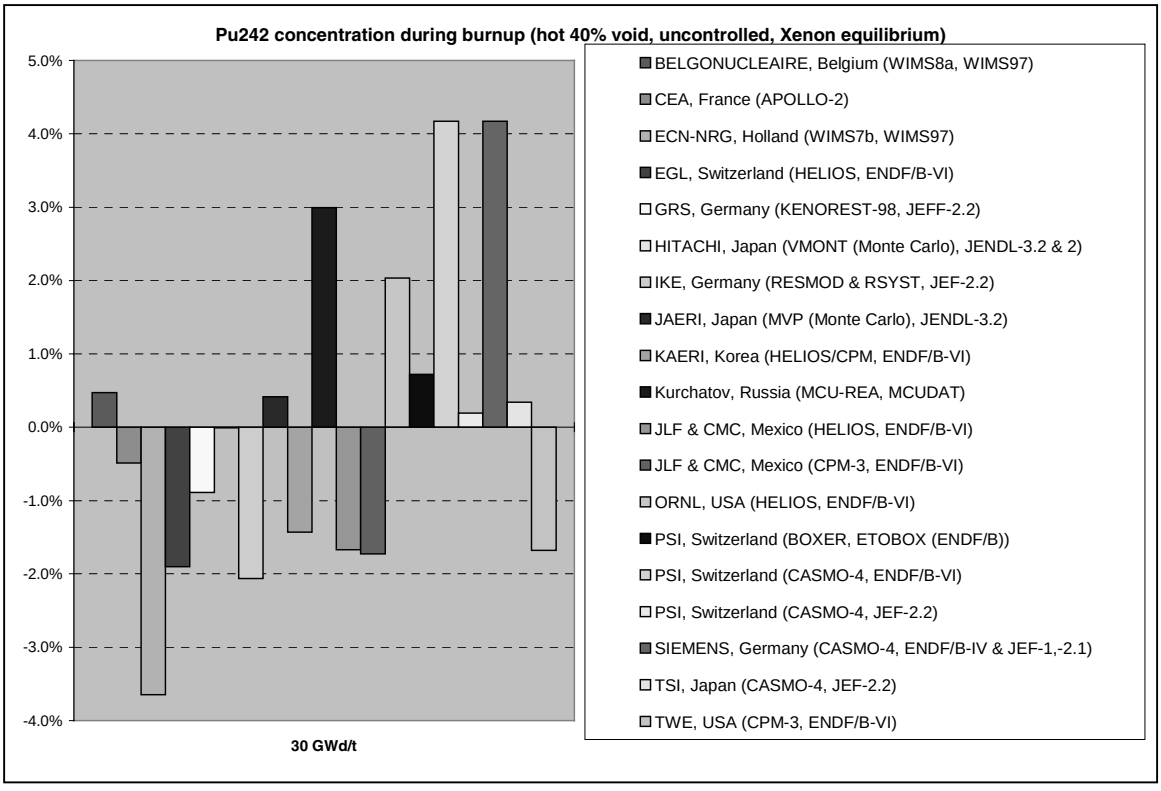
Pu242 concentration during burnup (hot 40% void, uncontrolled, Xenon equilibrium)
5.0%
4.0%
3.0%
2.0%
1.0%
0.0%
-1.0%
-2.0%
-3.0%
-4.0%
30 GWd/t
BELGONUCLEAIRE, Belgium (WIMS8a, WIMS97)
CEA, France (APOLLO-2)
ECN-NRG, Holland (WIMS7b, WIMS97)
EGL, Switzerland (HELIOS, ENDF/B-VI)
GRS, Germany (KENOREST-98, JEFF-2.2)
HITACHI, Japan (VMONT (Monte Carlo), JENDL-3.2 & 2)
IKE, Germany (RESMOD & RSYST, JEF-2.2)
JAERI, Japan (MVP (Monte Carlo), JENDL-3.2)
KAERI, Korea (HELIOS/CPM, ENDF/B-VI)
Kurchatov, Russia (MCU-REA, MCUDAT)
JLF & CMC, Mexico (HELIOS, ENDF/B-VI)
JLF & CMC, Mexico (CPM-3, ENDF/B-VI)
ORNL, USA (HELIOS, ENDF/B-VI)
PSI, Switzerland (BOXER, ETOBOX (ENDF/B))
PSI, Switzerland (CASMO-4, ENDF/B-VI)
PSI, Switzerland (CASMO-4, JEF-2.2)
SIEMENS, Germany (CASMO-4, ENDF/B-IV & JEF-1,-2.1)
TSI, Japan (CASMO-4, JEF-2.2)
TWE, USA (CPM-3, ENDF/B-VI)

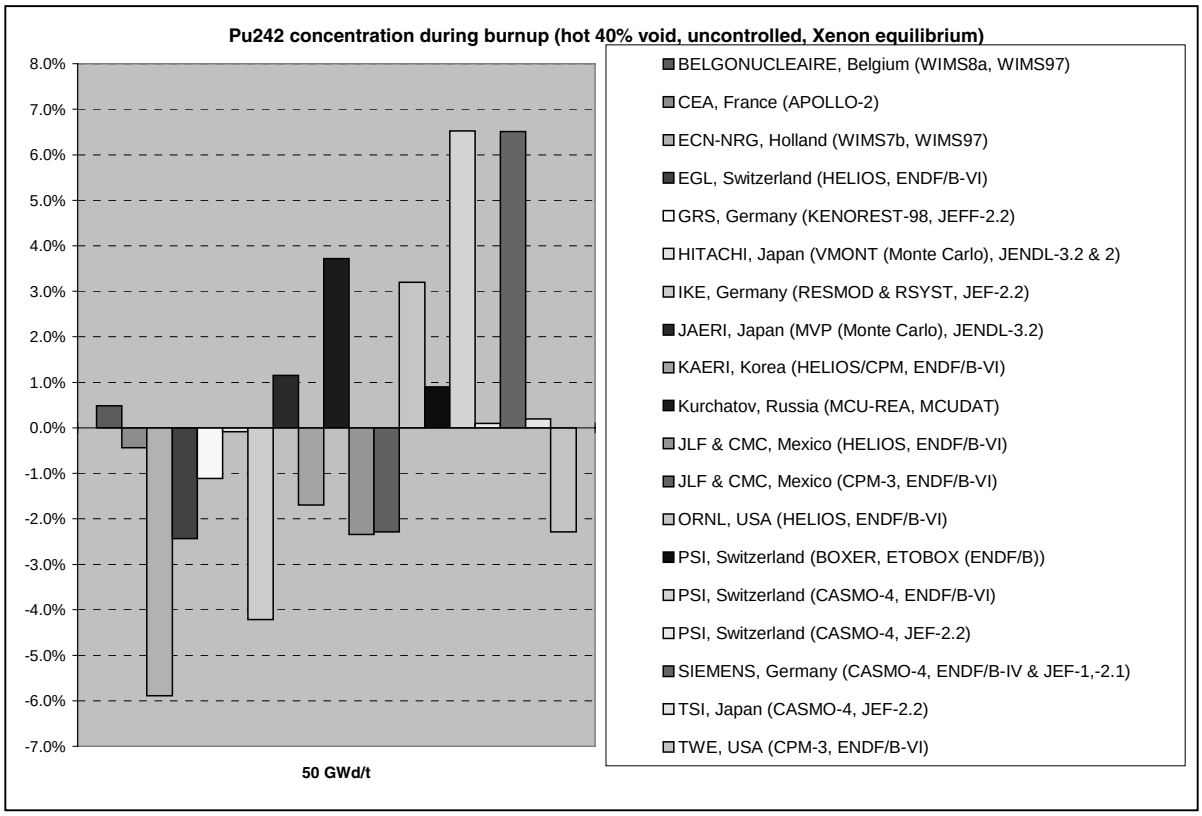

^{241}Am concentration (10^{24} a/cm^3)	5 GWd/t	10 GWd/t	30 GWd/t	50 GWd/t
Average =>	1.1341E-06	2.0944E-06	4.3451E-06	4.6573E-06
Discrepancy max. =>	8.70%	7.72%	3.66%	10.01%
Discrepancy min. =>	-2.32%	-2.19%	-6.04%	-11.41%
Average discrepancies (min./max.) =>	1.13%	1.19%	1.70%	3.02%
Average without extreme values =>	1.1299E-06	2.0876E-06	4.3512E-06	4.6612E-06
Average discrepancies (min./max.) =>	0.62%	0.74%	1.33%	2.12%

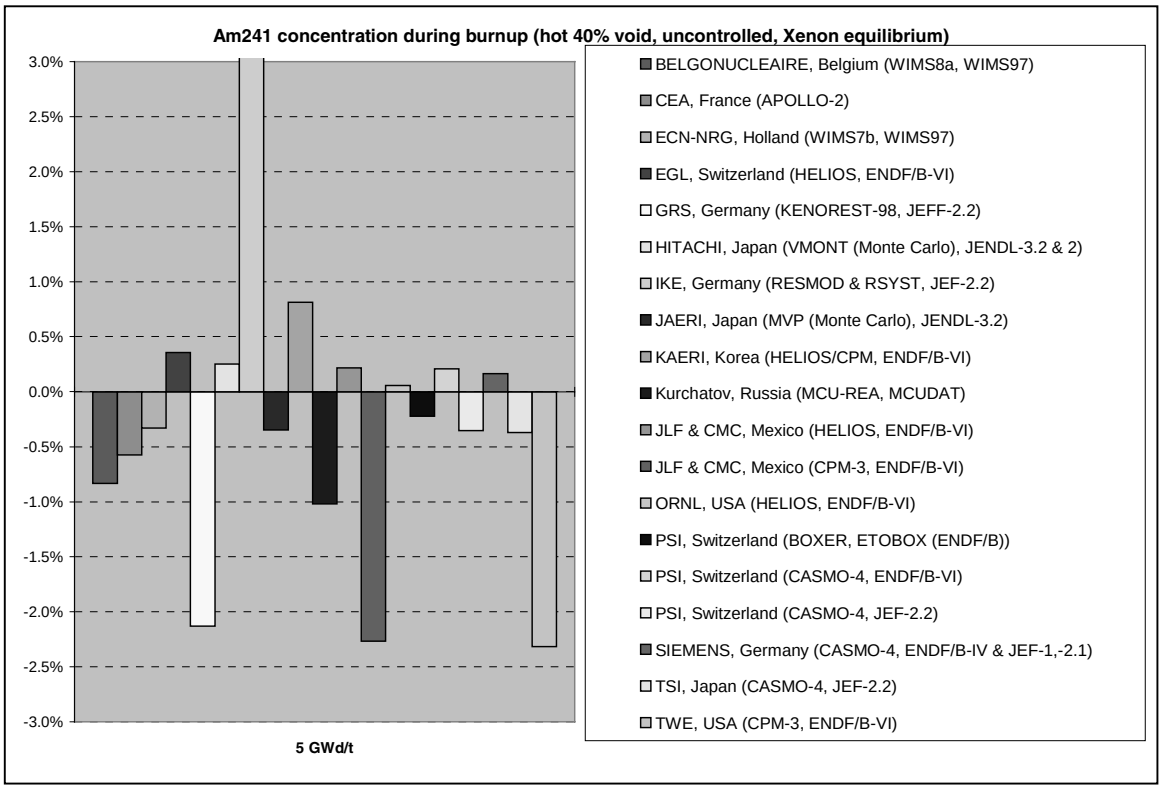
Am241 concentration during burnup (hot 40% void, uncontrolled, Xenon equilibrium)
3.0%
2.5%
2.0%
1.5%
1.0%
0.5%
0.0%
-0.5%
-1.0%
-1.5%
-2.0%
-2.5%
-3.0%
5 GWd/t
BELGONUCLEAIRE, Belgium (WIMS8a, WIMS97)
CEA, France (APOLLO-2)
ECN-NRG, Holland (WIMS7b, WIMS97)
EGL, Switzerland (HELIOS, ENDF/B-VI)
GRS, Germany (KENOREST-98, JEFF-2.2)
HITACHI, Japan (VMONT (Monte Carlo), JENDL-3.2 & 2)
IKE, Germany (RESMOD & RSYST, JEF-2.2)
JAERI, Japan (MVP (Monte Carlo), JENDL-3.2)
KAERI, Korea (HELIOS/CPM, ENDF/B-VI)
Kurchatov, Russia (MCU-REA, MCUDAT)
JLF & CMC, Mexico (HELIOS, ENDF/B-VI)
JLF & CMC, Mexico (CPM-3, ENDF/B-VI)
ORNL, USA (HELIOS, ENDF/B-VI)
PSI, Switzerland (BOXER, ETOBOX (ENDF/B))
PSI, Switzerland (CASMO-4, ENDF/B-VI)
PSI, Switzerland (CASMO-4, JEF-2.2)
SIEMENS, Germany (CASMO-4, ENDF/B-IV & JEF-1,-2.1)
TSI, Japan (CASMO-4, JEF-2.2)
TWE, USA (CPM-3, ENDF/B-VI)

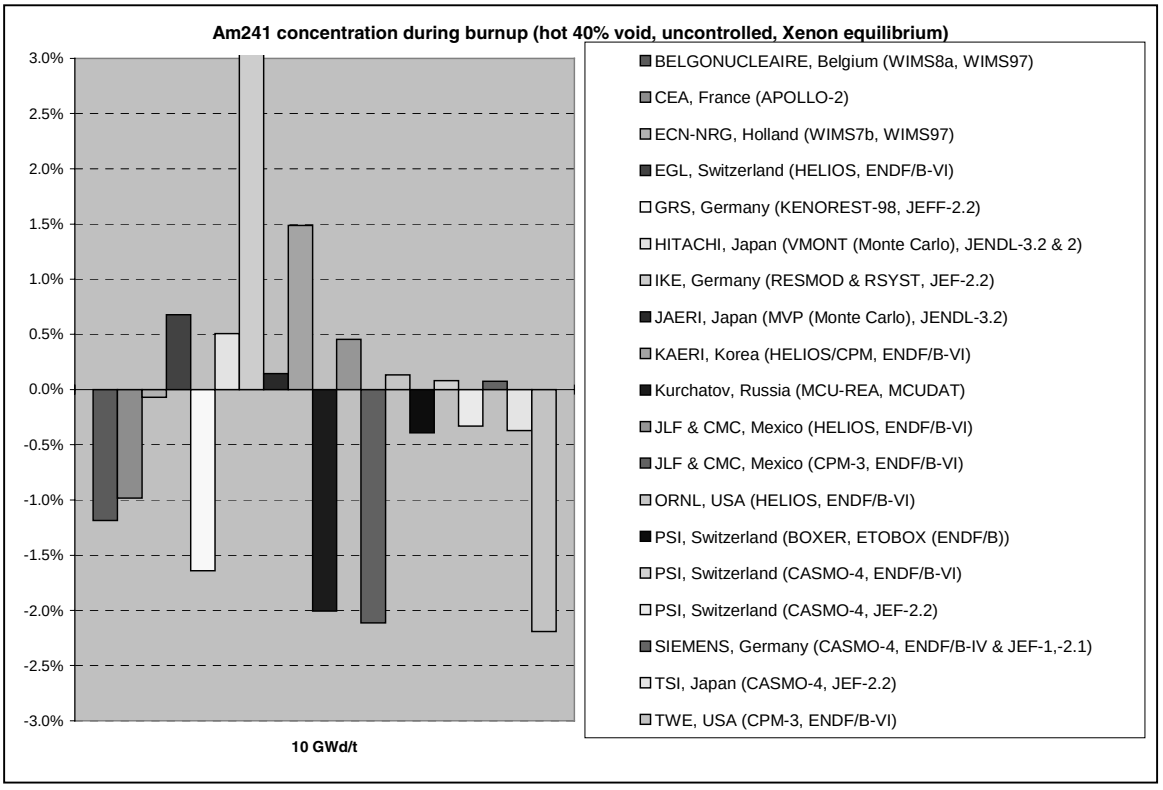
Am241 concentration during burnup (hot 40% void, uncontrolled, Xenon equilibrium)
3.0%
2.5%
2.0%
1.5%
1.0%
0.5%
0.0%
-0.5%
-1.0%
-1.5%
-2.0%
-2.5%
-3.0%
10 GWd/t
BELGONUCLEAIRE, Belgium (WIMS8a, WIMS97)
CEA, France (APOLLO-2)
ECN-NRG, Holland (WIMS7b, WIMS97)
EGL, Switzerland (HELIOS, ENDF/B-VI)
GRS, Germany (KENOREST-98, JEFF-2.2)
HITACHI, Japan (VMONT (Monte Carlo), JENDL-3.2 & 2)
IKE, Germany (RESMOD & RSYST, JEF-2.2)
JAERI, Japan (MVP (Monte Carlo), JENDL-3.2)
KAERI, Korea (HELIOS/CPM, ENDF/B-VI)
Kurchatov, Russia (MCU-REA, MCUDAT)
JLF & CMC, Mexico (HELIOS, ENDF/B-VI)
JLF & CMC, Mexico (CPM-3, ENDF/B-VI)
ORNL, USA (HELIOS, ENDF/B-VI)
PSI, Switzerland (BOXER, ETOBOX (ENDF/B))
PSI, Switzerland (CASMO-4, ENDF/B-VI)
PSI, Switzerland (CASMO-4, JEF-2.2)
SIEMENS, Germany (CASMO-4, ENDF/B-IV & JEF-1,-2.1)
TSI, Japan (CASMO-4, JEF-2.2)
TWE, USA (CPM-3, ENDF/B-VI)

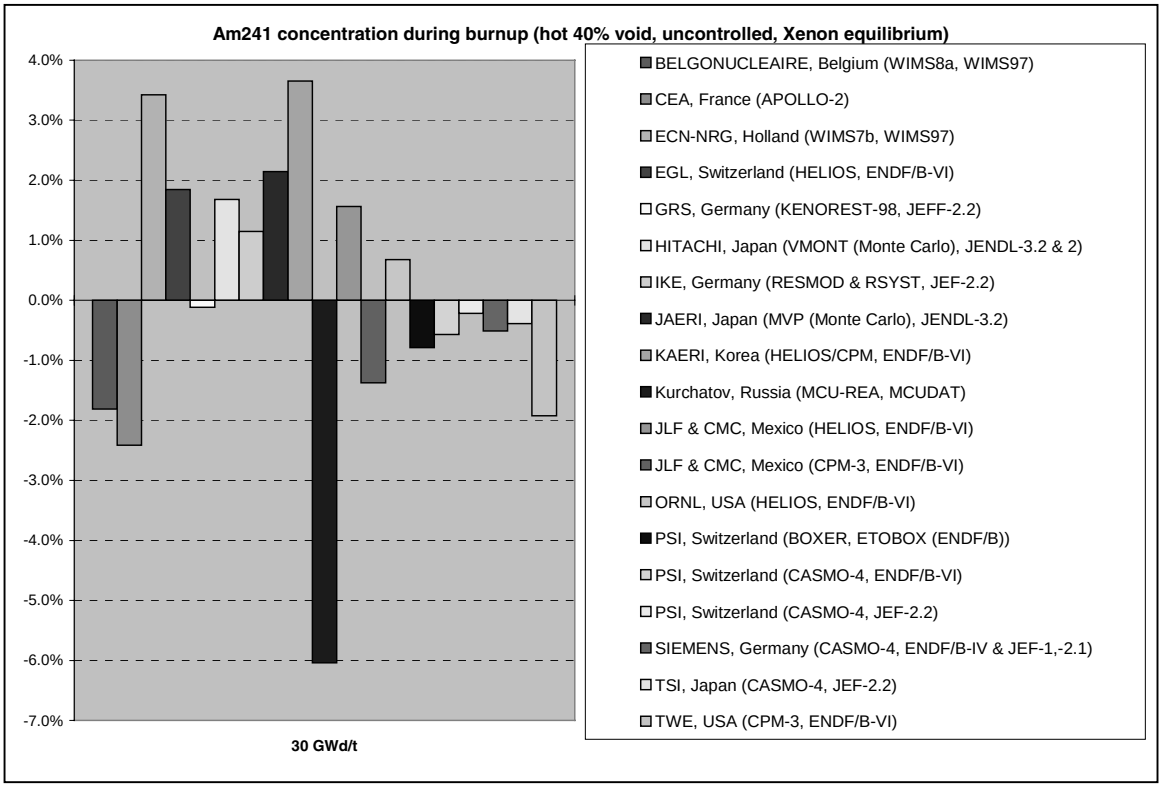
Am241 concentration during burnup (hot 40% void, uncontrolled, Xenon equilibrium)
4.0%
3.0%
2.0%
1.0%
0.0%
-1.0%
-2.0%
-3.0%
-4.0%
-5.0%
-6.0%
-7.0%
30 GWd/t
BELGONUCLEAIRE, Belgium (WIMS8a, WIMS97)
CEA, France (APOLLO-2)
ECN-NRG, Holland (WIMS7b, WIMS97)
EGL, Switzerland (HELIOS, ENDF/B-VI)
GRS, Germany (KENOREST-98, JEFF-2.2)
HITACHI, Japan (VMONT (Monte Carlo), JENDL-3.2 & 2)
IKE, Germany (RESMOD & RSYST, JEF-2.2)
JAERI, Japan (MVP (Monte Carlo), JENDL-3.2)
KAERI, Korea (HELIOS/CPM, ENDF/B-VI)
Kurchatov, Russia (MCU-REA, MCUDAT)
JLF & CMC, Mexico (HELIOS, ENDF/B-VI)
JLF & CMC, Mexico (CPM-3, ENDF/B-VI)
ORNL, USA (HELIOS, ENDF/B-VI)
PSI, Switzerland (BOXER, ETOBOX (ENDF/B))
PSI, Switzerland (CASMO-4, ENDF/B-VI)
PSI, Switzerland (CASMO-4, JEF-2.2)
SIEMENS, Germany (CASMO-4, ENDF/B-IV & JEF-1,-2.1)
TSI, Japan (CASMO-4, JEF-2.2)
TWE, USA (CPM-3, ENDF/B-VI)

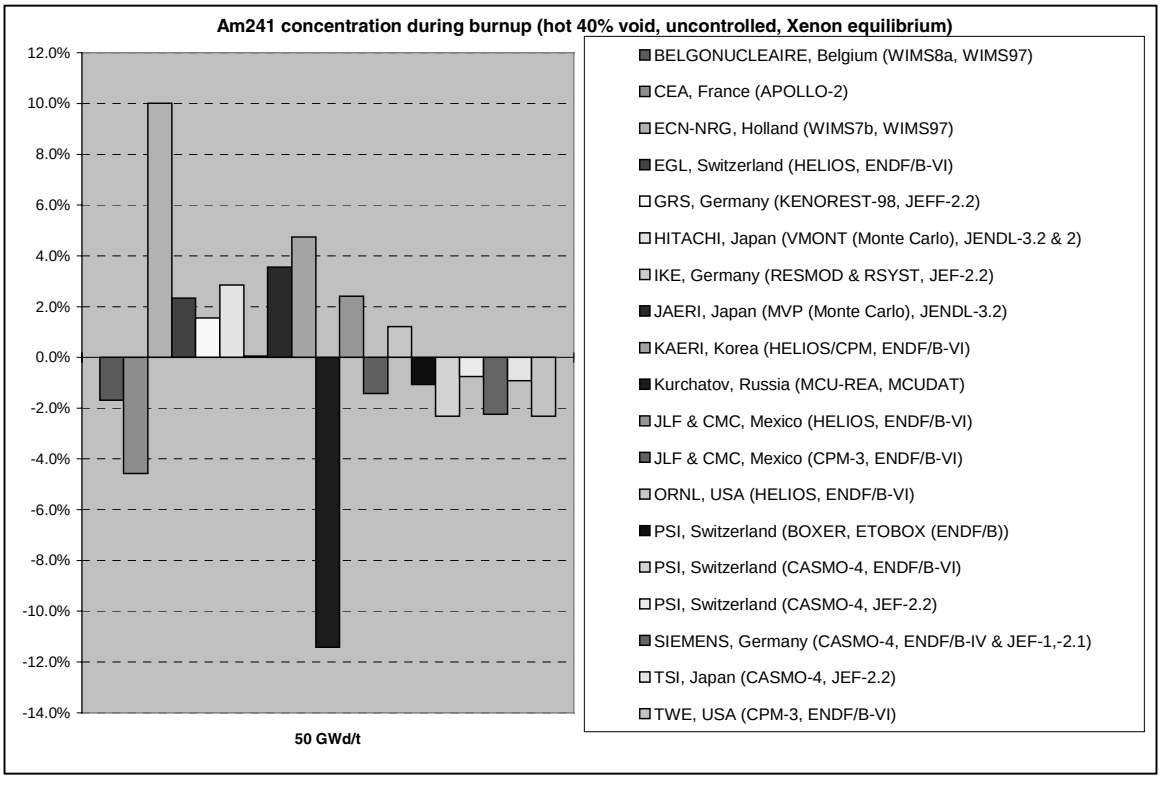
Am241 concentration during burnup (hot 40% void, uncontrolled, Xenon equilibrium)
12.0%
10.0%
8.0%
6.0%
4.0%
2.0%
0.0%
-2.0%
-4.0%
-6.0%
-8.0%
-10.0%
-12.0%
-14.0%
50 GWd/t
BELGONUCLEAIRE, Belgium (WIMS8a, WIMS97)
CEA, France (APOLLO-2)
ECN-NRG, Holland (WIMS7b, WIMS97)
EGL, Switzerland (HELIOS, ENDF/B-VI)
GRS, Germany (KENOREST-98, JEFF-2.2)
HITACHI, Japan (VMONT (Monte Carlo), JENDL-3.2 & 2)
IKE, Germany (RESMOD & RSYST, JEF-2.2)
JAERI, Japan (MVP (Monte Carlo), JENDL-3.2)
KAERI, Korea (HELIOS/CPM, ENDF/B-VI)
Kurchatov, Russia (MCU-REA, MCUDAT)
JLF & CMC, Mexico (HELIOS, ENDF/B-VI)
JLF & CMC, Mexico (CPM-3, ENDF/B-VI)
ORNL, USA (HELIOS, ENDF/B-VI)
PSI, Switzerland (BOXER, ETOBOX (ENDF/B))
PSI, Switzerland (CASMO-4, ENDF/B-VI)
PSI, Switzerland (CASMO-4, JEF-2.2)
SIEMENS, Germany (CASMO-4, ENDF/B-IV & JEF-1,-2.1)
TSI, Japan (CASMO-4, JEF-2.2)
TWE, USA (CPM-3, ENDF/B-VI)

^{243}Am concentration (10^{24} a/cm^3)	5 GWd/t	10 GWd/t	30 GWd/t	50 GWd/t
Average =>	1.1929E-06	2.2693E-06	5.8918E-06	8.7662E-06
Discrepancy max. =>	15.28%	15.35%	13.89%	13.85%
Discrepancy min. =>	-14.40%	-14.46%	-13.98%	-13.54%
Average discrepancies (min./max.) =>	7.38%	7.17%	6.02%	5.68%
Average without extreme values =>	1.1923E-06	2.2681E-06	5.8921E-06	8.7646E-06
Average discrepancies (min./max.) =>	6.51%	6.26%	5.09%	4.74%

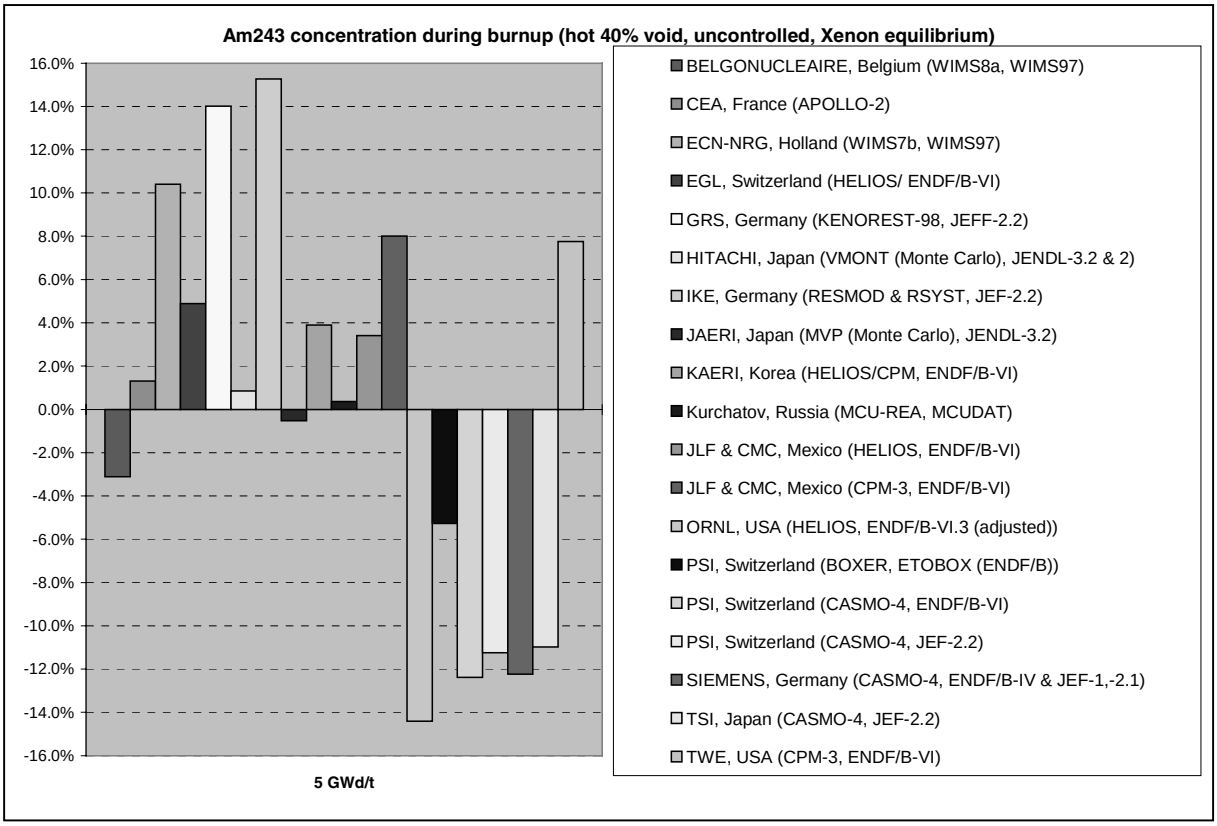

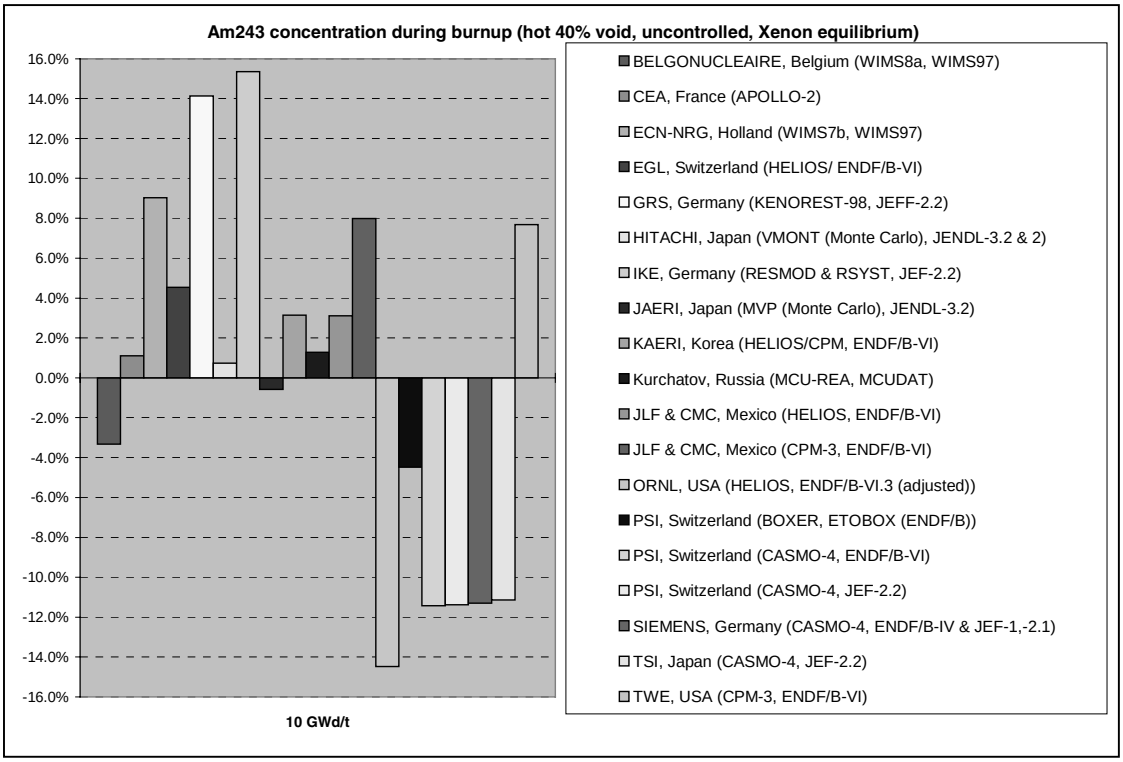
Am243 concentration during burnup (hot 40% void, uncontrolled, Xenon equilibrium)
16.0%
14.0%
12.0%
10.0%
8.0%
6.0%
4.0%
2.0%
0.0%
-2.0%
-4.0%
-6.0%
-8.0%
-10.0%
-12.0%
-14.0%
-16.0%
10 GWd/t
BELGONUCLEAIRE, Belgium (WIMS8a, WIMS97)
CEA, France (APOLLO-2)
ECN-NRG, Holland (WIMS7b, WIMS97)
EGL, Switzerland (HELIOS/ ENDF/B-VI)
GRS, Germany (KENOREST-98, JEFF-2.2)
HITACHI, Japan (VMONT (Monte Carlo), JENDL-3.2 & 2)
IKE, Germany (RESMOD & RSYST, JEF-2.2)
JAERI, Japan (MVP (Monte Carlo), JENDL-3.2)
KAERI, Korea (HELIOS/CPM, ENDF/B-VI)
Kurchatov, Russia (MCU-REA, MCUDAT)
JLF & CMC, Mexico (HELIOS, ENDF/B-VI)
JLF & CMC, Mexico (CPM-3, ENDF/B-VI)
ORNL, USA (HELIOS, ENDF/B-VI.3 (adjusted))
PSI, Switzerland (BOXER, ETOBOX (ENDF/B))
PSI, Switzerland (CASMO-4, ENDF/B-VI)
PSI, Switzerland (CASMO-4, JEF-2.2)
SIEMENS, Germany (CASMO-4, ENDF/B-IV & JEF-1,-2.1)
TSI, Japan (CASMO-4, JEF-2.2)
TWE, USA (CPM-3, ENDF/B-VI)

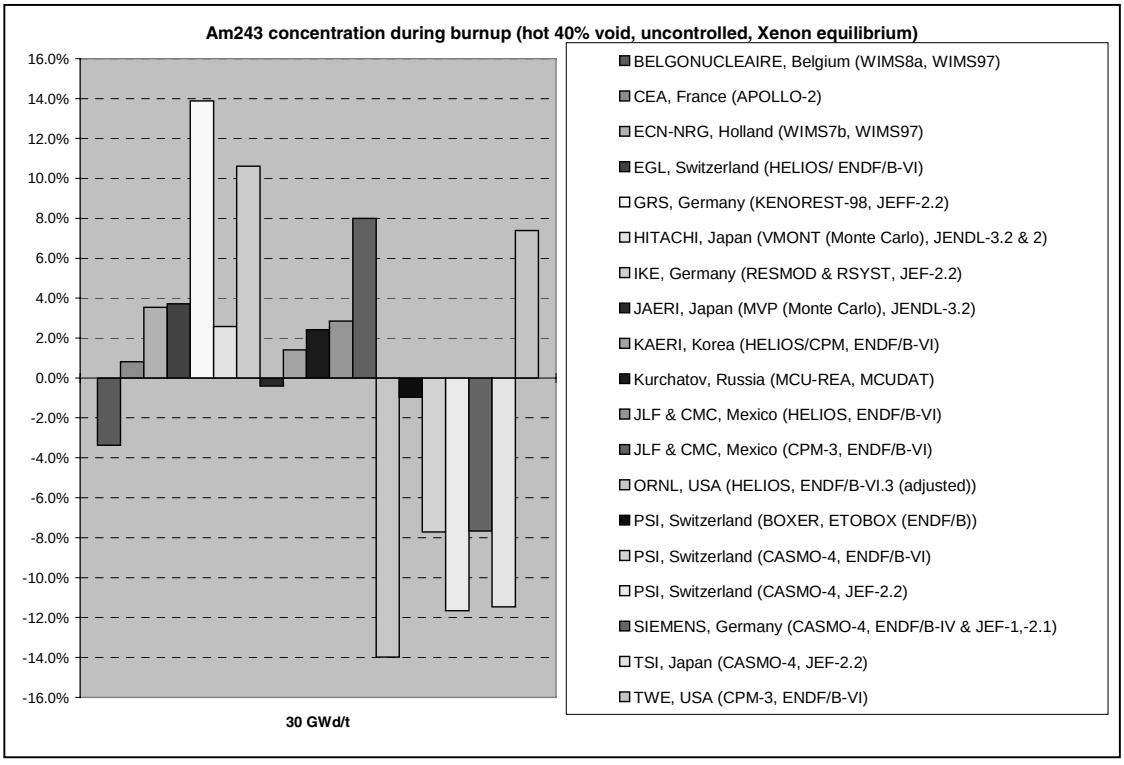
Am243 concentration during burnup (hot 40% void, uncontrolled, Xenon equilibrium)
16.0%
14.0%
12.0%
10.0%
8.0%
6.0%
4.0%
2.0%
0.0%
-2.0%
-4.0%
-6.0%
-8.0%
-10.0%
-12.0%
-14.0%
-16.0%
30 GWd/t
BELGONUCLEAIRE, Belgium (WIMS8a, WIMS97)
CEA, France (APOLLO-2)
ECN-NRG, Holland (WIMS7b, WIMS97)
EGL, Switzerland (HELIOS/ ENDF/B-VI)
GRS, Germany (KENOREST-98, JEFF-2.2)
HITACHI, Japan (VMONT (Monte Carlo), JENDL-3.2 & 2)
IKE, Germany (RESMOD & RSYST, JEF-2.2)
JAERI, Japan (MVP (Monte Carlo), JENDL-3.2)
KAERI, Korea (HELIOS/CPM, ENDF/B-VI)
Kurchatov, Russia (MCU-REA, MCUDAT)
JLF & CMC, Mexico (HELIOS, ENDF/B-VI)
JLF & CMC, Mexico (CPM-3, ENDF/B-VI)
ORNL, USA (HELIOS, ENDF/B-VI.3 (adjusted))
PSI, Switzerland (BOXER, ETOBOX (ENDF/B))
PSI, Switzerland (CASMO-4, ENDF/B-VI)
PSI, Switzerland (CASMO-4, JEF-2.2)
SIEMENS, Germany (CASMO-4, ENDF/B-IV & JEF-1,-2.1)
TSI, Japan (CASMO-4, JEF-2.2)
TWE, USA (CPM-3, ENDF/B-VI)

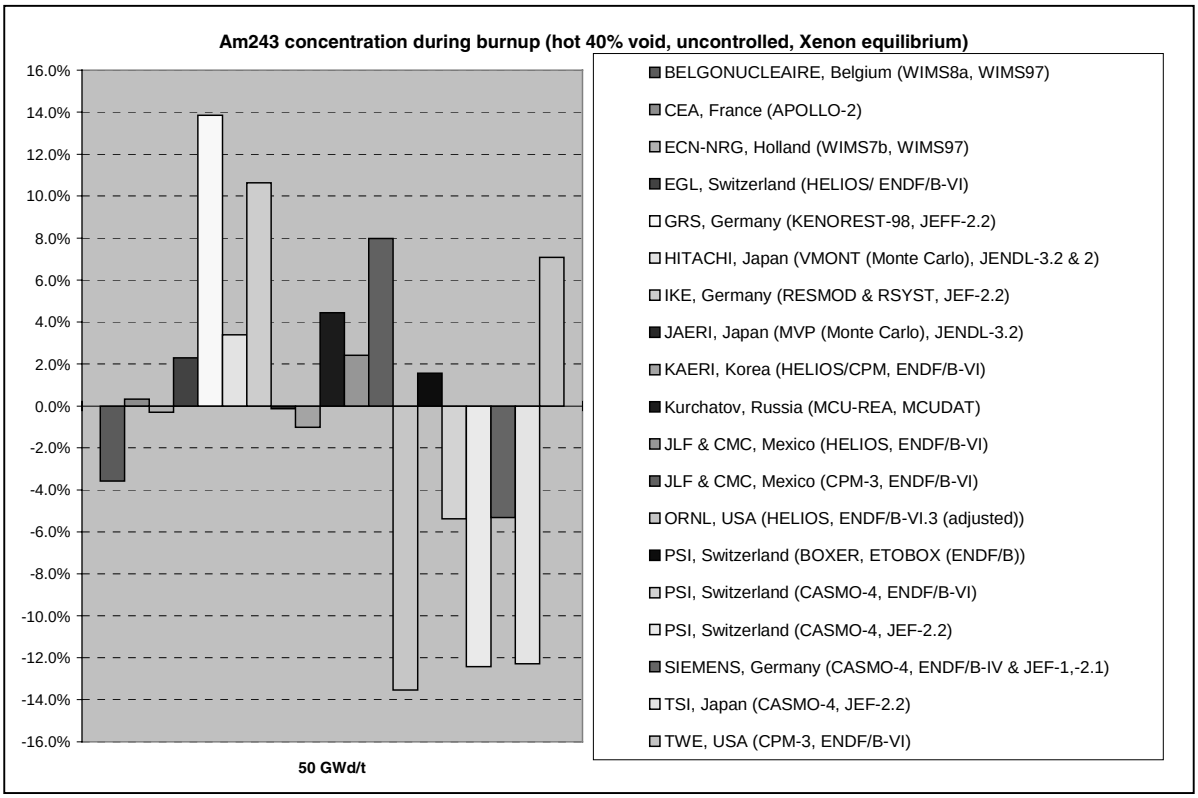

^{244}Cm concentration	5 GWd/t	10 GWd/t	30 GWd/t	50 GWd/t
Average =>	7.7445E-08	2.8812E-07	2.1299E-06	5.1206E-06
Discrepancy max. =>	31.71%	29.67%	19.31%	12.52%
Discrepancy min. =>	-28.36%	-27.28%	-22.30%	-18.45%
Average discrepancies (min./max.) =>	11.17%	10.83%	9.01%	7.98%
Average without extreme values =>	7.7292E-08	2.8771E-07	2.1336E-06	5.1384E-06
Average discrepancies (min./max.) =>	8.95%	8.75%	7.63%	7.08%

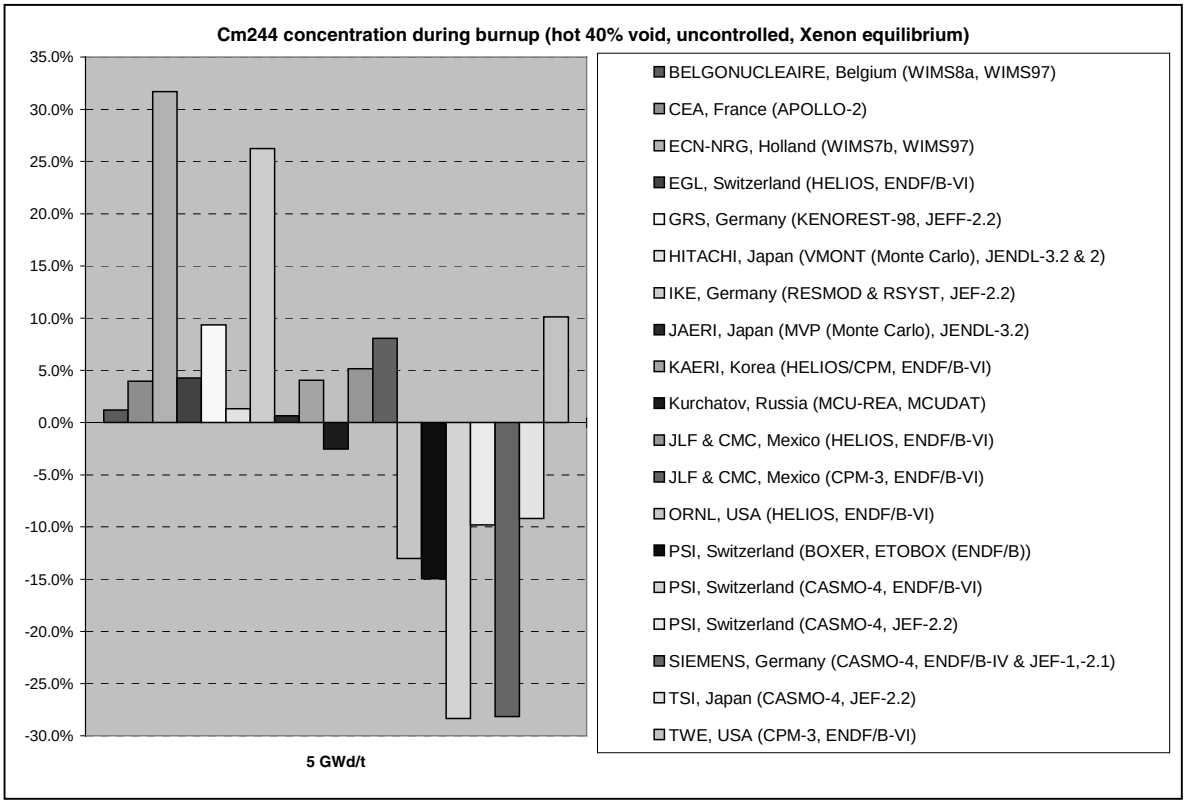
Cm244 concentration during burnup (hot 40% void, uncontrolled, Xenon equilibrium)
35.0%
30.0%
25.0%
20.0%
15.0%
10.0%
5.0%
0.0%
-5.0%
-10.0%
-15.0%
-20.0%
-25.0%
-30.0%
5 GWd/t
BELGONUCLEAIRE, Belgium (WIMS8a, WIMS97)
CEA, France (APOLLO-2)
ECN-NRG, Holland (WIMS7b, WIMS97)
EGL, Switzerland (HELIOS, ENDF/B-VI)
GRS, Germany (KENOREST-98, JEFF-2.2)
HITACHI, Japan (VMONT (Monte Carlo), JENDL-3.2 & 2)
IKE, Germany (RESMOD & RSYST, JEF-2.2)
JAERI, Japan (MVP (Monte Carlo), JENDL-3.2)
KAERI, Korea (HELIOS/CPM, ENDF/B-VI)
Kurchatov, Russia (MCU-REA, MCUDAT)
JLF & CMC, Mexico (HELIOS, ENDF/B-VI)
JLF & CMC, Mexico (CPM-3, ENDF/B-VI)
ORNL, USA (HELIOS, ENDF/B-VI)
PSI, Switzerland (BOXER, ETOBOX (ENDF/B))
PSI, Switzerland (CASMO-4, ENDF/B-VI)
PSI, Switzerland (CASMO-4, JEF-2.2)
SIEMENS, Germany (CASMO-4, ENDF/B-IV & JEF-1,-2.1)
TSI, Japan (CASMO-4, JEF-2.2)
TWE, USA (CPM-3, ENDF/B-VI)

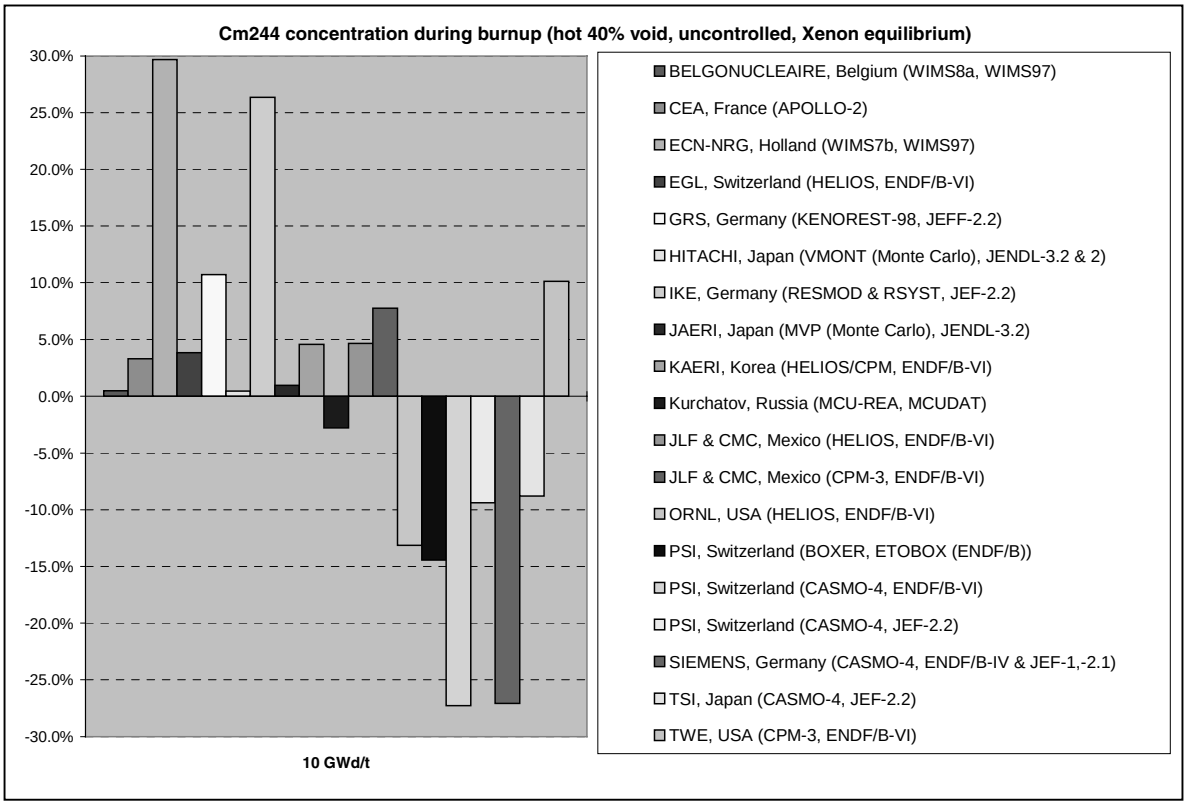
Cm244 concentration during burnup (hot 40% void, uncontrolled, Xenon equilibrium)
30.0%
25.0%
20.0%
15.0%
10.0%
5.0%
0.0%
-5.0%
-10.0%
-15.0%
-20.0%
-25.0%
-30.0%
10 GWd/t
BELGONUCLEAIRE, Belgium (WIMS8a, WIMS97)
CEA, France (APOLLO-2)
ECN-NRG, Holland (WIMS7b, WIMS97)
EGL, Switzerland (HELIOS, ENDF/B-VI)
GRS, Germany (KENOREST-98, JEFF-2.2)
HITACHI, Japan (VMONT (Monte Carlo), JENDL-3.2 & 2)
IKE, Germany (RESMOD & RSYST, JEF-2.2)
JAERI, Japan (MVP (Monte Carlo), JENDL-3.2)
KAERI, Korea (HELIOS/CPM, ENDF/B-VI)
Kurchatov, Russia (MCU-REA, MCUDAT)
JLF & CMC, Mexico (HELIOS, ENDF/B-VI)
JLF & CMC, Mexico (CPM-3, ENDF/B-VI)
ORNL, USA (HELIOS, ENDF/B-VI)
PSI, Switzerland (BOXER, ETOBOX (ENDF/B))
PSI, Switzerland (CASMO-4, ENDF/B-VI)
PSI, Switzerland (CASMO-4, JEF-2.2)
SIEMENS, Germany (CASMO-4, ENDF/B-IV & JEF-1,-2.1)
TSI, Japan (CASMO-4, JEF-2.2)
TWE, USA (CPM-3, ENDF/B-VI)

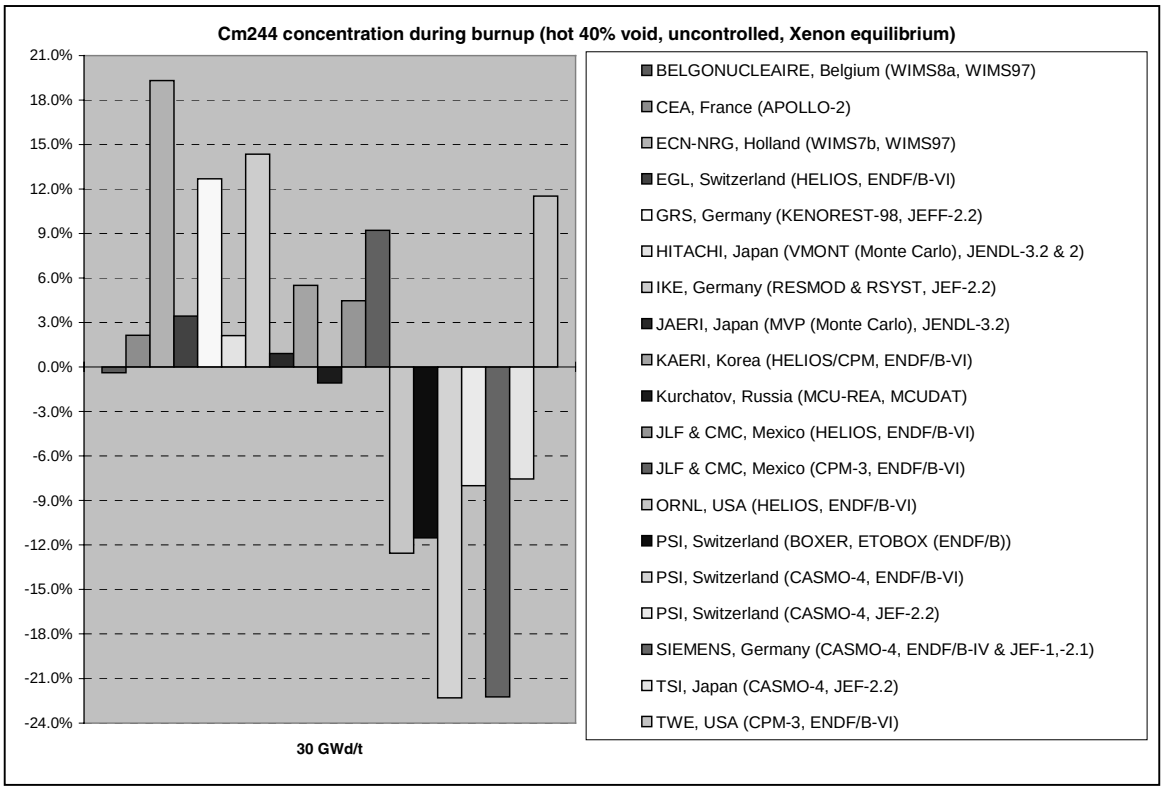
Cm244 concentration during burnup (hot 40% void, uncontrolled, Xenon equilibrium)
21.0%
18.0%
15.0%
12.0%
9.0%
6.0%
3.0%
0.0%
-3.0%
-6.0%
-9.0%
-12.0%
-15.0%
-18.0%
-21.0%
-24.0%
30 GWd/t
BELGONUCLEAIRE, Belgium (WIMS8a, WIMS97)
CEA, France (APOLLO-2)
ECN-NRG, Holland (WIMS7b, WIMS97)
EGL, Switzerland (HELIOS, ENDF/B-VI)
GRS, Germany (KENOREST-98, JEFF-2.2)
HITACHI, Japan (VMONT (Monte Carlo), JENDL-3.2 & 2)
IKE, Germany (RESMOD & RSYST, JEF-2.2)
JAERI, Japan (MVP (Monte Carlo), JENDL-3.2)
KAERI, Korea (HELIOS/CPM, ENDF/B-VI)
Kurchatov, Russia (MCU-REA, MCUDAT)
JLF & CMC, Mexico (HELIOS, ENDF/B-VI)
JLF & CMC, Mexico (CPM-3, ENDF/B-VI)
ORNL, USA (HELIOS, ENDF/B-VI)
PSI, Switzerland (BOXER, ETOBOX (ENDF/B))
PSI, Switzerland (CASMO-4, ENDF/B-VI)
PSI, Switzerland (CASMO-4, JEF-2.2)
SIEMENS, Germany (CASMO-4, ENDF/B-IV & JEF-1,-2.1)
TSI, Japan (CASMO-4, JEF-2.2)
TWE, USA (CPM-3, ENDF/B-VI)

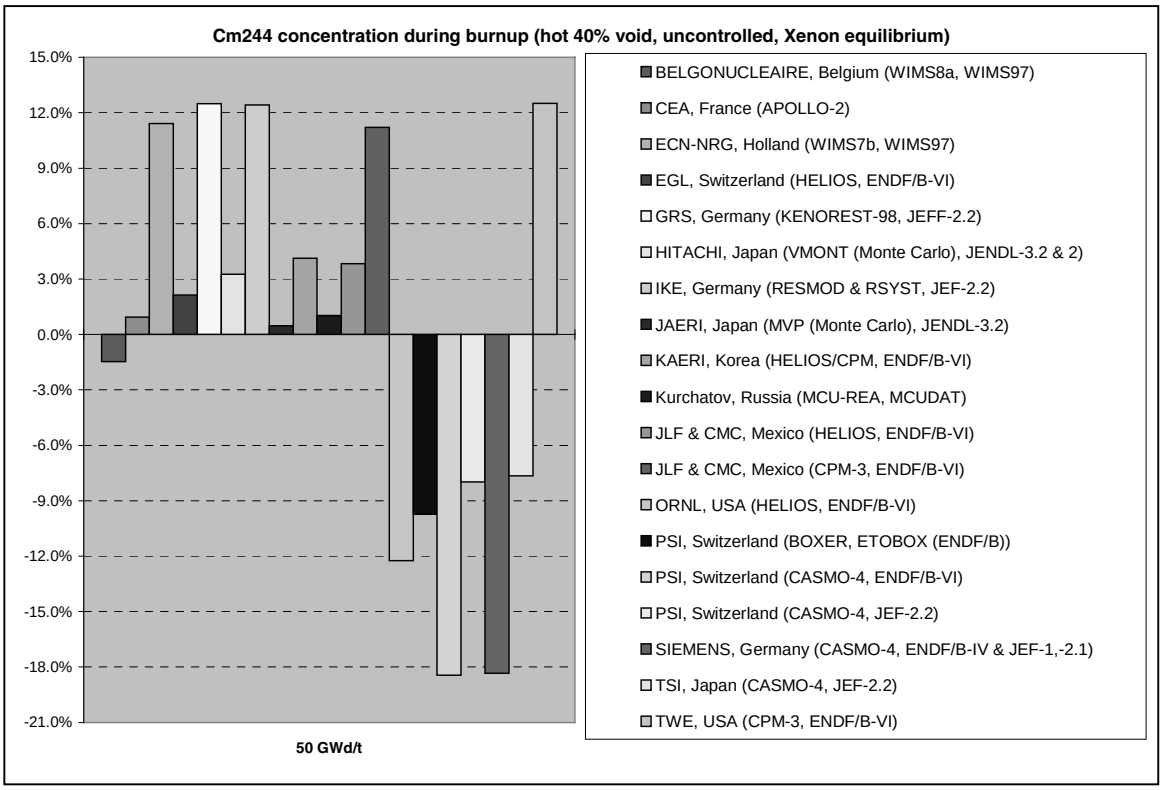
Cm244 concentration during burnup (hot 40% void, uncontrolled, Xenon equilibrium)
15.0%
12.0%
9.0%
6.0%
3.0%
0.0%
-3.0%
-6.0%
-9.0%
-12.0%
-15.0%
-18.0%
-21.0%
50 GWd/t
BELGONUCLEAIRE, Belgium (WIMS8a, WIMS97)
CEA, France (APOLLO-2)
ECN-NRG, Holland (WIMS7b, WIMS97)
EGL, Switzerland (HELIOS, ENDF/B-VI)
GRS, Germany (KENOREST-98, JEFF-2.2)
HITACHI, Japan (VMONT (Monte Carlo), JENDL-3.2 & 2)
IKE, Germany (RESMOD & RSYST, JEF-2.2)
JAERI, Japan (MVP (Monte Carlo), JENDL-3.2)
KAERI, Korea (HELIOS/CPM, ENDF/B-VI)
Kurchatov, Russia (MCU-REA, MCUDAT)
JLF & CMC, Mexico (HELIOS, ENDF/B-VI)
JLF & CMC, Mexico (CPM-3, ENDF/B-VI)
ORNL, USA (HELIOS, ENDF/B-VI)
PSI, Switzerland (BOXER, ETOBOX (ENDF/B))
PSI, Switzerland (CASMO-4, ENDF/B-VI)
PSI, Switzerland (CASMO-4, JEF-2.2)
SIEMENS, Germany (CASMO-4, ENDF/B-IV & JEF-1,-2.1)
TSI, Japan (CASMO-4, JEF-2.2)
TWE, USA (CPM-3, ENDF/B-VI)

Void effect

The void effect given here is the void of the coolant. The water hole and the water blade were not voided. Usually, this effect is small with MOX fuel.

k_{inf} (BOL)	100% Void	Void effect (40%-100%)	Void effect (80%-100%)
Average =>	1.09793	-0.03657	-0.00734
Discrepancy max. =>	0.02558	0.02313	0.01364
Discrepancy min. =>	-0.01433	-0.01366	-0.00854
Average discrepancies (min./max.) =>	0.00602	0.00685	0.00405
Average without extreme values =>	1.09667	-0.03760	-0.00791
Average discrepancies (min./max.) =>	0.00292	0.00428	0.00248

Eleven solutions were given for void effect. 8 solutions are very close. The void effect between nominal and voided conditions is negative (-3.5% in average) for all participants. The void effect between 80% and 100% of void is a small negative effect. Some participants find it positive. Nevertheless, the agreement between the values (extreme solutions excepted) is good (about less than 0.5% in reactivity).

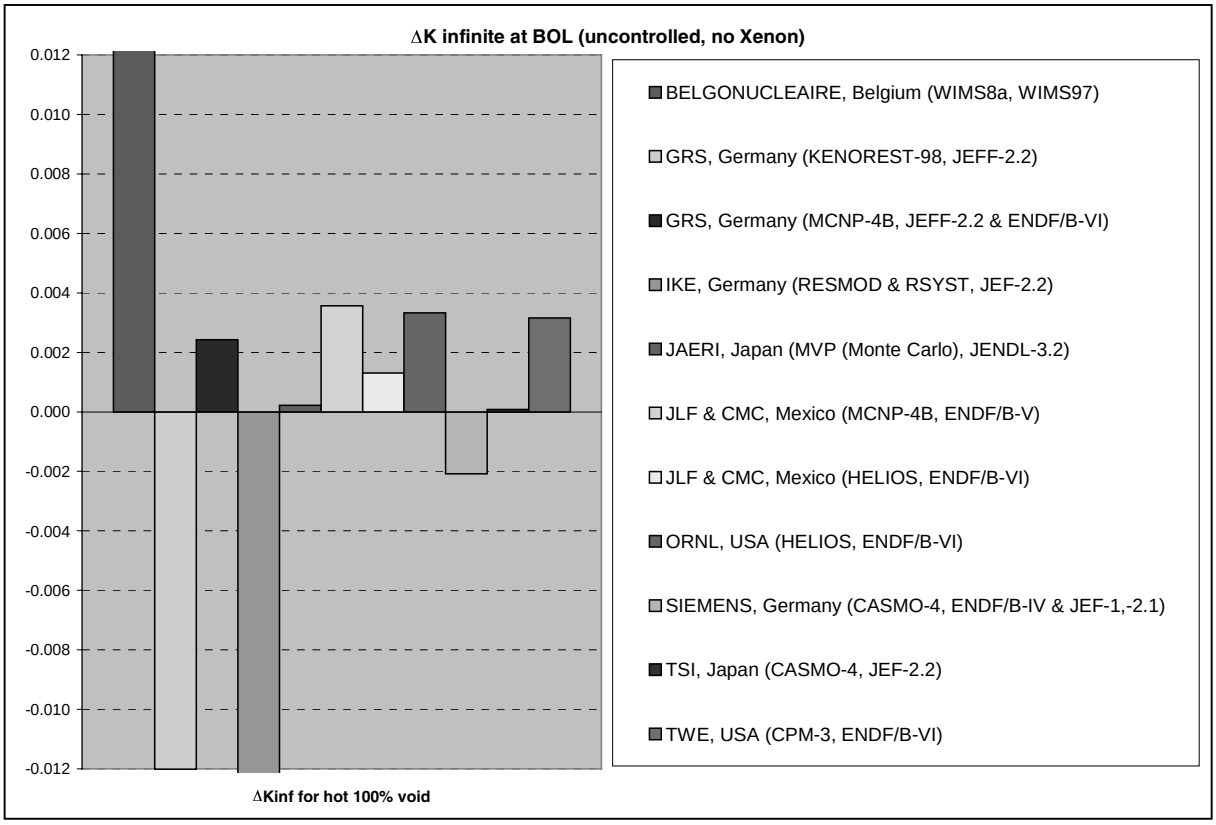

Controlled states

A simplified cruciform control rod model was specified by SIEMENS for a supplementary problem in the MOX BWR Benchmark for "controlled states", meaning core conditions in which control rods are fully inserted. The control rod was assumed to consist of a massive steel absorber in the centre and with cruciform steel blades containing cylindrical holes filled uniformly with B_4C powder. Control rods (CR) play an essential role in the reactivity control of BWRs. Accordingly a simplified cruciform control rod was defined for the present benchmark in order to investigate the influence of control rods on the reactivity and power distribution of a MOX assembly. The specification of this simplified control rod model (in which only B_4C is assumed as absorber material) is given in Appendix A.3 of Annex. Results of power distributions and reactivity were requested for all hot states with various void fractions and for the cold state.

Four participants submitted solutions for controlled states: ORNL with HELIOS, TSI with CASMO-4 (JEF2-lib), GRS with MCNP and Siemens/Framatome ANP with CASMO-4 (ENDF/B-lib). Generally, HELIOS and MCNP have the capability to model the control rod in finer detail than CASMO-4.

The following tables show k_{inf} and peaking factor for the rodded conditions.

1) ORNL, USA

Operating state	k_{inf}	Peaking factor
hot 0% void	0.9833	1.580
hot 40% void	0.9417	1.586
hot 80% void	0.9036	1.612
hot 100% void	0.8954	1.633
cold 0% void	1.0166	1.669

2) TSI, Japan

Operating state	k_{inf}	Peaking factor
hot 0% void	0.99430	1.590
hot 40% void	0.95056	1.597
hot 80% void	0.90662	1.583
hot 100% void	–	–
cold 0% void	1.02420	1.693

3) GRS, Germany

Operating state	k_{inf}	Peaking factor
hot 0% void	0.9891	1.595
hot 40% void	0.9466	1.596
hot 80% void	0.9040	1.582
hot 100% void	–	–
cold 0% void	1.0174	1.732

4) Siemens, Germany

Operating state	k_{inf}	Peaking factor
hot 0% void	0.98705	1.592
hot 40% void	0.94553	1.600
hot 80% void	0.90532	1.594
hot 100% void	–	–
cold 0% void	1.01812	1.699

The results of the reactivity (k_∞) of the controlled states are given are compiled in the table below. The average values and the reactivity of the corresponding uncontrolled states are given for comparison. Generally, the k_∞-values do not spread very much. There is a trend that the TSI k_∞-results are somewhat higher than the others, indicating a small k_∞-basis compared to the other methods, but the general trend is identical for all methods.

k_{inf} (reactivity) of controlled and uncontrolled states

Case controlled	**ORNL Helios**	**TSI C4 JEF 2**	**GRS MCNP**	**FANP/Siem. C4 ENDF**	**average**
hot 0% void contr.	0.9833	0.99430	0.9891	0.98705	0.9884
hot 40% void contr.	0.9417	0.95056	0.9466	0.94553	0.9461
hot 80% void contr.	0.9036	0.90662	0.9040	0.90532	0.9049
hot 100% void contr.	0.8954	–	–	–	0.8954
cold 0% void contr.	1.0166	1.02420	1.0174	1.01812	1.0191
Uncontrolled					
hot 0% void uncontr.	1.1600	1.17093	1.1673	1.16080	1.1648
hot 40% void uncontr.	1.1312	1.14021	1.1384	1.13230	1.1355
hot 80% void uncontr.	1.1038	1.10705	1.1071	1.10340	1.1053
hot 100% void uncontr.	1.1000	–	1.0991	1.09460	1.0979
cold 0% void uncontr.	1.1752	1.18154	1.1758	1.17350	1.1765

In the next table, the control rod worths (i.e. the k_∞-differences between controlled and uncontrolled states) are compiled for all operating states. The results are very similar for all participants: There is the general trend that the control rod worth increases with decreasing water density (e.g. higher voidage).

CR worth (Δk_{inf})	**ORNL**	**TSI**	**GRS**	**FANP/Siem.**	**average**
hot 0% void contr.	-0.1767	-0.17663	-0.1782	-0.17375	-0.1763
hot 40% void contr.	-0.1895	-0.18965	-0.1918	-0.18677	-0.1894
hot 80% void contr.	-0.2002	-0.20043	-0.2031	-0.19808	-0.2005
hot 100% void contr.	-0.2046	–	–	–	-0.2046
cold 0% void contr.	-0.1586	-0.15734	-0.1584	-0.15538	-0.1574

The next table shows the influence of the control rods on void reactivity. For the controlled states the void reactivity is considerably more negative than for the uncontrolled state. It should be

noted that the void reactivities are more variable than the rod worths. In particular, the TSI results show more negative void reactivities than the other solutions.

Hot void reactivity of controlled and uncontrolled states

	ORNL	TSI	GRS	FANP/Siem.	average
k_{inf} 40%-0% contr.	-0.0416	-0.04374	-0.0425	-0.04152	-0.0423
k_{inf} 80%-40% contr.	-0.0381	-0.04394	-0.0426	-0.04021	-0.0412
k_{inf} 40%-0% uncontr.	-0.0288	-0.03072	-0.0289	-0.0285	-0.0292
k_{inf} 80%-40% uncontr.	-0.0274	-0.03316	-0.0313	-0.0289	-0.0302

An important parameter for BWR safety is the hot-cold-reactivity swing. This is the reactivity difference between the hot operating state (with around 40% void) and the cold shutdown state. For the cold shutdown state it has to be assumed that one (the most reactive) control cell is not controlled ("stuck-rod"-criterion). On a simple lattice base the reactivity of this "stuck-rod" case can be taken roughly as the k_∞-average of the controlled and uncontrolled cold state. The hot-cold-swing on a lattice base is then the difference between this cold state and the 40% void uncontrolled case. This hot-cold reactivity is shown in the table below. The results are quite close with GRS/MCNP showing the largest hot-cold-swing and ORNL/HELIOS showing the smallest.

Hot-cold-swing	ORNL	TSI	GRS	FANP/Siem.	average
Delta k_{inf} (cold-hot)	-0.0353	-0.03734	-0.0418	-0.03649	-0.0377

The local peaking factors of the fission rate distributions are shown in the last table. Despite the very heterogeneous geometry of the controlled cell the local peaking factors are almost identical in all solutions, i.e. close to 1.6 for the hot states and around 1.7 for the cold state. Here the ORNL/HELIOS results show a slight increase of the peaking factors with increasing void which is not seen in the other solutions. The location of the peaking rod is always in the corner opposite to the control rod corner. For the cold state it is always on pos. l-10, for hot 0% void it is always on pos. h-10. The location may vary for the hot voided states: l-10, h-10 and k-9 may be the leading rod positions here for the different solutions.

Peaking factor

Case controlled	ORNL Helios	TSI C4 JEF 2	GRS MCNP	FANP/Siem. C4 ENDF	average
hot 0% void contr.	1.580	1.590	1.595	1.592	1.5893
hot 40% void contr.	1.586	1.597	1.596	1.600	1.5948
hot 80% void contr.	1.612	1.583	1.582	1.594	1.5928
hot 100% void contr.	1.633	–	–	–	1.6330
cold 0% void contr.	1.669	1.693	1.732	1.699	1.6983

Chapter 4

DISCUSSION AND INTERPRETATION OF RESULTS

The purpose of this chapter is to comment on the significance of the results obtained in this benchmark from the perspective of commercial reactor operation and support. Each of the main reactor physics parameters discussed in Chapter 3 is considered in the individual sub-sections.

4.1 BOL k_{inf}

Of the BOL k_{inf} calculations performed in the benchmark, the most important one for reactor operation is the result for hot 40% void, since this determines approximately the critical condition of the core for the nominal operational conditions. For both 0% and 40% voidage, the spread of k_{inf} is within ±0.009% Δk when the clear outlier is excluded. This spread is very similar to that obtained in an earlier WPPR benchmark [refer to Volume 6] which modelled PWR MOX in the context of multiple recycle; in the first recycle generation, which corresponds most closely to that considered in the present benchmark, the spread of results for EOC k_{inf} was also ±0.009% Δk. While it is difficult to compare the two results directly, since the PWR benchmark considered EOC conditions, it is encouraging that the BWR benchmark appears to give roughly the same level of agreement. This suggests that the methods are capable of dealing with the many calculational complications of a BWR MOX assembly, including the effect of gadolinia.

The results for hot 80% void and cold 0% void are slightly more difficult to interpret. The overall spread appears somewhat larger than the ±0.009% Δk, but this is due to a larger number of outlying solutions and there appears to be a sub-set of solutions that are tightly clustered within ±0.002% Δk for the hot 80% void case and ±0.004% Δk for the cold 0% void case. The hot 80% void calculation is relevant to normal operation in that it describes the contribution of those areas near the top of the core where voidage is a maximum. The contribution from this region to overall reactivity is slightly reduced because of the relatively low neutron importance, however the correct void content (spectral index) in the upper core regions strongly influences the build-up of heavy metal isotopes with local burn-up and thus is important for cold conditions where the upper regions dominate the reactivity behaviour. The cold 0% void condition is important for shutdown margin calculations.

The comparison between the Monte Carlo and deterministic methods shows a difference of less than ±0.005% Δk. Assuming that the Monte Carlo results can be taken as a kind of "virtual experiment", this indicates that the approximations of the deterministic codes introduce an error in BOC k_{inf} of this order. Interestingly, the difference between ENDF/B and JEF-based nuclear data libraries appears to contribute ±0.010% Δk and combining the two sources of "error" in quadrature (assuming they are statistically independent) would suggest an overall uncertainty band of ~ ±0.011% Δk.

It is difficult to make the connection between these observations and the calculation of the critical condition of an actual core. Firstly, these calculations are for an isolated MOX assembly,

which does not account for the close interaction between MOX and UO_2 assemblies in the practical situation. Secondly, in an actual core there are complex 3-D neutronics and thermal-hydraulic feedback effects to consider and the various assemblies are all at different stages of burn-up. Furthermore, with no experimental measurement such as from BWR mock-up criticals, it is not possible to say which result, if any, is the correct one.

The only comment that can be made is that in the event that the observed discrepancies between the different codes and nuclear data libraries were actually to be representative of a real core loaded entirely with MOX assemblies, the calculation of the critical core condition would not meet the precision required for operational purposes. Having said this, it should be noted that only a sub-set of the solutions presented here come from organisations with a large database of practical experience of actual BWR operation and it is likely that the spread of results from this sub-set would be smaller. Moreover, those organisations with the operational experience also know of any systematic biases between their code predictions for UO_2 cores and actual measurements and are able to correct for them. Any systematic differences between UO_2 and MOX assemblies would also be well known by the time a utility was ready to proceed with full scale MOX loading. Therefore, it is likely that any underlying discrepancies in the nuclear data libraries and codes such as those seen in the BOL k_{inf} data would not be a significant obstacle in practice.

Nevertheless, prior to any of the methods used for this benchmark being applied to the nuclear design of a BWR with a substantial fraction of MOX fuel assemblies, it is recommended (or even necessary) to obtain actual plant measurements. In practice, a large fraction of MOX assemblies would not be loaded for the first time without being preceded by smaller scale batches in which a reduced number of MOX assemblies are loaded and the physics parameters monitored closely (in fact this has been the procedure in the Gundremmingen plant). With the spread of results observed, it is likely that most of the methods would be acceptable for carrying out the nuclear design work provided that they are already validated for UO_2 cores. The impact on the BOL reactivity of the whole core is reduced in proportion to the fraction of the core loaded with MOX assemblies such that the uncertainty is expected to be acceptable. It is suggested that an overall uncertainty target of ±0.002 to ±0.003% Δk would probably be acceptable and achievable for part MOX loadings. In practice, a first-time loading of MOX assemblies would probably proceed initially at a low level and this would allow the operating plant measurements to be accumulated without significant detriment to the prediction of BOL reactivities. Ultimately the data so acquired would allow the gradual build up to the desired equilibrium MOX core fraction.

4.2 Variation of k_{inf} with burn-up

The variation of k_{inf} with burn-up is very consistent between the various solutions and the bias at 0 GWd/t with respect to the average tends to be preserved during irradiation, behaviour which is very similar to that seen in an earlier WPPR benchmark with PWR MOX assemblies [refer to Volume 6]. The difference in reactivity gradients between solutions based on JEF-2.2 and ENDF/B-VI is slightly worrying and invites further investigation. Differences in the evolution with burn-up implies that there will be small differences in the radial flux/power distribution across the core.

The variation of k_{inf} with burn-up is an important design parameter for determining the mean anticipated discharge burn-up and thus the economics of a fuel assembly. The present benchmark design has been chosen in such a way that the mean k_{inf} at hot uncontrolled 40% void state between 10 and 50 GWd/t is around (or slightly above) 1.0, thus allowing mean discharge burn-ups of close to 50 GWd/t in one-year cycles with some coastdown operation. This is of course biased by the

CASMO(ENDF/B) k_{inf} which was used by Siemens (not knowing the "real" k_{inf}) for the benchmark design. For design studies a prediction accuracy of around 1 GWd/t mean discharge burn-up should be acceptable. Taking as a (rather rough) rule of thumb that an increase of the mean k_{inf} by 0.01 corresponds to an increase of the mean discharge burn-up of around 2 GWd/t, a k_{inf} spread of around 0.005 around the "real" value seems to be acceptable. Taking the k_{inf} values at 30 GWd/t as an indicator, the spread of solutions (outliers excepted) is around 0.005. This suggests that most of the codes will predict similar mean discharge burn-ups.

4.3 Power peaking factor

The spread of results of ±2.0% in BOL power peaking factor (outlying solutions excluded) at hot conditions is acceptable for nuclear design applications, being less than the uncertainty accepted on the calculations It should be borne in mind that the interaction between UO_2 and MOX fuel has not been subject of the present Benchmark. The direct neighbourhood of UO_2 assemblies to MOX assemblies will normally increase the peaking factors of the outer row in the BWR MOX assembly by a few percent. The process of introducing MOX assemblies into the core would likely proceed in stages and it would be prudent to load the MOX assemblies initially in core locations where they are unlikely to be the lead assemblies and where any bias between the calculations and the actual power peaking will not limit the core.

4.4 Gadolinia depletion behaviour

The gadolinia design strongly influences the important core characteristics, particularly the core power peaking factors, control rod densities and shutdown margins (although, particularly for the present benchmark design, the effect is considerably less pronounced than in uranium fuel). There are some large differences between participants with respect to the ^{155}Gd and ^{157}Gd concentrations at burn-ups in the range 6 to 10 GWd/t where the gadolinia is approaching complete burn-out and the reactivity versus burn-up curve varies rapidly with burn-up. Although the absolute concentrations of ^{155}Gd and ^{157}Gd are quite small in the 6 to 10 GWd/t range of interest, the discrepancies in the residual concentrations may have an effect on reactivity and peaking factor, particularly since self-shielding effects are by then very weak. As the reactivity effect of gadolinium itself is rather low in the present Benchmark, the most interesting feature here (compared with uranium fuel) is the hard neutron spectrum and the strong spectral gradient in the gadolinia rods located between the internal water channel and the MOX rods with high Pu content. The differences in the reactivity behaviour of the various solutions during gadolinium burn-out are generally small enough that they will only have a marginal influence on core parameters.

4.5 Heavy nuclide concentrations

Although the heavy nuclide concentrations are not of direct interest as a core parameter, discrepancies do have an indirect impact on the core characteristics through the influence that they have on the evolution of core multiplication factor with burn-up. Heavy nuclide inventories are, however, important for safeguards calculations and also for spent fuel inventory calculations (especially if the MOX fuel is intended for further reprocessing).

The values obtained seem to be in reasonably good agreement, at least for the lower plutonium isotopes. The higher plutonium isotopes tend to be more discrepant, as do the minor actinides. As might be expected, the spread of results increases with mass number, being most significant for ^{244}Cm,

reflecting the accumulation of errors as we proceed up the mass chain and the progressively smaller concentrations of high mass nuclides. With appropriate benchmarking to experimental measurements, the spread of results would probably be adequate for safeguards applications. Sometimes the nuclear design codes are used to perform the spent fuel inventory calculations. Alternatively, specialised codes such as ORIGEN can be used for this purpose, in which case the nuclear design codes are used to pass few-group fluxes and cross-sections to the inventory codes and any biases in the nuclear design codes are likely to pass over to the inventory codes. Irrespective of which approach is used, the spread of values suggests that for at least the higher mass nuclides, benchmarking of the inventory calculations to experimental measurements would be needed.

4.6 Void effect

The void effect is a crucial parameter in BWRs both in view of normal operating conditions and in view of safety related areas such as transients and stability. There is a large spread of results, when all the solutions are included, although the spread is narrowed if the outlying solutions are excluded. The void effect on the single assembly basis is difficult to verify from operational data, also a voidage approaching 100% is well outside the range of normal operating experience. Some integral validation might be inferred from operational data for typical core averaged void fractions around 40%, but the largest discrepancies occur at higher values. Perhaps there is a case for benchmarking the calculations to measurements for voided configurations in a critical facility? A good indication may be the (cold) moderator temperature coefficient which is normally measured at the startup of each BWR cycle. This is to a large extent a moderator density effect and the measurements can give valuable hints at the influence of inserted MOX assemblies and on the accuracy of the code system calculating the moderator temperature coefficient.

4.7 Concluding remarks

It is encouraging that the various solutions presented here are generally in reasonable agreement and that the spread of values seen is comparable to those seen in previous PWR benchmarks. This is in spite of the significantly higher complexity of BWR assembly calculations compared with PWR assemblies and the loading of gadolinia.

The data presented here are insufficient to validate the nuclear design methods, because there is no experimental data with which to benchmark the code predictions. However, the generally reasonable agreement, when clear outlying solutions are excepted, does suggest that satisfactory validation of the codes and methods could be demonstrated safely in a programme in which MOX assemblies were phased in gradually with the MOX core fraction being allowed to increase once the operational data have confirmed the satisfactory performance of the nuclear design methods for lower core fractions.

There is the suggestion that critical experiments for a BWR mock-up with voidage might be helpful to provide validation for the calculation of the void effect.

Annex

BWR MOX BENCHMARK SPECIFICATION

G. Schlosser, W. Timm
Siemens/KWU

1. Physical motivations

The layout of the present benchmark proposal has been chosen for the following reasons:

- a modern 10×10 BWR design with large internal water structure is most meaningful;
- the fissile content should enable mean discharge burn-ups of up to 50 GWd/t;
- the isotopic composition of the plutonium should correspond to Pu in burnt UO_2 fuel with discharge burn-ups of >50 GWd/t (Pu quality less than 60%).

2. Geometrical and physical data

The geometric description of the fuel assembly (ATRIUM-10 (10-9Q) type with symmetrical water gaps) is given in Figure A.1. Only uncontrolled single assemblies with reflective boundary conditions are considered. The rod enrichment distribution in the assembly is given in Figure A.2. Note that 6 of the 91 fuel rods are U/Gd-rods.

The material temperatures and the power density are given in Table A.1. The isotopic concentrations of all materials are listed in Table A.2 (MCNP-type input with comments beginning with "C", which should be rather self-explanatory). These nuclide concentrations should correspond to the material densities given in Appendix A.1. Although we have made some effort to compile these data, there is no warranty that these concentrations correspond 100% accurately to the densities in this appendix. The concentrations [in units of 10^{24}] in Table A.2 are the reference anyway. If codes with comfortable input options (such as CASMO or SCALE allowing for simple integral material input due to internal material library) are used it should be checked that the number densities in Table A.2 are reproduced.

Control rods (CR) play an essential role in reactivity control of BWRs. Therefore also a simplified cruciform control rod has been defined for the present benchmark in order to investigate the influence of control rods on the reactivity and power distribution of a MOX assembly. The specification of this simplified control rod model are provided in Appendix A.3 of this Annex.

3. Calculations and results

Calculations are split into two parts.

1) Begin of life (BOL), uncontrolled, no Xenon

- k_∞, fission rate distribution (normalised to 1) and local peaking factors (fission rate)
- Hot 0% void
- Hot 40% void
- Hot 80% void
- Hot 100% (i.e. void reactivity as a function of void fraction)

  Note: 100% void should be taken as 100% steam density which is 0.03676 g/cm^3 at 286°C. The concentrations for "saturated steam" are n(H) = 2.458E-3 and n(O) = 1.229E-3.

- Cold 0% void
- Void reactivity will be presented as a function of void fraction (i.e. 0-40%, 40-80%, 80-100%).
- For a better estimation of the shutdown margins a table with the 40% void hot-cold 0% void reactivity swing will be included.

  Note: Only the coolant surrounding the fuel rods is voided, **not** the water outside the channel box and inside the water channel.

- Results to be reported as in Table A.3/Figure A.3.

Burn-up calculation for hot, uncontrolled operating conditions with 40% void assuming Xenon equilibrium. Power normalisation as in the respective bundle code (normally including gamma-contributions).

- Calculation of k_∞, total flux, fission rate distribution (normalised to 1), local peaking factors and selected heavy nuclide concentrations as a function of lattice exposure for the exposure points 0.0, 0.2, 1, 2, 3, 4, 5, 6, 7, 8, 9, 10, 30, 50 GWd/t
- Results to be reported as in Table 4/Figure A.3.
- *Whenever possible*: (provided the information is easily available)
- Microscopic fission and capture (n, γ) cross-sections for the same heavy nuclides, also total macroscopic cross-sections integrated over all energy groups (one-group) for burn-ups of 0, 5, 10, 30 and 50 GWd/t for hot uncontrolled conditions with 40% void.
- Results to be reported as in Table A.5.
- The same information should also be provided for pins **d6** (U/Gd low power), **d7** (high Pu content, peaking factor), **e10** (average type of pin) for the following three energy groups:

  Group 1 (**fast**): $\rightarrow$ 5.53 keV Group 2: $\rightarrow$ ~4.0 eV Group 3 (**thermal**): $\rightarrow 10^{-5}$ eV

- Results should be reported as in Tables A.6.1, 6.2 and A.6.3.

Results concerning gadolinia depletion including individual isotopes should be reported as outlined in Table A.7:

- Nuclide concentrations and absorption rates for the following exposure points: 0.0, 0.2, 1, 2, 3, 4, 5, 6, 7, 8, 9, 10, 30, 50 GWd/t for pins **d6, f8, g8**.

Figure A.1. Geometry layout

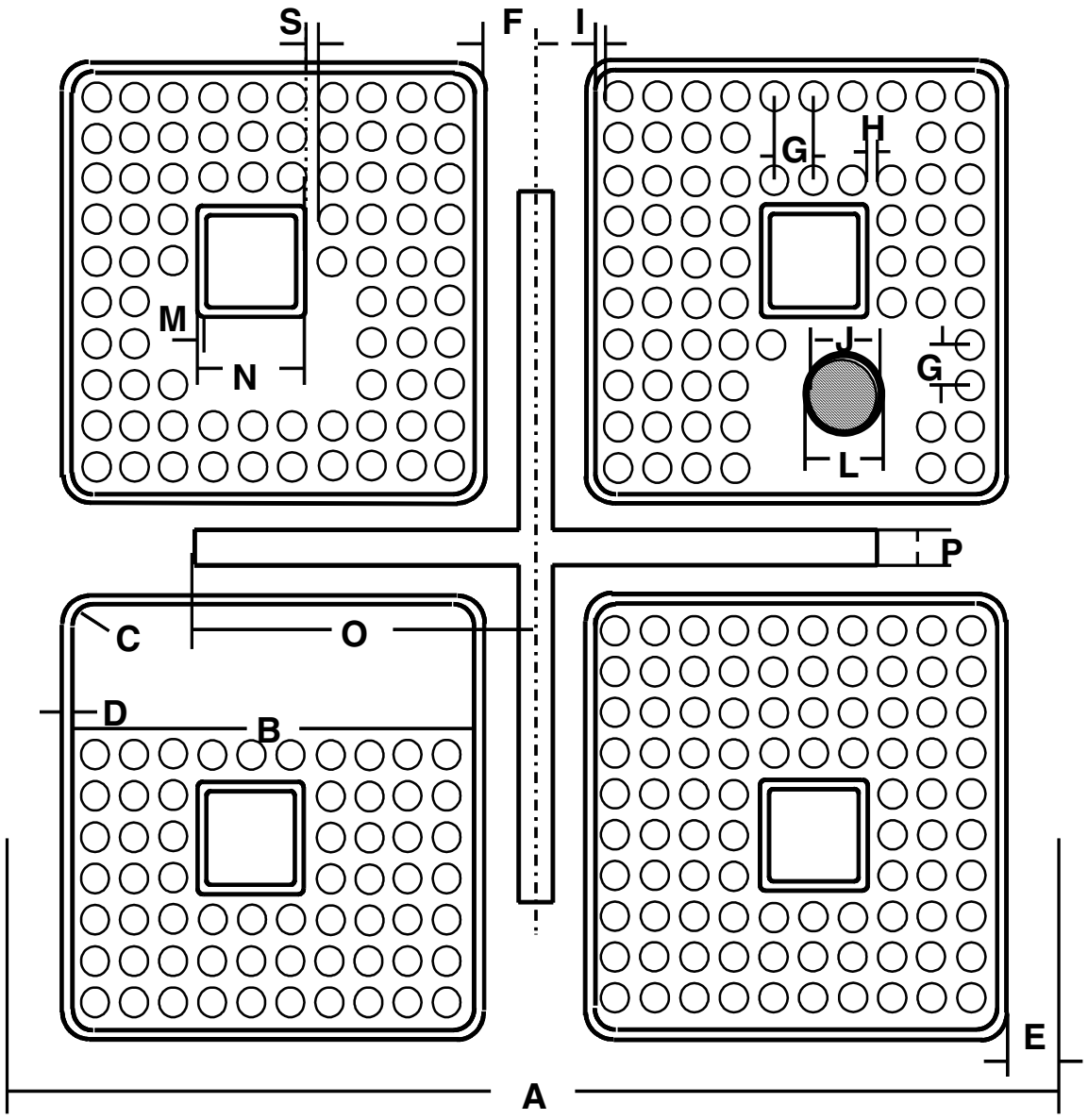

A 305.00	G 12.95	N 35.00
B 134.00	H 2.90	O 122.4
C 0.0	I 3.70	P 6.37
D 2.50	J 8.84	S 3.375
E 6.75	L 10.05	
F 6.75	M 0.725	

Note: 2S+N = 3G+H.

Figure A.2. Fuel rod distribution in the lattice 10CQL043/393–6G1.5

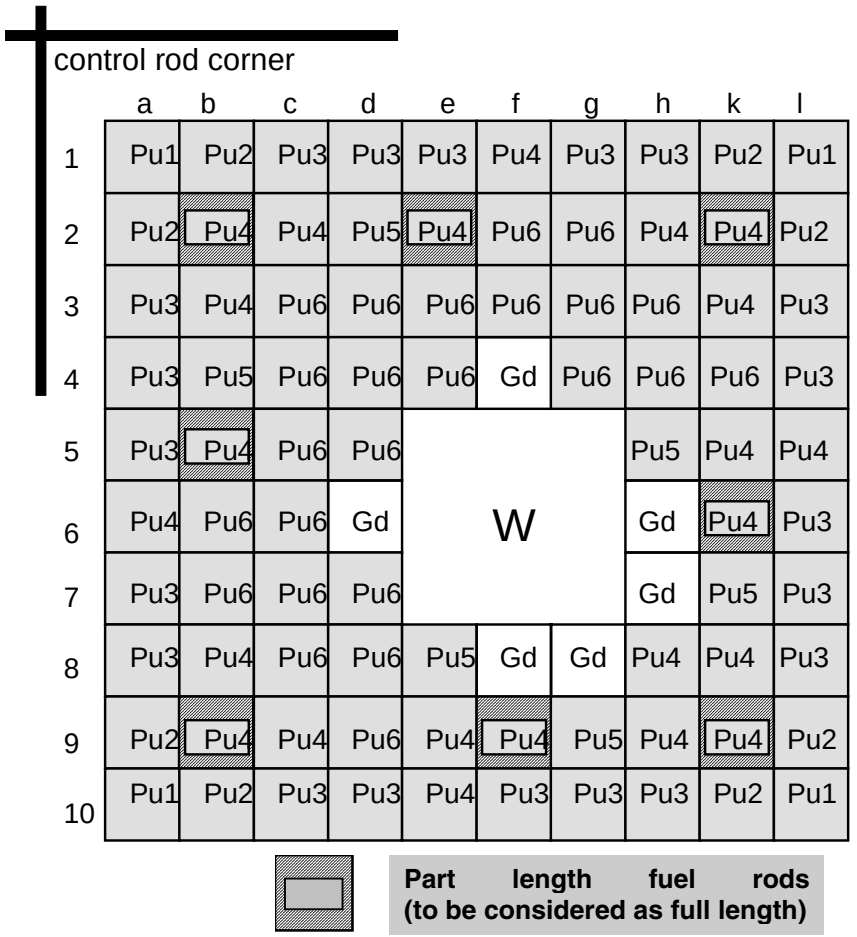

rod type	w/o ^{235}U in U	w/o Pu_{fiss} in U_{tails}, 0.2 ^{235}U	Pu_{tot}	w/o Gd_2O_3	no.
Gd	**3.95**	**0.00**		**1.5**	**6**
Pu1	**0.2**	**1.6**	**2.69**	**–**	**4**
Pu2	**0.2**	**2.3**	**3.86**	**–**	**8**
Pu3	**0.2**	**3.1**	**5.20**	**–**	**20**
Pu4	**0.2**	**4.0**	**6.71**	**–**	**23**
Pu5	**0.2**	**4.5**	**7.55**	**–**	**6**
Pu6	**0.2**	**6.3**	**10.57**	**–**	**24**
	mean fissile content in w/o				
	0.43 ^{235}U	**3.93 Pu_{fiss}**			

Figure A.3. Results to be reported: Local fission rate distribution (normalised to 1); only half the assembly (including diagonal) is required

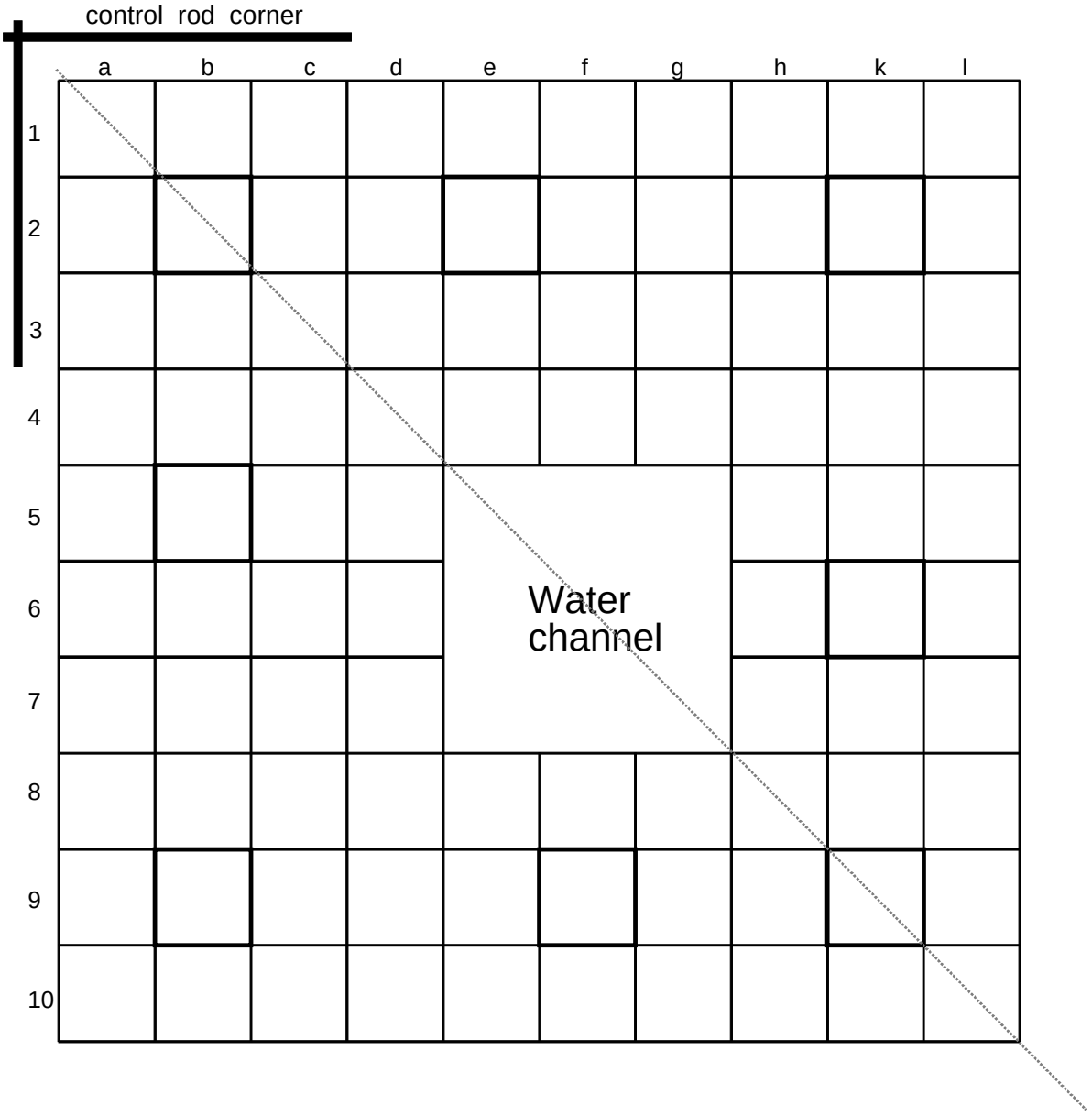

Note: In order to avoid confusion with the letters i and j, these letters have not been used for pin positioning.

Table A.1. Material temperatures and power density

Temperatures		
Fuel	hot	900 K**
Fuel	cold	293 K
Clad/Box	hot	600 K
Clad/Box	cold	293 K
H_2O	hot	559 K (573 K)*
H_2O	cold	293 K
Power density		25 W/gHM**

* 559 K corresponds to hot BWR operating conditions and the H_2O concentrations in Table A.2, if only 573 K is available in the library, this temperature is also acceptable at the given nuclide densities calculated for the real temperature and pressure.

** For typical BWR power densities of 25 W/gHM (Heavy Metal) fuel temperatures in a 10×10 bundle are usually lower than 900 K but this temperature should be used in the calculation.

Table A.2. Isotopic compositions (I)

```
C Cold geometry and densities!
C
C k-boltzmann =8.6153E -5 eV / K
C                    DENSITIES G/CM3
C   H2O (NORMAL cold)          0.998
C   H2O (NORMAL hot)           0.740
C   H2O (VOIDING 40%)          0.458
C   H2O (VOIDING 80%)          0.177
C   CLAD-MATERIAL              6.550
C   WATERBOX  / -CHANNEL       6.550
C   FUEL        (MOX    )      9.921
C   FUEL  (UO2 /GD)            9.737
CC
C-----------------------------------------------
C  concentrations of mixtures , in units of 10**24
C-----------------------------------------------
C H2O: unvoided  cold 0  RHO = 0.998
C H:   1001.92C JEF2 305.9 C 99.985%
C O:   8016.92C JEF2 305.9 C 99.756%
M0     1001.51C  6.672E-02   8016.92C  3.336E-02
C

C-----------------------------------------------
C H2O: unvoided  hot  1  RHO = 0.740
C H:   1001.92C JEF2 305.9 C 99.985%
C O:   8016.92C JEF2 305.9 C 99.756%
M1     1001.51C  4.94479E-02 8016.92C  2.47256E-02
C

C-----------------------------------------------
C H2O: voided     2  RHO = 0.458  (40% void)
C H:   1001.92C JEF2 305.9 C 99.985%
C O:   8016.92C JEF2 305.9 C 99.756%
M2     1001.51C  3.06491E-02 8016.92C  1.53256E-02
C

C-----------------------------------------------
C H2O: voided     3   RHO = 0.177  (80% void)
C H:   1001.92C JEF2 305.9 C 99.985%
C O:   8016.92C JEF2 305.9 C 99.756%
M3    1001.51C  1.183E-02   8016.92C  5.914E-03
C

C-----------------------------------------------
C ZRY4 Clad + box     4
C ZR: 40000.92C JEF2 305.9 C
M4    40000.92C 4.32444-02
```

Table A.2. Isotopic compositions (II)

```
C-----------------------------------------------
C
C MOX1.60:        5
C U235:  92235.91C JEF2 659.9 C
C U238:  92238.91C JEF2 659.9 C
C O:      8016.91C JEF2 659.9 C
C PU238: 94238.91C JEF2 659.9 C
C PU239: 94239.91C JEF2 659.9 C
C PU240: 94240.91C JEF2 659.9 C
C PU241: 94241.91C JEF2 659.9 C
C PU242: 94242.91C JEF2 659.9 C
C U234:  92234.91C = 3.53299E-07
M5    92235.91C 4.36070E-05 92238.91C 2.14883E-02  8016.91C 4.42551E-02
      94238.91C 1.30671E-05 94239.91C 2.73272E-04 94240.91C 1.73178E-04
      94241.91C 7.85925E-05 94242.91C 5.13948E-05 92234.91C 3.50411E-07

C-----------------------------------------------
C
C MOX2.30:        6
C U235:  92235.91C JEF2 659.9 C
C U238:  92238.91C JEF2 659.9 C
C O:      8016.91C JEF2 659.9 C
C PU238: 94238.91C JEF2 659.9 C
C PU239: 94239.91C JEF2 659.9 C
C PU240: 94240.91C JEF2 659.9 C
C PU241: 94241.91C JEF2 659.9 C
C PU242: 94242.91C JEF2 659.9 C
C U234:  92234.91C = 3.49157E-07
M6    92235.91C 4.30914E-05 92238.91C 2.12290E-02  8016.91C 4.42551E-02
      94238.91C 1.87845E-05 94239.91C 3.92821E-04 94240.91C 2.48940E-04
      94241.91C 1.12984E-04 94242.91C 7.38936E-05 92234.91C 3.46269E-07

C-----------------------------------------------
C
C MOX3.10:        7
C U235:  92235.91C JEF2 659.9 C
C U238:  92238.91C JEF2 659.9 C
C O:      8016.91C JEF2 659.9 C
C PU238: 94238.91C JEF2 659.9 C
C PU239: 94239.91C JEF2 659.9 C
C PU240: 94240.91C JEF2 659.9 C
C PU241: 94241.91C JEF2 659.9 C
C PU242: 94242.91C JEF2 659.9 C
C U234:  92234.91C = 3.44475E-07
M7    92235.91C 4.24864E-05 92238.91C 2.09326E-02  8016.91C 4.42551E-02
      94238.91C 2.53115E-05 94239.91C 5.29446E-04 94240.91C 3.35518E-04
      94241.91C 1.52291E-04 94242.91C 9.95910E-05 92234.91C 3.41407E-07
```

Table A.2. Isotopic compositions (III)

```
C-----------------------------------------------
C
C MOX4.00:        8
C U235:  92235.91C JEF2 659.9 C
C U238:  92238.91C JEF2 659.9 C
C O:      8016.91C JEF2 659.9 C
C PU238: 94238.91C JEF2 659.9 C
C PU239: 94239.91C JEF2 659.9 C
C PU240: 94240.91C JEF2 659.9 C
C PU241: 94241.91C JEF2 659.9 C
C PU242: 94242.91C JEF2 659.9 C
C U234:  92234.91C = 3.41054E-07
M8    92235.91C 4.18141E-05 92238.91C 2.05992E-02  8016.91C 4.42551E-02
      94238.91C 3.26793E-05 94239.91C 6.83168E-04 94240.91C 4.32935E-04
      94241.91C 1.96492E-04 94242.91C 1.28509E-04 92234.91C 3.36005E-07


C-----------------------------------------------
C
C MOX4.50:        9
C U235:  92235.91C JEF2 659.9 C
C U238:  92238.91C JEF2 659.9 C
C O:      8016.91C JEF2 659.9 C
C PU238: 94238.91C JEF2 659.9 C
C PU239: 94239.91C JEF2 659.9 C
C PU240: 94240.91C JEF2 659.9 C
C PU241: 94241.91C JEF2 659.9 C
C PU242: 94242.91C JEF2 659.9 C
C U234:  92234.91C = 3.33491E-07
M9    92235.91C 4.14332E-05 92238.91C 2.04139E-02  8016.91C 4.42551E-02
      94238.91C 3.67504E-05 94239.91C 7.68567E-04 94240.91C 4.87043E-04
      94241.91C 2.21051E-04 94242.91C 1.44567E-04 92234.91C 3.32944E-07


C-----------------------------------------------
C
C MOX6.30:        11
C U235:  92235.91C JEF2 659.9 C
C U238:  92238.91C JEF2 659.9 C
C O:      8016.91C JEF2 659.9 C
C PU238: 94238.91C JEF2 659.9 C
C PU239: 94239.91C JEF2 659.9 C
C PU240: 94240.91C JEF2 659.9 C
C PU241: 94241.91C JEF2 659.9 C
C PU242: 94242.91C JEF2 659.9 C
C U234:  92234.91C = 3.33491E-07
M11   92235.91C 4.00887E-05 92238.91C 1.97470E-02  8016.91C 4.42551E-02
      94238.91C 5.14638E-05 94239.91C 1.07599E-03 94240.91C 6.81853E-04
      94241.91C 3.09476E-04 94242.91C 2.02402E-04 92234.91C 3.22140E-07
```

Table A.2. Isotopic compositions (IV)

```
C-----------------------------------------------
C
C GD 1.5 + U235=3.95 w/o        10
C U235:  92235.91C JEF2 659.9 C
C U238:  92238.91C JEF2 659.9 C
C O:      8016.91C JEF2 659.9 C
C U234:  92234.91C
C GD-154 = 1.05498E-05   (64154.99C)
C GD-155 = 7.24224E-05
C GD-156 = 1.00672E-04
C GD-157 = 7.70670E-05
C GD-158 = 1.22311E-04

M10   92235.91C 8.66996E-04 92238.91C 2.08160E-02  8016.91C  4.40859E-02
      92234.91C 6.96691E-06 64154.99C 1.05498E-05  64155.99C 7.24224E-05
      64156.99C 1.00672E-04 64157.99C 7.70670E-05  64158.99C 1.22311E-04
```

RESULTS TO BE SUBMITTED

(Preference is for EXCEL format)

Table A.3. Results to be reported (3a)

operating state	k_∞	peaking factor (fission rates)
hot 0% void		
hot 40% void		
hot 80% void		
hot 100% void*		
cold 0% void		

* 100% steam density: 0.03676 g/cm^3 at 286°C [n(H) = 2.458E-3, n(O) = 1.229E-3]

Table A.4. Results to be reported (3b)

Burn-up calculation for hot uncontrolled conditions with 40% void
Lattice averaged nuclide concentrations in units of 10^{24} per cm^3

to be calculated \ exposure [GWd/t]	0*	0.2	1	2	3	4	5	6	7	8	9	10	30	50
k_∞														
peaking factor														
total neutron flux														
n. c. ^{235}U														
^{238}U														
^{238}Pu														
^{239}Pu														
^{240}Pu														
^{241}Pu														
^{242}Pu														
^{241}Am														
^{243}Am														
^{244}Cm														

* No xenon.

Table A.5. Results to be reported (3b, optionally)

*Lattice averaged (**one-group**) fission and capture(n,γ) cross-sections*
Macroscopic [cm^{-1}] and microscopic [barn]
For hot uncontrolled conditions with 40% void

exposure [GWd/t]	**0***	**5**	**10**	**30**	**50**
fission Σ_{mac}					
σ_{mic} ^{235}**U**					
^{238}**U**					
^{238}**Pu**					
^{239}**Pu**					
^{240}**Pu**					
^{241}**Pu**					
^{242}**Pu**					
^{241}**Am**					
^{243}**Am**					
^{244}**Cm**					

exposure [GWd/t]	**0***	**5**	**10**	**30**	**50**
capture Σ_{mac}					
σ_{mic} ^{235}**U**					
^{238}**U**					
^{238}**Pu**					
^{239}**Pu**					
^{240}**Pu**					
^{241}**Pu**					
^{242}**Pu**					
^{241}**Am**					
^{243}**Am**					
^{244}**Cm**					

* No xenon.

Table A.6.1. Results to be reported (3b, optionally) for each of the following pins: d6, d7, e10

*Lattice averaged (**first** group → 5.53 keV) fission and capture (n,γ) cross-sections*
Macroscopic [cm^{-1}] and microscopic [barn]
For hot uncontrolled conditions with 40% void

exposure [GWd/t]	**0***	**5**	**10**	**30**	**50**
fission Σ_{mac}					
σ_{mic} ^{235}**U**					
^{238}**U**					
^{238}**Pu**					
^{239}**Pu**					
^{240}**Pu**					
^{241}**Pu**					
^{242}**Pu**					
^{241}**Am**					
^{243}**Am**					
^{244}**Cm**					

exposure [GWd/t]	**0***	**5**	**10**	**30**	**50**
capture Σ_{mac}					
σ_{mic} ^{235}**U**					
^{238}**U**					
^{238}**Pu**					
^{239}**Pu**					
^{240}**Pu**					
^{241}**Pu**					
^{242}**Pu**					
^{241}**Am**					
^{243}**Am**					
^{244}**Cm**					

* No xenon.

Table A.6.2. Results to be reported (3b, optionally) for each of the following pins: d6, d7, e10

*Lattice averaged (**second** group → ~4 eV) fission and capture (n,γ) cross-sections*
Macroscopic [cm^{-1}] and microscopic [barn]
For hot uncontrolled conditions with 40% void

exposure [GWd/t]	**0***	**5**	**10**	**30**	**50**
fission Σ_{mac}					
σ_{mic} ^{235}**U**					
^{238}**U**					
^{238}**Pu**					
^{239}**Pu**					
^{240}**Pu**					
^{241}**Pu**					
^{242}**Pu**					
^{241}**Am**					
^{243}**Am**					
^{244}**Cm**					

exposure [GWd/t]	**0***	**5**	**10**	**30**	**50**
capture Σ_{mac}					
σ_{mic} ^{235}**U**					
^{238}**U**					
^{238}**Pu**					
^{239}**Pu**					
^{240}**Pu**					
^{241}**Pu**					
^{242}**Pu**					
^{241}**Am**					
^{243}**Am**					
^{244}**Cm**					

* No xenon.

Table A.6.3. Results to be reported (3b, optionally) for each of the following pins: d6, d7, e10

*Lattice averaged (**third** group → 10^{-5} eV) fission and capture (n,γ) cross-sections*
Macroscopic [cm^{-1}] and microscopic [barn]
For hot uncontrolled conditions with 40% void

exposure [GWd/t]	**0***	**5**	**10**	**30**	**50**
fission Σ_{mac}					
σ_{mic} ^{235}**U**					
^{238}**U**					
^{238}**Pu**					
^{239}**Pu**					
^{240}**Pu**					
^{241}**Pu**					
^{242}**Pu**					
^{241}**Am**					
^{243}**Am**					
^{244}**Cm**					

exposure [GWd/t]	**0***	**5**	**10**	**30**	**50**
capture Σ_{mac}					
σ_{mic} ^{235}**U**					
^{238}**U**					
^{238}**Pu**					
^{239}**Pu**					
^{240}**Pu**					
^{241}**Pu**					
^{242}**Pu**					
^{241}**Am**					
^{243}**Am**					
^{244}**Cm**					

* No xenon.

Table A.7. Additional output information for the BWR MOX benchmark

exposure GWd/t	n.c. ^{155}Gd 10^{24} per cm^3	n.c. ^{157}Gd 10^{24} per cm^3	$R_{abs}(^{155}Gd)$	$R_{abs}(^{157}Gd)$	$R_{abs}(Gd)$
0.0					
0.2					
1.0					
2.0					
3.0					
4.0					
5.0					
6.0					
7.0					
8.0					
9.0					
10.0					

Comments

1) n.c. ^{155}Gd (10^{24} per cm^3) – System average nuclides concentrations (may be averaged over three Gd pins, **d6, f8, g8**)

$R_{abs}(^{155}Gd)$ – absorption rate on the ^{155}Gd isotope in the system

$R_{abs}^{(i)}(x)$ – relative reaction rate type *x* for *i* th isotope in this region:

$$R_{abs}^{(1)} = \frac{\int_{three\ Gd\ pins} \Sigma_{abs}^{(155)}(\alpha)\Phi(\alpha)d\alpha}{\int_{System} \Sigma_{abs}(\alpha)\Phi(\alpha)d\alpha} \qquad (1)$$

where: *abs* – a absorption reaction rate;

$\alpha = \{\vec{r}, \vec{V}\}$ – phase space co-ordinates

$\int_{System} \Sigma_{abs}(\alpha)\Phi(\alpha)d\alpha$ – the total absorption rate in the system

In the case when computer codes uses the following normalisation:

$$R_{abs}^{(155)} = \int_{System} \Sigma_{abs}(a)\Phi(\alpha)d\alpha = 1$$

then $R_{abs}^{(155)} = \int_{three\ Gd\ pins} \Sigma_{abs}^{(155)}(a)\Phi(\alpha)d\alpha = 1$

2) $R_{abs}(Gd)$ – absorption rate for all Gd isotopes.

3) Reaction rates may be submitted also for each of the three energy groups separately.

Appendix A.1

MATERIAL DENSITIES AND PU COMPOSITION

Densities

Oxide	MOX fuel rods (U_{tails} 0.2 w/o ^{235}U in U)	9.921 g/cm^3
Oxide	U-Gd rods (3.95% ^{235}U, 1.5 wt.% Gd_2O_3)	9.737 g/cm^3
Zr (cladding + box)		6.550 g/cm^3
H_2O	286°C (0% void)	0.740 g/cm^3
	286°C (40% void)	0.458 g/cm^3
	286°C (80% void)	0.177 g/cm^3
	20°C (0% void)	0.998 g/cm^3

Pu isotopic composition [wt%]

^{238}Pu	^{239}Pu	^{240}Pu	^{241}Pu	^{242}Pu	Pu_{fiss}
2.2	46.2	29.4	13.4	8.8	59.6

Appendix A.2

DETAILS TO BE PROVIDED ABOUT THE CALCULATIONAL SCHEME USED

1. Name of participant.

2. Establishment.

3. Name of code system(s) used.

4. Bibliographic references for the codes used.

5. Origin of cross-section data (e.g. ENDF/B-VI, JEF-2.2, JENDL-3.2, etc.)
   (Describe deviations of standard libraries, e.g. mix from different libraries, details.)

6. Spectral calculations and data reduction methods used:
   (Please describe your scheme, through a graph and explanatory words provide details about assumptions made.)

   a. Resonance shielding: specify method(s) and specify energy range, and the nuclides (actinides, clad, fission products, oxygen, unresolved resonance treatment).

   b. Mutual shielding (overlapping of resonances).

   c. Fission spectra: specify whether only a single spectrum was used or a weighted mix from all fissile nuclides, explain procedure.

   d. How was the (n, 2n) reaction treated?

   e. Weighting spectrum for scattering matrices, e.g. correction of the out-scatter and self-scatter terms considering the differences between the original weighting spectrum and realistic cell spectrum.

7. Number of energy groups used in the different phases.

8. Cell calculation:

   a. Type of calculation: i.e. heterogeneous, homogenous.

   b. Theory used: diffusion, transport.

   c. Method used: finite difference, finite elements, nodal, S_n(order), collision probability, Monte Carlo, J+/-, etc.

d. Calculation characteristics: meshes, elements/assembly, meshes/pin, number of histories, multi-group, continuous energy, etc.

9. Other assumptions and characteristics:

   a. How many regions with different spectra have been used (different spectrum averaged cross-section sets)? Which ones?

   b. How many burn-up zones have been used (one for each pin or one for each enrichment…)? (Note: these parameters can have an important effect in determining the host spot position.)

10. Other comments that are useful for correctly interpreting the results.

Appendix A.3

DEFINITION OF A SIMPLIFIED CRUCIFORM CONTROL ROD MODEL FOR THE MOX BWR BENCHMARK

In the attached Figure A.A.3.1 a simplified cruciform BWR control rod is defined for the MOX BWR Benchmark. The control rod is assumed to consist of massive steel in the center and of steel blades containing cylindrical holes filled uniformly with B_4C powder. This represents a rather rough model, however the areas of the absorber material (B_4C) and steel should be realistic. More modern designs of BWR control rods may contain additional absorber materials like Hf and may have larger volume fractions of absorber material. Some water fractions in the control blades are not taken into account here.

The densities are assumed to be 1.76 g/cm^3 for B_4C (natural Boron) and 7.9 g/cm^3 for stainless steel. In fact these are the default densities in CASMO. As for the material composition of stainless steel, we have also chosen the CASMO default values, which are attached together with the isotopic concentrations in the table below. Although we checked the data, the participants of the benchmark may feel free to check the consistency (underlying awk-script is also attached in Annex). As for the steel isotopes, we have only calculated one lumped concentration for each metal element in the steel. It should be left to the participants to decide which isotopes of, say , Fe, Cr or Ni should be taken into account in the calculations. Neutron absorption in the steel material does have a significant effect on k-effective. For CASMO-users we have also appended the corresponding "CRD-card" for this control rod. Participants using CASMO may feel free to check this.

Concerning the benchmark calculations, we suggest to consider the following controlled states:

- BOL, cold, no void;
- BOL, hot, 0%, 40% and 80% void;

k-effective, relative pin-wise fission rate distribution and local peaking factors are certainly worth to be calculated and to be compared in this benchmark.

As for the definition of the "hot-cold-swing" $\Delta\rho_{hc}$ we then suggest to include the cold controlled state by the formula:

$$\Delta\rho_{hc} = [k(\text{cold, contr.})+k(\text{cold, uncontr.})]/2-k(\text{hot, uncontr., 40\% void}).$$

The argument for this formula is the fact that for the cold "stuck rod" case the k_{inf} values of the controlled state and the ones of the uncontrolled state contribute with almost the same weighting factor to the k-effective of the whole core.

Figure A.3.1. Simplified cruciform control rod model for MOX BWR benchmark

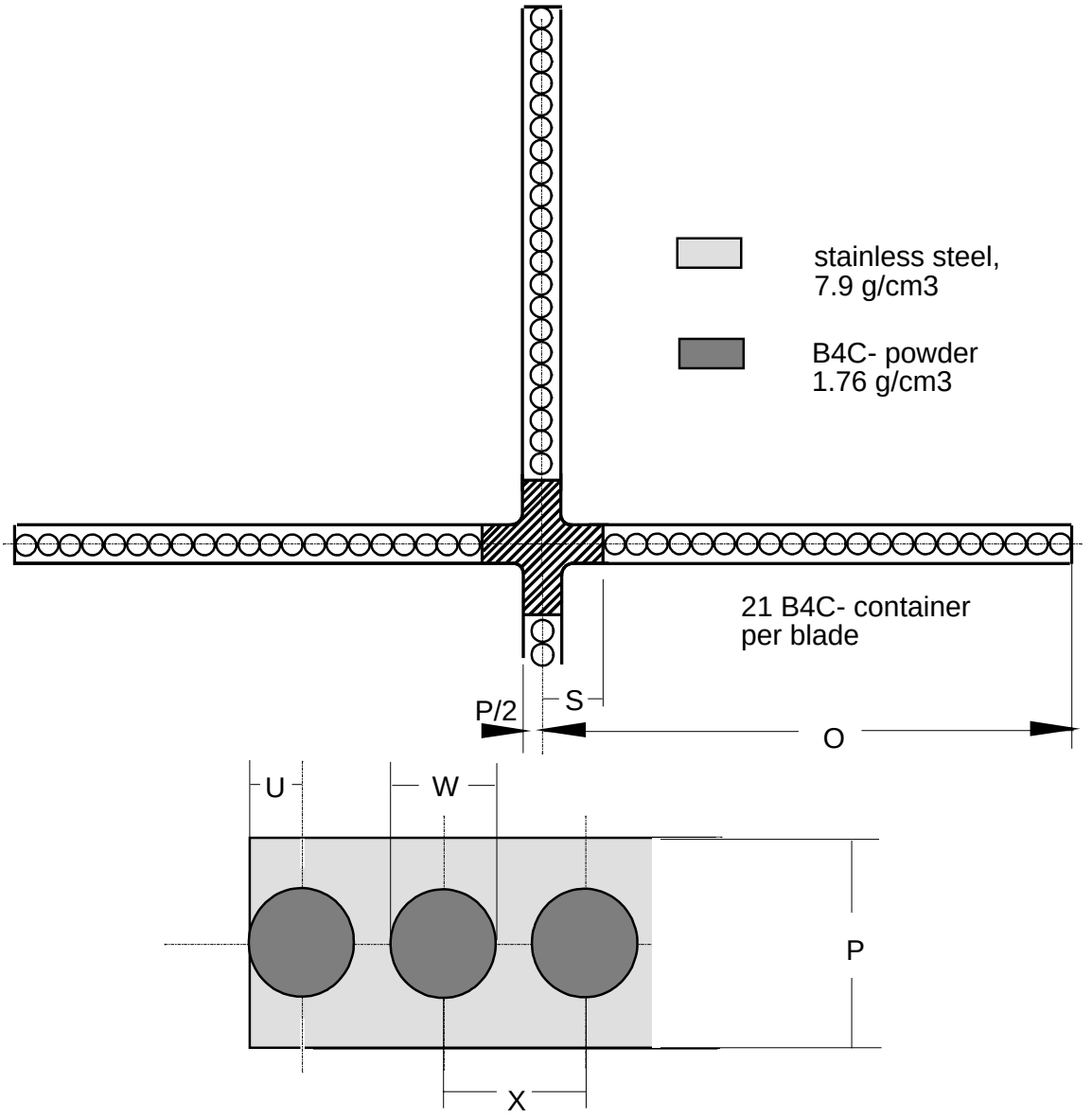

Dimensions in mm:

O	120	U	1.8
P	6.37	W	3.6
S	20	X	4.82

Table A.3.1. MCNP-like input for CR-materials
(nuclide concentrations in $10^{-24}/cm^3$)

```
C-------------------------------
C B4C cold    12  , RHO = 1.76
C  B: 0.183 w/o B10, 0.817 w/o B10, boron 0.78261 w/o in B4C
C  C: 0.21739 w/o in B4C
M12
    5010  0.0151794
    5011  0.0616072
    6012  0.019183


C-------------------------------
C stainless steel cold    13  , RHO = 7.9
C  Si:  0.0051  w/o in st
C  Cr:  0.1740  w/o in st
C  Mn:  0.0199  w/o in st
C  Fe:  0.6835  w/o in st
C  Cr:  0.1170  w/o in st
M13
    14000  0.000863754
    24000  0.0159191
    25000  0.0017232
    26000  0.058222
    28000  0.00948404
```

*** CASMO "CRD-card":**

```
* only of relevance to CASMO users
CRD 0.3185   0.0  2.0  10.0  0.18  0.4762
*  CRP = 0.4762 = 10/21 is used instead of 0.482 (X in CR Fig.)
*  because only this will give correct B4C area in CASMO
*  difference to taking value of 0.482 should be negligible
```

Annex. Awk-script for generating atomic concentrations of CR materials

```
#! /usr/bin/awk -f
# on most unix machines
# comments start with "#"
BEGIN {
 NL = 6.02205e23  # avogadro constant
# the atomic / isotopic masses (At_..) have been taken from
# "Karlsruher Nuklidkarte 1981"
# newer values may differ slightly
#
# boron carbide (absorber)
 rho_b4c = 1.76   # density
 is_b4c =3        # no. of isotopes
# weighting factor                    ;  isotopic weight
# natural boron
 fakt_b4c [1] = 0.78261 * 0.183       ; At_b4c [1] = 10.0
 fakt_b4c [2] = 0.78261 * 0.817       ; At_b4c [2] = 11.0
 fakt_b4c [3] = 0.21739               ; At_b4c [3] = 12.011

# Isotope Id
 namis_b4c [1] = "B10"                ; ideis_b4c [1] = "5010"
 namis_b4c [2] = "B11"                ; ideis_b4c [2] = "5011"
 namis_b4c [3] = "C12"                ; ideis_b4c [3] = "6012"

# stainless steel casmo-like (347)
 rho_st = 7.9
 is_st = 5

 fakt_st[1] = 0.0051                  ;  At_st [1] = 28.09
 fakt_st[2] = 0.1740                  ;  At_st [2] = 52.00
 fakt_st[3] = 0.0199                  ;  At_st [3] = 54.94
 fakt_st[4] = 0.6835                  ;  At_st [4] = 55.85
 fakt_st[5] = 0.1170                  ;  At_st [5] = 58.69
# note: the total sum is only 0.9995 ; the rest is some "dummy" isotope
# Isotope Id
 namis_st [1] = "Si"                  ;  ideis_st [1] = "14000"
 namis_st [2] = "Cr"                  ;  ideis_st [2] = "24000"
 namis_st [3] = "Mn"                  ;  ideis_st [3] = "25000"
 namis_st [4] = "Fe"                  ;  ideis_st [4] = "26000"
 namis_st [5] = "Ni"                  ;  ideis_st [5] = "28000"
```

```
sumfakt = 0
printf "\n"
print " B4C"
print " ---"
for (i=1 ; i<=is_b4c ; i++) {
    sumfakt += fakt_b4c [i]
    conc_b4c [i] = rho_b4c * fakt_b4c [i] * NL / At_b4c [i]
    print " Isotope : ", namis_b4c [i] , " Concentration : " conc_b4c [i]
    }
print " check sum =" sumfakt

sumfakt = 0
printf "\n"
print " Steel"
print " -----"
for (i=1 ; i<=is_st ; i++) {
    sumfakt += fakt_st [i]
    conc_st [i] = rho_st * fakt_st [i] * NL / At_st [i]
    print " Isotope : ", namis_st [i] , " Concentration : " conc_st [i]
    }
print " check sum =" sumfakt
print " "
print " "
print "MCNP-like input"
print "C###############"
print " "
print "C------------------------------"
print "C B4C cold    12  , RHO =" , rho_b4c
print "C  B : 0.183 w/o B10, 0.817 w/o B10, boron 0.78261 w/o in B4C
print "C  C : 0.21739 w/o in B4C"
print "M12"
for (i=1 ; i<=is_b4c ; i++) {
        print "    " ideis_b4c [i] , " " conc_b4c [i] * 1.0e-24
    }
print " "
print " "
print "C------------------------------"
print "C stainless steel cold    13  , RHO =" , rho_st
print "C  Si:  0.0051  w/o in st"
print "C  Cr:  0.1740  w/o in st"
print "C  Mn:  0.0199  w/o in st"
print "C  Fe:  0.6835  w/o in st"
print "C  Cr:  0.1170  w/o in st"
print "M13"
for (i=1 ; i<=is_st ; i++) {
        print "    " ideis_st [i] , " " conc_st [i] * 1.0e-24
    }
       }
```

Addendum

PARTICIPANTS IN THE BWR MOX BENCHMARK

BELGIUM

LANCE, Benoit
Belgonucléaire S.A.
Avenue Ariane 2-4
B-1200 BRUXELLES

FRANCE

DELPECH, Marc (Benchmark co-ordinator)
CE Cadarache, DER/SERI/LCSI
Bâtiment 212
F-13108 SAINT-PAUL-LES-DURANCE CEDEX

GASTALDI, Bernard
CEA Cadarache
F-13108 SAINT-PAUL-LES-DURANCE CEDEX

LEE ,Yi-Kang
CEA/DRN/DMT/SERMA/LEPP
Bâtiment 470,
F-91191 GIF-SUR-YVETTE CEDEX

MAGAT, Philippe
CEA Saclay, SERMA/LENR
Bâtiment 470
F-91191 GIF-SUR-YVETTE CEDEX

PENELIAU, Yannick
CEA Saclay, CEA/DEN/DM2S/SERMA/LEPP
Bâtiment 470
F-91191 GIF-SUR-YVETTE CEDEX

ROHART, Michelle
CEA Saclay, CEA/DRN/DMT
SERMA/LCA
F-91191 GIF-SUR-YVETTE CEDEX

TCHISTIAKOV, Andrei
29, le Tivoli, Allée des Peupliers
F-13090 AIX-EN-PROVENCE

GERMANY

HESSE, Ulrich
Gesellschaft fuer Anlagen- und Reaktorsicherheit
Forschungsgelaende
Postfach 1328
D-85739 GARCHING

LUTZ, Dietrich
Universitaet Stuttgart
Institut fuer Kernenergetik und Energiesysteme
D-70550 STUTTGART

MATTES, Margarete
Universitaet Stuttgart
Institut fuer Kernenergetik und Energiesysteme
D-70550 STUTTGART

MISU, Stefan
FRAMATOME-ANP GmbH
Postfach 3220, Freyeslebenstr. 1
D-91050 ERLANGEN

SCHLOSSER, Gerhard
FRAMATOME-ANP GmbH
Power Generation (KWU) Dep. NBTI
Postfach 3220, Bunsenstr. 43
D-91050 ERLANGEN

TIMM, Wolf
FRAMATOME-ANP GmbH
Postfach 3220, Freyeslebenstr. 1
D-91050 ERLANGEN

ZWERMANN, Winfried
Gesellschaft fuer Anlagen- und Reaktorsicherheit (GRS) GmbH
Forschungsgelaende
D-85748 GARCHING

JAPAN

INOUE, Yuichiro
Toden Software, Inc
In-Core Fuel Management Dept.
Tokyo Bijyutsu Club Bldg.
6-19-15 Shimbashi, Minato-ku
TOKYO 105-0004

ISHII, Kazuya
Energy Research Laboratory Hitachi, Ltd.
1168 MORIYAMA-CHO,
7-2-1 Omika-cho, Hitachi-shi
Ibaraki-ken

OKUMURA, Keisuke
Reactor Analysis Laboratory (JAERI)
Department of Nuclear Energy System
TOKAI-MURA, Naka-gun
Ibaraki-ken 319-1195

KOREA (REPUBLIC OF)

KIM, Young-Jin
Director, HANARO Utilization
Technology Development
Korea Atomic Energy Research Institute
P.O. Box 105, YUSEONG

KIM, Taek Kyum
Nuclear Design Technology Development
Korea Atomic Energy Research Institute KAERI
P.O. Box 105 Yusong-gu
Daeduk-Danji, TAEJON 305-600

JOO Hyung Kook
Nuclear Design Technology Development
Korea Atomic Energy Research Institute KAERI
P.O. Box 105 Yusong-gu
Daeduk-Danji, TAEJON 305-600

MEXICO

FRANCOIS. Juan Luis
Universidad Nacional Autonoma De Mexico
Apartado Postal 6-58
Col. Buenavista
62131, CUERNAVACA, Morelos.

MARTIN-DEL-CAMPO, Cecilia
Universidad Nacional Autonoma de Mexico
A.P. 20-364
MEXICO 01000 DF

THE NETHERLANDS

DAMEN, Patricia
NRG
Westerduinweg 3
Postbus 25
NL-1755 ZG PETTEN

RUSSIAN FEDERATION

KALUGIN, Mikhail A.
RRC (Kurchatov Institute)
Dept. Physical and Technical Research of Advanced Reactors
Kurchatov Square, 1
123182 MOSCOW

SWITZERLAND

KROUTHEN, Jan
Head Incore Fuel Management
EGL/KKL Nuclear Fuel Department
Kernkraftwerk Leibstadt AG
CH-5325 LEIBSTADT

PARATTE, Jean-Marie
Paul Scherrer Institute
CH-5232 VILLIGEN PSI

UNITED STATES OF AMERICA

BAKER, Steven
TransWare Enterprise Inc.
266 Pennsville Pedricktown Road
PEDRICKTOWN NJ 08067

CUEVAS-VIVAS, Gabriel
Nuclear Engineering Dept.
Texas A&M University, College Station
TEXAS 77843-3133

GEHIN, Jess C.
Oak Ridge National Laboratory
Building 6025, MS-6363
Bethel Valley Road, P.O.Box 2008
OAK-RIDGE, Tennessee 37831-6363

PARISH, Theodore A.
Nuclear Engineering Dept.
Texas A&M University, College Station
TEXAS 77843-3133

CHAIRMAN

HESKETH, Kevin
British Nuclear Fuels plc
Research and Technology
B709 Springfields
PRESTON, Salwick
Lancashire PR4 0XJ
United Kingdom

SECRETARIAT

SARTORI, Enrico
OECD/NEA Data Bank
Le Seine Saint-Germain
12, boulevard des Iles
F-92130 ISSY-LES-MOULINEAUX
France

ALSO AVAILABLE

NEA Publications of General Interest

2001 Annual Report (2002) *Free: paper or Web.*

NEA News
ISSN 1605-9581 Yearly subscription: € 40 US$ 45 GBP 26 ¥ 4 800

Nuclear Science

Physics of Plutonium Recycling (2002)
Volume VI – Multiple Pu Recycling in Advanced PWRs
ISBN 92-64-1995768 Price: € 45 US$ 45 GBP 28 ¥ 5 250

Advanced Reactors with Innovative Fuels (2002)
ISBN 92-64-19847-4 Price: € 130 US$ 113 GBP 79 ¥ 15 000

Basic Studies in the Field of High-temperature Engineering(2002)
ISBN 92-64-19796-6 Price: € 75 US$ 66 GBP 46 ¥ 8 600

Fission Gas Behaviour in Water Reactor Fuels (2002)
ISBN 92-64-19715-X Price: € 120 US$ 107 GBP 74 ¥ 12 100

Shielding Aspects of Accelerators, Targets and Irradiation Facilities – SATIF 5 (2001)
ISBN 92-64-18691-3 Price: € 84 US$ 75 GBP 52 ¥ 8 450

Nuclear Production of Hydrogen (2001)
ISBN 92-64-18696-4 Price: € 55 US$ 49 GBP 34 ¥ 5 550

Utilisation and Reliability of High Power Proton Accelerators (2001)
(ISBN 92-64-18749-9 Price: € 130 US$ 116 GBP 80 ¥ 13 100

Pyrochemical Separations (2001)
ISBN 92-64-18443-0 Price: € 77 US$ 66 GBP 46 ¥ 7 230

Evaluation of Speciation Technology (2001)
ISBN 92-64-18667-0 Price: € 80 US$ 70 GBP 49 ¥ 7 600

Comparison Calculations for an Accelerator-driven Minor Actinide Burner (2002)
ISBN 92-64-18478-3 *Free: paper or web.*

Speciation, Techniques and Facilities for Radioactive Materials at Synchrotron Light Sources (2002)
Workshop Proceedings, Grenoble, France, 10-12 September 2000
ISBN 92-64-18485-5 *Free: paper or web.*

Forsmark 1 & 2 Boiling Water Reactor Stability Benchmark (2001)
ISBN 92-64-18669-4 *Free: paper or web.*

Pressurised Water Reactor Main Steam Line Break (MSLB) Benchmark (Volume III) (2002)
ISBN 92-64-18495-3 *Free: paper or web.*

A VVER-1000 LEU and MOX Assembly Computational Benchmark (2002)
Specification and Results
ISBN 92-64-18491-0 *Free: paper or web.*

Order form on reverse side.

ORDER FORM

OECD Nuclear Energy Agency, 12 boulevard des Iles, F-92130 Issy-les-Moulineaux, France
Tel. 33 (0)1 45 24 10 15, Fax 33 (0)1 45 24 11 10, E-mail: neapub@nea.fr**, Internet: www.nea.fr**

Qty	Title	ISBN	Price	Amount
			Total*	

* Prices include postage fees.

❑ Payment enclosed (cheque payable to OECD Publications).

Charge my credit card ❑ VISA ❑ Mastercard ❑ American Express

Card No.	Expiration date	Signature
Name		
Address	Country	
Telephone	Fax	
E-mail		

OECD PUBLICATION, 2, rue André-Pascal, 75775 PARIS CEDEX 16
PRINTED IN FRANCE
(66 2003 02 1 P) – No. 52915 2003